

INTELLIGENT FACADES FOR HIGH PERFORMANCE GREEN  
BUILDINGS

Property of Rensselaer Polytechnic Institute

Intelligent Facades for High Performance Green Buildings

Final Report

Award Numbers:

DE-FG36-06GO86070

09EE0002285

March 1, 2017

Rensselaer Polytechnic Institute

Contact: Anna Dyson

Phone: 212.618.3965

Email: [dysona@rpi.edu](mailto:dysona@rpi.edu)

Working Partners: Syracuse University

DOE Field Project Officer:

Steve Palmeri

## Contents

1. Executive Summary .....	3
2. Comparison of Accomplishments with the Goals and Objective of the Project .....	11
3. Summary of Project Activity .....	22
4. Appendix .....	256
5. Publications and Patents.....	280
6. Computer Modeling Descriptions .....	283

# 1. Executive Summary

## **Progress Towards Net-Zero and Net-Positive-Energy Commercial Buildings and Urban Districts Through Intelligent Building Envelope Strategies**

Previous research and development of intelligent facades systems has been limited in their contribution towards national goals for achieving on-site net zero buildings, because this R&D has failed to couple the many **qualitative** requirements of building envelopes such as the provision of daylighting, access to exterior views, satisfying aesthetic and cultural characteristics, with the **quantitative** metrics of energy harvesting, storage and redistribution. To achieve energy self-sufficiency from on-site solar resources, building envelopes can and must address this gamut of concerns **simultaneously**. With this project, we have undertaken a high-performance building-integrated combined-heat and power concentrating photovoltaic system with high temperature thermal capture, storage and transport towards multiple applications (BICPV/T).

The critical contribution we are offering with the *Integrated Concentrating Solar Façade* (ICSF) is conceived to improve daylighting quality for improved health of occupants and mitigate solar heat gain *while* maximally capturing and transferring on-site solar energy. The ICSF accomplishes this **multi-functionality** by intercepting only the direct-normal component of solar energy (which is responsible for elevated cooling loads) thereby transforming a previously problematic source of energy into a high-quality resource that can be applied to building demands such as heating, cooling, dehumidification, domestic hot water, and possible further augmentation of electrical generation through organic Rankine cycles. With the ICSF technology, our team is addressing the global challenge in transitioning commercial and residential building stock towards **on-site clean energy self-sufficiency**, by fully integrating innovative environmental control systems strategies within an intelligent and responsively dynamic building envelope. The advantage of being able to use the entire solar spectrum for active and passive benefits, along with the potential savings of avoiding transmission losses through direct current (DC) transfer to all buildings systems directly from the site

of solar conversion, gives the system a compounded economic viability within the commercial and institutional building markets.

With a team that spans multiple stakeholders across disparate industries, from CPV to A&E partners that are responsible for the design and development of **District and Regional Scale Urban Development**, this project demonstrates that **integrating utility-scale high efficiency CPV installations with urban and suburban environments is both *viable and desirable within the marketplace***. The historical schism between utility scale CPV and BIPV has been one of differing scale and cultures. There is no technical reason why utility-scale CPV cannot be located within urban embedded district scale sites of energy harvesting. New models for leasing large areas of district scale roofs and facades are emerging, such that the model for utility scale energy harvesting can be reconciled to commercial and public scale building sites and campuses. This consortium is designed to unite utility scale solar harvesting into building applications for smart grid development.

The team has demonstrated a keen and large market interest from the most important A&E firms globally, having collaborated on the speculative application of this technology for multiple commercial projects with globally leading firms such as SOM LLP, KPF, Buro Happold, Arup, SHoP Architects, and NBBJ. The projects that have emerged from these collaborations demonstrate that the impediments such as split incentives amongst multiple stakeholders, and the complexity of implementation and maintenance strategies, can be managed and overcome because of the powerful value equation of clean on-site district scale energy self-sufficiency.

The inevitable rise within the construction industry of increasingly large units of modular, pre-fabricated assemblies containing integrated systems within plug in units will give a major boost towards the necessary coupling of energy harvesting at the building envelope alongside multiple ECS applications. The crucial advantage of concentrating solar energy at the building envelope is in maintaining the high exergy content of solar energy as much as possible, by developing high temperatures and high temperature deltas, rather than allowing insolation to degrade to a state of low-potential, as typically happens when it sinks into the building structure, with conventional building envelopes. Thus, with this integrated system concept, the conventional approach to

sustainable commercial building design that attempts to ‘off-load’ solar heat gain, is eschewed in favor of maximally capturing and transforming all of the resource, which results in significant benefits for urban areas susceptible to heat island effect.

Theoretical (expected) at-module electrical and thermal generation efficiencies are calculated to be over 32% and over 41%<sup>1</sup>, respectively for a combined collection efficiency of 73%. In experimentation to date, we have observed simultaneous efficiencies of 21% electrical and 22% thermal collection at the module, for a combined efficiency of 43%. We are in discussion with our collaborators in the concentrating PV industry about the discrepancy between our observed energy output and expected values.

---

<sup>1</sup> Based on published CPV cell efficiency from Dimroth, Frank, Matthias Grave, Paul Beutel, Ulrich Fiedeler, Christian Karcher, Thomas N. D. Tibbits, Eduard Oliva, et al. “Wafer Bonded Four-Junction GaInP/GaAs//GaInAsP/GaInAs Concentrator Solar Cells with 44.7% Efficiency.” *Progress in Photovoltaics: Research and Applications* 22, no. 3 (March 1, 2014): 277–82. doi:10.1002/pip.2475. And, Green, M. A., Emery, K., Hishikawa, Y., Warta, W., & Dunlop, E. D. (2016). Solar cell efficiency tables (version 47). *Progress in Photovoltaics: Research and Applications*, 24(1), 3–11. <http://doi.org/10.1002/pip.2728>.

Based on ideal concentrating optical train efficiency reported in Benitez, P., Minano, J., Zamora, P., Mohedano, R., Cvetkovic, A., Buljan, M., ... Hernandez, M. 820 (2010). High performance Fresnel-based photovoltaic concentrator. *Optics Express*, 821 18(S1). Retrieved from <http://www.ipi-llc.com/Papers/FresnelPVCentrator.pdf>



Figure 1. Proposed district-scale distributed generation project: Aerospace City, Qatar.

Directed submission of multiple CASE Systems which were proposed to be integrated into building, landscapes and urban infrastructure of this radically projective, energy self-sufficient sustainable city of the future. Images courtesy of SOM LLP, Buro Happold Consulting Engineers, and CASE.



Figure 2. Illustrative Site Plan, Aerospace City, Qatar. CASE systems modeled at district/utility scale in projective city construction project.

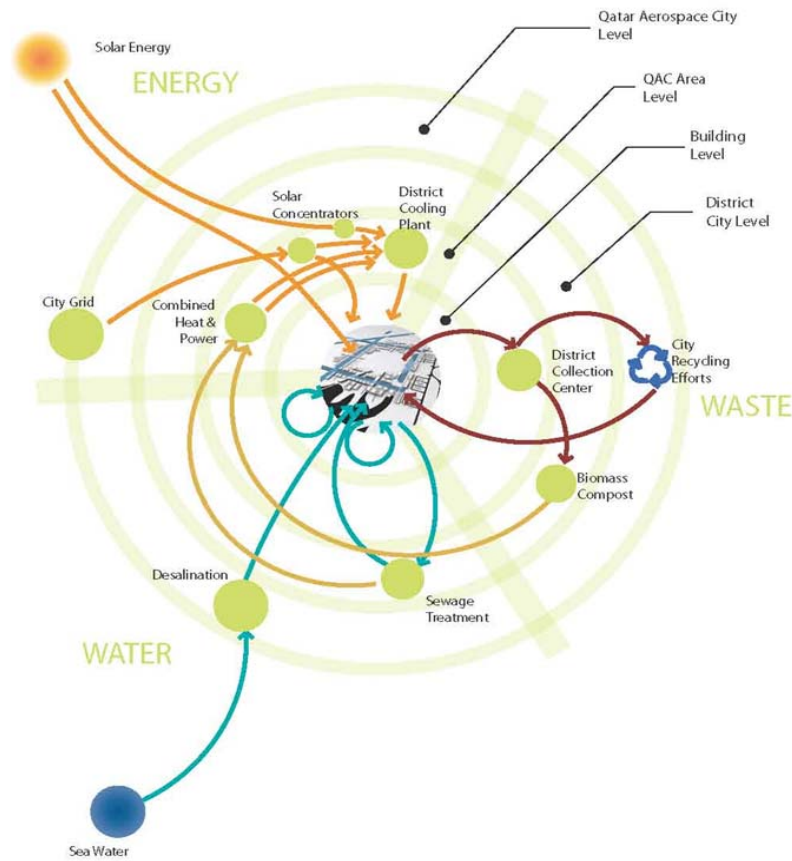


Figure 3. District Scale Concept for integration of Distributed Building-Integrated Concentrating PV towards utility and building scale applications.

Aerospace City Proposal, Qatar. CASE in collaboration with Skidmore Owings and Merrill, LLP (SOM) and Buro Happold Consulting Engineering.

In this granting period, we tested and iterated prototypes through three distinct generations, refined simulation tools for the assessment of the system's energy production and energy cost savings, and specified our conceptual framework in a demonstration of the significant benefits of optimally managing the cascading potentials of energy flows towards multiple applications. Thus far we have verified electrical and thermal production at the module scale, and we are proceeding with array-scale characterization over multiple diurnal cycles. We have simulated the potential for significant energy generation capacity of this system across a range of different climate

types and in most commercial building types, approaching or surpassing net-zero-energy goals for multiple commercial building types and climates.

Multiple technical reassessments of the thermal collection and application strategies have been iterated throughout the process, while certain setbacks have been offset by innovations in systems design from our team and by synergistic advances in the cell types, optics, heat transfer and transport, refrigeration technologies, and electrical distribution technologies from our industrial collaborators. Future work will continue with a more thorough characterization of CPV operational characteristics in the building setting, the full integration of our simulation into a building energy modeling environment (to increase the accessibility of the technology), further refinement of our cost-benefit analysis, experimental optimization in relationship to sorption chilling technology, deployment of our current prototype along both passively-cooled and thermal-harvesting forks, and exploration of multi-phase thermal transfer and short-term storage.

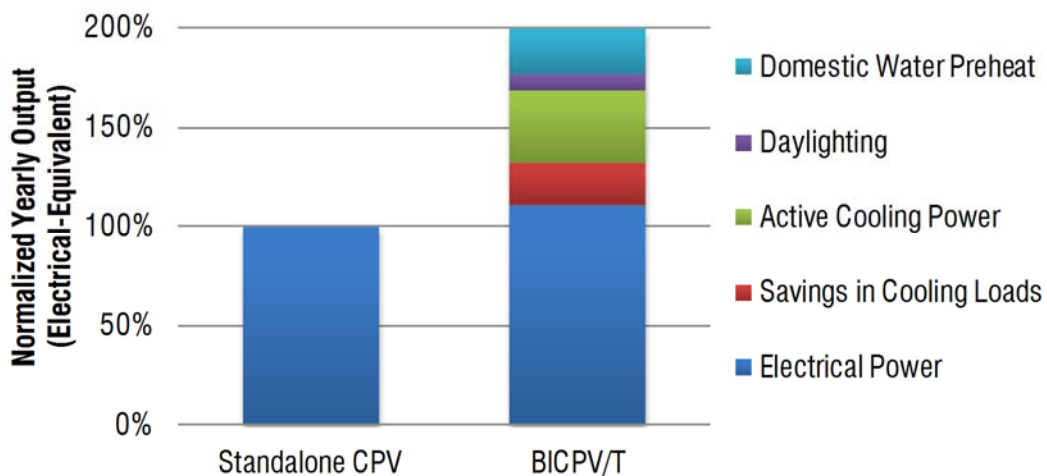


Figure 4. CPV output comparison, stand-alone (power plant) vs. BICPV/T.

BICPV/T has greater impact than stand-alone arrays due to attendant benefits of integrating into the building context combined with grid losses in communicating remotely-generated electricity to a building site. Thermal and electrical power are equated by their relative building system COPs (assumed: 3.1 for vapor cycle chilling and .55 for sorption chilling).

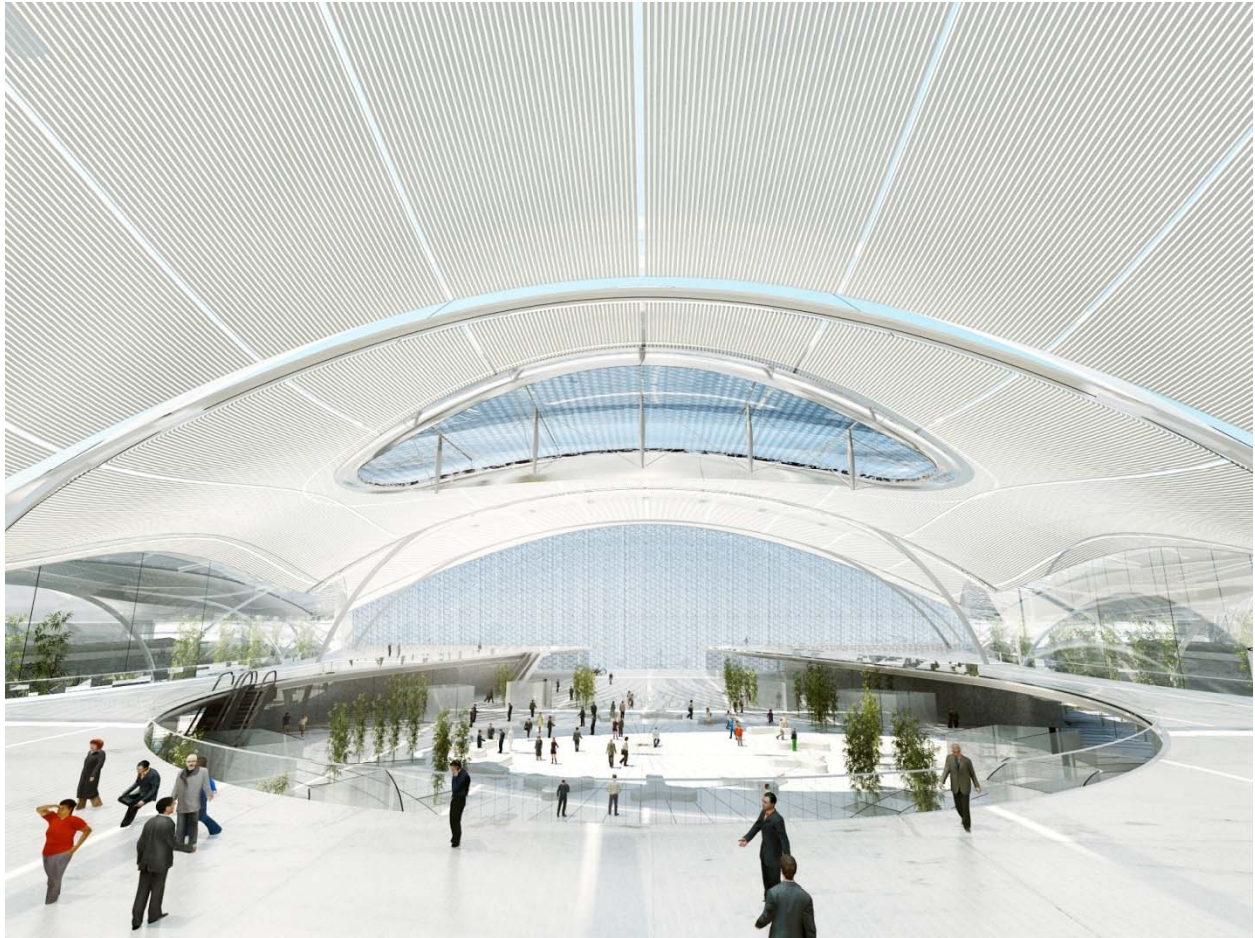


Figure 5. Utility-scale BICPV/T, Skidmore Owings and Merrill LLP Undisclosed Airport Project  
Integration of BICPV/T at full-scale in master plan enabling power generation at district scale.

## **2. Comparison of Accomplishments with the Goals and Objective of the Project**

## Project Objectives

### ***Strategy for Utilization of Climate Resources via Intelligent Façade Technology***

To maximize the usefulness of climate resources, a tiered approach is followed where a climatic resource is applied to a building demand in, as nearly as possible, its original form and quality.

The highest priority is in modulating the use of sunlight for interior lighting. Although this may seem intuitive, sunlight is often blocked out of office spaces with blinds, in favor of overhead electrical lighting, because the positioning of windows creates glare issues (especially with computer-based work). In terms of light quality, however, full-spectrum sunlight is preferred over most electrical sources. Electrical light is inefficient, as well: even modern light-emitting diodes (LEDs) convert electricity to visible light at a rate of only 15 to 25%,<sup>2</sup> while the rest of the energy dissipates as heat gain, which is typically undesired. Attendant to daylighting is the potential for views to the exterior, which are a fundamental intention of including windows in a building design.

The second priority is to address direct-normal insolation (DNI), a highly-ordered climatic energy flow. Current mass-market terrestrial concentrating photovoltaic modules convert DNI to electricity at peak efficiency of 35.9%<sup>3</sup> and an installation collecting energy at this rate, even when heavily discounted for operating losses, would still generate roughly double the average energy use of commercial building stock in the United States on a per-area basis.<sup>4,5</sup> Prioritizing DNI is equally valuable, though, because the energy is typically detrimental in the commercial built environment, driving up cooling loads and contributing to glare issues. The simultaneous reduction of cooling loads from insolation and electric lighting are essentially passive benefits, reducing a building's peak electrical demand before considering any generated energy.

---

<sup>2</sup> Thermal Management of White LEDs. (2007). US DOE.

<sup>3</sup> Amonix Achieves World Record 35.9% Module Efficiency Rating at NREL | [www.amonix.com](http://www.amonix.com). (2013).

<sup>4</sup> CBECS. (2008). 2003 CBECS Detailed Tables: Summary.

<sup>5</sup> Ratio of 2X generation-to-consumption based on 260kWh/m<sup>2</sup>-yr building EUI, 850W/m<sup>2</sup> DNI, net CPV efficiency = 34%, 5 hours of collection.

Although the conversion efficiency of currently-available CPV is high, over half of the energy concentrated on the cell is dissipated as heat. Within the context of potential building applications, the value of this energy can be still quite high, since the elevated temperatures can be generated at the CCA, using solar power that would otherwise drive up cooling loads (if the irradiation passed into the building or to heat the outer surface of the facade). Within the limits of current CPV technology, temperatures can be raised high enough to drive low-pressure organic Rankine cycles, generating still more electricity, or at even better efficiencies, the energy can be applied to active (sorption) chilling processes.<sup>6</sup> Driving temperatures of 65°C are nominally useful for current commercially-available chilling machinery operating at COPs of 0.5 to 0.6, so the thermal collection method of a near-term intelligent façade strategy should be geared towards providing energy of that quality.

Thermal energy is useful at temperatures below sorption-driving temperature as well, for controlling humidity in indoor air. Mitigating the latent moisture loads in outdoor air can account for most of the power in cooling systems in humid environments. Instead, mid-grade heat—between 50°C and 65°C—can be used to power desiccant regeneration strategies, displacing another major power demand in many climates. Thermal energy at all temperatures can be applied to interior heating loads, of course, and to pre-heating of domestic or process hot water supplies.

Cascading the applications of climate-sourced energy according to their potential is crucial for matching available resources to a building's demands, and the lack of this concise framework is a fundamental reason that efforts in building-integrated generation typically fall short. As an accompaniment to the conceptual ranking of energy potentials, a diagrammatic cascade of thermal-only energy and applications is shown in Figure 31.

---

<sup>6</sup> With future cell types that function at temperatures in excess of 150°C, (under development by collaborators at RPI) double-effect chillers could be driven with combined COPs in excess of 1.3.

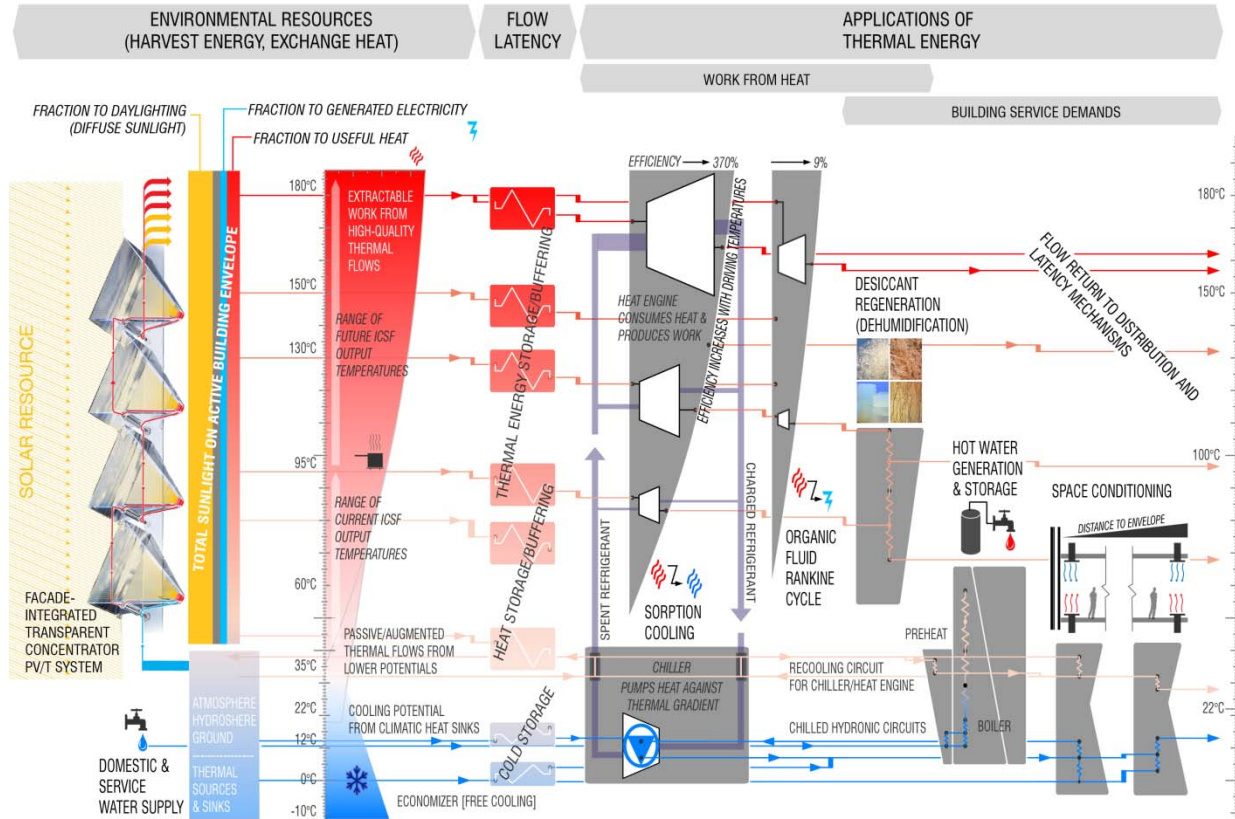


Figure 6. Thermal cascade network diagram: framework for solar energy capture and transfer for building systems applications through ranges of temperature.

Cascading a thermal flow from processes that require high temperatures to processes that require lower temperatures enables the most complete use of all availability (exergy) in the thermal flow.

### ***Building Energy Model Including Integrated Concentrating Solar Façade + Revised Systems***

By integrating with a robust and widely accepted building energy modeling (BEM) framework such as Energy Plus, the ICSF strategy can be more widely applied, not only in our own internal analyses, but by external collaborators and interested parties. In this phase of work the necessary interface points between our system simulator and a BEM engine have been identified, and a procedure has been developed for combining the two engines in post-processing. In the next phase, a module for active solar façade systems will be developed that can be accessed by the BEM engine on a time step basis, allowing us to more accurately observe system states, proscribe control procedures, and forecast results.

### ***Corroboration with Empirical/Prototype Demonstration***

Rensselaer developed and tested prototypical installations of three iterations of a next generation curtain wall unit that directly transfers heat and power captured from a building-integrated concentrating photovoltaic (CPV) system(s) into integrated systems for heating, lighting and cooling. The development of optimization strategies for these application systems for captured solar energy through the integration and simultaneous testing of three functions: 1) thermal capture, transfer and distribution; 2) distributed cooling system strategies; 3) direct current transfer to interior applications. Although this research focused specifically on developing trade-off optimization strategies for the simultaneous capture and transfer of heat and power to building applications, the façade system that was integrated into this testing schedule, by necessity, focused on the Integrated Concentrating Solar Façade (ICSF) System that was developed by Rensselaer with previous grants from the New York State Energy Research and Development Authority (NYSERDA), The New York State Foundation for Science, Technology and Innovation (NYSTAR), and the US Department of Energy (DOE).<sup>7</sup> The ICSF System is a building-integrated photovoltaic (PV) system that increases daylighting quality, reduces cooling loads, generates electricity, and produces high-grade thermal energy. We are currently seeking and negotiating with strategic industrial partners to help develop transformative systems for distributed heat capture and transfer, transport, storage and cooling.

### **Project History**

Beginning with the insight that concentrating PV and building envelopes could be integrated, Experimental Prototypes have been developed with a new concept for a two-axis tracking assembly and concentrating modules that are embedded within the curtain wall of a building. Small-scale prototypes were first tested in 2003 and showed expected PV generation efficiencies (relative to original computational models). With this current

---

<sup>7</sup> A.H. Dyson, P.R.H. Stark, M.K. Jensen, S. Elliott Gruen “Integrated Concentrating (IC) Solar Façade System”, Solar Energy Technology Program, DOE, 2008 and 2009. (total average score on both technical and demonstration reviews - 3.7 out of 4)

grant, further prototype iterations have been of an integrated and optimized delivery system for a 'whole building matrix' suite environmental control systems (ECS) with heat and power applications that have been designed and tested for cost and energy payback periods that would be a fraction on existing disparate systems, within retrofits for new and existing construction. Part of the on-going mission of this research is to demonstrate the synergy of retrofitting ECS in complete integration with a building envelope retrofit that both mitigates cooling and lighting loads, while maximizing on-site energy capture.

## **Progress Overview**

### ***ICSF Prototype Iteration***

The physical manifestation of the integrated concentrating solar façade (ICSF) system has evolved substantially through many prototype iterations, from a lab-scale PV-only proof-of-concept through the current iteration, a full-building-scale machine in occupied space. During operation, the prototype generates electricity and thermal power on a per-module basis that is relevant to the commercial office environment. Furthermore, development for the next, larger iteration has been incorporated into the current design, in order to streamline deployment in an optimized location once it becomes available. The prototype can be reconfigured or replicated to operate at a larger scale at that time.

The team has refined the system as a completely integrated unit to test heat capture, transfer, storage and redistribution within the more confined interior lab spaces that we have at our constant disposal at CASE and Rensselaer. We continue to gather data from the CASE prototypes which will be submitted for publication in Spring 2014, as ongoing testing at the CoE was unfortunately interrupted by construction schedules and delays in the acquisition of testing equipment and space. However, we hope to finish all data acquisition through the two prototypes at CASE and the HT lab, in view to building another larger assembly at the CoE with all integrated features associated with interior conditions in another future phase.

For design validation and verification to continue during periods of the calendar without solar access, we had to embark upon an indoor testing regime. Our indoor

testing at this point has been limited to tracking accuracy verification. We propose, now, to complete indoor performance testing at our heat transfer laboratory at Rensselaer Polytechnic Institute, that will parallel track the testing at CASE for the larger building integrated prototypes. In that way, we can ensure more consistent and reliable conditions that are necessary in our development of systems for capture, storage and redistribution of the heat energy.

## **Assessment of Results and Projections for Ongoing Research**

It is absolutely critical in the next phase of research, that the consortium works closely with industry and with NREL to bring into closer alignment the projection of potential electrical efficiencies of the systems with the testing results. Multiple refinements of the system can be made rapidly with greater industrial support. The second critical step for future research is to ensure support for ‘whole building matrix’ testing that can demonstrate the power of this integrated approach towards on-site net zero, by tying the demonstration to global building requirements for heating, lighting, cooling and plug loads, throughout diurnal and seasonal shifts. The work has thus far been predominantly undertaken within an academic context, but to enjoy further progress, it is essential that the system be co-developed with an alliance of industrial entities that is capable of the design-for-manufacturing and scale-up that is required.

### ***Create Systematic Architectural and Energy Related Payback Options for varied applications***

The building application has a large effect on the potential of ICSF due to correlation between peaks of generation from ICSF and peaks of consumption from the building. An office building provides the ideal program for installation. ICSF peak generation hour correlate with the peak consumption hours of an office building. In other words, as ICSF produces energy between the hours of 9:00am and 5:00pm, with the maximum from noon to 3:00pm, the office consumes energy within the same time interval. Additionally, as the solar generation ceases in the later hours of the work day, so does the consumption of the office building. This correlation of peak generation and demand reduces the need for thermal and electrical storage, can be used to down size mechanic systems, and reduce capital system costs.

When the generated electrical and thermal loads are not needed, the energy is stored for a demand response. An apartment complex does not provide the same potential as an office building but could would substantial electrical and thermal storage. This is due to the apartment complex peak demands being in early morning and evening. ICSF will be just ramping up and down at those times and would need to have stored potential to meet the building's peak demands. The utilization of additional electrical and thermal storage can be expensive, negatively effecting the payback period.

As the simulation process becomes more interconnected and the link of data becomes streamline the ability to run simulations for varying building types, applications, and locations is easier. Currently, office building simulations have been the model of interest but future simulations will explore the relationship between building applications peak demands and ICSF peak generation. The stronger correlated peaks will provide greater direct offset of electrical and thermal consumption in the building and a faster payback. The linking of system and building simulation with a conversation of data flow that informs both generation and consumption will, not only, more accurately inform the building context but provide results more quickly. With the streamline of the ICSF generation and building benefits, advanced simulations can be done exploring application in a wider range of building types. As linked simulations provide better results of building energy consumption after the implementation of ICSF, the payback analysis can be complete from the value of the generated electrical and thermal energy in the building context.

### ***Identify and Develop New Relationships between Building Management and Planning***

With this project, we have analyzed new opportunities for the integration of high-efficiency solar systems to be integrated into building envelopes within many building typologies. Within dense urban zones, with tall building types, the principal opportunities to accumulate district scale solar energy collection are within the vertical facades, presenting a particular geometric and tectonic challenge with respect to the optimization of solar energy collection, a problem that we have studied at length. There is a global opportunity to retrofit failing modern curtain wall systems within integrated retrofits

synchronizing the transfer of energy to electrical lighting and HVAC systems. (Please see Appendix for a comprehensive assessment of solar markets and associated strategies for solar energy collection.) For maximum reduction of grid-dependency for building systems delivery, all environmental control systems need to be interdependently synchronized with the conditions of collection and redistribution of daylighting, lighting, heating, cooling and plug loads.

Modern building management systems (BMS) employ greater amounts of feedback and control of operational states, thanks to increasing availability of and facility with distributed sensors and actuator technology. This feedback enables intelligent façade deployment, as the active elements in a system can be modified continuously to optimize the environmental and energy flow conditions with respect to prioritized criteria. In the case of multiple-effect harvesting strategies such as ICSF, this development offers the capacity to direct operational states towards predicted future building demands, with techniques such as model predictive control.<sup>8</sup> Experts in controls at RPI who are current researcher collaborators include Dr. Sandipan Mishra and Dr. Riccardo Bevilacqua.

During discussions with the MEP professionals responsible for designing the mechanical systems for our recent collaboration on SOM's medical campus design, we initiated the inclusion of additional sensors within the ICSF installation that would control airflow through the curtain wall cavity based on temperature differentials and external prevailing wind patterns. With relative ease, thanks to the applications of sensors and remote louver actuators already included in the project specification, the performance of ICSF, and therefore the balance of thermal regulation in the building, could be optimized based on real-time climate conditions. As the distributed sensing and feedback capabilities of building systems continues to increase, multi-variable control strategies will proliferate beyond classic negative feedback loops and manual interventions, and investigating BICPV/T in this context will provide rich further avenues of investigation.

---

<sup>8</sup> Oldewurtel, F., Parisio, A., Jones, C. N., Gyalistras, D., Gwerder, M., Stauch, V., Lehmann, B., et al. (2012). Use of model predictive control and weather forecasts for energy efficient building climate control. *Energy and Buildings*, 45(0), 15–27.

### ***Identify Material Assembly Strategies for Use in New Systems***

The extended research group has been working on co-development strategies for integrating the ICSF into innovative building envelopes with multiple façade manufacturers, including Island Building Envelope (who fully cost shared the curtain wall unit that was installed in the Syracuse Center for Excellence in Phase 1 of this project), Seele, and Vector Foiltec. Vector Foiltec is the market leader in ETFE building envelope systems, with 80% market share and the greatest portfolio of ETFE buildings. Seele is a diverse company that specializing in the research and development of high end curtain wall systems deploying a range of emerging materials.

Perhaps the most promising aspect of ETFE pneumatic membranes is that they are extremely lightweight with optical clarity and exterior geometries that are superior for optimal solar capture, and that they are optimally suited for long span stadia and other structures that support programs such as sporting venues, airports, transportation hubs, shopping malls and other public programs that by definition prefer to have as much daylight and connection to the outdoors, thereby constituting an optimal programmatic opportunity for ICSF.



Figure 7. Scale model of an Air-Cooled ETFE.

Proposed ETFE Building Envelope Unit from Vector Foiltec that has been retrofitted with IC Solar Modules with Passive Heat sinks. This fully mechanically ventilated air cooling system from Vector Foiltec has been implemented at stadium scale on the left.

Similarly, these building types, provide an optimal typology for district scale energy harvesting and redistribution for peer to peer sharing within districts. They are also at the optimal scale to maximize DC transfer and transport, thereby providing a highly

attractive value equation for large scale owner-occupiers such as municipalities and private consortia.

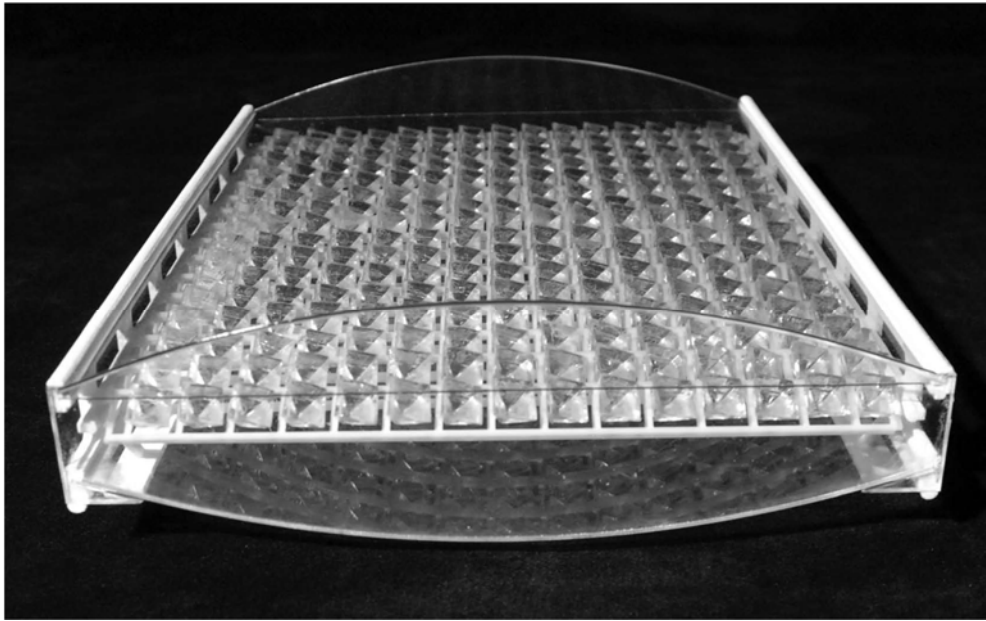


Figure 8. Scale model of an Air-Cooled ETFE Building Envelope Unit from Vector Foiltec that has been retrofitted with IC Solar Modules with Passive Heat sinks.

### **3. Summary of Project Activity**

## Contents: Summary of Project Activity

Contents.....	2
1. Executive Summary .....	3
2. Comparison of Accomplishments with the Goals and Objective of the Project .....	11
Project Objectives .....	12
Project History.....	15
Progress Overview.....	16
Assessment of Results and Projections for Ongoing Research .....	17
3. Summary of Project Activity .....	22
Contents: Summary of Project Activity .....	23
List of Tables.....	27
List of Figures.....	30
List of Equations.....	38
Glossary of Terms and Abbreviations .....	42
Nomenclature for Equations.....	42
3.1 Introduction: Contemporary Context for Intelligent Façade Research .....	45
Assessment Criteria for Integrating Intelligent Facades into High-Performance Green Buildings .....	53
Gallery: Prototypes and Experiments.....	72
Project Objectives .....	76
Project History.....	79
Progress Overview.....	80
3.2 Development of Analysis and Design Tools for Responding to Dynamic Building Energy Consumption Profiles and Performance Criteria.....	83
3.2.1 Modeling the Energy Requirements for Conventional Lighting, Heating, Ventilating and Cooling Systems.....	84

3.2.2	Synchronizing Variable Solar Resource to Fluctuations in Demand Applications .....	90
3.2.3	Identification of Performance Criteria for Building Integration .....	94
3.3	Simulation of Existing and Projected Systems for Performance Evaluation and Design Optimization .....	96
3.3.1	Modeling Existing Systems for Performance Optimization .....	99
3.3.2	Trade-Off Optimization: Electrical vs. Thermal .....	101
3.3.3	Trade-Off Optimization: Construction Costs vs. Performance .....	103
3.3.4	Modeling Effects of ICSF on Buildings in Context: Process.....	106
3.3.5	Simulation Routine for ICSF Performance.....	111
3.3.6	Thermal Energy Utilization Simulations for Internal Systems Applications .....	133
3.3.7	Case Study: Towards Energy-Positive Buildings Through a Quality-Matched Energy Flow Strategy.....	138
3.4	Development of Integrated Optimized System Using Solar Energy for Electrical and Heat Applications .....	176
3.4.1	Localized Thermal Management and Onsite Energy Distribution .....	177
3.4.2	Applications for Thermal Energy Captured at the Building Envelope.....	177
3.4.3	Passive Thermal Storage Techniques for Access to Thermal Energy According to Demand .....	178
3.4.4	Applications for Electrical Energy Generated at the Building Envelope: Novel Techniques for integrating Harvested Daylighting with ICSF with Bioresponsive Electrical Lighting .....	179
3.5	Building, Testing and Evaluation of Integrated System Using Solar Energy for Electrical and Heat Applications.....	197
3.5.1	Generation 6 ICSF Prototype Experiments.....	199
3.5.2	Generation 7 ICSF Prototype Experiments.....	201
3.5.3	Generation 8 ICSF Prototype Experiments.....	209
3.5.4	Experimental Investigation of a Building Envelope-Integrated, Transparent Concentrating Photovoltaic and Thermal Collector.....	214
3.5.5	PHASE III: Assessment of Research Field of Inquiry .....	245

3.6	Overall Assessment for Future Research and Development for this Area of Inquiry: Implications for Envelope and Thermal Transfer Integration and Optimization Strategies for Building Integrated Solar Energy.....	247
3.6.1	Integrating Device Scale Finite Element Analysis with Building Energy Modeling Methods for the Adaptation of Future Energy Systems in a Double Skin Façade.....	247
3.7	Requirements for Ongoing Research .....	250
3.7.1	Proposal for Low-Cost Solar Simulator.....	251
3.7.2	Phase Change Material Incorporation and Sizing.....	255
4.	Appendix.....	256
A.	Tracking Control System .....	256
A.1	Hardware .....	256
A.2	Software .....	258
B.	ICSF Simulation Details.....	264
C.	ICSF Module Heat Sink Specifications .....	267
D.	Electrical Distribution Efficiency Characterization .....	268
E.	Electrical Power Pricing .....	269
F.	BICSF Façade Retrofit Analysis .....	270
G.	ICSF Test Bed: Sheikh Khalifa Medical City, Abu Dhabi, UAE.....	274
5.	Publications and Patents.....	280
5.1	Publications and Patents .....	280
6.	Computer Modeling Descriptions .....	283
6.1	Computer Modeling Description.....	283
6.2	HelioOptix Simulation Engine Model Description. (2012) .....	284
6.3	Description of ICSF Modelica Model Development of a Modeling Strategy for Adaptive Multifunctional Solar Energy Building Envelope Systems.....	300

Abstract..... 300

Introduction ..... 301

BITCOPT Model Description..... 307

Initial Results and Discussion..... 313

Conclusion ..... 316

References..... 317

## List of Tables

Table 1. Building Energy Use Intensity (EUI): DoE baselines relative to buildings with active façade systems. ....	48
Table 2. Key physical parameters of active façade energy collection and application strategy. ....	51
Table 3. Performance criteria and metrics for evaluating intelligent active façade strategies. ....	54
Table 4. Parameters of building simulation: 10-story, high-rise commercial architecture, segmented curtain wall envelope. ....	88
Table 5. Grades (temperature ranges) of thermal resources relevant to the built environment. ....	91
Table 6. Total irradiation on envelope surfaces of a building, New York City and Phoenix Climates. ....	93
Table 7. Performance criteria and metrics for evaluating intelligent active façade strategies. ....	94
Table 8. Steps in co-simulating ICSF and a building energy model. ....	107
Table 9. HeliOptix simulation engine input and output variables. ....	112
Table 10. Variables in calculation of glazing attenuation. ....	113
Table 11. Sample conditions of concentrator-receiver steady-state thermal model. ....	125
Table 12. Energy use intensity, per floor area, relative to incident insolation. ....	140
Table 13. Analyzed climate types. ....	148
Table 14. Thermal capacities of modeled thermal energy storage (NYC climate). ....	150
Table 15. Model configuration parameters. ....	152
Table 16. COP Chiller Function Coefficients. ....	161
Table 17. Lighting loads under daylighting controls. ....	164
Table 18. Yearly facility heating and cooling loads of twelve configurations. ....	166
Table 19. Summary of thermal collection and heating applications. ....	167

Table 20. Solar cooling systems summary. ....	169
Table 21. Summary: net energy use intensities, by demand type (kWh/m <sup>2</sup> -yr).....	171
Table 22. Utility annual cost summary.....	173
Table 23. Target Commercial Building Types and Campus Equivalents. ....	184
Table 24. Representative Before and After Installation Comparison. ....	184
Table 25. Proposed components of energy savings of LED smart lighting system integration (not including solar energy capture or solar heat gain mitigation from ICSF).....	187
Table 26. 50,000 ft <sup>2</sup> Education Building Annual Energy Savings Estimate.....	191
Table 27. Phases of ICSF Development.....	193
Table 28. U.S. Commercial Building Types and Features, as percent of total.....	195
Table 29. U.S. Commercial Sector. ....	195
Table 30. U.S. Commercial Sector Projected Floor Space.....	196
Table 31. Observed module efficiency (Electrical + Thermal), Generation 7 prototype.....	204
Table 32. Inputs and outputs of active envelope model.....	220
Table 33. Insolation quantities defined. ....	221
Table 34. Glazing loss parameters.....	223
Table 35: List of Uncertainties. ....	236
Table 36. Decision matrix for optimal mass of PCM in ICSF/VTR system.....	255
Table 37. Front panel of original ICSF simulation developed at CASE/Rensselaer (constructed in Microsoft Excel). (3 pages) .....	264
Table 38. Electricity Service Costs (simulated), baseline building vs. building with ICSF strategies. ....	270
Table 39. HeliOptix simulation engine input and output variables.....	284

Table 40. Variables in calculation of glazing attenuation. ....	285
Table 41. Inputs and outputs of active envelope model.....	308
Table 42. Parameters for measured-modeled data calibration.....	315

## List of Figures

Figure 1. Proposed district-scale distributed generation project: Aerospace City, Qatar. ....	7
Figure 2. Illustrative Site Plan, Aerospace City, Qatar. CASE systems modeled at district/utility scale in projective city construction project. ....	7
Figure 3. District Scale Concept for integration of Distributed Building-Integrated Concentrating PV towards utility and building scale applications. ....	8
Figure 4. CPV output comparison, stand-alone (power plant) vs. BICPV/T. ....	9
Figure 5. Utility-scale BICPV/T, Skidmore Owings and Merrill LLP Undisclosed Airport Project .....	10
Figure 6. Thermal cascade network diagram: framework for solar energy capture and transfer for building systems applications through ranges of temperature. ....	14
Figure 7. Scale model of an Air-Cooled ETFE. ....	20
Figure 8. Scale model of an Air-Cooled ETFE Building Envelope Unit from Vector Foiltec that has been retrofitted with IC Solar Modules with Passive Heat sinks. ....	21
Figure 9. ICSF Generation 6 View prototype, by CASE, Rensselaer Polytechnic Institute. ....	45
Figure 10. ICSF installed in clerestory of proposed FIT expansion (render). NY, NY. ....	46
Figure 11. ICSF Generation 8 Heat and Power Prototype, Operational at CASE studio, NY, NY. ....	46
Figure 12. Section view of ICSF module showing concentration and components. ....	49
Figure 13. Energy Flow at the Modular Scale through ICSF. ....	49
Figure 14. Comparison of benefits between ICSF and baseline low-SHGC IGU. ....	50
Figure 15. Sample case study from 2010 of an undisclosed commercial building in UAE. ....	50
Figure 16. Summary of spatial and energy benefits of intelligent envelope (ICSF) strategies. ....	52
Figure 17. Performance criteria for building envelopes and intelligent facade systems. ....	53
Figure 18. Conceptual ranking of energy sources and demands of the built and natural environments. ....	55

Figure 19. Ecosystem of collaborators and research partners in intelligent facades and distributed systems. .... 57

Figure 20. Vascular Thermal Redistribution schematic across core-dominated building floorplate. .... 60

Figure 21: Perimeter HVAC Systems Reduction. .... 66

Figure 22: Angled Curtain Wall Façade Retrofit with clerestory window panel for solar collection and shading above, and clear vision glass below. .... 66

Figure 23. Glazing mullions channel water for heating, cooling, and moisture control at EMPAC at Rensselaer. (Images: Brandon Andow, 2011) ..... 69

Figure 24. Synthetic Energy Flow Diagram for the capture, transformation, and redistribution of solar energy into electrical and thermal power at the façade. .... 71

Figure 25. ICSF Generation 6 Heat & Power prototype. (Syracuse, NY, 2010-2012). .... 72

Figure 26. ICSF Modified Generation 6 Prototype. .... 72

Figure 27. ICSF Generation 7 prototype, deployed at CASE studio, Manhattan, NY. .... 73

Figure 28. Improvements from Generation 7 to Generation 8 prototype. .... 74

Figure 29. Generation 8 water block heat sink, customized to ICSF. .... 74

Figure 30. Passive heat sink design alternative for ICSF installation with fan assisted air cooling. .... 75

Figure 31. Thermal cascade network diagram: framework for solar energy capture and transfer for building systems applications through ranges of temperature. .... 78

Figure 32. Thermal redistribution strategy (schematic). .... 81

Figure 33. Commercial buildings energy consumption by end use (2010, projected). .... 86

Figure 34. National energy usage by sector, building sector breakdown and energy carriers. .... 86

Figure 35. Energy carriers used in building sector. .... 87

Figure 36. Primary fuels for electric power in United States, 2010. .... 87

Figure 37. Simulated building typology is typical for large, core-dominated commercial architecture. .... 89

Figure 38. Cumulative thermal loads on mid-building floor plate for the representative large commercial building design, modeled in Phoenix, AZ.....	90
Figure 39. Cumulative thermal loads on mid-building floor plate for the representative large commercial building design, modeled in New York City, NY.....	90
Figure 40. Process diagram for harvesting solar energy, transforming it, and applying it to service demands through active façade strategies.....	98
Figure 41: Performance Comparison between ICSF, mono-Silicon solar cells, and water heating with evacuated tube collectors.....	100
Figure 42. Exergy ratio of incident sunlight to electrical output and thermal output of BICP/T.....	101
Figure 43. Power developable by BICPV/T increases with increasing collector temperature.....	102
Figure 44 - Generation 7 lower stack actuator block (left) and Generation 8 lower stack actuator block (right).....	104
Figure 45. Generation 7 (left) and Generation 8 (right) marionette assemblies.....	105
Figure 46. Chiller best-performance state: drive circuit T = 65°C, recooling T = 25°C.....	106
Figure 47. The relationship between incident direct normal insolation (from NYC TMY data) and ICSF temperature output for a stack of 15 modules from the ICSF simulation engine.....	118
Figure 48. Electrical output of ICSF (kWh/m <sup>2</sup> of envelope area, yearly).....	119
Figure 49. Comparison of simulated electrical generation between SAM and ICSF models for New York, NY.....	122
Figure 50: Comparison of simulated electrical generation between SAM and ICSF models for Phoenix, AZ.....	122
Figure 51: Comparison of simulated electrical generation between SAM and ICSF models for New York, NY.....	123
Figure 52: Comparison of simulated electrical generation between SAM and ICSF models for Phoenix, AZ.....	123
Figure 53. Thermal energy balance control volume of the hydronically cooled concentrator-receiver.....	124

Figure 54. Energy losses of concentrator-receiver at steady state and operating temperature ranges. ....	126
Figure 55. Measurements of thermal conductivity of tubing runs interstitial to module heat exchangers...	127
Figure 56. Coolant pumping losses relative to electrical generation. ....	128
Figure 57: Equivalent Thermal Resistance of the Hydronic Distribution System. ....	130
Figure 58: Simplified Model (Radiation and Contact Resistance removed). ....	130
Figure 59: Equivalent Thermal Resistance from combining series resistance.....	130
Figure 60: Alternate coolant flow paths, short (left) and long (right).....	132
Figure 61: Collection efficiency relative to tank temperature for short and long coolant flow paths. ....	132
Figure 62. SorTech chiller performance curves. ....	134
Figure 63. Chiller performance (COP) augmented with evaporative cooling. ....	136
Figure 64. Energy produced by 5-bay ICSF system, hourly, and by daily totals.....	137
Figure 65. Per-module total energy output per day.....	137
Figure 66. Relation of studio space cooling demand and ICSF production (hourly). ....	138
Figure 67. Sizing of buffer tank vs. expected energy collected by ICSF.....	138
Figure 68. Transitioning from centralized systems (grid-source optimized) to distributed, integrated systems (climate-sourced optimized).....	141
Figure 69. Q-MEF model, structure and variable flow.....	143
Figure 70. Building configurations and components from modeling environments. ....	144
Figure 71. Plumbing schematic showing chilled and rejection-range distribution. ....	146
Figure 72. Modeled method of flushing excess heat from cavity. ....	158
Figure 73. Thermal energy transfers, yearlong cumulative summary. ....	168
Figure 74. Utility costs, three climates, yearly.....	172

Figure 75. Utility costs breakdown, Mountain View, yearly. ....	172
Figure 76. Schematic for introducing PCM to thermal storage buffer in ICSF.....	178
Figure 77. Comparison of daylighting performance: ICSF & Electroactive Dynamic Daylighting System. .	189
Figure 78. ICSF Generation 6 working prototypes.....	199
Figure 79. Secondary optical element and heat sink assembly in Generation 7 design. ....	201
Figure 80. Pyrheliometer mounted to measure sensitivity to flux.....	206
Figure 81. Re-calibration of pyrheliometers.....	207
Figure 82. Potential heat sink designs.....	207
Figure 83. ICSF receiver and heat sink evolution.....	208
Figure 84. Secondary optical element and heat sink assembly in Generation 7 design. ....	209
Figure 85. Balance of system measurement and control hardware for Generation 7. ....	211
Figure 86. Trailing end of Generation 8 tracker stacks.....	211
Figure 87. Motor specification evolution, past and current tracker design.....	212
Figure 88: Tracking Embedded Controller: Concerto F28M36PX MCU (on dev board). ....	213
Figure 89. Cassette assembly (exploded view). Façade installation shown with 20° tilt and glass infill. .	215
Figure 90. Installed BITCoPT prototype (photograph).....	216
Figure 91. BITCoPT prototype module components.....	217
Figure 92. Thermal collection scheme: hydronic circuits, heat exchanger.....	219
Figure 93. Simulation of angle-dependent shading conditions ( $F_{POE}$ ).....	224
Figure 94. Control volume for energy balance at module receiver.....	225
Figure 95. BITCoPT prototype as tested, with sensor placements.....	232
Figure 96. Experimental setup: thermocouples installed at module receivers. ....	232

Figure 97. Observed prototype power generation.....	238
Figure 98. Energy efficiencies (measured) of homogeneous sub-array.....	239
Figure 99. Observed cogeneration efficiencies $\eta_{\text{cogen}}$ , $\epsilon_{\text{cogen}}$ , for homogenous modules (functions of $T_{\text{HTF,in}}$ ).....	240
Figure 100. Exergetic efficiencies for homogenous sub-array on February 20 <sup>th</sup> .....	241
Figure 101. Observed and projected cogeneration energy and exergetic efficiencies.....	242
Figure 102. Exergetic efficiencies for projected setup, February 20 <sup>th</sup> input data.....	243
Figure 103. Projected Price Per Module for Mass Produced ICSF.....	246
Figure 104. Testing facility with co-located labs that accelerates scale-up from 'hotbox' testing to integration within building.....	251
Figure 105: Distribution of rotational feedback steady state error from mean (n = 1000). ....	256
Figure 106: Tracking servos step response to an introduced position change. ....	258
Figure 107. ICSF Control System flow chart.....	259
Figure 108. Tracking servo PID control pseudocode.....	260
Figure 109: Tracking servo PID control psuedocode.....	261
Figure 110: ICSF Control System One-Line Schematic.....	262
Figure 111: Circuit Diagram for Bi-Directional H-Bridge servo motor drivers.....	262
Figure 112: Fabricated Motor Control Board to House Motor Drivers.....	263
Figure 113. Datasheet provided by Mikros, characterizing heat sink in Generation 8 module.....	267
Figure 114. Circuit Diagram for Electrical Transmission Efficiency Calculation. ....	268
Figure 115. Calculated Voltage Drop for 3 Modules in Series. ....	268
Figure 116: Facade Retrofit Exploded Component Axonometric (ICSF installation at 15 tilt).....	271

Figure 117: Installation of ICSF Mega-panels onto Existing Curtain Wall Conditions (Vertical Orientation).....	272
Figure 118. SKMC Hospital City .....	274
Figure 119: SKMC Hospital Entrance .....	274
Figure 120. SKMC General Hospital Lobby with transparent ICSF roof modules that bathe the interior space with cool diffuse daylight and allow for a clear view to the sky while removing solar heat gain and glare from the space. ....	275
Figure 121. General Hospital Lobby, with and without active façade intervention. ....	275
Figure 122. Design Weighted Daylight Glare Probability Matrix showing the progressive reduction in glare resulting from the integration of ICSF in the SKMC lobby.....	278
Figure 123. The relationship between incident direct normal insolation (from NYC TMY data) and ICSF temperature output from HeliOptix simulation engine. ....	286
Figure 124. Simulated ICSF installation output temperatures.....	287
Figure 125. Simulated ICSF Output Temperatures, relative to hourly DNI data, for NYC climate. Heat loss effect of hydronic cooling circuit simulated with vacuum-insulated tubing. ....	288
Figure 126. Simulated thermal energy gains from a 6 module stack, given short- and long-tubing configurations, and HeliOptix simulation output, for reference.....	288
Figure 127. Electrical output of ICSF (kWh/m <sup>2</sup> of envelope area, yearly). ....	289
Figure 128. Data collected from ICSF module.....	290
Figure 129. Thermal energy and net DC electricity production from installed ICSF.....	291
Figure 130. Sortech chiller performance curves. ....	293
Figure 131. Chiller performance (COP) augmented with evaporative cooling. ....	295
Figure 132. Cumulative effects of ICSF on the thermal loads, NYC climate.....	297
Figure 133. Cumulative effects of ICSF on the thermal loads, Phoenix climate.....	298

Figure 134. The BITCOPT system. Photographs of CASE Integrated Concentrating Solar Façade (ICSF) installation and data acquisition, with a diagram showing the adaptable energy conversion, storage and redistribution strategy. .... 302

Figure 135. BITCOPT energy balance model and variable flow diagram. Component tags (denoted by #) are referred to in text. .... 305

Figure 136. Model control volumes: BITCOPT receiver (left, #BM) and cassette (right, #BEC). .... 309

Figure 137. Measured and modeled power generation. .... 315

Figure 138. Year-long simulation of energy collection with experimentally-derived model parameters. .... 315

Figure 139. As modeled BITCOPT intercepts 96% (yearly) of  $I_{DN}$  transmitted past exterior glazing of south and west façades. .... 316

## List of Equations

Equation 1. Empirical formula for determining Fresnel efficiency factor of concentrating the light on high efficiency solar cell, based on the magnitude of concentration.....	112
Equation 2. Empirical equation for determining thermal resistance based on the flow rate of liquid through the system. ....	113
Equation 3. Radiation power transmitted through glass, relative to angle of incidence. ....	114
Equation 4. Transverse angle.....	114
Equation 5. Parallel transmission coefficient. ....	114
Equation 6. Perpendicular transmission coefficient. ....	114
Equation 7: Equation to determine the percentage of module overlap. ....	115
Equation 8: Energy-In-Per-Cell equation, used to calculate the maximum amount of solar energy reaching the cell before electrical and thermal conversion.....	115
Equation 9: Equation for determining the cell electrical conversion efficiency. ....	116
Equation 10: Electrical power (POWER) generation based on energy in per cell (EIPC) and PV cell efficiency (CELLEFF).....	116
Equation 11: After the power is calculated for one module, a For loop is run to sum up the values dependent on the number of cells in a vertical stack. This generated the electrical power for one stack (EPOW). ....	116
Equation 12: The electrical power (EPOW) for one stack is multiplied but the number of stacks (HSTACKS) to determine the new EPOW for the entire array. ....	116
Equation 13: Amount of heat into the cell ( $HEAT_{IN}$ ) after a percentage is converted it electrical power. ...	116
Equation 14: Equation to determine the temperature of the fluid ( $T_{OUT}$ ) after the initial fluid temperature ( $T_{IN}$ ) flowing past the cell heat source ( $HEAT_{IN}$ ) with a user defined mass flow rate ( $m_{dot}$ ) and specific heat capacity ( $c_p$ ).....	117
Equation 15: Averaging equation to determine the temperature of the cell ( $T_{MEAN}$ ) for the use of transferring more heat to a heat transfer fluid.....	117

Equation 16: The thermal power generated (TPOW) is determined from HTF outlet temperature. ....	118
Equation 17. Incompressible pumping power. ....	128
Equation 18: Equivalent thermal resistance.....	130
Equation 19: Heat loss for section on pipe. ....	130
(20) .....	149
(21) .....	149
(22) .....	149
(23) .....	149
(24) .....	155
(25) .....	156
(26) .....	157
(27) .....	159
(28) .....	159
(29) .....	160
(30) .....	161
(31) .....	162
(32) .....	221
(33) .....	221
(34) .....	222
(35) .....	222
(36) .....	225
(37) .....	226

(38) ..... 226

(39) ..... 226

(40) ..... 227

(41) ..... 227

(42) ..... 227

(43) ..... 228

(44) ..... 228

(45) ..... 229

(46) ..... 229

(47) ..... 229

(48) ..... 229

(49) ..... 230

(50) ..... 230

(51) ..... 230

(52) ..... 235

(53) ..... 235

Equation 54. Daylight Glare Probability ..... 277

Equation 55. Radiation power transmitted through glass, relative to angle of incidence. .... 285

Equation 56. Transverse angle..... 285

Equation 57. Parallel transmission coefficient. .... 285

Equation 58. Perpendicular transmission coefficient. .... 285

Equation 59. Solar power incident on CPV (#GP, #MG, #LT). .... 308

Equation 60. Effective flux concentration ratio as function of geometric concentration, CPV-incident irradiance, and AM1.5 reference insolation (#LT).....	308
Equation 61. Energy balance for a module receiver (#REB).....	309
Equation 62. Relationship between HTF and CPV driving temperatures and collected heat at module receiver (#WBHS).....	311
Equation 63. Thermal energy lost at the receiver (#REB).....	311
Equation 64. Thermal transport loss as a function of tubing insulation and temperature difference (#TTL).....	311
Equation 65. Energy balance of hydronic tubing (#TTL).....	311
Equation 66. Thermal transport efficiency of tubing (#TTL).....	312
Equation 67. Energy balance across cassette control volume (#BEC, #EF).....	312
Equation 68. Conductivity across outer cassette glazing (#EF).....	312
Equation 69. Conductivity across inner cassette glazing (#EF).....	313

## Glossary of Terms and Abbreviations

BICPV/T	Combined photovoltaic and thermal energy-producing building-integrated system
ICSF	Building-Integrated Concentrating Solar Facade
CCA	Concentrator Cell Assembly
CPV	Concentrator Photovoltaic Cell
HTF	Heat Transfer Fluid, working fluid
ORC	Organic Rankine cycle for rotational work (electrical generation)
PCM	Phase changing material (typically a paraffin or a eutectic salt, used to store thermal energy at a specific temperature by melting or freezing)
PV	Photovoltaic
SHGC	Solar Heat Gain Coefficient

## Nomenclature for Equations

<i>MAG</i>	Concentration magnitude
<i>EVC</i>	Cell electrical efficiency - extrapolated from IV performance charts (%)
<i>EVT</i>	Cell thermal efficiency (%)
<i>TR</i>	Thermal resistance of system (K/W)
<i>MDOTGAL</i>	Mass flow rate of fluid (kg/s)
<i>P</i>	Transmitted power (watts)
<i>N<sub>AIR</sub></i>	Index of refraction, air
<i>N<sub>GLASS</sub></i>	Index of refraction, glass
$\theta$	Angle of incidence
$\theta_t$	Transverse angle
<i>T<sub>p</sub></i>	Transmission coefficient, parallel
<i>T<sub>t</sub></i>	Transmission coefficient, perpendicular
<i>SELF<sub>SH</sub></i>	Percent of modules that are self-shaded in the array (%)
<i>HSPACE</i>	Horizontal spacing between modules in the array (m)
<i>VSPACE</i>	Vertical spacing between modules in the array (m)
<i>DNIAOI</i>	Direct normal incidence angle of incidence

<i>LENS</i>	Lens size (m <sup>2</sup> )
<i>EIPC</i>	Energy in per cell (Wh)
<i>DNI</i>	Direct normal incidence solar radiation – from TMY3 (W/m <sup>2</sup> )
<i>g<sub>eff</sub></i>	Transmission efficiency (%)
<i>Fresnel</i>	Lens efficiency (%)
<i>CELLEFF</i>	Overall cell efficiency
<i>E<sub>Peak</sub></i>	Maximum efficiency peak (%)
<i>TPVGUESS</i>	Estimate cell temperature (°C)
<i>POWER</i>	Electrical power generation for one module (W)
<i>EPOW</i>	Electrical power for one stack of modules (W)
<i>HSTACKS</i>	Number of stacks
<i>HEAT<sub>IN</sub></i>	Thermal energy produce per module (W)
<i>T<sub>OUT</sub></i>	Temperature of fluid leaving module ((°C)
<i>T<sub>IN</sub></i>	Temperature of fluid entering module (°C)
<i>T<sub>MEAN</sub></i>	Mean fluid temperature(°C)
<i>TPOW</i>	Thermal power for one stack of modules (W)
<i>T<sub>ORIG</sub></i>	Original temperature of fluid (°C)
<i>R</i>	Heat loss factor (k/Wh)
<i>ṁ</i>	mass flow rate (kg/s)
<i>C<sub>p</sub></i>	Heat capacity of fluid (J / K or C)
<i>P<sub>h</sub></i>	Pumping power (W)
<i>η<sub>p</sub></i>	Pump efficiency
<i>g</i>	Gravitational acceleration (m/s <sup>2</sup> )
<i>h</i>	Pump head (m)
<i>R<sub>eqv</sub></i>	Equivalent total thermal resistance
<i>R<sub>conv,i</sub></i>	Thermal convection resistance between inside fluid and tube wall
<i>R<sub>cond,t</sub></i>	Thermal conduction resistance for tube wall
<i>R<sub>cond,i</sub></i>	Thermal conduction resistance for tube insulation
<i>R<sub>conv,o</sub></i>	Thermal convection resistance between tube insulation and air
<i>Q<sub>loss</sub></i>	Heat loss from thermal distribution

$T_{water}$	water temperature (°C)
$T_{air}$	air temperature (°C)
$\dot{Q}$	heat transfer rate, W

### 3.1 Introduction: Contemporary Context for Intelligent Façade Research

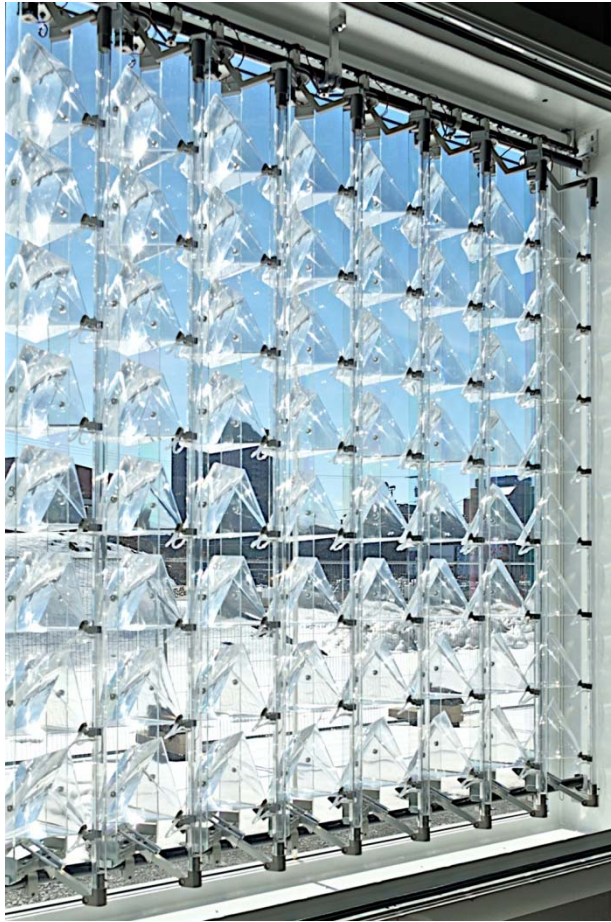


Figure 9. ICSF Generation 6 View prototype, by CASE, Rensselaer Polytechnic Institute. Full-scale model used to explore motion studies, daylighting qualities, and alignment changes due to differential thermal expansion. Installed in Syracuse, NY, 2010.<sup>9,10</sup>

---

<sup>9</sup> Dyson, A. H., Jensen, M. K., & Borton, D. N. (2007, March 13). United States Patent: 7190531 - Concentrating type solar collection and daylighting system within glazed building envelopes.

<sup>10</sup> Dyson, A. H., Jensen, M. K., & Borton, D. N. (2010, June 29). United States Patent: 7745723 - Concentrating type solar collection and daylighting system within glazed building envelopes.



Figure 10. ICSF installed in clerestory of proposed FIT expansion (render). NY, NY.

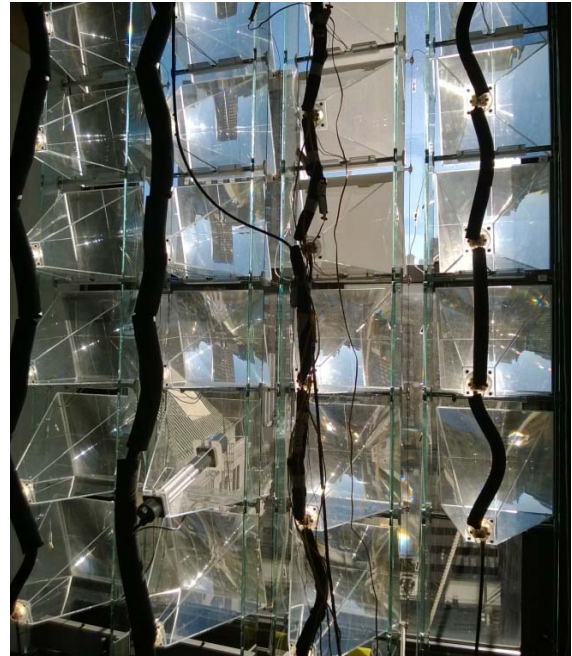
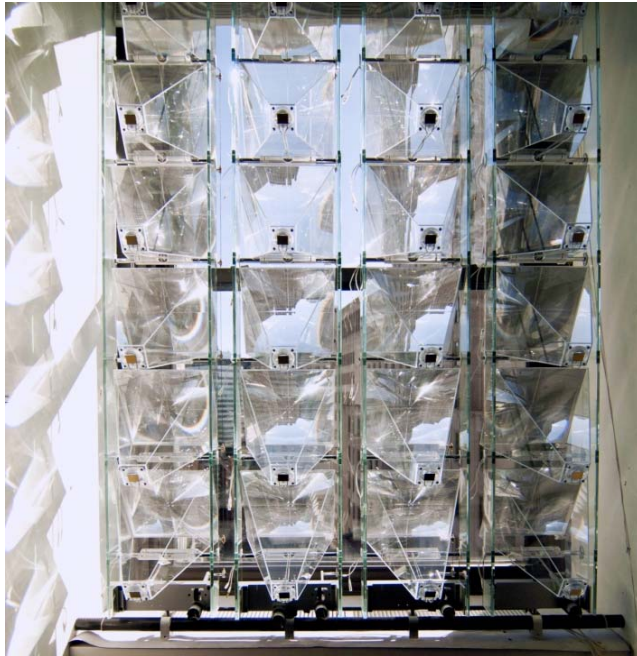


Figure 11. ICSF Generation 8 Heat and Power Prototype, Operational at CASE studio, NY, NY.

Improvements over Generations 6 and 7 include reduced parts count, return to low-cost servo tracking actuation and low-profile heat sink design, configuration for multiple thermal transport methods, and interface to building cooling systems. Array is pictured here with and without insulated hydronic cooling circuits, which are included for experimental characterization. Proposed design comprises all transparent or light-hued components (no black insulation).

Buildings are responsible for consuming roughly 40% of the energy that is produced, world-wide. Addressing energy use in the built environment is crucial to maintaining stability, growth, and health in the 21st century and beyond.<sup>15</sup> The built environment is everywhere presented, however, with sources of power (and other benefits) from conditions in the immediate natural environment, such as solar energy. With present building stock, natural conditions typically serve to drive energy consumption, as when solar irradiation heats a commercial building, causing cooling loads. Rather than counteracting natural conditions with grid-sourced energy, if buildings could draw on and benefit from these conditions—climatic energy resources—buildings of a range of typologies in many climates could be net producers, with systems that internalize and manipulate available climatic energy sources.

To benefit fully from available climatic resources, buildings must interface proactively with the natural environment by collecting, directing, and transforming the energy flows that are available, to address the building's demands. The present inquiry explores the physical interface between built and natural environments: a building's façade. Currently researched BICPV/T strategies ignore critical context of the occupied built environment, and either fail to meet criteria that make them desirable for a building project, or fail to collect the maximal exergy available from insolation because of lack of deep integration with the energy demands of the conditioned space.

An intelligent façade concept is proposed and developed which manipulates solar energy in order to provide electricity, active and passive cooling, and thermal energy to be used in the building. The concept performs thus while remaining largely transparent, thereby enhancing daylighting conditions and maintaining outdoor views for building occupants. The façade technology is termed the Integrated Concentrating Solar Façade, or ICSF, and is a specific example of a broader class of building-integrated combined concentrating PV and thermal collection (BICPV/T) technologies. To gain traction as a successful technology, ICSF is envisioned to function within a larger,

---

<sup>15</sup> Perez-Lombard, L., Ortiz, J., & Pout, C. (2008). A review on buildings energy consumption information. *Energy and Buildings*, 40.

revised strategy of building design where mechanical systems are arrayed around the floor plate perimeter, proximate to their energy source (the façade), rather than be clustered in centralized locations (the logical placement when all energy is supplied via connection to power grids). As a specific example of the broader climate-interactive paradigm, ICSF and the distributed systems strategy are evaluated not only as a method for efficient solar collection, but as a successful, integral element of the built environment.

Table 1. Building Energy Use Intensity (EUI): DoE baselines relative to buildings with active façade systems. Comparative analysis of energy and cost benefits of active façade systems, parameterized by building type and climate, showing both reductions in baseline energy use due to ICSF and energy generated by ICSF.

BUILDING ENERGY USE/GENERATION AND YEARLY BUDGET COMPARISON, WITH/WITHOUT INTELLIGENT FACADE SYSTEMS

		Energy Consumption			Cost-Profit projection		
		Baseline (ASHRAE)	With Active Envelope Systems			Baseline (ASHRAE)	With Active Envelope Systems
Building Type	Climate	Energy Use Intensity (kWh/m <sup>2</sup> -yr) ↓	Energy Use Intensity with ICSF (kWh/m <sup>2</sup> -yr) ↓	ICSF Generation (kWh/m <sup>2</sup> -yr) ↑	Net Energy Use Intensity (kWh/m <sup>2</sup> -yr) ↓↑	Yearly Consumption Budget (\$/yr) ↓	Yearly Consumption/Profit Budget (\$/yr) ↓↑
Small Office	NYC	-125	-106	209	103	\$ -59,000	\$ -150
	Phoenix	-147	-104	339	235	\$ -27,000	\$ 5,900
	Mountain View	-99	-93	280	187	\$ -25,000	\$ 8,800
Medium Office	NYC	-139	-128	81	-47	\$ -170,000	\$ -52,000
	Phoenix	-150	-127	130	3	\$ -102,000	\$ -3,800
	Mountain View	-106	-103	109	6	\$ -88,000	\$ 200
Large Office	NYC	-143	-125	31	-94	\$ -1,226,000	\$ -790,000
	Phoenix	-133	-110	46	-64	\$ -395,000	\$ -175,000
	Mountain View	-137	-125	39	-86	\$ -850,000	\$ -525,000

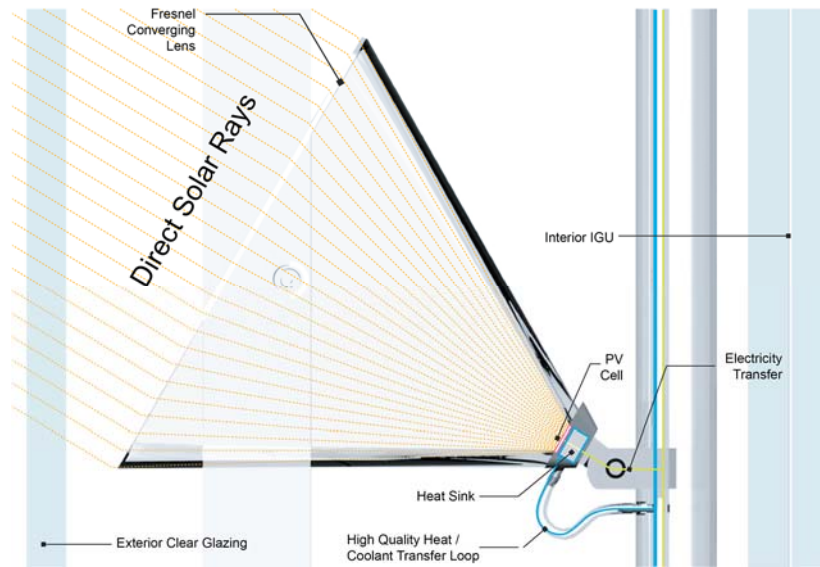


Figure 12. Section view of ICSF module showing concentration and components.

### ENERGY FLOWS THROUGH IC SOLAR FACADE

Solar radiation enters the cavity and is concentrated onto the PV cell where it is transformed into electricity and thermal energy.

Cold water is supplied for optimal energy transfer.

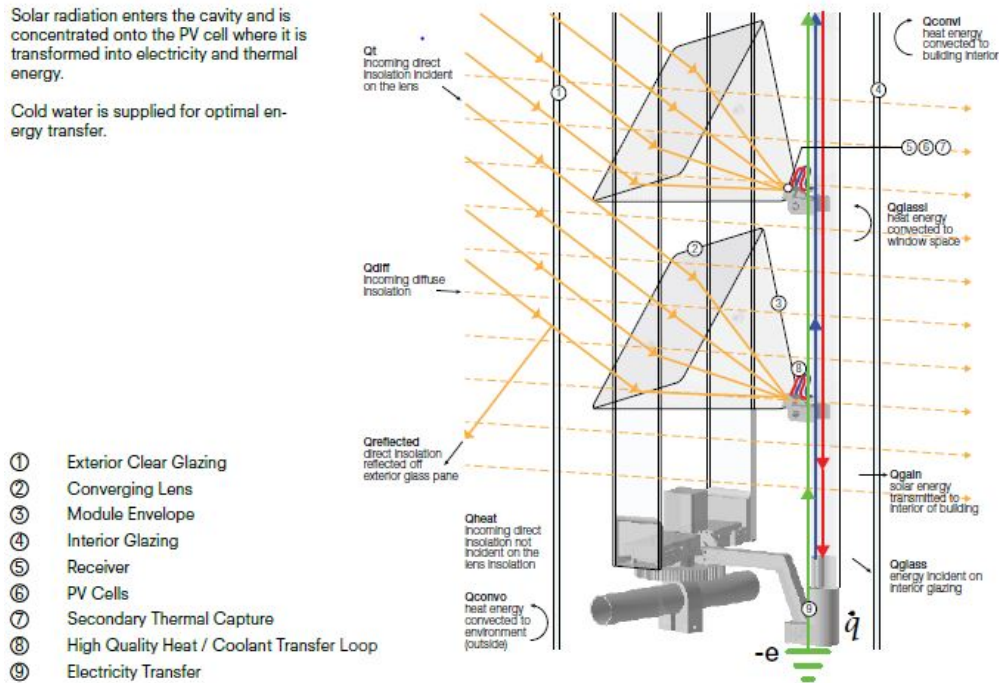
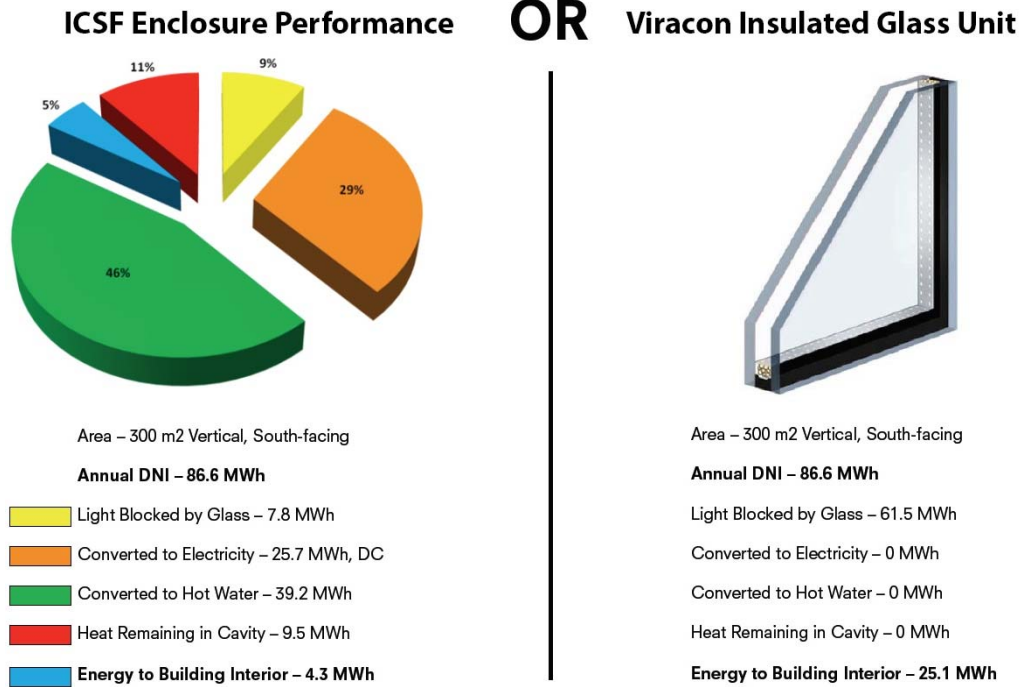


Figure 13. Energy Flow at the Modular Scale through ICSF.



**82.9% Decrease in Solar Heat Gain compared to Viracon IGU-** (VE 15-40, 1/4"-1/2"-1/4", SHGC 0.29.)

Figure 14. Comparison of benefits between ICSF and baseline low-SHGC IGU

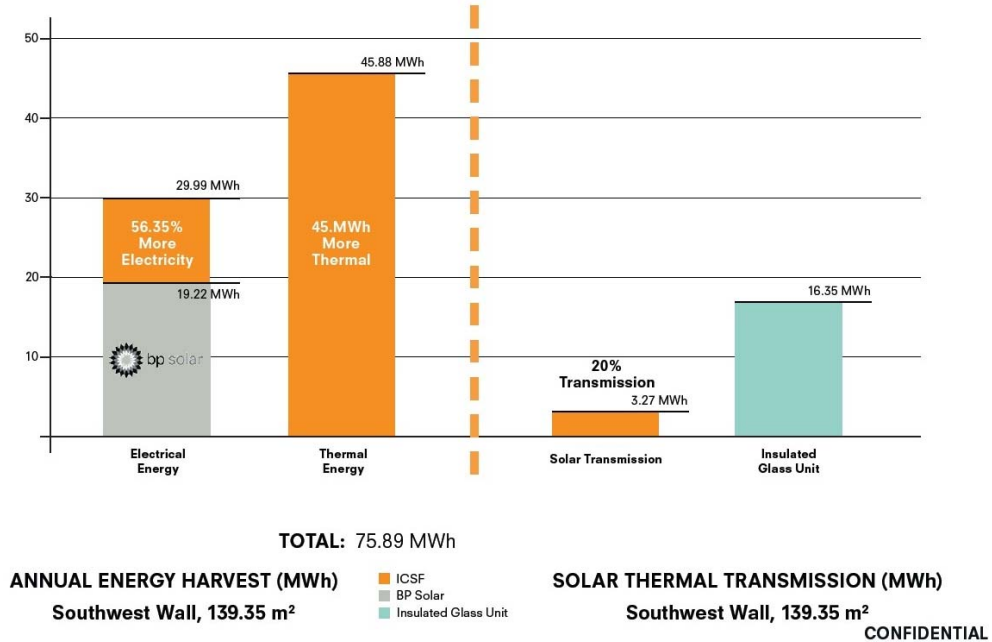


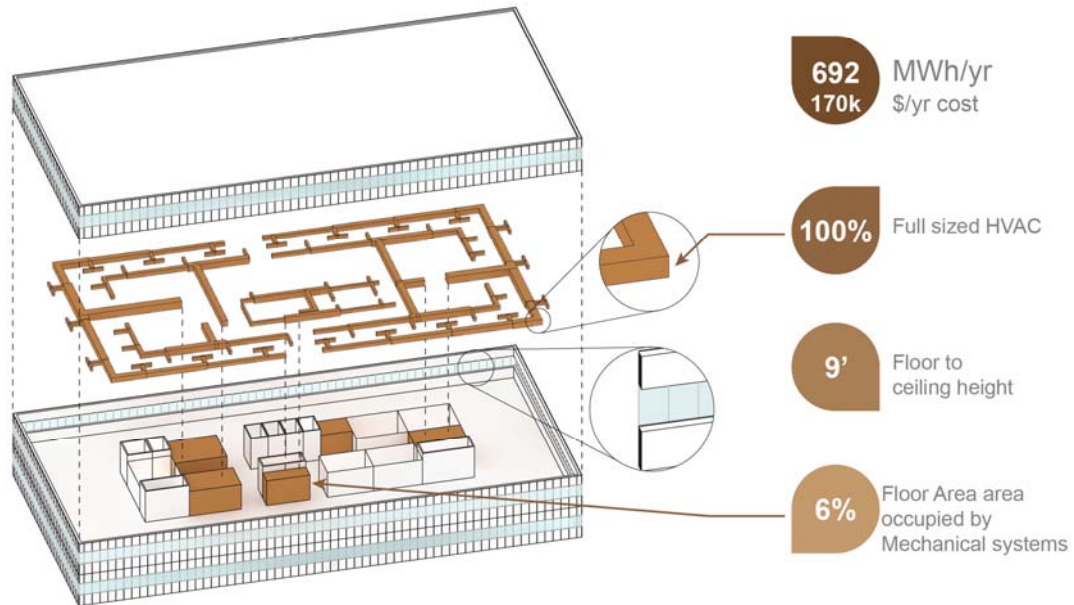
Figure 15. Sample case study from 2010 of an undisclosed commercial building in UAE  
Courtesy of SHoP Architects - ICSF installed on southwest façade with synergistic energy benefits (CPV/T) vs BP's Solar PV cells. Additional benefits are shown from decreased thermal transmission into occupied spaces vs. typical IGUs.

Table 2. Key physical parameters of active façade energy collection and application strategy.

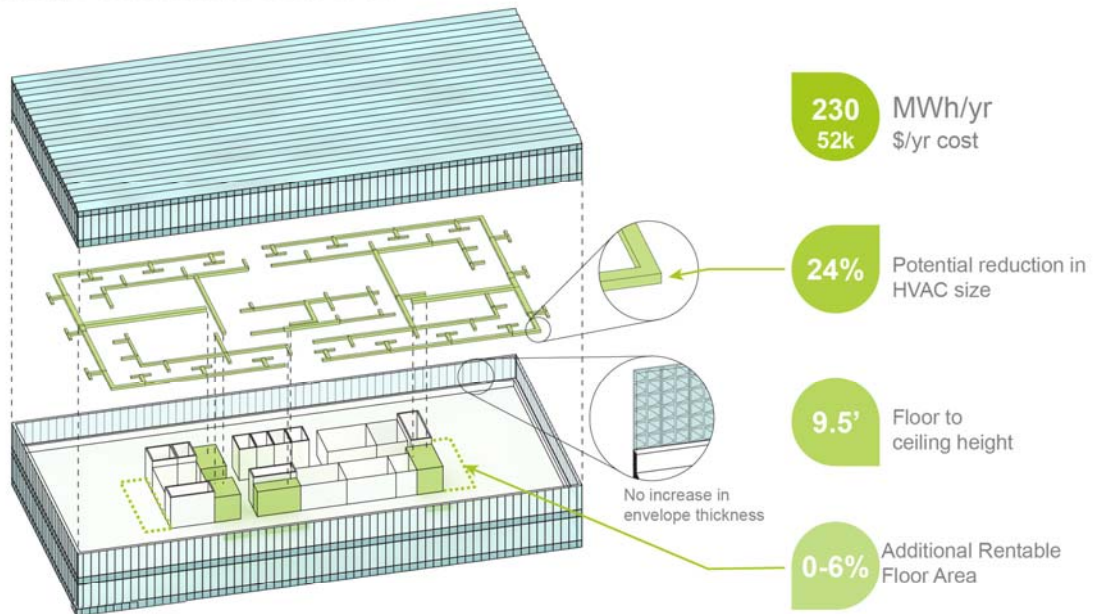
<b>Parameter</b>	<b>Description</b>	<b>Metric</b>
Photovoltaic Conversion Efficiency	Ability of PV technology to convert solar energy to electricity	%
Thermal Conversion Efficiency	Ability of façade technology to convert solar energy to thermal energy	%
Thermal Transport Efficiency	Ability to transfer collected thermal energy to point of application (work extraction)	%
Thermal Quality Maintenance	Ability to maintain temperature (quality) of collected thermal energy over required distance or time	W/K, $\tau$
Building Energy Supply Fraction	Fraction of energy supply that a building requires that can be climatically sourced (via active envelope)	%
Net Energy Production	Electrical and thermal power generation of active envelope, less power consumed	kWh/yr, kWh/m <sup>2</sup> -yr
Energy Opportunity Cost	Expenditures for powering building relative to benchmark alternative	Present Value (\$)

SPACE ALLOCATION AND ENERGY BENEFITS FOR CONVENTIONAL MEDIUM SIZE OFFICE IN NEW YORK CITY CLIMATE WITH AND WITHOUT ICSF

- Baseline Building Performance



- Building Performance With ICSF



Solar Energy: Direct+Diffuse Insolation on south, east, west, and inclined roof exposures of reference building, from TMY3 data. Building: CBECS Medium Office Building Reference (3 story, 5000m<sup>2</sup>/54,000sf, ASHRAE 90.1 - 2007 standards). Active Envelope Systems include PV and thermal effects of HeliOptix Integrated Concentrating Solar Façade. Building energy use simulated in Energy Plus. Envelope systems output simulated with HeliOptix alpha tool. Simulation cross referencing by CASE (48% Thermal transport efficiency, 0.6 Sorption COP). Electricity costs estimated at \$0.15/kWh. Preliminary HVAC calculation based on Based on: Grondzik, Walter T., Alison G. Kwok, Benjamin Stein, and John S. Reynolds. Mechanical and electrical equipment for buildings. John Wiley & Sons, 2011.

Figure 16. Summary of spatial and energy benefits of intelligent envelope (ICSF) strategies.

Data shown for: 3-story, 50,000sf office building in Mid-Atlantic coastal climate.

## Assessment Criteria for Integrating Intelligent Facades into High-Performance Green Buildings

### *Health, Productivity, Vitality*

The overriding mandate for a building project is to provide an environment that supports the health, productivity, and vitality of its inhabitants and stakeholders in a conscientious manner with environmentally benign energy resources. To create circumstances in which people thrive a variety of criteria must be met, as shown in Figure 17. A successful façade strategy addresses this full range of criteria.

### *Building Façade as Layered Performance Criteria*

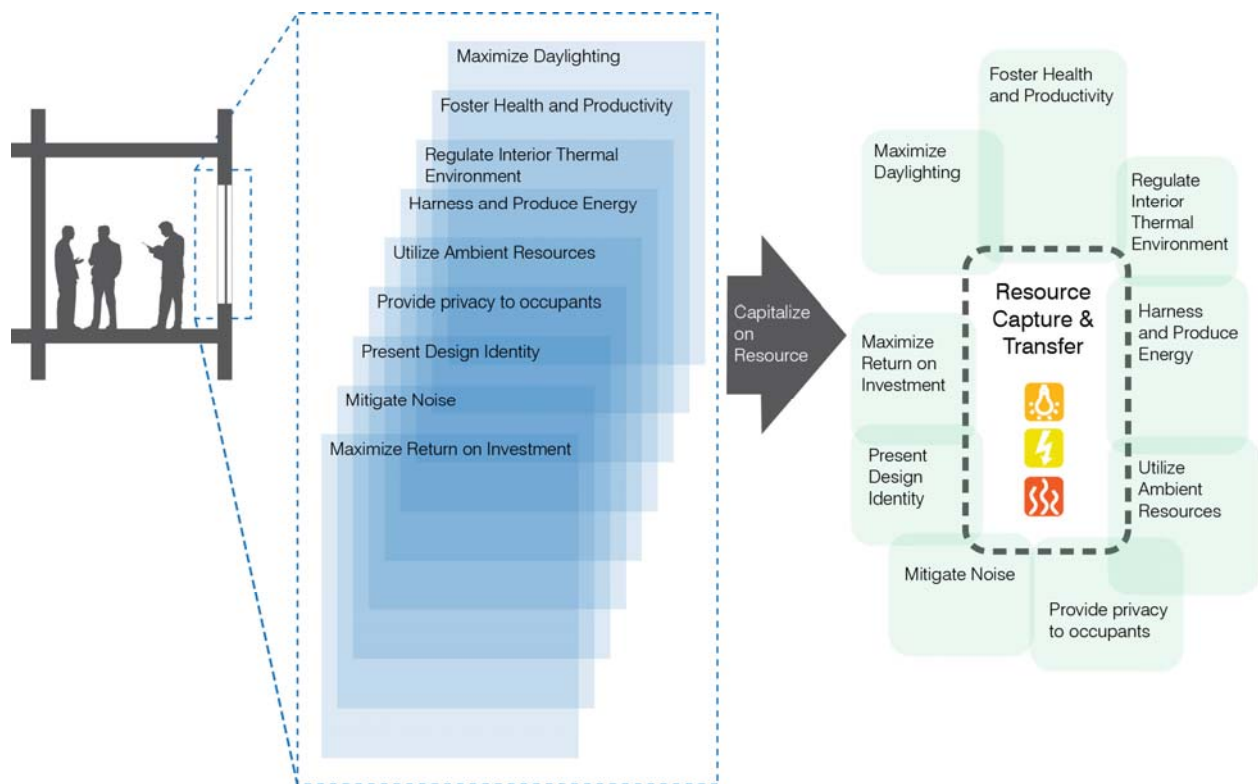


Figure 17. Performance criteria for building envelopes and intelligent facade systems.

Table 3. Performance criteria and metrics for evaluating intelligent active façade strategies.

<b>Performance Criteria</b>	<b>Description</b>	<b>Metric</b>
Maximize Daylighting	use of diffuse daylight to reduce lighting load and increase visual comfort	Present value (\$)
Foster Health and Productivity	healthier heat distribution, ventilation, material selection, etc. increases occupant productivity	fraction, lux
Regulate Interior Thermal Environment	control of thermal gradients and temperature swings to maximize thermal comfort	DGP
Harness and Produce Energy	electrical and thermal power generation at the building façade	Present value (\$)
Utilize Ambient Resources	transformation of ambient energy flows from loads to resources	Present value (\$)
Provide Privacy to Occupants	lensing filters both solar rays and views	kWh/yr, kWh/m <sup>2</sup> -yr
Present Design Identity	contribution of technology to architectural design character and building aesthetic	kWh/yr, kWh/m <sup>2</sup> -yr
Mitigate Noise	intermediate layer in IGU provides increased sound absorption	Subjective
Maximize Return on Investment	creating of short and long term dividends	LCA matrix

### ***Managing Energy Flows of Varying Qualities***

To maximize the effects of manipulating bioclimatic energy flows, one must apply the fact that all energy is not equally useful. The built environment demands energy at a range of qualities: from the full-spectrum radiation of daylight for illumination, down through the ordered, cyclical electromagnetic flow of alternating current, to the minimal enthalpy changes of heating or cooling a conditioned space to maintain thermal comfort. With current building systems, nearly all forms of work are accomplished by transforming delivered electricity. This reliance wastes potential, as relatively little of the work done in the built environment requires the high potential of grid mains electrical supplies. Rather than this singular focus on grid electricity, a new paradigm can be

imagined where energy that available from the natural environment (in a given form and at a given potential) can be applied directly to demands of the built environment, with minimal transformations. The rubric for this concept is embodied in Figure 18.

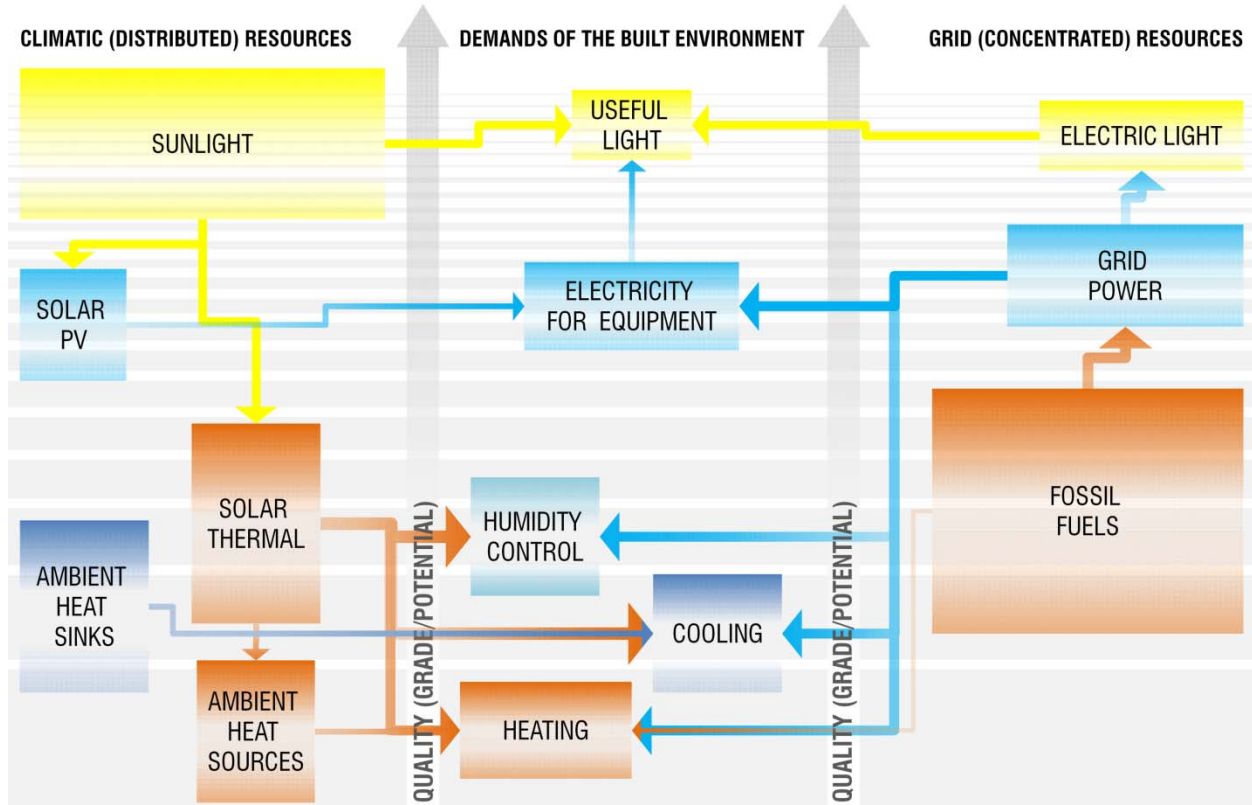


Figure 18. Conceptual ranking of energy sources and demands of the built and natural environments. Satisfying demands for services at a given potential with energy sources at similar potentials avoids the inefficiency of boosting the quality of an energy source (such as when lighting with electricity) or the waste of exergy when addressing a low-potential demand with a high-potential energy flow (such as heating with electricity).

Therefore, a building-integrated system must treat an energy resource as dynamic on multiple levels. Using ICSF as an example, its systems must respond in geometry to track solar angles during the course of the day; in transparency to reduce glare to the interior while daylighting as much inhabited space as possible; in thermal flows to collect, redistribute, and dissipate waste heat produced through solar electric generation; and in envelope to encourage engaged views to the exterior and provide a unique visual identity to buildings that is both aesthetically pleasing and economically

viable. An integrated system must therefore be holistic, and will require the incorporation of electric, thermal, daylighting, and façade criteria allowing for an environmental responsiveness embedded within an envelope that collapses exterior and interior conditions to balance multiple criteria in a single integrative strategy.

### ***Energy storage***

Energy storage contributes to grid resiliency by off-setting peak demand, and end-use thermal storage demonstrates near-100% efficiency relative to electrical use.<sup>16</sup> and on-site generation is critical to achieving highest-grade NZEB(A) performance.<sup>17</sup>

Air conditioning drives peak power demands in certain climates, and this effect is spreading as urbanization and standards of living increase across warmer regions of the planet (including the United States).<sup>18</sup>

### ***Architecture and Industrial Design Awards***

In terms of design and prototyping progress, the system development has been recognized by many design awards, including prestigious design awards in Industrial Design (Spark, 2012), Architectural (Merit Award in the International AIA Curtain Wall Open Competition, 2010), Metropolis Next Generation Design Competition (2003), The Museum of Modern Art (MoMA) Young Architects Series (2001), and Chicago Athenaeum, Good Green Design Awards (2011).

---

<sup>16</sup> Denholm, P., Ela, E., Kirby, B., & Milligan, M. (2010). NREL. *The Role of energy storage with renewable electricity generation* (No. TP-6A2-47187).

<sup>17</sup> Crawley, D., Pless, S., & Torcellini, P. (2009). Getting to Net Zero. *ASHRAE Journal*, 51(9).

<sup>18</sup> Sebzali, M. J., & Rubini, P. A. (2007). The impact of using chilled water storage systems on the performance of air cooled chillers in Kuwait. *Energy and Buildings*, 39(8), 975–984.

## Academic and Industrial Collaborators

Potential impacts of Research Cluster:

Energy production, energy reduction, reduced carbon foot-print, on-site "Net Zero"

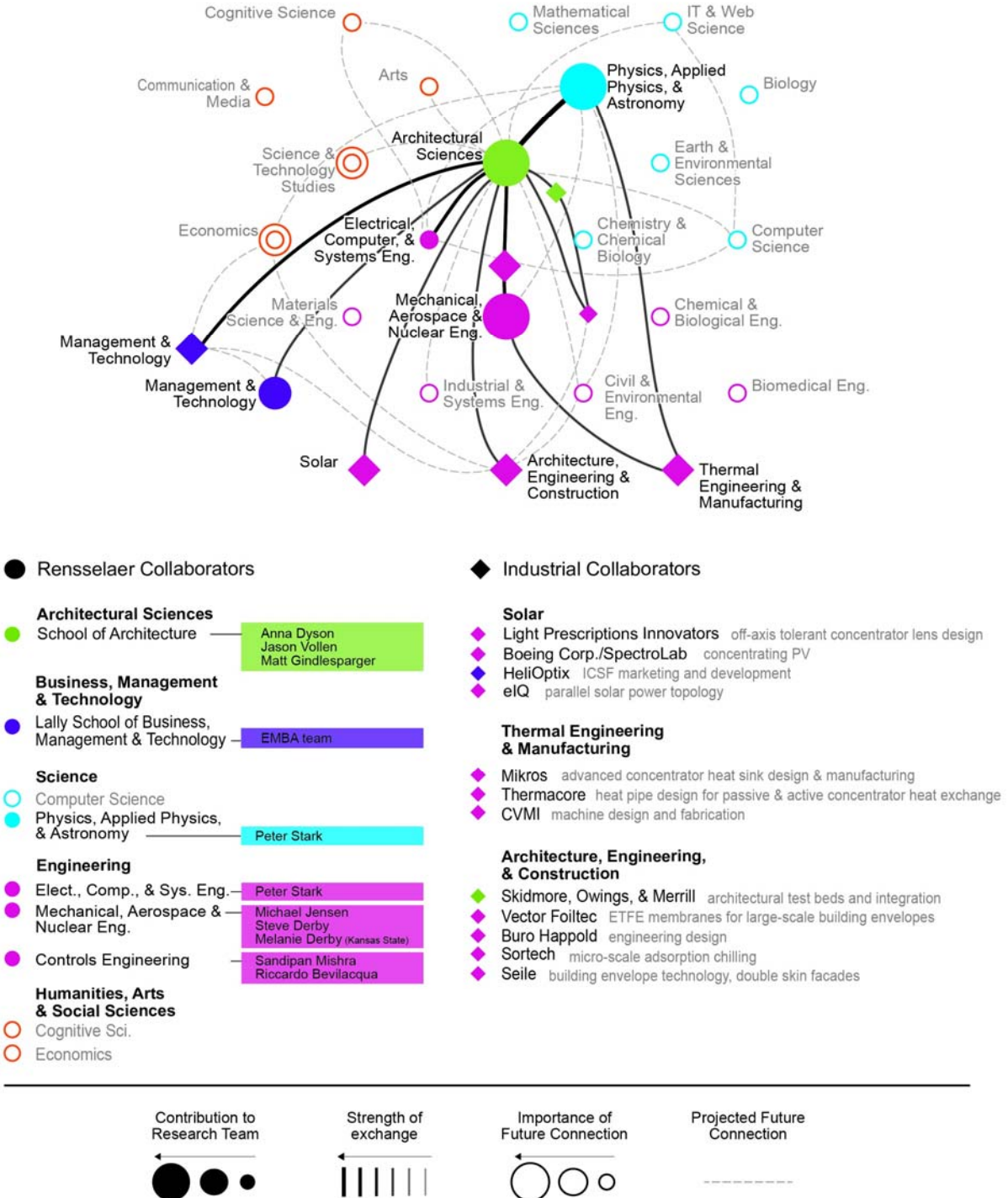


Figure 19. Ecosystem of collaborators and research partners in intelligent facades and distributed systems.

### ***Synergistic Intersection of CPV and Inhabited Built Environment***

Through integration into the building context, ICSF leverages the benefits of concentrator technology and diminishes the disadvantages. CPV is capable of the highest electrical efficiencies of PV technologies, while incorporating lower amounts of complex and expensive semiconductor materials and assemblies. Balance-of-system and maintenance costs tend to run higher, however, for the stiff physical structures that enable accurate tracking and cleaning schedules. Since a building is inherently structural, and façade cleaning schedules are standard in commercial building maintenance, the cost-benefit relationship for BI-CPV is fundamentally better than with stand-alone CPV. Although it is the case that buildings are constructed to looser dimensional tolerances than early-generation CPV might tolerate, advanced lens design (from our industrial partners), curtain wall installation techniques (from the building industry), and control strategies (developed internally) have combined to resolve this issue.

### ***Thermal Energy Storage replaces inherent latency of fuel-sourced power***

Mechanisms for thermal energy storage (TES) are a critical component of an overall intelligent façade strategy—and for BICPV/T strategies in particular—because these mechanisms make it possible to synchronize the availability of a resource with the demand for that resource. The modern-day power grid relies on the inherent latency of fuel-based power: when power is demanded, fuel is consumed; otherwise, it remains stable. Climatic energy sources, rather, are transient. A storage mechanism therefore contributes the dispatchable functionality that is missing from renewable resources.

In current practice, TES typically refers to the production of a reservoir of cooling capacity, either via ice generation, or simply chilled water. In this form, storage is an economically viable method of performing the work that a commercial building requires (cooling) during the times when electrical power is inexpensive (overnight). Successful installations have been done at building scales, campus scales, and district scales.<sup>19</sup> Although in the context of BICP/T the resource (solar energy) and the demand (cooling)

---

<sup>19</sup> MacCracken, M. (2010). Energy Storage: Providing for a Low-Carbon Future. *ASHRAE Journal*, 52(9), 28–35.

are often simultaneous, storage of cooling capacity is valuable if cooling is to be re-distributed throughout a building, or applied beyond the daytime hours (or into the next day, to address morning heat gain spikes).

Locating the space for cool TES is flexible. By locating the mass and equipment for TES at the façade, directly adjacent to the chiller and BICPV/T system, the resource of cooling capacity is close at hand to the spaces that require it. However, pumping a chilled working fluid from the chiller at the façade to in-board storage mass is effective too, because pumping chilled working fluid through pipes is relatively thermally efficient, and core zones of buildings demonstrate the most consistent cooling loads.

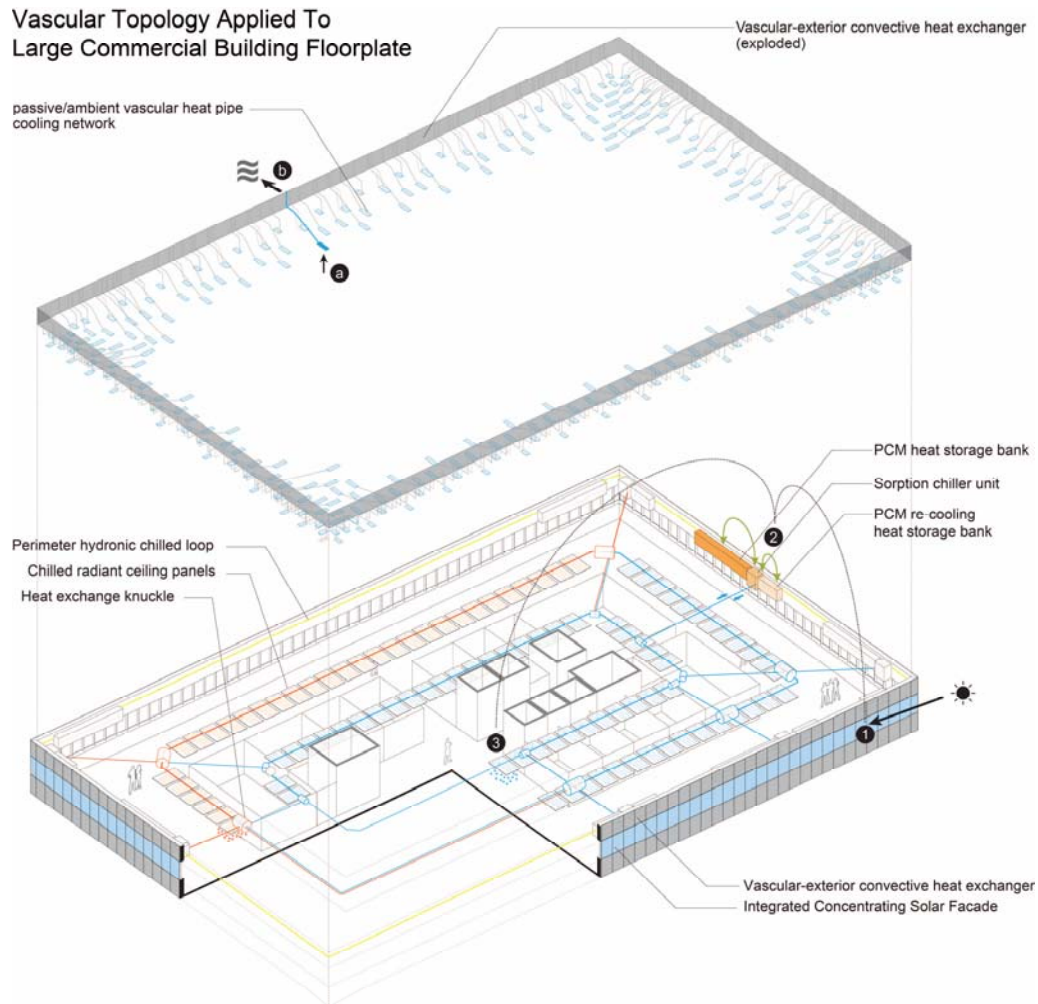


Figure 20. Vascular Thermal Retribution schematic across core-dominated building floorplate.

Regardless of the locations of coolth storage, the distribution of reserve cooling capacity throughout the building floor plate allows for smaller, multiple hydronic circuits to deliver cooling power when necessary. Multiple small pumps with lower head demands could be used to drive cooling circulation, in commonality with modern single-pipe distribution, which, as with TES, is a maturing technology in the building systems sector, and gaining visibility.<sup>20</sup> BICPV/T interfaces naturally with the realm of modern, maturing thermal regulation strategies for buildings, in part because of the advantages of TES.

<sup>20</sup> Cunniff, G., & Zerba, B. (2006). Single-Pipe Systems for Commercial Applications. *Heating/Piping/Air Conditioning Engineering : HPAC*, 78(10), 42–46.

In addition to the building of cooling capacity, thermal energy storage takes on expanded meanings when discussing BICPV/T, meanings which correlate to the three thermal flows involved in the thermodynamic chilling cycle: driving temperatures to power the cycle, chilled output, and re-cooling flow to collect the effluent heat. By providing thermal storage capacity at the discrete temperature ranges for each of these flows,<sup>21</sup> an unconstrained system is created where decisions can be made regarding the most efficient times to run different processes. This three-tiered approach carries through and informs equipment sizing and distribution, and provides a theoretical framework for the valuation of harvested thermal energy in the building context.

### ***Energy Benefits: Peak Demand and Total Use***

Two factors are important when evaluating the energy use profile of the built environment, total use and peak demand, and active façade technology has specific benefits for both factors. Total use is the equivalent of our drain on finite energy resources, and the attendant concerns (pollution, climatic instability) of this draining. Peak demand determines required grid capacity: an overburdened grid will fail, but sizing infrastructure to handle peak loads means it goes un-used during the majority fraction of time when demand is not highest. The energy generated and saved by deploying active façade strategies such as ICSF can drastically reduce a building's consumption, in some cases transforming the building into a net generator. In addition, because these strategies draw on the same force—the sun—that drives up cooling demand (and therefore peak demand), their benefits are maximal when demand is maximal.

### ***Leading by example: Zero-net-energy by 2030***

The US government has set a series of increasing performance goals for energy use in the built environment, and intelligent façades strategies provide a clear path towards meeting these goals. The Obama Administration's Executive Order 13514, "Federal Leadership in Environmental, Energy, and Economic Performance," mandates that 15% of federal agencies' existing buildings and all new construction of federal

---

<sup>21</sup> Three temperature ranges are roughly 0°C to 17°C, 30 to 55°C, and 50°C to 100°C (some overlap).

buildings must comply with the *Guiding Principles for Federal Leadership in High Performance and Sustainable Buildings* (Guiding Principles) by 2015. Incorporation of ICSF into new construction and retrofit projects meets the “Optimize Energy Performance” requirements outlined in the Guiding Principles. Additionally, in 2020 all new federal buildings that enter the planning process will be designed to achieve zero-net-energy by 2030. On-site zero-net-energy, which eliminates inefficiencies from energy distribution and transport, is an ever-greater challenge, towards which to strive through leading by example. Intelligent façade strategies such as ICSF are able to produce an energy surplus for a given year (as will be shown in greater detail), given a range of common building types and across a range of climates: Rather than net-zero-energy, buildings become power plants. ICSF could achieve this performance where previous solutions have struggled because it is a holistic and radical strategy for the manipulation of climatic energy flows. ICSF reduces demand loads to the interior spaces while collecting and distributing multiple forms of harvested energy through use of integrated systems. ICSF embodies the spirit of zero-net-energy mandates by creating clean, sustainable, and carbon neutral energy for the built environment.

### ***Leveraging Key Enabling Technologies***

Key enabling technologies from business collaborators such as eIQ, SorTech, and Spectrolab which are being leveraged by ICSF, are also simultaneously beneficial for the contributing partners. Furthermore, orchestration of these proven technologies will streamline production of ICSF from R&D, to future commercialization. It is incorrect to define ICSF as a conglomerate of off-the-shelf / commercially available components, rather it is a novel, integrated system whose development is allied with growing market trends that have been identified and vetted by our business collaborators. For example, SorTech, the leading manufacturer of adsorption (sorption) refrigeration for small and medium cooling units has recognized the growing business opportunity for heat driven cooling technologies at the residential scale. Centralized adsorption cooling systems at the large multi-family residential, and commercial scale are less popular than their vapor-compression (v-c) refrigeration counterpart, because they are less efficient and have low response times to fluctuating demand scenarios. Unlike v-c systems which

employ multiple compressors that can cycle “On/Off” to quickly meet cooling demands loads, larger adsorption units have long start up times, which translate to thermal discomfort for the occupied space until the cooling unit reaches operating conditions. A more appropriate strategy for large residential and commercial spaces that is not yet intended for SorTech products, but recognized by ICSF is distributed adsorption cooling. The start-up time decreases with unit size therefore, cooling demand response time is no longer a design issue with the smaller units. Additionally, adsorption cooling is more applicable for distributed cooling compared to v-c because there are no acoustic concerns. Typically, compressors are isolated from occupied spaces due to permissible sound levels set by municipalities. This holistic union ICSF and key enabling technologies is only further established by incorporation of eIQ’s maximum power point tracker (MPPT) for parallel solar PV arrays.

MPPT systems (such as eIQ’s vBoost) fluctuate the load resistance connected to the PV cells to determine the maximum power that can be produced for the given environmental conditions. This is beneficial for ICSF because the entire electrical collection efficiency for a link of cells in series would degrade if even one module were shaded. Because the solar resource is not uniform for all modules, and due to self-shading, MPPTs are integral components that isolate regions of modules which optimize performance output without hindering overall solar conversion efficiency.

### ***ETFE***

ETFE (Ethylene tetrafluoroethylene) is a commercially available architectural cladding / buildings envelope technology that consists of translucent pneumatic cushions typically framed in an aluminum structure. The cushions are pressurized with air, to provide stability from wind loads and to perform as a thermal barrier. Building skins that have incorporated ETFE include; the Eden Project (Cornwall, UK), Beijing National Aquatics Centre (Beijing, China) and the Experimental Media and Performing Arts Center at RPI (Troy, NY). One possible design for ICSF would be to insert an array of modules in the ETFE cushion, between the exterior and interior foils. This would provide as an adequate and long last barrier from weather elements, while allowing for diffuse light transmission; adding value to the space in the form of daylighting benefits.

### ***Identifying Stakeholders and Performance Criteria for Façade Retrofits***

In planning for the future, large stakeholders in the built environment, such as corporate headquarters, universities, hospitals, and government campus groups, must consider façade renewal. The cycles of ownership for such institutions, which consist of multitudes of buildings, usually exceeds 100 years. Managing and operating aging, existing buildings is typically a large part of a corporation's budget. Productivity cost factors alone indicate the special value of a façade retrofit which allows normal operations to continue or may actually enhance the normal operations. The increasing relevance of retrofit facades also re-affirms the need for planners and architects to understand the potential of improved utilization of energy production, daylight, thermal capture, and glare reduction, so these benefits may be integrated into plans for a building's renewal. With the wave of 1950s and 60s-era buildings in need of retrofit world-wide, large office buildings have an opportunity to be at the forefront of incorporating solar autonomy in façade renewal. Availability of ICSF to this retrofit market would act as a conduit for façade contractors, consultants, building engineers, and architects to consult each other at all stages of the design process. ICSF would contribute to how building owners, tenants, and maintenance personnel currently engage their buildings, packaging conservation, health, and comfort with long-term economic advantages. (See Appendix F for further analysis and a retrofit case study.)

### ***Reduction of Mechanical Equipment***

Many conventional HVAC systems comprise separate pieces of equipment which are referred to with the comprehensive term "air-handling units." For instance, the boiler generates hot water or steam for heating, and requires large amounts of fuel and air supplies. The fan room contains air-handling equipment, which supplies the boiler in large buildings. Sometimes individual fan rooms are located on each floor or in each zone, while chimneys exhaust gases from the burning fuel. On the other end, cooling towers extract heat from the water that has been used for cooling by blowing air over the water to create water vapor, and release the latent heat. Cooling towers are typically located on the roof and use a large quantity of outdoor air, creating an unpleasant microclimate, with fog in cold weather. The evaporation and exposure of water to the

outdoors in hot, humid conditions leads to scaling and corrosion in pipes. The growth of bacteria and algae in cooling towers has been linked to sick building syndrome, and thus vapor from cooling towers must be isolated from fresh air intakes, neighboring buildings, and parked cars. However, it is difficult to shield the noise and view of the cooling tower without a solid barrier that would limit access to air. Cooling towers are also noisy due to forced air motion, and require special acoustic isolation from the structural frame of the building.

Centralized HVAC systems distribute heating and cooling through distribution trees. Distribution trees take up a lot of space, both horizontally and vertically, and occupy, on average, 6% of the total occupiable floor area in high-rise construction<sup>22</sup>. They require coordination with lighting, ceiling design, and other interior design elements. Similar to the tree which the term references, these distribution networks have roots - the machines heating or cooling the air. The trunk of the tree is the main duct or pipe running vertically from the mechanical equipment to the zones served. The tree's branches are the many smaller ducts running horizontally, leading to individual spaces. Finally, the leaves are the point of interchange between the ducted heating or cooling and the space served. The point of interchange is typically a large, bulky fan-coil unit that dictates the depth of the drop ceiling.

---

<sup>22</sup> Grimm, Nils, HVAC Systems and Components Handbook, McGraw-Hill, New York 1998.

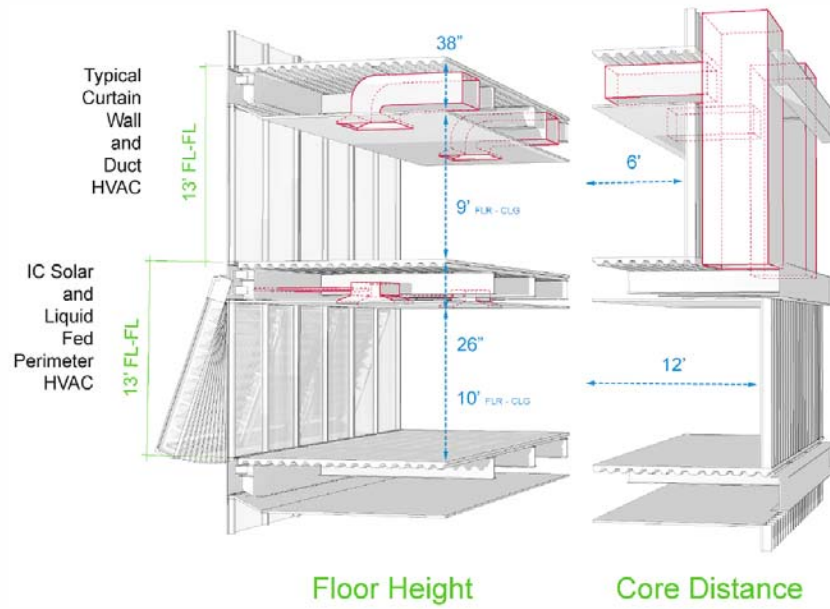


Figure 21: Perimeter HVAC Systems Reduction.

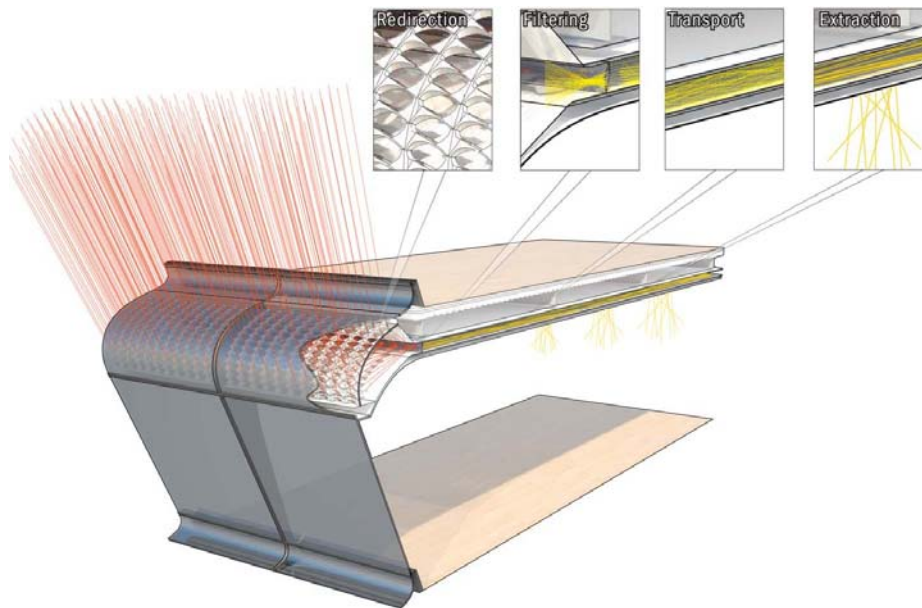


Figure 22: Angled Curtain Wall Façade Retrofit with clerestory window panel for solar collection and shading above, and clear vision glass below.

### ***Vertical HVAC Reduction and Real Estate Premium***

Decentralized air handling units (connected directly to facade panels) have the potential to reduce the peak thermal load offset for existing HVAC systems, resulting in smaller vertical air distribution trees. The vertical distribution tree is generally located on the perimeter of a building's core, outside of the structure, allowing for an easily accessible reduction in duct sizes, and the subsequent addition of usable floor area for rent or purchase. As an example of the possible extents of this seemingly minor change, a case-study office tower in Phoenix, Arizona, with a geometrically optimized south-facing IC Solar retrofit façade and panel-installed absorption coolers, has a 170ft x 170ft building footprint, of which 30% is assigned as core. Phoenix, with its intense direct solar climate, can provide all the hot water needed to supply absorption cooling through locally distributed floor plate networks from the facade panels. As a result, the existing vertical ductwork could be reduced, and the space refitted as rentable floor area. This would allow the building to regain 6% of its total floor area, or 44,640 square feet over 31 floors. With the average yearly Phoenix office rental rate of \$60 per square foot, this would work out to approximately \$2.2 million in additional income per year for the building owner, enough to pay for the install of an optimized IC Solar retrofit façade in 6 years.<sup>23</sup>

### ***Horizontal HVAC Reduction and Health***

If the case study office tower in Phoenix, Arizona is again used, and 100% of the hot water needed to maintain thermal comfort through locally distributed floor plate networks from the facade panels is provided, then the need for horizontal distributive ducts would also be eliminated. Because water is a much more efficient thermal medium than air, the pipes to distribute the water from the facade panels need only to be 1" in diameter, compared to air ducts which are a few feet in diameter. By eliminating these ducts, the drop ceiling can be raised increasing the floor to ceiling height. The increase in floor to ceiling height can be coordinated with the retrofit building integrated facade through the installation of taller glazing for increased day lighting. By moving the circulation system of the building out to the skin, and in re-thinking the process of

---

<sup>23</sup> ASHRAE Greenguide: The Design, Construction and Operation of Sustainable Buildings, 2006.

distribution locally, there emerge great possibilities to creating more flexible, healthier spaces for building occupants.

### ***Interface with DC/Micro grid***

Intelligent facades Momentum for building-scale DC power distribution is increasing due to reinforcing trends of:

- Increasing DC end-use
- Improving solid-state power handling technology
- Peak loading on traditional grid capacity and aging infrastructure
- Increasing viability of distributed generation methods<sup>24</sup>

### ***Concentrating Façade Precedents: Hydronic and BICPV/T***

As a study of precedents, hydronic façade systems have been successfully deployed for thermal regulation in high performance building designs. These systems, however, do not demonstrate energy harvesting capabilities. At Carnegie Mellon University, The Intelligent Workplace Laboratory (IW) incorporates a Gartner-designed façade<sup>25,26</sup> which flows water through mullions to perimeter building zones using existing heat and coolth resources such as district steam and, potentially, waste energy from other processes.<sup>27,28</sup> Heating is the primary thermal concern as the building is designed with an extended, thin floor plate. This building type does not exhibit the same cooling loads as deeper-floor plate commercial buildings, which have been identified as

---

<sup>24</sup> Collier, S. (2013). Self-sufficiency in electricity grid outages with DC microgrids. The Energy Collective.

<sup>25</sup> Josef Gartner & Co., Gundelfingen (September 28, 1968). German Patent Office: 1,784,864 – Integrated Façade System Gartner.

<sup>26</sup> Gartner, K. (1985). United States Patent: 4535833 - Vertical mullion having heat transfer medium flow passage.

<sup>27</sup> Hartkopf, V., Loftness, V., Mahdavi, A., Lee, S., & Shankavaram, J. (1997). An integrated approach to design and engineering of intelligent buildings--The Intelligent Workplace at Carnegie Mellon University. *Automation in Construction*, 6(5-6), 401-415.

<sup>28</sup> Gong, X., & Claridge, D. E. (2007). Impact of the Position of the Radiators on Energy Consumption and Thermal Comfort in a Mixed Radiant and Convective Heating System. *ASHRAE Transactions*, 5(113).

the initial target for active façade research. However, the IW full-scale experiment still demonstrates the viability of re-distributing heat locally<sup>29</sup> (bypassing centralized systems) with hydronic circulation between interior heat exchangers, which is a tenet of this research.



Figure 23. Glazing mullions channel water for heating, cooling, and moisture control at EMPAC at Rensselaer. (Images: Brandon Andow, 2011)

Hydronic facades have had successes in curtain wall architecture, although their potential for redistributing heat between interior and exterior zones has not been explored.

The piped-mullion façade system designed by Gartner has been used in other projects as well, such as the Curtis Priem Experimental Media Performing Arts Center (EMPAC) at Rensselaer Polytechnic Institute.<sup>30</sup> The building's curtain wall temperature is maintained by heated water that flows in the mullions, thereby regulating indoor temperatures as well as preventing dew formation on the glass envelope.

Similar BICPV strategies have been investigated in prior research, at the University of Patras, Greece, and University of Lleida, Spain, with positive indications for energy generation, cooling load reduction, and life cycle analysis relative to non-concentrating

---

<sup>29</sup> Interview, Vivian Loftness, February 13, 2013.

<sup>30</sup> Design by Grimshaw and Partners, with Davis Brody Bond and Aedas.

BI systems.<sup>31,32,33</sup> The transparency benefit is noted, but research to date has yet to address the full gamut of architectural performance criteria required for a successful implementation nor the potential for revising building systems topology around façade energy generation.

### ***Precedents of heat pipes in the built environment***

Heat pipes are being investigated at multiple scales and applications as an enabling technology for BICPV/T and distributed cooling strategies. Heat pipes are chambers (typically elongated, hence “pipes”) that contain a working fluid in liquid-gas equilibrium and stay relatively isothermal when exposed to disparate temperatures, experiencing thermal flow in the form of vapor transport (and liquid re-circulation) along their length. Due to the simplicity, effectiveness, versatility and robustness of the heat pipe principle and construction, they are used in a variety of applications, and across a range of scales. Certain solar thermal systems (evacuated tubes, for example) leverage heat pipe principles, and they have been investigated actively in solar and BI-solar applications, for example towards improving the conductivity of passive heat sinks for CPV.<sup>34,35</sup> In the building systems industry, heat pipe solutions are commercially available for upgrading the efficiency of HVAC systems.<sup>36,37</sup>

---

<sup>31</sup> Tripanagnostopoulos, Y., Siabekou, C., & Tonui, J. K. (2007). The Fresnel lens concept for solar control of buildings. *Solar Energy*, 81(5), 661–675.

<sup>32</sup> Menoufi, K., Chemisana, D., & Rosell, J. I. (2013). Life Cycle Assessment of a Building Integrated Concentrated Photovoltaic scheme. *Applied Energy*, 111, 505–514.

<sup>33</sup> Chemisana, D. (2011). Building Integrated Concentrating Photovoltaics: A review. *Renewable and Sustainable Energy Reviews*, 15(1), 603–611.

<sup>34</sup> Du, D., Darkwa, J., & Kokogiannakis, G. (2013). Thermal management systems for Photovoltaics (PV) installations: A critical review. *Solar Energy*, 97, 238–254

<sup>35</sup> Anderson, W., Tamanna, S., Sarraf, D. B., Dussinger, P. M., & Hoffman, R. W. (2008). Heat Pipe Cooling of Concentrating Photovoltaic Systems (pp. 1–6). Presented at the Photovoltaic Specialists Conference. 33rd IEEE, San Diego, CA: IEEE.

<sup>36</sup> Jouhara, H. (2009). Economic assessment of the benefits of wraparound heat pipes in ventilation processes for hot and humid climates. *International Journal of Low-Carbon Technologies*, 4(1).

<sup>37</sup> Heat Pipe Technology. Retrieved April 25, 2012, from [www.heatpipe.com](http://www.heatpipe.com).

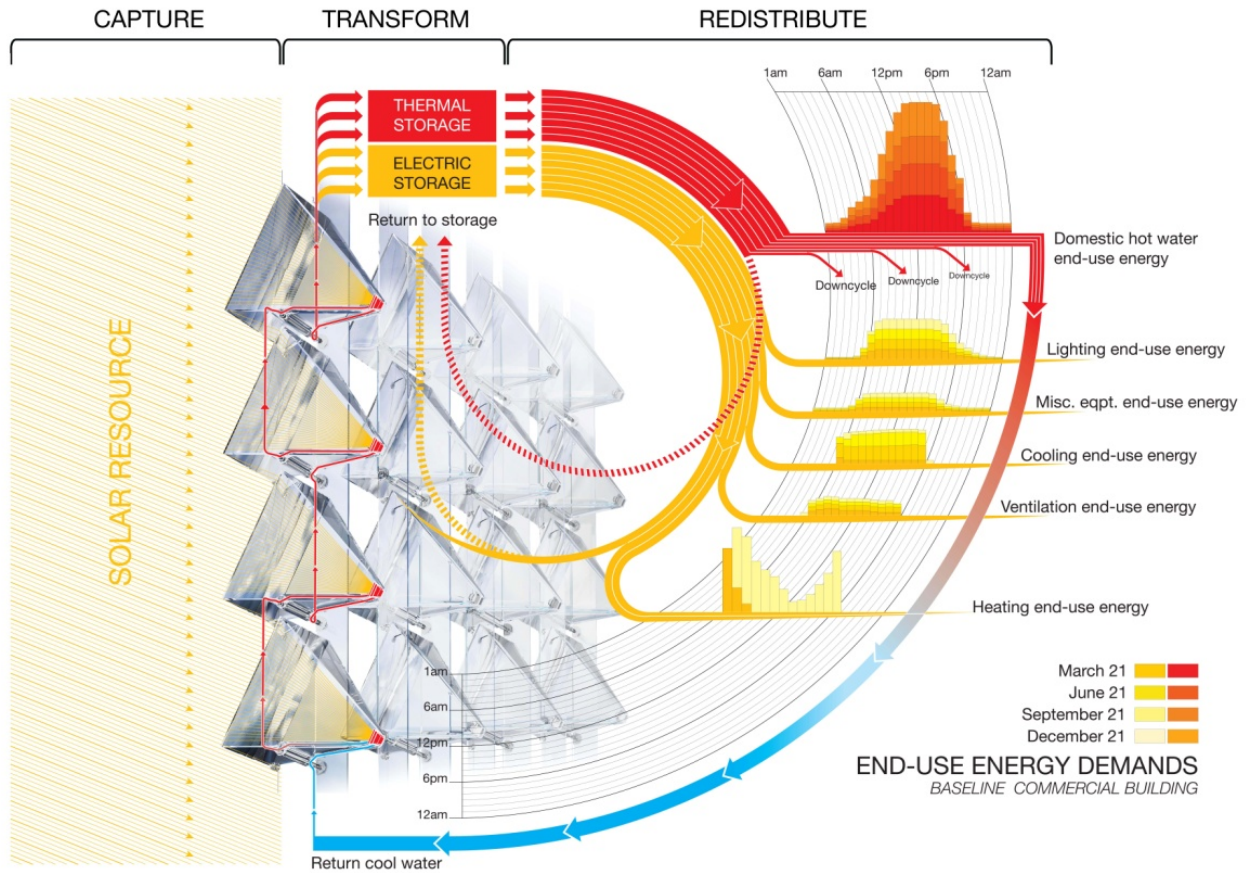


Figure 24. Synthetic Energy Flow Diagram for the capture, transformation, and redistribution of solar energy into electrical and thermal power at the façade.

Heat transfer fluid is circulated through ICSF to raise the temperature and exergy content, and then circulated to processes that consume the thermal exergy flow.

## Gallery: Prototypes and Experiments

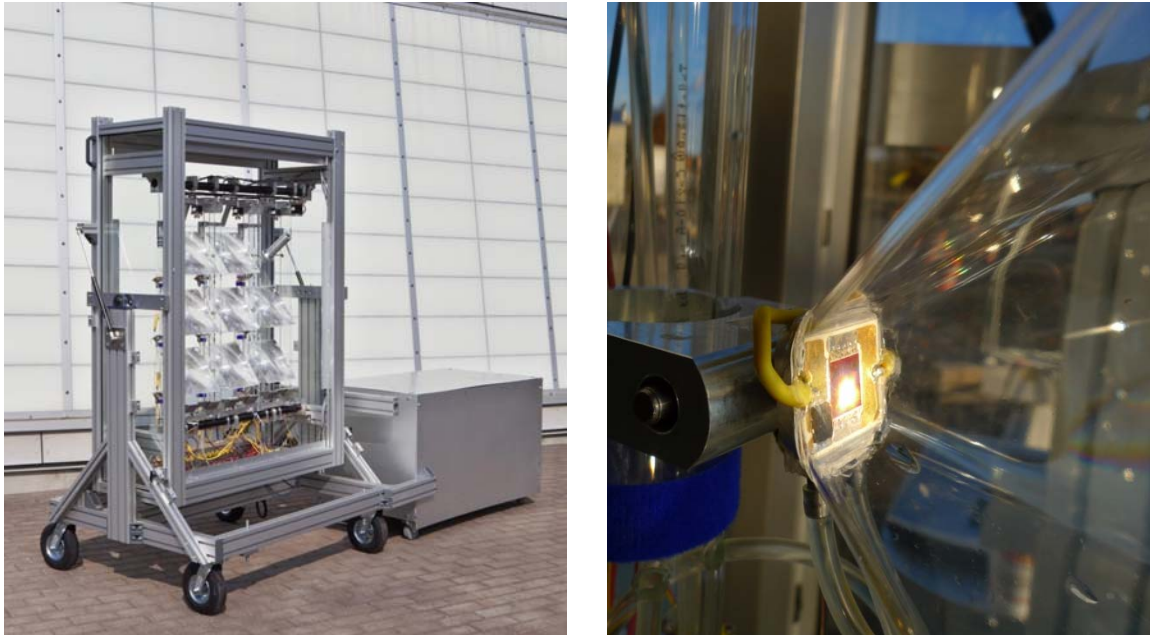


Figure 25. ICSF Generation 6 Heat & Power prototype. (Syracuse, NY, 2010-2012).

Portable and instrumented nine-position prototype used to develop tracking and control systems, cooling methods, and mechanical updates to module and tracker towers. Precursor optical design was efficient but overly sensitive to tracking error.



Figure 26. ICSF Modified Generation 6 Prototype.

On display at the AIA Integrate / Innovate Exhibition in New York City, October 6<sup>th</sup> 2010 to January 25<sup>th</sup> 2011.

The ICSF system won the Merit Prize in the International Curtain Wall Competition.

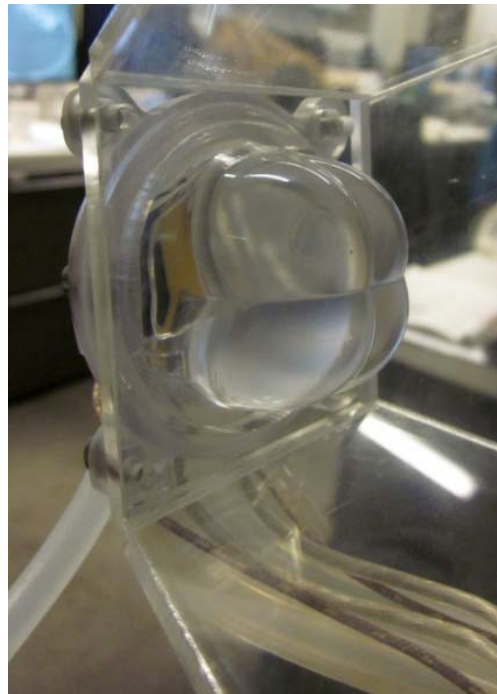
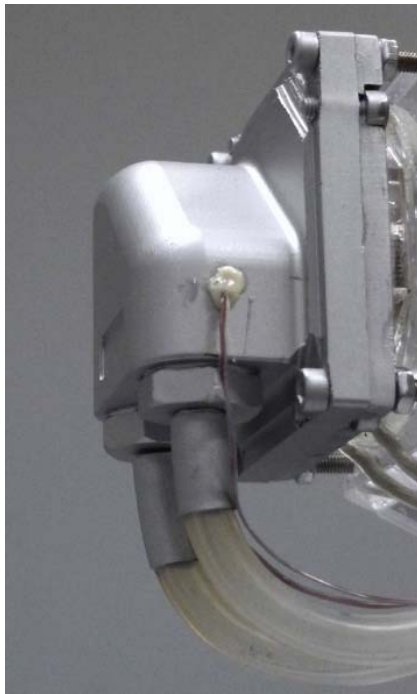
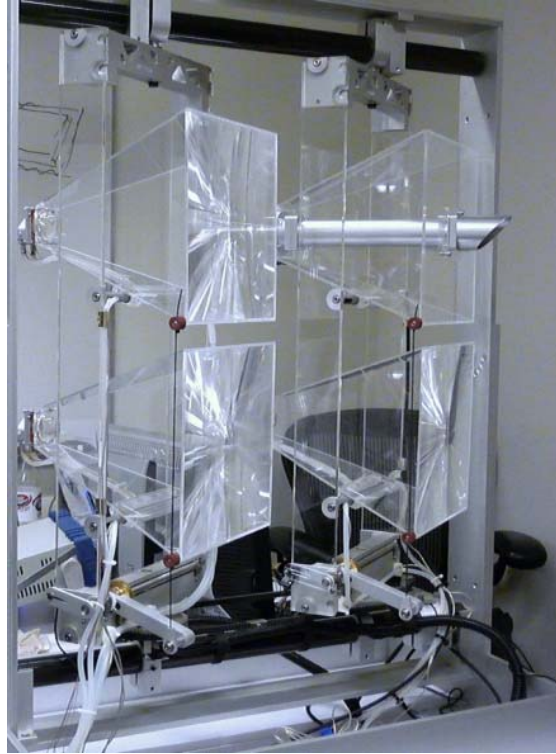


Figure 27. ICSF Generation 7 prototype, deployed at CASE studio, Manhattan, NY. Improvements include an optimized optical design, and simplified mechanical design for manufacture, assembly, and operational robustness. Coolant-fed heat sink revised. The Fresnel-Kohler primary and secondary optics provide uniform flux on the CPV cell while easing the tracking accuracy requirements.

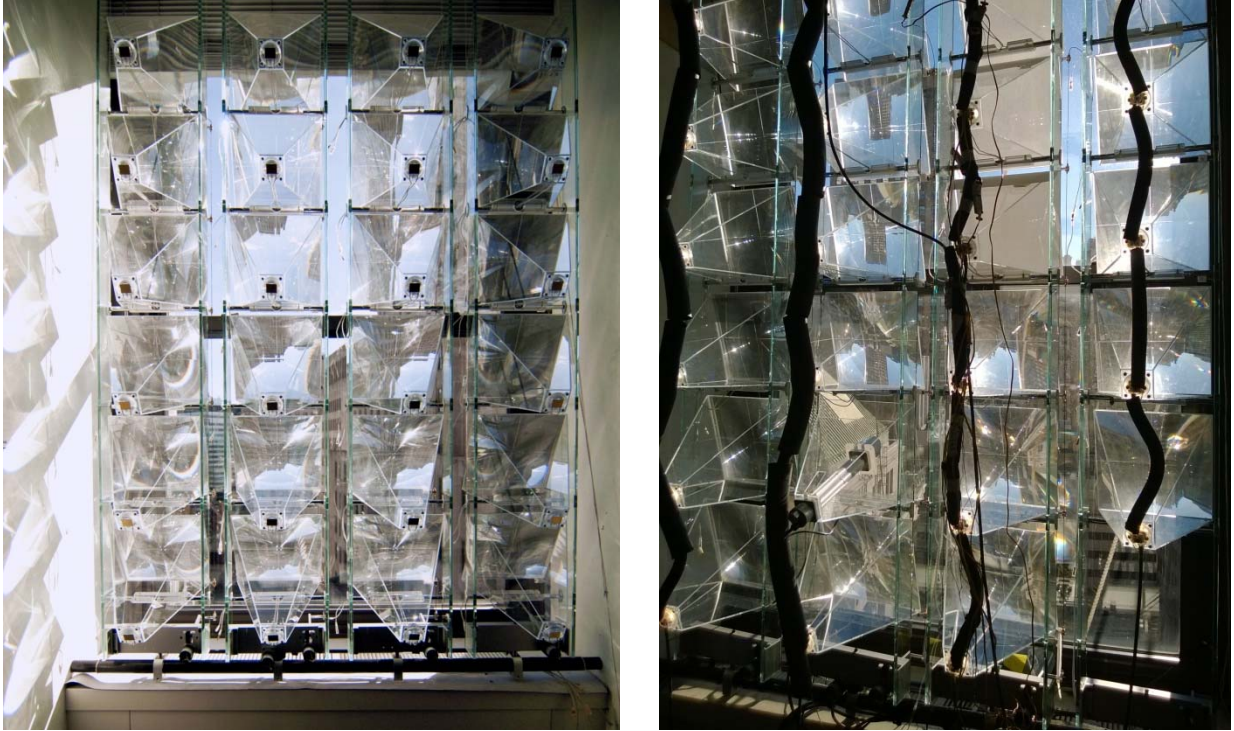


Figure 28. Improvements from Generation 7 to Generation 8 prototype. Improvements include over 50% reduction in parts count, return to low-cost servo tracking actuation and low-profile heat sink design, configurable for multiple thermal transport methods.

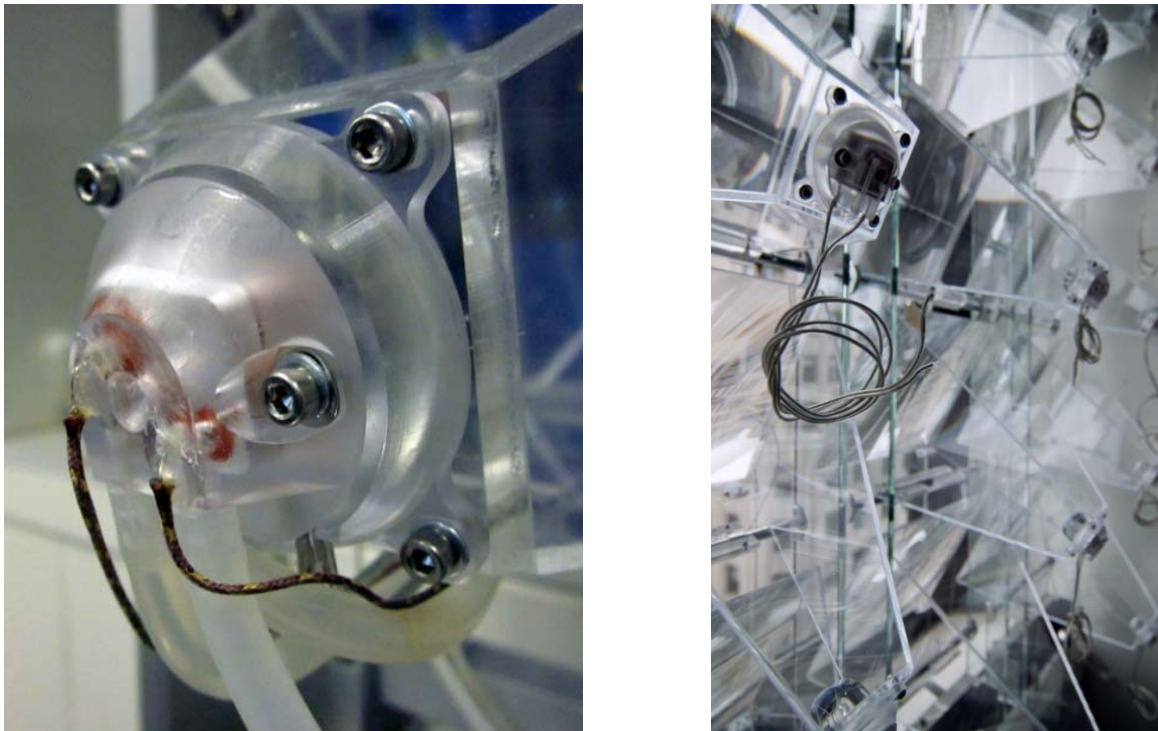


Figure 29. Generation 8 water block heat sink, customized to ICSF.

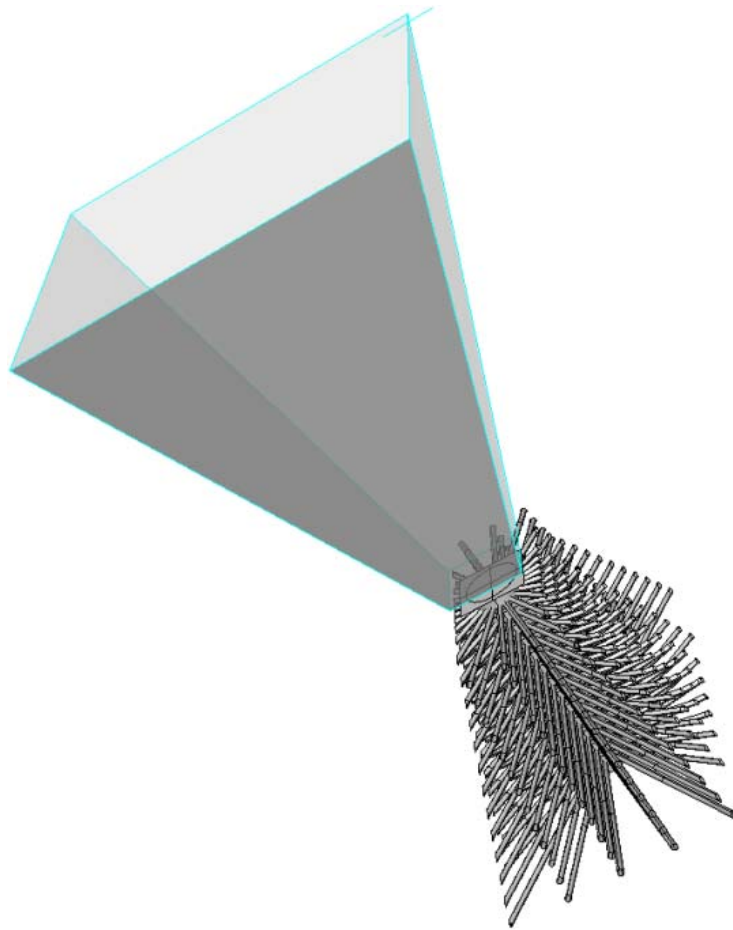


Figure 30. Passive heat sink design alternative for ICSF installation with fan assisted air cooling. Passive (air-cooled) design proposed for the Sheik Khalifa Medical Center Atrium, projected to be Installed in 2016. Top: design study. Bottom: Prototype heat sink for testing air cooled modules for incorporation into ETFE pneumatic panels.

## Project Objectives

### ***Strategy for Utilization of Climate Resources via Intelligent Façade Technology***

To maximize the usefulness of climate resources, a tiered approach is followed where a climatic resource is applied to a building demand in, as nearly as possible, its original form and quality (refer to conceptual ranking in Figure 18).

The highest priority is in modulating the use of sunlight for interior lighting. Although this may seem intuitive, sunlight is often blocked out of office spaces with blinds, in favor of overhead electrical lighting, because the positioning of windows creates glare issues (especially with computer-based work). In terms of light quality, however, full-spectrum sunlight is preferred over most electrical sources. Electrical light is inefficient, as well: even modern light-emitting diodes (LEDs) convert electricity to visible light at a rate of only 15 to 25%,<sup>39</sup> while the rest of the energy dissipates as heat gain, which is typically undesired. Attendant to daylighting is the potential for views to the exterior, which are a fundamental intention of including windows in a building design.

The second priority is to address direct-normal insolation (DNI), a highly-ordered climatic energy flow. Current mass-market terrestrial concentrating photovoltaic modules convert DNI to electricity at peak efficiency of 35.9%<sup>40</sup> and an installation collecting energy at this rate, even when heavily discounted for operating losses, would still generate roughly double the average energy use of commercial building stock in the United States on a per-area basis.<sup>41,42</sup> Prioritizing DNI is equally valuable, though, because the energy is typically detrimental in the commercial built environment, driving up cooling loads and contributing to glare issues. The simultaneous reduction of cooling loads from insolation and electric lighting are essentially passive benefits, reducing a building's peak electrical demand before considering any generated energy.

---

<sup>39</sup> Thermal Management of White LEDs. (2007). US DOE.

<sup>40</sup> Amonix Achieves World Record 35.9% Module Efficiency Rating at NREL | [www.amonix.com](http://www.amonix.com). (2013).

<sup>41</sup> CBECS. (2008). 2003 CBECS Detailed Tables: Summary.

<sup>42</sup> Ratio of 2X generation-to-consumption based on 260kWh/m<sup>2</sup>-yr building EUI, 850W/m<sup>2</sup> DNI, net CPV efficiency = 34%, 5 hours of collection.

Although the conversion efficiency of currently-available CPV is high, over half of the energy concentrated on the cell is dissipated as heat. Within the context of potential building applications, the value of this energy can be still quite high, since the elevated temperatures can be generated at the CCA, using solar power that would otherwise drive up cooling loads (if the irradiation could pass into the building or to heat the outer surface of the facade). Within the limits of current CPV technology, temperatures can be raised high enough to drive low-pressure organic Rankine cycles, generating still more electricity, or at even better efficiencies, the energy can be applied to active (sorption) chilling processes.<sup>43</sup> Driving temperatures of 65°C are nominally useful for current commercially-available chilling machinery operating at COPs of 0.5 to 0.6, so the thermal collection method of a near-term intelligent façade strategy should be geared towards providing energy of that quality.

Thermal energy is useful at temperatures below sorption-driving temperature as well, for controlling humidity in indoor air. Mitigating the latent moisture loads in outdoor air can account for most of the power in cooling systems in humid environments. Instead, mid-grade heat—between 50°C and 65°C—can be used to power desiccant regeneration strategies, displacing another major power demand in many climates. Thermal energy at all temperatures can be applied to interior heating loads, of course, and to pre-heating of domestic or process hot water supplies.

Cascading the applications of climate-sourced energy according to their potential is crucial for matching available resources to a building's demands, and the lack of this concise framework is a fundamental reason that efforts in building-integrated generation typically fall short. As an accompaniment to the conceptual ranking of energy potentials, a diagrammatic cascade of thermal-only energy and applications is shown in Figure 31.

---

<sup>43</sup> With future cell types that function at temperatures in excess of 150°C, (under development by collaborators at RPI) double-effect chillers could be driven with combined COPs in excess of 1.3.

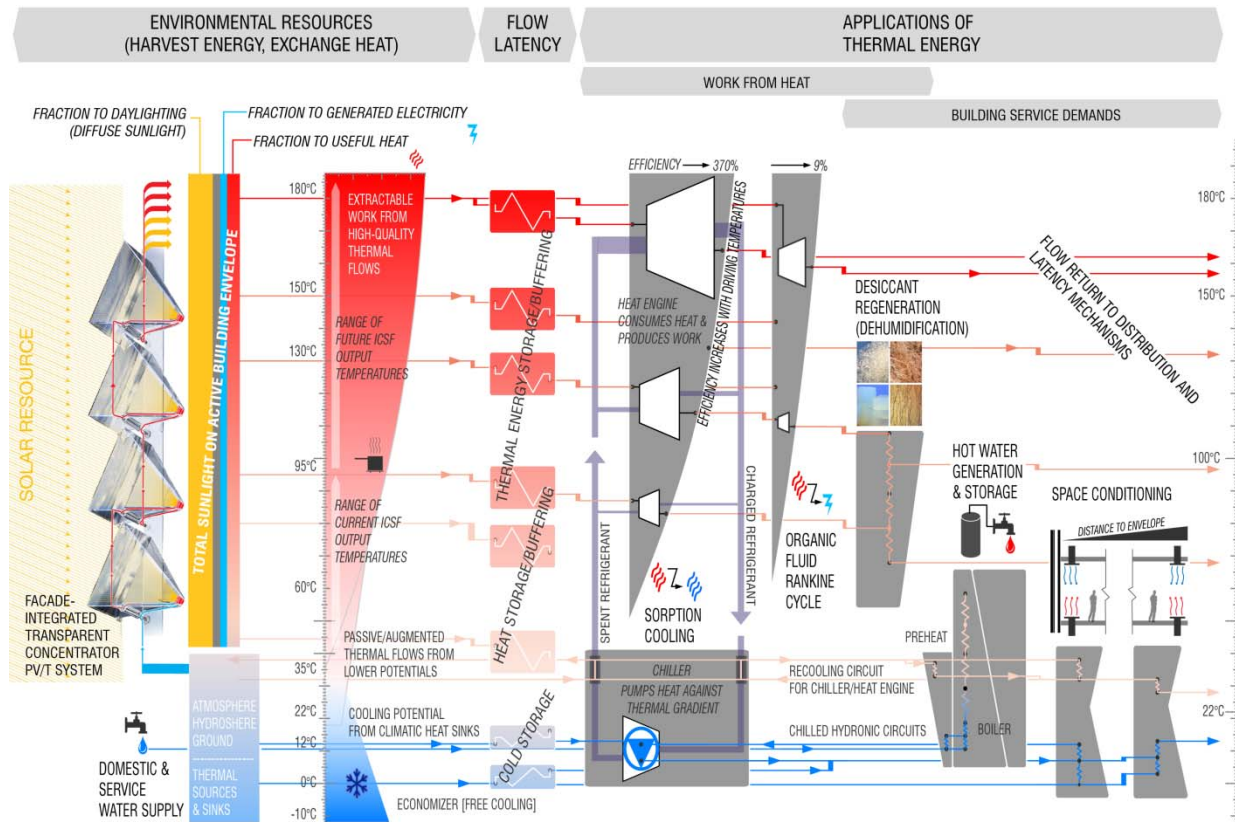


Figure 31. Thermal cascade network diagram: framework for solar energy capture and transfer for building systems applications through ranges of temperature.

Cascading a thermal flow from processes that require high temperatures to processes that require lower temperatures enables the most complete use of all availability (exergy) in the thermal flow.

### ***Building Energy Model Including Integrated Concentrating Solar Façade + Revised Systems***

By integrating with a robust and widely accepted building energy modeling (BEM) framework such as Energy Plus, the ICSF strategy can be more widely applied, not only in our own internal analyses, but by external collaborators and interested parties. In this phase of work the necessary interface points between our system simulator and a BEM engine have been identified, and a procedure has been developed for combining the two engines in post-processing. In the next phase, a module for active solar façade systems will be developed that can be accessed by the BEM engine on a time step basis, allowing us to more accurately observe system states, proscribe control procedures, and forecast results.

### ***Corroboration with Empirical/Prototype Demonstration***

Rensselaer developed and tested prototypical installations of three iterations of a next generation curtain wall unit that directly transfers heat and power captured from a building-integrated concentrating photovoltaic (CPV) system(s) into integrated systems for heating, lighting and cooling. The development of optimization strategies for these application systems for captured solar energy through the integration and simultaneous testing of three functions: 1) thermal capture, transfer and distribution; 2) distributed cooling system strategies; 3) direct current transfer to interior applications. Although this research focused specifically on developing trade-off optimization strategies for the simultaneous capture and transfer of heat and power to building applications, the façade system that was integrated into this testing schedule, by necessity, focused on the Integrated Concentrating Solar Façade (ICSF) System that was developed by Rensselaer with previous grants from the New York State Energy Research and Development Authority (NYSERDA), The New York State Foundation for Science, Technology and Innovation (NYSTAR), and the US Department of Energy (DOE).<sup>44</sup> The ICSF System is a building-integrated photovoltaic (PV) system that increases daylighting quality, reduces cooling loads, generates electricity, and produces high-grade thermal energy. We are currently seeking and negotiating with strategic industrial partners to help develop transformative systems for distributed heat capture and transfer, transport, storage and cooling.

### **Project History**

Beginning with the insight that concentrating PV and building envelopes could be integrated, Experimental Prototypes have been developed with a new concept for a two-axis tracking assembly and concentrating modules that are embedded within the curtain wall of a building. Small-scale prototypes were first tested in 2003 and showed expected PV generation efficiencies (relative to original computational models). With this current

---

<sup>44</sup> A.H. Dyson, P.R.H. Stark, M.K. Jensen, S. Elliott Gruen "Integrated Concentrating (IC) Solar Façade System", Solar Energy Technology Program, DOE, 2008 and 2009. (total average score on both technical and demonstration reviews - 3.7 out of 4)

grant, further prototype iterations have been of an integrated and optimized delivery system for a 'whole building matrix' suite environmental control systems (ECS) with heat and power applications that have been designed and tested for cost and energy payback periods that would be a fraction on existing disparate systems, within retrofits for new and existing construction. Part of the on-going mission of this research is to demonstrate the synergy of retrofitting ECS in complete integration with a building envelope retrofit that both mitigates cooling and lighting loads, while maximizing on-site energy capture.

## **Progress Overview**

### ***ICSF Prototype Iteration***

The physical manifestation of the integrated concentrating solar façade (ICSF) system has evolved substantially through many prototype iterations, from a lab-scale PV-only proof-of-concept through the current iteration, a full-building-scale machine in occupied space. During operation, the prototype generates electricity and thermal power on a per-module basis that is relevant to the commercial office environment. Furthermore, development for the next, larger iteration has been incorporated into the current design, in order to streamline deployment in an optimized location once it becomes available, and the prototype can be reconfigured or replicated to operate at a larger scale at that time.

The team has refined the system as a completely integrated unit to test heat capture, transfer, storage and redistribution within the more confined interior lab spaces that we have at our constant disposal at CASE and Rensselaer. We continue to gather data from the CASE prototypes which will be submitted for publication in Spring 2014, as ongoing testing at the CoE was unfortunately interrupted by construction schedules and delays in the acquisition of testing equipment and space. However, we hope to finish all data acquisition through the two prototypes at CASE and the HT lab, in view to building another larger assembly at the CoE with all integrated features associated with interior conditions in another future phase.

For design validation and verification to continue during periods of the calendar without solar access, we had to embark upon an indoor testing regime. Our indoor

testing at this point has been limited to tracking accuracy verification. We propose, now, to complete indoor performance testing at our heat transfer laboratory at Rensselaer Polytechnic Institute, that will parallel track the testing at CASE for the larger building integrated prototypes. In that way, we can ensure more consistent and reliable conditions that are necessary in our development of systems for capture, storage and redistribution of the heat energy.

### ***Building Context Analysis Framework Progress***

### ***Thermal Redistribution Strategy Progress***

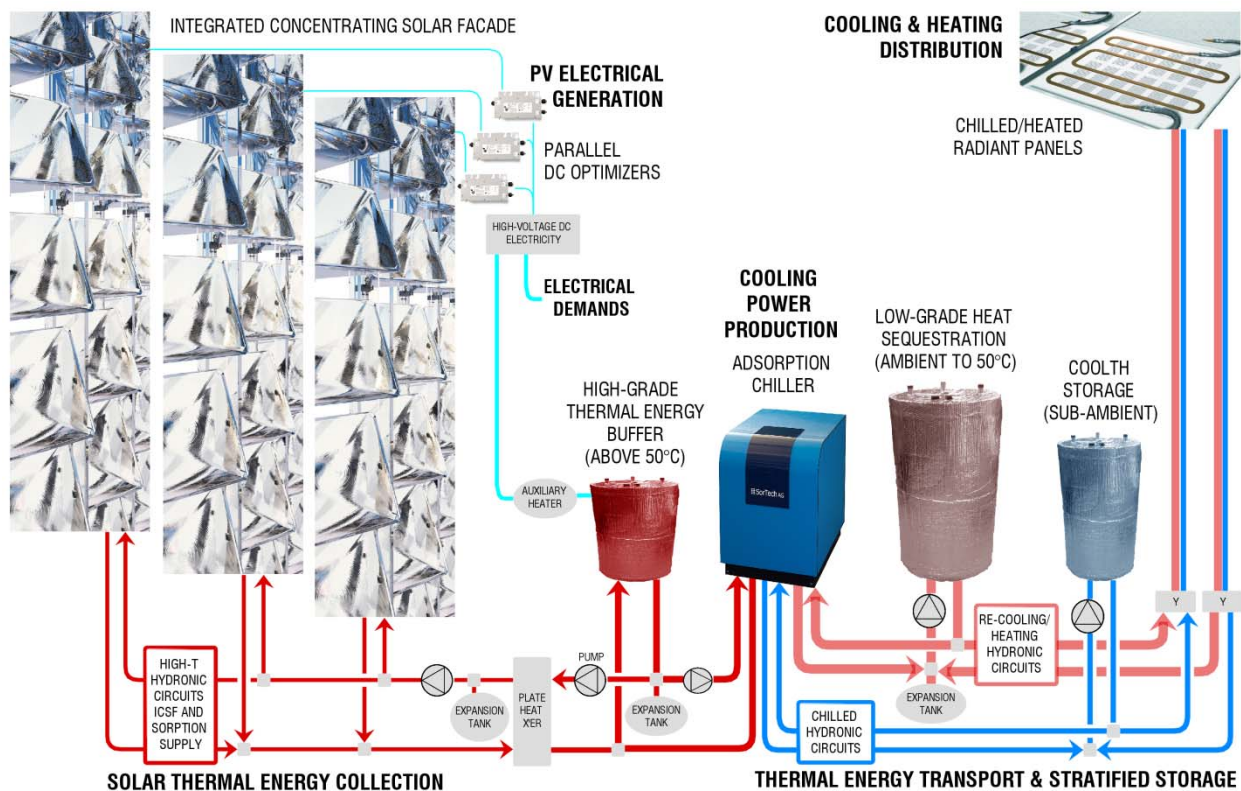


Figure 32. Thermal redistribution strategy (schematic).

To effectively use climatic thermal resources, façade-integrated harvesting systems are interlinked with thermal storage at three distinct temperature regimes, thermally-driven chilling devices, and radiant/mixed cooling and heating distribution units.

### ***Full-scale Architecture View Mockup and 1/2-Scale CPV/T Prototype (Generation 6)***

The testing of this integrated active facade system was initially planned in collaboration with Syracuse University. Two casement curtain wall units were installed

at the Syracuse Center for Excellence in Environmental and Energy Systems (CoE): one as a full-scale, fully-tracking Architectural View mockup, and the second as a half-scale CPV + Thermal collecting experimental rig. Due to unforeseen infrastructural and funding delays at the CoE, this testing was ultimately relocated to the CASE labs in New York, NY, with the aspiration towards future research with a 'whole building systems' heating, lighting and cooling loop installation in the Rensselaer Heat Transfer Lab in the Jonsson Engineering Center, and a fully integrated system-of systems installation at the Smart Lighting Research Center in 2014.

### ***Iterated Full-Scale CPV/T Prototypes (Generations 6 & 7)***

The latest iteration of the integrated concentrating solar façade (ICSF) system has been constructed at the CASE labs and is undergoing testing. The array comprises 72 modules will fill 6m<sup>2</sup> of façade (window) area when complete. Alongside the electrical harness which collects PV output, a hydronics-based thermal transport system manages the heat production of the array, providing the energy to an adsorption chiller (scheduled for installation in the first half quarter of 2014). Thermal and electrical characterization has been done through operation and data acquisition, and optimization of the thermal transport circuits is underway. The experimental setup has been constructed to accept future experimentation with multi-phase thermal transport for in-façade segments of the thermal network, to address parasitic pumping losses and eventual architectural / productization concerns.

### ***Simulator***

While parallel tracking the ICSF prototyping development, multiple computational models at different scales have been written, including characterization at the module/receiver level to an overall system distribution simulation. Initial models for ICSF were written in Microsoft Excel to calculate energy collection potential from TMY data while accounting for module/array self-shading. The ICSF simulation has since evolved and was re-coded in the Visual Basic programming language to include the new optical components found in ICSF Generation 7 and Generation 8.

### ***Experimental work***

The balance-of-system design is critical to the development of building-integrated CPV systems, since we incorporate concentrating photovoltaic technology into a synergistically integrated building system that effectively utilizes available solar energy for maximum impact on the overall energy consumption profile of the building. We utilize the high-quality heat and electricity produced by CPV systems directly at the building envelope, and further reduce building cooling and lighting loads. To achieve this goal, post-occupancy testing of full-scale prototype(s) at CASE and the HT lab will assess the operating constraints on power generation, capture and transfer, as well as assess and develop optimum techniques for direct transfer of the PV generated electricity and high quality heat to distributed building systems.

### **3.2 Development of Analysis and Design Tools for Responding to Dynamic Building Energy Consumption Profiles and Performance Criteria**

The technological development and market penetration of intelligent façade systems (and architectural technologies more broadly) is dependent on the ease of modeling the systems in the early phases of project design and performance specification. In current practice, architectural designers have few tools with which they can model the integration of new systems, or describe the character and benefits of these systems to clients and other stakeholders. It's therefore crucial to the advancement of new technologies to simultaneously develop tools that will aide their modeling and description. In the process of our research in ICSF, a suite of tools has been developed for description of its interactive and behavioral effects and modeling the effects of thermal manipulation and electrical generation. Existing building modeling tools have been combined with synthetic diagramming, system and thermal models with graphical user interfaces, interactive parametric environments, and real-time feedback displays, to improve our ability to describe and interrogate the systems.

### **3.2.1 Modeling the Energy Requirements for Conventional Lighting, Heating, Ventilating and Cooling Systems**

Not all tools involved in ICSF research are purpose-built: fundamental tools for the practice of architectural sciences exist in mature states, such as building energy modeling (BEM). To establish baseline energy consumption characteristics with which to compare the effects of ICSF and distributed thermal strategies, BEM is used to simulate the operational states of representative classes of buildings. The modeling of conventional buildings is an important and informative process to describing the potential of ICS as a building integrated solution. Using the Commercial Building Energy Consumption Survey (CBECS) provides average building types to work from for baseline analysis. The CBECS reviewed 5,215 buildings and determined the specifications of 16 building types from the canvassed data. From those building types, the small, medium, and large office buildings are studied as baselines.

The CBECS small, medium, and large office building types were selected for dimensions and size. These building types allow the comparison of energy consumption across parameters of average size and use. The dimensions and parameters of each building type are selected as the industrial average for each building type.

Each building type has parameters of floor area, number of floors, aspect ratio, floor-to-floor height, and glazing fraction. The small office building has a floor area of 511m<sup>2</sup>, aspect ratio of 1.5, and a single floor. The small office building represents a very large stock of office building across the country in less densely populated regions. The medium office building, with 4,982m<sup>2</sup> floor area, 1.5 aspect ratio, and 3 floors, represents office buildings in tech-park/office complexes, a common typology in suburban areas. The large office building has a floor area of 46,320m<sup>2</sup>, 1.5 aspect ratio, and 12 floors. The large office building represents office buildings in densely populated regions, like cities, where there is a necessity to build vertical to fit higher volumes of people.

### **3.2.1.1 Determine Thermal Loads in Representative Building Style: Large Commercial**

Commercial architecture is a target platform for the installation of building-integrated concentrating solar façade technology, since these buildings suffer high cooling loads across climates and typically show high glazing ratios.

Additionally, in larger buildings, floor plans are deep enough so that a major fraction of the building's space is physically removed from the building's envelope. This aspect results in particular patterns of building systems design and operation. Heat is constantly generated internally (from people, equipment, and the systems themselves), but is generated in space that borders only on other spaces that generate heat. Compounding this, solar irradiation warms the building's exterior during the same hours that the most heat is generated internally. Consequently, large amounts of energy must be actively removed on a continual basis. This is done (with only negligible exceptions) by centralized systems. This energy is sourced remotely and, because of the broad impact of the building sector, compromises environmental conditions at both the macro and micro scale. When tallied together, thermal climate control operations—heating, cooling, ventilation—and the related tasks of refrigeration and water heating require over half of the national commercial building energy budget (Figure 33). If it can be assumed that these figures are similar for residential and other building types, thermal control therefore consumes a rough quarter of the energy used in the nation as a whole.<sup>45</sup> Reducing the electrical and cooling requirements of this sector of building stock would have useful impacts on the electrical consumption—and primary fuel use—of the country, as seen in Figure 34.

---

<sup>45</sup> Data source: U.S. EIA. (2011). *Annual Energy Review* ( No. DOE-EIA-0384 (2010)). DOE.

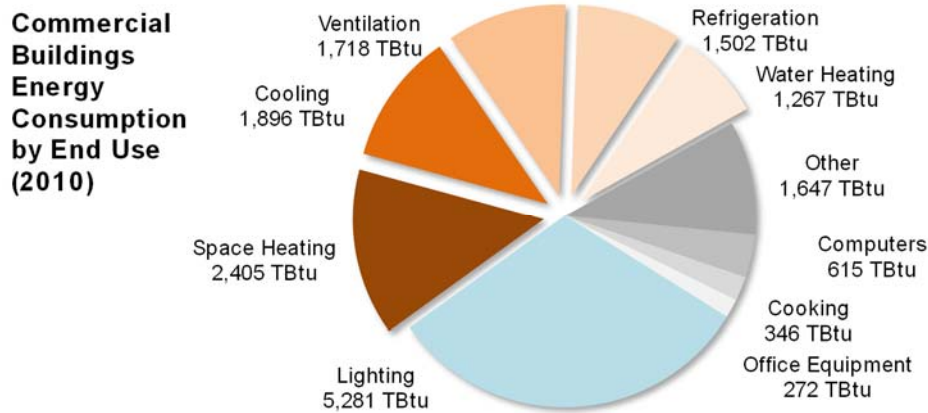


Figure 33. Commercial buildings energy consumption by end use (2010, projected).<sup>46</sup> Cooling, ventilation, and heating together account for over half of the energy consumption of buildings; lighting is well over 25%. Because of the amount of energy used in the commercial building sector (see Figure 34), these operations account for a significant fraction of the nation’s energy budget.

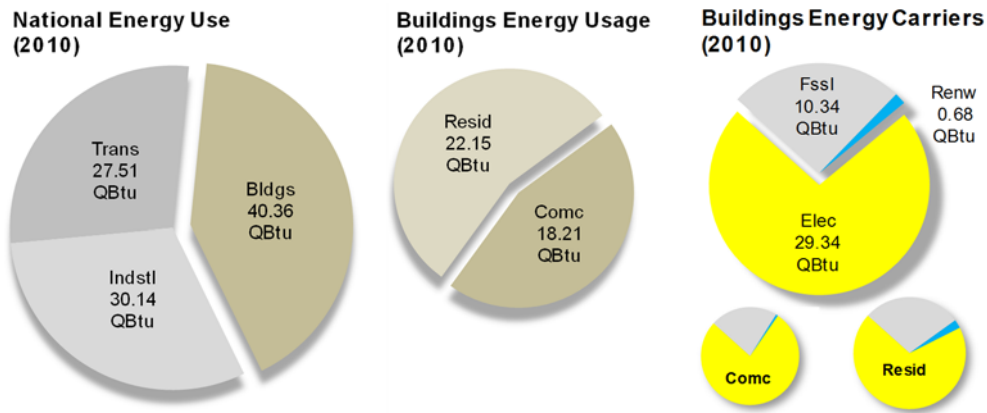


Figure 34. National energy usage by sector, building sector breakdown and energy carriers.<sup>47</sup> The building sector (combined residential and commercial) consumes over 40% of the energy used in the country, largely through consumption of electricity.

<sup>46</sup> Data source: U.S. EIA. (2011). *Annual Energy Review* ( No. DOE-EIA-0384 (2010)). DOE.

<sup>47</sup> Data source: U.S. EIA. (2011). *Annual Energy Review* ( No. DOE-EIA-0384 (2010)). DOE.

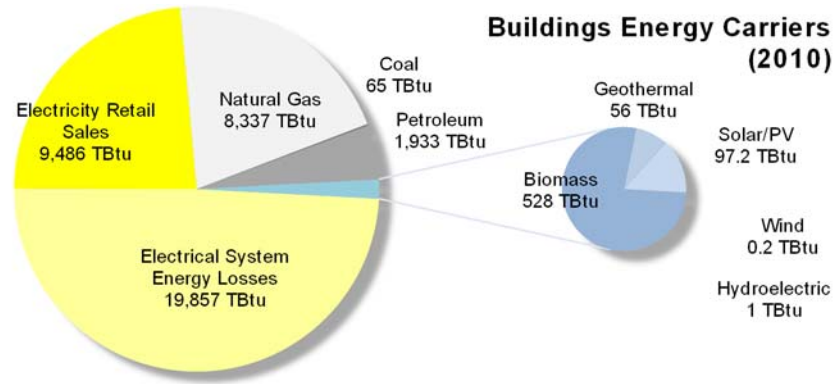


Figure 35. Energy carriers used in building sector.<sup>48</sup>

Electricity is the major carrier of energy for the building sector, but nearly one half of building energy consumption is in losses in electrical generation and delivery.

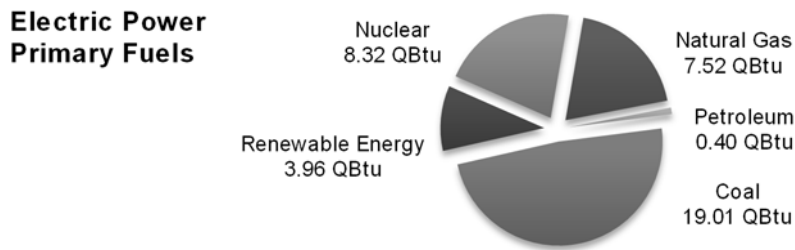


Figure 36. Primary fuels for electric power in United States, 2010.<sup>49</sup>

Electrical power in the U.S. is primarily from non-renewable primary fuel sources, compounding the impact of the electrical consumption of the commercial building sector.

### 3.2.1.2 Building Simulation: Large Office Building

To predict how a building-integrated concentrating solar collection system would operate at full scale, the different types of energy transformations performed by ICSF are related to thermal loads present in a generic large office building with a highly-glazed envelope. The building thermal loads are calculated using the DOE-2 simulation engine, using the eQUEST interface, the parameters of which are described in Table 4 and Figure 37.

<sup>48</sup> Data source: U.S. EIA. (2011). *Annual Energy Review* ( No. DOE-EIA-0384 (2010)). DOE.

<sup>49</sup> Data source: U.S. EIA. (2011). *Annual Energy Review* ( No. DOE-EIA-0384 (2010)). DOE.

Table 4. Parameters of building simulation: 10-story, high-rise commercial architecture, segmented curtain wall envelope.

<i>Building Description</i>	
Building type	10 story office building (high-rise)
Construction type	concrete flat-plate construction, metal frame w all and glazing
Floor plate shape	rectangular
Orientation	broad face due south
Floor plate dimensions (E-W x N-S)	48.8 x 30.5 m
Floor plate area	1486 (16,000) m <sup>2</sup> (sq. ft)
South perimeter zone area	305 m <sup>2</sup>
East perimeter zone area	168 m <sup>2</sup>
North perimeter zone area	305 m <sup>2</sup>
West perimeter zone area	168 m <sup>2</sup>
Core zone area	540 m <sup>2</sup>
Floors	10
Total building area	14860 (160,000) m <sup>2</sup> (sq. ft)
Floor to floor height	3.96 (13) m (ft)
Floor to ceiling height	3.81 (12.5) m (ft)
<i>Exterior construction</i>	
Roof construction	Built-up
Roof R value	3 h-ft <sup>2</sup> -°F/Btu
Ground floor	Earth contact, 6" concrete slab. No perimeter insulation
Envelope construction	Segmented curtain w all
<i>Glazing</i>	
Percentage of façade (all exposures)	92 %
Solar transmittance (normal to plane)	60 %
Visible transmittance	78 %
Construction	single, non-op., no thermal breaks. Plk. Supergrey/Air1/Clear3
U-Factor (conductance)	0.60 Btu/hr-ft <sup>2</sup> -F
<i>Lighting</i>	
Power density	10.76 W/m <sup>2</sup>
Daylighting modeled?	No
<i>Systems</i>	
Domestic hot water design temperature	135 °F
DHW loop design temperature	80 °F
DHW heat input ratio	1.37 Btu/Btu
HVAC system type	Packaged multizone
Fans	Variable speed
Night venting	Not Available
Economizer	Yes, below 65°F outdoor DBT
Cooling electric input ratio	36% Btu/Btu
Cooling coefficient of performance (COP)	2.78
Furnace heat input ratio	1.24 Btu/Btu
<i>*Details from eQUEST model.</i>	

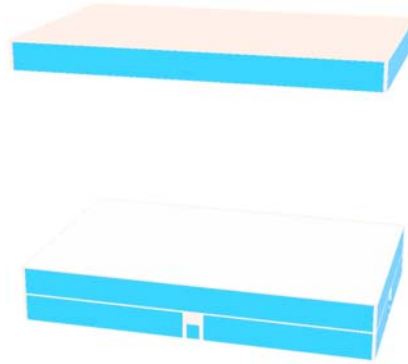


Figure 37. Simulated building typology is typical for large, core-dominated commercial architecture. Middle floors are repeated in the simulation, assuming similar conditions prevail.

The thermal loads in each zone are represented by the latent and sensible energy that the simulated building systems remove (or add) during every time step, to maintain the zone temperature and humidity within specified parameters of thermal comfort and building maintenance. In the simulation we designed, the environmental control systems are capable of counteracting loads completely during each time step, meaning that the simulation variable “current hour heat extraction rate (Btu/hr)” is an accurate representation of the zonal thermal loads that must be addressed in the building description. Figure 38 and Figure 39 show the cumulative thermal loads for the simulated building, zone by zone, in the test climates of New York City, NY, and Phoenix, AZ. It’s notable that even in New York, a relatively cold climate, the cumulative thermal loads increase almost monotonically over the course of the year. In Phoenix there is no period where heating is noticeable. This is characteristic of the chosen building typology: with a relatively low ratio of envelope area to floor area, it is “core dominated,” and representative of commercial high-rise architecture.

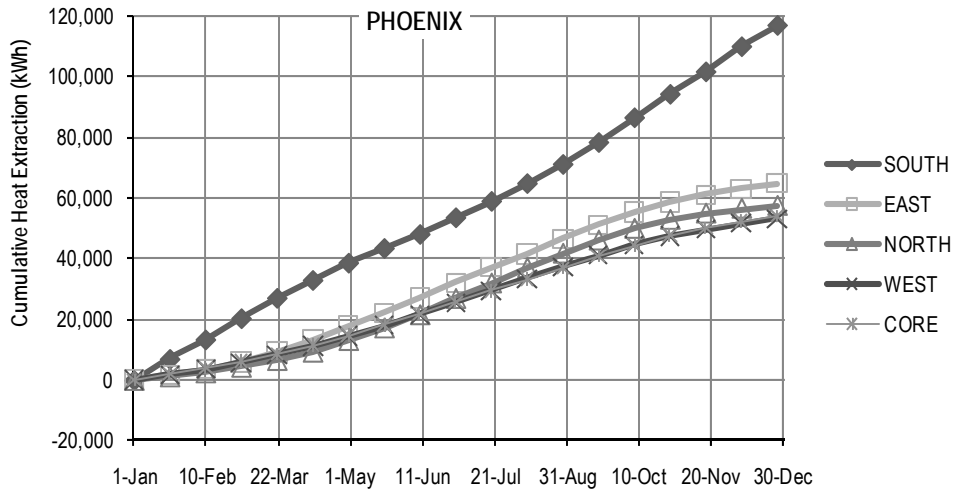


Figure 38. Cumulative thermal loads on mid-building floor plate for the representative large commercial building design, modeled in Phoenix, AZ.

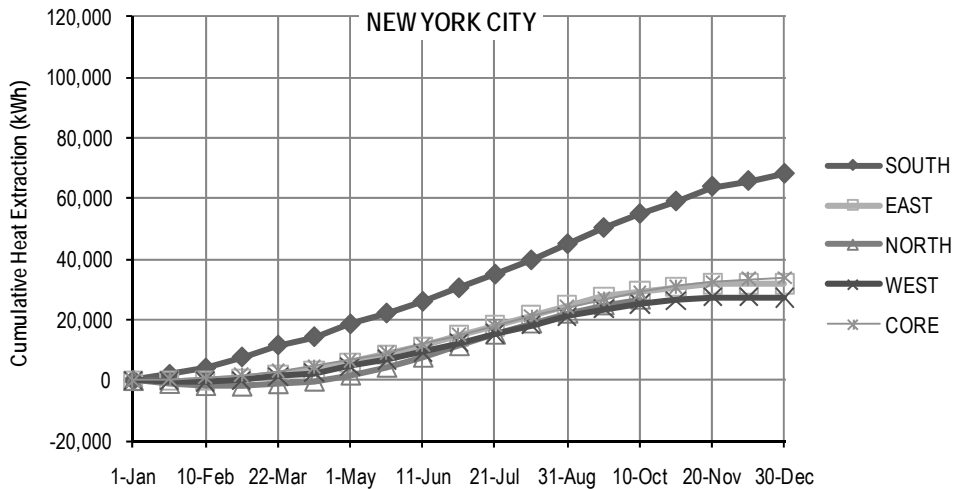


Figure 39. Cumulative thermal loads on mid-building floor plate for the representative large commercial building design, modeled in New York City, NY.

### 3.2.2 Synchronizing Variable Solar Resource to Fluctuations in Demand Applications

Buffering thermal resources at three distinct temperature regimes is an optimal approach for synchronizing solar resources to building service demands. This buffering should occur via systems that are discrete from the bulk thermal mass of the building

and can be charged or drained with heat at useful rates. Appropriate temperature ranges for the separate grades are determined by the eventual use of the energy, and explained in Table 5.

Table 5. Grades (temperature ranges) of thermal resources relevant to the built environment.

Heat sources and heat sinks available to or generated in the built environment can be applied to a range of service demands, based on the temperature regime of the resource.

Thermal Energy Type	Temperature Range	Utility of Energy
High-grade thermal energy	over 50°C	Driving active (thermodynamic work extraction) processes, dessicant regeneration/dehumidification, heating domestic/process water
Low to mid-grade heat source	7°C over indoor thermal comfort range to 65°C	Heating and pre-heating domestic/process hot water, zone heating, re-cooling for work-extraction processes
Ambient sink	near indoor thermal comfort range	Sinking thermal flow from work-extraction processes
Low-grade heat sink	7°C below indoor thermal comfort range and lower	Zone cooling, long-term storage of harvested energy

Work can be extracted from high grade thermal energy (above 60°C in this context), but insulation must be more intensive for energy storage and transportation at higher temperatures. This requirement implies that high temperature storage should be done close to the point of generation, and for the minimum possible duration. Low to mid-grade thermal energy can be used for zone heating and heating/pre-heating domestic or process hot water supplies. The low-grade end of this regime can serve dual purposes – a thermal mass in the temperature range of 30 to 40 °C can both sink thermal flow from an active process and source heating to zones that require it.

### **3.2.2.1 Characterization of Resource: Insolation on Building Envelope**

As buildings increase in height, effects of insolation incident on roof diminish, relative to the insolation incident on the building’s facades. Building-integrated energy collection is highly dependent on the orientation and tilt of its installation. Therefore, it’s important to develop an understanding of these relative quantities with respect to

variables of site, orientation, and climate. Surface-incident insolation is shown in Table 6, which sums the amount of insolation (according to TMY data), by month, to indicate how that sum varies over the course of the year, relative to envelope orientation and climate.

Table 6. Total irradiation on envelope surfaces of a building, New York City and Phoenix Climates.

Tilt	Orient	Jan	Feb	Mar	Apr	May	Jun	Jul	Aug	Sep	Oct	Nov	Dec	Total
Vertical	East	63	74	95	122	131	128	117	115	106	91	66	58	1168
	SE	113	113	120	127	116	105	103	114	125	132	114	110	1393
	South	141	134	129	106	80	64	73	93	123	157	146	143	1389
	SW	106	109	125	120	115	103	108	117	122	136	117	108	1386
	W	57	71	100	113	131	125	123	118	102	94	69	56	1160
45	East	89	105	140	182	204	201	189	178	157	129	93	79	1746
	SE	138	148	176	203	208	196	192	194	189	180	143	130	2096
	South	159	167	193	204	202	185	190	198	199	204	168	155	2225
	SW	132	145	180	195	207	193	197	197	185	182	146	129	2089
	W	82	101	146	173	204	198	196	182	152	133	96	78	1740
33.5	East	92	109	149	194	218	216	205	192	166	136	97	82	1857
	SE	134	146	180	212	224	214	209	207	194	179	139	125	2163
	South	150	161	195	215	222	207	210	211	204	199	159	144	2277
	SW	129	143	184	206	224	212	214	209	191	181	141	124	2158
	W	87	107	153	185	218	213	211	194	162	139	100	81	1851
Flat (roof)		96	115	162	205	239	236	230	211	177	146	104	86	2007

Total Incident Radiation (kWh/m<sup>2</sup> of surface), Phoenix (TMY2 data)

Tilt	Orient	Jan	Feb	Mar	Apr	May	Jun	Jul	Aug	Sep	Oct	Nov	Dec	Total
Vertical	East	39	50	67	82	91	94	98	95	73	59	35	31	812
	SE	71	78	86	92	91	91	95	101	91	90	61	62	1008
	South	89	94	96	90	79	77	81	92	97	108	75	81	1060
	SW	68	75	89	90	89	92	95	94	93	89	58	63	994
	W	36	47	69	78	89	95	98	87	75	58	33	32	798
45	East	52	69	96	123	141	151	152	142	107	84	49	43	1209
	SE	81	98	122	142	151	159	161	158	132	118	73	71	1466
	South	95	111	134	147	152	159	161	159	143	133	84	85	1564
	SW	79	96	124	139	149	159	161	151	134	117	72	72	1453
	W	49	66	99	120	138	152	152	133	110	84	47	45	1194
33.5	East	53	72	102	131	151	163	163	150	114	89	52	46	1285
	SE	78	96	124	147	160	170	171	164	135	117	71	69	1502
	South	88	107	134	152	162	172	173	167	145	129	80	79	1587
	SW	76	94	126	145	159	171	171	158	137	116	70	69	1492
	W	51	69	104	128	149	164	163	142	116	88	50	46	1271
Flat (roof)		55	75	111	141	165	180	179	159	124	95	54	49	1387

Total Incident Radiation (kWh/m<sup>2</sup> of surface), New York City (TMY2 data)

### 3.2.3 Identification of Performance Criteria for Building Integration

Table 7. Performance criteria and metrics for evaluating intelligent active façade strategies.

Performance Criteria	Description	Metric
Maximize Daylighting	use of diffuse daylight to reduce lighting load and increase visual comfort	Present value (\$)
Foster Health and Productivity	healthier heat distribution, ventilation, material selection, etc. increases occupant productivity	fraction, lux
Regulate Interior Thermal Environment	control of thermal gradients and temperature swings to maximize thermal comfort	DGP
Harness and Produce Energy	electrical and thermal power generation at the building façade	Present value (\$)
Utilize Ambient Resources	transformation of ambient energy flows from loads to resources	Present value (\$)
Provide Privacy to Occupants	lensing filters both solar rays and views	kWh/yr, kWh/m <sup>2</sup> -yr
Present Design Identity	contribution of technology to architectural design character and building aesthetic	kWh/yr, kWh/m <sup>2</sup> -yr
Mitigate Noise	intermediate layer in IGU provides increased sound absorption	Subjective
Maximize Return on Investment	creating of short and long term dividends	LCA matrix

**Fostering Health and Productivity** is a vital criterion of performance in the built environment. Spaces that improve the physical health of occupants and the perceptual experience also improve the efficiency of work produced by occupants. ICSF helps to increase health and productivity by capturing and transforming heat for a healthier heating/cooling delivery system through radiant panels.

The building envelope's ability to **Maximize Daylighting** reduces artificial lighting requirements. Lighting is the second largest energy consumer in large buildings. Therefore, reduction of this load can significantly reduce a building's energy use. In addition, natural daylight provides a healthier, more productive and temperature-stable

environment for occupants. The ICSF system has considerable capacity for daylighting, by allowing diffuse sunlight through to the interior.

**Regulating Interior Thermal Environments** is necessary and desirable for human comfort. Stable regulation of interior temperature shifts and thermal gradients provides for the physical and perceptual thermal comfort of the occupants. ICSF reduces undesirable solar heat gain by capturing and redirecting direct solar rays while allowing the more thermally and visually comfortable diffuse light to pass through.

**Harnessing and Producing Energy** at the building site is an increasingly vital performance criterion in our current energy crisis. ICSF works to harness bioclimatic flows for electrical and thermal power generation at the building façade.

**Utilizing Ambient Resources** rather than relying on primary energy sources is crucial to the future of the built environment. ICSF works to reduce the building's reliance on fossil fuels and high-quality energy inputs by capturing and transforming the ambient flows around the building. the system re-envision the "loads" of ambient flows as "resources."

In typical practice, **Providing Privacy to Occupants** is accomplished with opaque shading devices, louvers, or highly reflective surfaces. While these solutions do provide the comfort of privacy, they create other issues such as reduces natural daylight, maintenance, glare to the exterior environment, etc. However, the lensing system used to redirect solar rays in the ICSF provides a visual filter for the façade while allowing diffuse sunlight and views to the exterior.

**Presenting Design Identity** through the building façade is an important aspect of the technology's contribution to the character of an architectural design. The ICSF system demonstrates a clean aesthetic that flows visually with modern glass curtain wall systems.

**Mitigating Noise** through the building façade is also directly related to an increase in perceived human comfort and occupant productivity. With an additional intermediate layer added to the Insulated Glass Unit, ICSF provides increased absorption of the unwanted noise pollution from dense urban streets.

**Maximizing Return on Investment** in an active façade strategy ensures that the technology offers short and long term dividends. ICSF leverages the initial cost by the energy savings, increased productivity, and energy production of the system.

Performance criteria for an integrated system includes the flexibility of adaptation to new as well as existing architectural conditions, building systems and components, as well as a diversity of interior requirements by occupants and programs. For the system to be viable, it must simultaneously respond to the movement and intensity of the external resource (if applicable), provide energy for specific programmatic requirements, and provide thermal comfort, ample daylighting, and a reduction of glare. This convergence of complex criteria into a single dynamic solution at multiple scales, including thermal flows, bodies, equipment, and HVAC systems, requires mapping of variable links to precisely control the relationship between interconnected entities. Because these relationships affect interior environments containing occupants and programs that have very different internal and external requirements, flexibility within the system must be able to be directly linked to factors of cost, energy production, spatial effect, and effect on the rest of the building's connected systems.

Within this larger context sits intelligent, energy-manipulating façade technologies. At the façade, climatic energy resources can be not only harvested, but redistributed and transformed into building resources. The façade is the innate region for these energy manipulations, as the point of contact between built and natural environments. An intelligent façade technology is not responsible simply for power generation--this undervalues its potential.

### **3.3 Simulation of Existing and Projected Systems for Performance Evaluation and Design Optimization**

Co-simulation is the methodology used here for projecting the performance of buildings enhanced by active envelope energy collection and redistribution. Baseline performance of a building typology is determined, given the context of site, morphology, and baseline-spec systems. Simulation is also done for the output and effects of the active façade technology in the equivalent contexts of façade orientation and site. The

results are then combined on a time-step basis to produce results for the integrated system.

To properly value ICSF in the building context, separate simulations are tied together to make current and future projections of system and building performance. Due to the linking of models, assumptions are applied throughout the process. Assumptions are made for solar heat gain interception, energy conversion, heat losses, and system performance. Current simulations of ICSF are idealized on a per-module basis and scaled up to system size. This creates ideal results that model the potential of what the system can be in the future. There are inherent challenges, heat transfer problems, and system operations that must be considered when scaling up to a full-scale façade system. In future work, the simulation process and linking of models will refine the results. Linking the ICSF simulation within an entire building context will inform value propositions of not just electrical and thermal generation but whole building benefits of cooling load reduction, day light supply, and visibility to the outdoors.

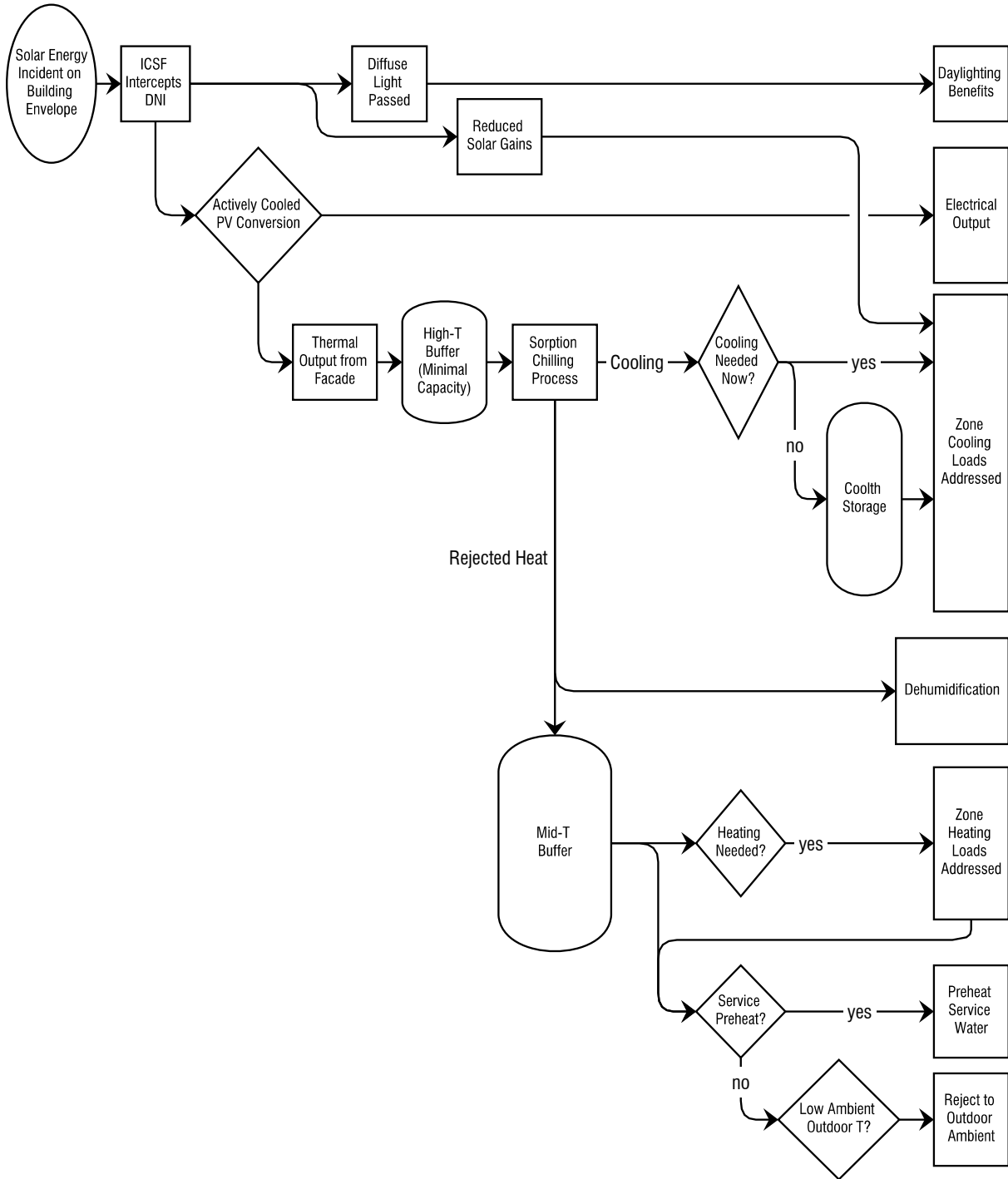


Figure 40. Process diagram for harvesting solar energy, transforming it, and applying it to service demands through active façade strategies.

### **3.3.1 Modeling Existing Systems for Performance Optimization**

#### **3.3.1.1.1 Simulated Comparison with Existing Systems for Performance Optimization**

To evaluate the effects of ICSF, its power generation must be compared to existing solar harvesting systems. Mono-silicon photovoltaic modules provide a comparative technology for electrical generation, as a mature, commodity-scale technology. Likewise, for a baseline of thermal power harvesting, evacuated-tube solar water heaters convert solar energy to thermal energy relatively efficiently, and are widely available (though not as common as PV). The three system's simulated performance (in a theoretical roof installation of a medium-sized office building) can be seen in Figure 41. Although ICSF does not outpace either precedent technology relative to their native energy output types, the combined effects, in addition to daylighting benefits and cooling-load reductions, show the BICPV/T strategy to provide improvements against baseline solar harvesting systems, even when installed in roof-type settings.

Mono-silicon photovoltaic cells generate with an electrical conversion efficiency around 20%. Comparing ICSF to mono-silicon PV cells, ICSF employs Fresnel lenses and small, high efficiency concentrator PV cells to produce electric power, equal to or greater than mono-silicon PV cells. Additionally, ICSF produces thermal power, where PV cannot, adding to the potential value of ICSF.

Evacuated-tube solar collectors can produce high-grade heat at high efficiencies. As an example for comparison, the ergSol 100-6 panel was chosen from available Solar Rating & Certification Corporation data sets, for its high performance.<sup>50</sup> The evacuated tubes generate more thermal energy than ICSF due to their vacuum insulation, heat pipe transfer, and high flow rates. But although evacuated tubes produce higher quantities of thermal energy, the conversion of heat to electricity is not as energetically efficient as PV generation.

---

<sup>50</sup> Solar Rating & Certification Corporation. "Certified Solar Collector 10001807." ergSol 100-6 df. Expiration Date: January 30, 2025. 400 High Point Drive Suite 400, Cocoa, Florida. [www.solar-rating.org](http://www.solar-rating.org).

ICSF provides potential due to its ability to produce electrical and thermal energy. The generation of electricity is equivalent to mono-silicon PV cells but instead of letting the heat go as waste, the energy is harvested. ICSF generates energy similar to both systems and combines them into a building integrated system capable of offsetting large fractions of (if not all) a building's electrical and thermal consumption.

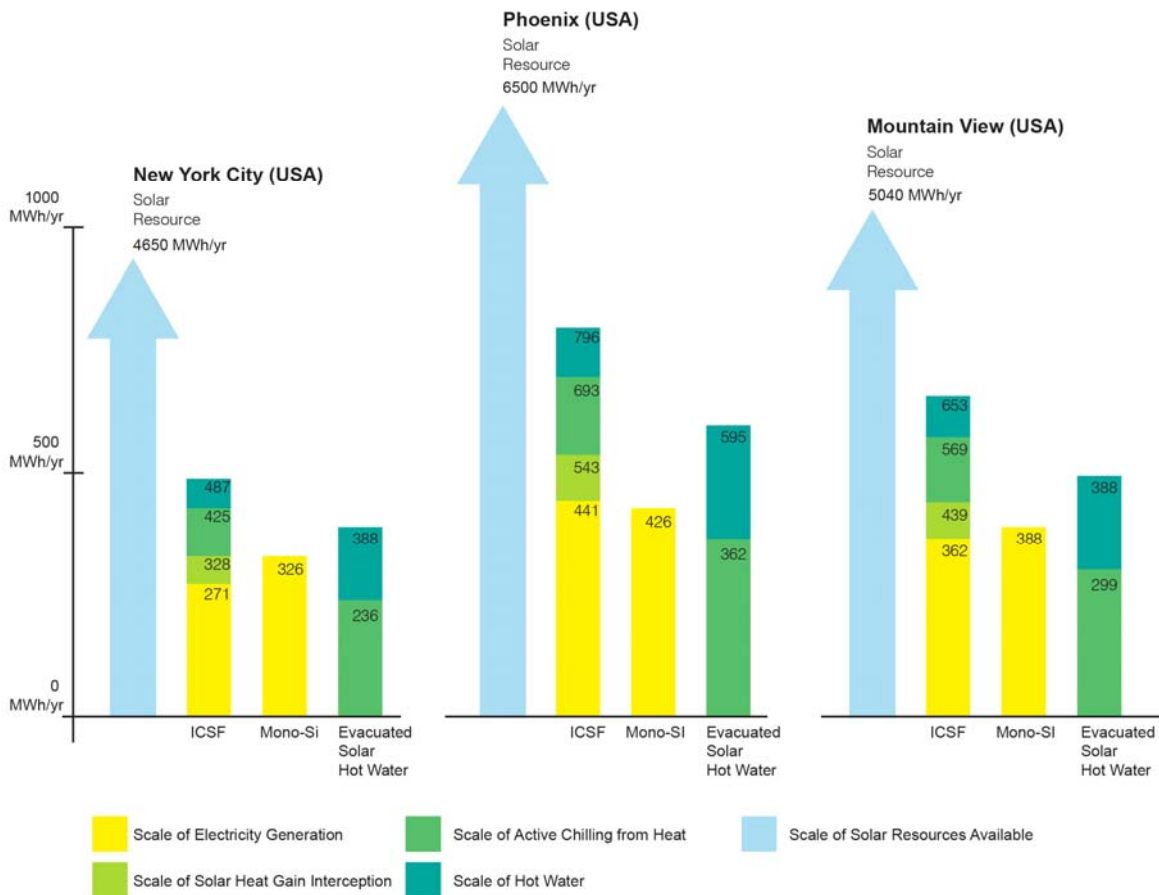


Figure 41: Performance Comparison between ICSF, mono-Silicon solar cells, and water heating with evacuated tube collectors.

### 3.3.2 Trade-Off Optimization: Electrical vs. Thermal

The ability to transform direct beam insolation—a highly-ordered form of energy—into electricity, which is nearly as highly-ordered, is the critical advantage of photovoltaic technology over other forms of electrical generation, which, as heat engines, are limited by the Carnot efficiency which puts an upper bound on a process’s efficiency based on the temperatures of the processes energy sources and sinks. However, since a BICPV/T system provides both electrical and thermal flows, it is useful to be able to compare the utility of the thermal flow to that of the electrical flow, as shown in Figure 42.

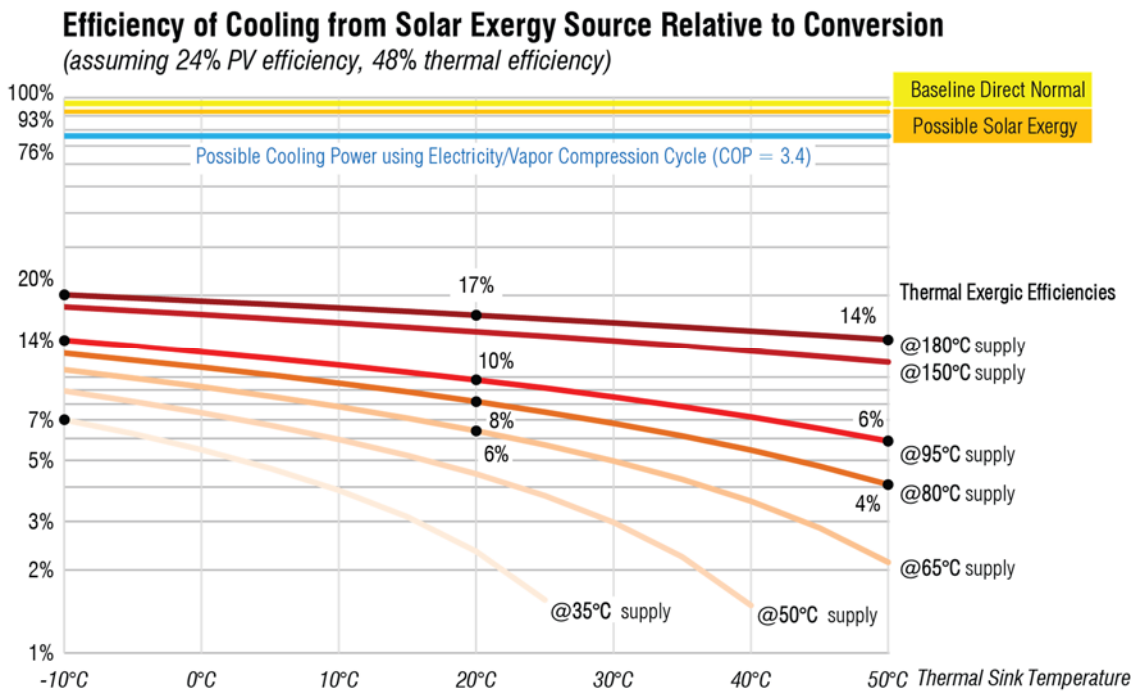


Figure 42. Exergy ratio of incident sunlight to electrical output and thermal output of BICPV/T.

The electrical and thermal outputs of BICPV/T are evaluated by the amount of cooling power they can theoretically produce.

Relative to simple CPV, CPV/T can provide additional work output according to the temperatures produced through concentration, and the available sink temperatures (such as the ambient temperatures of the natural environment). The further advantage of a tightly building-integrated CPV/T strategy over stand-alone CPV/T is in the re-

direction of solar gains which typically cause cooling loads (and therefore demands for energy), especially in core-dominated building types.

As with all PV, the electrical generation efficiency of ICSF decreases as CPV temperatures are allowed to rise. The losses are better than offset, however, by the increase in the utility of the thermal energy that can be collected, provided the systems for thermal transport are effective. This relationship is explained in Figure 43.

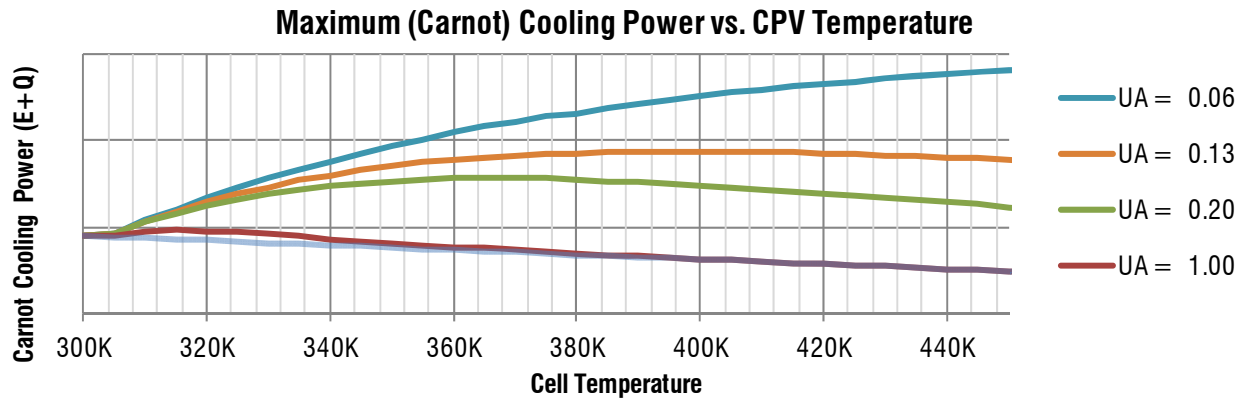


Figure 43. Power developable by BICPV/T increases with increasing collector temperature.

Based on Carnot process efficiencies, the utility of thermal energy collected from CPV cells increases as cell temperatures increase (as measured by the common metric of produceable cooling power). This increase of thermal utility offsets (with surplus) the decrease in electrical generation efficiency due to elevated cell temperatures. The increase is contingent on the effectiveness of the method of thermal transport.

The observation of increasing power output relative to system temperature is based on the interaction of Carnot efficiencies of heat engine and refrigeration cycles and the heat transfer through insulation in the BICPV/T system's thermal transport mechanisms. As CPV cell temperatures rise above ambient temperatures, they become a source of thermal energy. If the elevated temperatures can be maintained and transmitted to useful work-extracting processes (such as sorption chilling), the system output is increased by the development of high-grade thermal energy.

In the specific case of using ICSF to drive a sorption chilling process, the generated high-grade thermal energy should be delivered to the process at a temperature of 65°C or higher for useful work output.<sup>51</sup>

### **3.3.3 Trade-Off Optimization: Construction Costs vs. Performance**

Projected cost for installing the ICSF system range from \$10 per watt to \$13.75 per watt of electrical energy production<sup>52</sup> for a simple 3000w installation. A comparable 3000w installation of typical PV technology can cost up to \$8 per watt<sup>53</sup> electrical energy production. These figures do not take into consideration the added, multi-pronged energy savings measures associated with an ICSF installation such as:

- Down-sizing of HVAC systems relative to reduction in peak demand
- Reduction of electrical lighting loads in response to the systems daylighting effectiveness.

The current generation (Generation 8) of the ICSF prototype represents progress towards the projection of \$8-\$13.75 per watt for system cost by means of reducing individual part cost, and complexity, overall reduction of the number of parts within the system, and reducing assembly complexity while simultaneously improving the systems overall tolerance and alignment. In the design and re-configuration of the optical assembly for Generation 8, a specialized cold plate assembly was implemented into the system to better match the thermal loads to the cold plate assembly. On a parallel track the design team has engaged with industry collaborator Mikros Manufacturing, Inc, to design an integrated cold-plate/PV cell assembly to reduce the package resistance (63% of the total at 0.1 LPM) and improve reliability by better matching the CTE of the components. That would also allow the team to buy bare cells at a reduced cost rather than pre-fabricated assemblies. To optimize the design (lowest cost for a given target operating conditions), consideration for the entire system would be made so that the proper trades could be made between flow rate, pressure drop, and package thermal

---

<sup>51</sup> According to Sortech, manufacturer of small-scale adsorption chillers. Cooling work is performed at inlet temperatures as low as 55°C, but the COP at that operating state is low.

<sup>52</sup> Heliopix cost projections.

<sup>53</sup> <http://www.cleanpower.com/products/powerbill/clean-power-estimator/>

resistance. An optimized design could potentially reduce the approach temperature by about a factor of two. That would allow operation with the fluid exit temperature around 90C (to more efficiently drive an absorption chiller for example) while keeping the junction temperature below 100 °C.

With an eye toward robustness and design-for-manufacturing, several system components were re-designed with considerations made for part complexity, system tracking tolerance, weight reduction, and mechanical robustness.

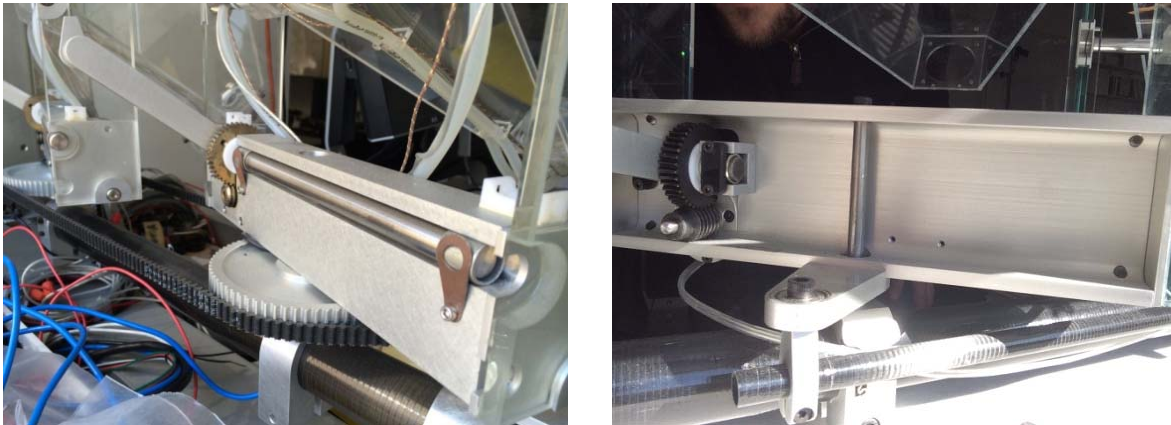


Figure 44 - Generation 7 lower stack actuator block (left) and Generation 8 lower stack actuator block (right).

In the case of the upper and lower stack actuator blocks, the Generation 7 prototype design of the components required machining of solid rectangular aluminum stock, where the Generation 8 prototype makes use of an extruded channel profile as the stock material to significantly reduce the weight as well as machining and processing time of the individual parts.



Figure 45. Generation 7 (left) and Generation 8 (right) marionette assemblies.

At the mechanical connection between individual system modules and stack altitude actuator, a low friction, bearing surface is required to maintain tracking accuracy. Prior iterations make use of cartridge bearings and holder assemblies that mate to the module envelopes, requiring a high degree of placement precision. Generation 8 prototype makes use of a 1 piece machined Rulon J part as both mechanical interface and bearing surface, relying on inexpensive dowel pins for placement and alignment. This part, at production scale could be inexpensively injection molded.

### **3.3.3.1 Design/material drivers for thermal transport system**

A tradeoff optimization exists between the effectiveness of the ICSF thermal transport system and the system's capital costs of design and materials. Better overall resistance to thermal leakage—better insulation—results in higher transferred temperatures and a better coefficient of performance from the driven sorption process, per the Carnot limit.

The efficiency peak of the selected sorption technology, however, peaks not at the upper limit of driving circuit temperatures but at lower temperatures, due to mechanical

limitations.<sup>54</sup> This simplifies the operational tradeoff: lowering system temperature increases both transport efficiency and work extraction efficiency, but the up-front costs remain subject to analysis.

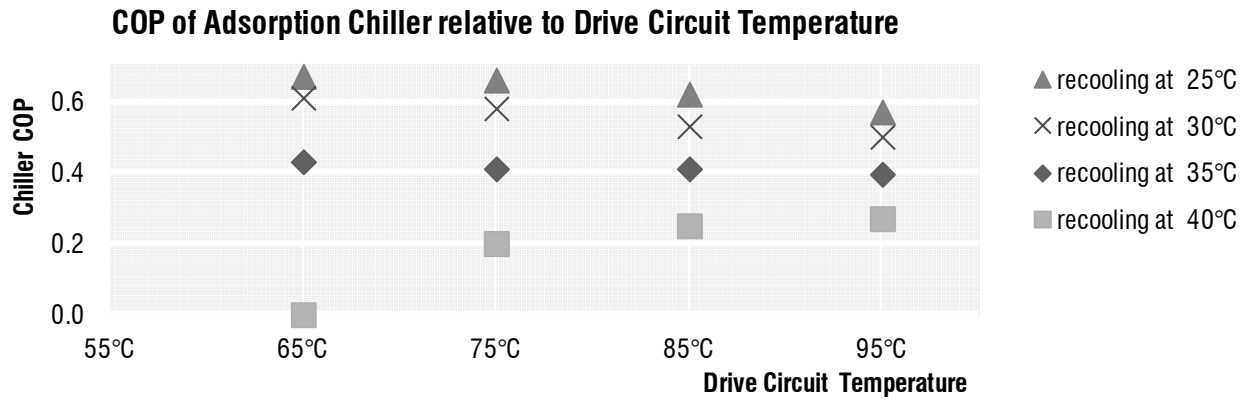


Figure 46. Chiller best-performance state: drive circuit T = 65°C, recooling T = 25°C.

Adsorption chiller performance is determined by mechanism design as well as Carnot efficiency; empirical COP peaks at lower range of driving temperatures.

### 3.3.4 Modeling Effects of ICSF on Buildings in Context: Process

By co-simulating ICSF and a building energy model, the energy savings, economic value, and environmental benefits can be deduced. The current method for combining these simulations is to run them with equivalent parameters, and post-process the data in a spreadsheet. The steps are explained in Table 8.

<sup>54</sup> The maximum cooling power of the selected technology, the Sortech eCoo, does increase with drive circuit T, as predicted by the Carnot relationship.

Table 8. Steps in co-simulating ICSF and a building energy model.

#### **Steps to Model BICSF-Supplied Cooling Capacity in Building Setting**

- Define site location, building orientation, wall directions, and available façade and roof area for installation.
- Run ICSF simulation with weather data, site specific parameters, and array specifications to simulate electrical and thermal power generation from building façade.
- Repeat simulation for each building façade (with array dimensions and orientation).
- Run a building energy simulation for the chosen building context; Retrieve lighting, electrical, heating and cooling loads (by zone, hourly).
- Reduce lighting electrical loads in perimeter zones by fraction to account for daylighting benefits of ICS.
- Reduce cooling loads by fraction relative to ICS power generation, to account for interception of solar gain.
- Calculate cooling power available from ICS-generated thermal energy, according to sorption chiller performance specs; apply cooling to remaining zone cooling loads.
- Calculate electrical draw of standard mechanical equipment required to balance remaining.
- Report revised sum for electrical power required for building.

#### ***Define location, building orientation, wall directions, and available façade and roof area for installation.***

Building orientation is very important in determining solar tracking. Due to the close packing of Fresnel lens, the tracking arrays have limited movement before self-shading and mechanical interference. To determine the shading percentage and range of motion, a shading and movement analysis was done for the current system design. Future analysis is required in finding the ideal spacing that maximizes generation with a minimal restriction of movement. It was assumed that 75% of the area of each of the façades and the roof was available for ICSF integration. The roof installed arrays are inclined at 45° to maximize summer and winter solar tracking. The roof array size remains 75% of the total horizontal roof area. In reality, the arrays will be installed in staggering 45° stacks of modules. This will project shading between angled arrays. In future studies, analysis will be done to more accurately determine the available roof area without shading the solar tracking roof array.

***Run ICSF simulation with weather data, site specific parameters, and array specifications to simulate electrical and thermal power generation from the building façade.***

TMY3 weather data files are fed to the ICSF simulation to acquire the DNI, corresponding hour of year, latitude, and longitude for the location. The data imported is used with solar position equations to determine the angle of incidence, solar energy in per cell, shading, and generation of electrical and thermal power. To simplify the model, an empirical heat loss equation is used to determine the loss of thermal potential. A future model will combine an already completed heat loss simulation with the ICSF simulation. Please refer to the ICSF Simulation Engine section, below, for a more detailed explanation of this process.

***Repeat simulation for each building façade (with array dimensions and orientation).***

Due to the ICSF simulation program, each façade must be modeled individually. Array orientation has a considerable effect on the production potential due to self-shading. The ICSF simulation uses a self-shading equation to determine the quantity of energy reaching each of the cells. This method works well but future work is necessary to implement harder solar tracking stops to the range of motion in the tracking maneuverability. Currently, cells are space to reduce the amount of solar heat gain into the building and maximize the amount of solar energy capture.

***Run a building energy simulations for the chosen building context; Retrieve lighting, electrical, heating and cooling loads (by zone, hourly).***

The DOE EnergyPlus Example IDF Generator was used to create the input files for the building energy simulations. Using the IDF generator was beneficial for constructing buildings that followed the ASHRAE 90.1-2007 standards for each local climatic condition. Each building follows the CBECS office building types. The three building types studied were:

- The small office building with a floor area of 5,500 ft<sup>2</sup> (511 m<sup>2</sup>) and one story
- The three-story medium office building type with a floor area of 53,626 ft<sup>2</sup> (4,982 m<sup>2</sup>)

- The twelve-story medium office building type with a floor area of 498,588 ft<sup>2</sup> (46,320 m<sup>2</sup>).

The building types were modeled in New York, NY, Phoenix, AZ, and Mountain View, CA. New York, NY was selected due to the market and local understanding of seasonal swings. Phoenix, AZ provided what may be the highest potential market location with a strong solar resource and high cooling loads. Mountain View, CA was studied as a temperate climate with low cooling and heating loads.

***Reduce lighting loads in perimeter zones by fraction to account for daylight benefits of ICS.***

Through the interception of beam radiation, ICSF will block the direct beam light that causes glare while allowing diffuse daylight to past through the modules, into the space. For accurate tracking of daylight on materials and into the space a Radiance analysis is required. Radiance will simulate a daylight analysis projected on the ICSF modules to find the amount of high quality daylight that reaches the interior space. This amount of sufficient daylight can be used to reduce the light loads in the perimeter zones. In the future, a daylight analysis will be coupled with the building energy simulation program to reduce perimeter lighting loads when there is sufficient daylight provided to the space.

***Reduce building loads by a fraction relative to ICSF power generation, to account for interception of solar heat gain.***

ICSF is a façade mounted system that intercepts much of the direct normal irradiance and converts it into electricity and thermal energy that is transported away from the facade before reaching the interior building zones. ICSF benefits the building's cooling loads by intercepting much of the solar heat gain that would normally increase the cooling loads. An assumption is made that energy intercepted by ICS can be used to reduce the heat gain before it reaches the interior space. The electrical generation from ICSF is not used in the reduction of heat gain into a building zone due to the utilization of the energy as building equipment and lights that will add heat to the space. On the other hand, the thermal energy captured and transported is a subtraction of heat that would otherwise be entering the adjacent building zone. It is assumed that 50% of

the heat captured is lost in transport and added into the building as heat gain. The remaining 50% of the thermal power is not entering the space and is used to reduce the inherent heat gain from the exterior. The 50% reduction of heat gain (from the thermal capture) is used to reduce the cooling rate of the building systems. When coupling the reduction in cooling rate, with the system COP, the reduction in electricity can be determined. In the next step, the heat captured can be utilized in a sorption chiller process to add cooling to the building zones and further reduce electrical cooling loads. Future research is required to more accurately account for the interception of energy, the heat loss, and interaction with the adjacent space.

***Calculate cooling power available from ICS-generated thermal energy, per sorption chiller performance specs, applying cooling to remaining zone cooling loads.***

The thermal energy generated from ICS can be utilized in a sorption chiller process to generate cooling for the building zones. The amount of cooling required for each building was determined from the EnergyPlus simulations. An adsorption chiller COP of 0.55 was applied to determine the required thermal throughput for a certain amount of cooling. The amount of thermal energy captured from ICSF (discounted 50% for heat loss) was applied to the amount of sorption heat required. The reduction in the cooling load can be applied from the amount of cooling generated through the sorption process. Future work will be done in determining the potential of thermal energy at each sorption chiller and its ability to convert heat to cooling. Additionally, with increased working temperatures, alternative sorption chilling technologies (such as double effect absorption, with COPs of 1.2 and higher) could be considered, increasing the potential of the systems to offset large cooling loads.

***Calculate electrical draw of standard mechanical equipment required to balance remaining.***

The electrical power generated from ICSF can be applied directly to building energy systems. The electrical loads are determined from the EnergyPlus simulations. The loads vary greatly from building type and location. In an ideal circumstance, the DC generation from ICS can be applied to DC systems and equipment. To account for

transmission losses 90% of the electrical generation was used to offset electrical loads in the building.

***Report revised sum for electrical power required for building.***

After offsetting heat gain from interception, cooling loads with thermal energy, and electrical loads from electrical generation, the new building energy consumption can be determined. The intercept of heat gain and the utilization of thermal energy substantially reduce, if not completely offset, the cooling loads in the building. The electricity demand offset from ICSF generation is dependent on the roof area available for installation and the density of the building.

***3.3.5 Simulation Routine for ICSF Performance***

With the innovation of a new energy capture technology, it is a necessity to develop new, accurate methods for modeling its potential. To model ICSF solar tracking and concentration technology, sun path algorithms and climate data input into refraction and energy conversion efficiency functions and heat transfer relationships. The outputs of the model are the system's electrical and thermal generation potential. These outputs can be related to outputs from other models, such as a building energy simulation, or used as inputs to other models. With the electrical and thermal potential calculated, projections can be made for zero energy architecture solutions and designs.

To extrapolate the known operative characteristics of ICSF into a larger context, a simulation tool for ICSF has been constructed (implemented in Visual Basic, based on an original design implemented in a spread sheet).

***3.3.5.1 ICSF Simulation Engine***

The ICSF simulation tool generates electrical and thermal generation data, based on several inputs, as summarized in . The program starts by importing and reading weather data from a chosen TMY3 data file. After the file is imported the code extracts the user inputs of array orientation, area, and material properties from a GUI. With all the necessary data imported, the code runs through the calculations to determine the electrical and thermal outputs for the array, iterating hourly over the course of a year.

Table 9. HeliOptix simulation engine input and output variables.

The engine is a consolidation version of an earlier model developed at CASE.

<i>HeliOptix Simulation Engine</i>	
<i>Inputs</i>	<i>Outputs</i>
Climate Data (TMY2 or TMY3 in .epw format)	DNI (from climate data)
Fresnel Lens Width	Array Coolant Output Temperature
CPV Cell Width	Electrical Power Output (W, hourly)
F#	Thermal Power Output (W, hourly)
Fresnel Lens Material	
Vertical Module Spacing	
Horizontal Module Spacing	
Window Area	
Modules per Stack (Modules in Thermal Series)	
Number of Stacks (calculated automatically)	
Front Glass Pane Refraction Index	

### 3.3.5.1.1 Initial Calculations

The first portion of the program calculates the potential of the Fresnel lens. The F-number and lens material are specified to calculate the focusing concentration of the solar radiation on lens to the radiation on the PV cell.

Based on the concentration magnitude the efficiency of the cell is determined using a current-voltage empirical equation:

$$EVC = \frac{11.22 + MAG}{(14.65 + 1.041(MAG) + (0.02543MAG) \sin(0.1589 + MAG) - 0.3238 \sin(MAG))}$$

Equation 1. Empirical formula for determining Fresnel efficiency factor of concentrating the light on high efficiency solar cell, based on the magnitude of concentration.

where *EVC* is the efficiency of the cell based on the Fresnel lens geometry and *MAG* is the magnitude of concentration determined from the Fresnel lens and F-number.

The thermal resistance of system through the flow of water between modules is determined using an empirical equation for heat loss based on the flow rate.

$$TR = (0.0427 * MDOTGAL^{-0.239}) + 0.22$$

Equation 2. Empirical equation for determining thermal resistance based on the flow rate of liquid through the system.

where  $TR$  is the thermal resistance and  $MDOTGAL$  is the flow rate of the fluid through the system.

### 3.3.5.1.2 Angle of Incidence

After the weather data, user specifications, cell and lens properties are defined, the sun position calculations are done for each hour of the year. Through 8760 iterations, the Angle of Incidence (AOI), insolation, electrical and thermal power generations are calculated. The AOI function uses the day of year, hour, latitude, longitude, site azimuth offset, and site altitude offset to determine at which angle the sun is in relation to the facade. AOI is then fed to the insolation function (Glazing Attenuation).

### 3.3.5.1.3 Glazing Attenuation

As the sun impinges on the outer glass surface of a building, a certain fraction of the radiation is attenuated or reflected from the surface, relative to the angle of incidence between the surface normal and the solar rays. This effect must be accounted for in a consideration of the amount of energy expected to reach the cell of ICSF.

To be precise, the refraction results in lowered input to the solar modules. The resultant solar energy reaching the PV cells is modeled as a function between the incident angle of solar rays and surface normal of outer glazing. Variables used in the calculation are explained in Table 10. This attenuation due to exterior glazing is incorporated into the ICSF simulation engine as part of the Insolation function.

Table 10. Variables in calculation of glazing attenuation.

<i>Glazing attenuation variable</i>	<i>Symbol</i>	<i>Value</i>
Transmitted power	P	
Index of refraction, air	Nair	1
Index of refraction, glass	Nglass	1.5
Angle of incidence	$\theta$	
Transverse angle	$\theta_t$	
Transmission coefficient, parallel	T_p	
Transmission coefficient, perpendicular	T_t	

$$P = \frac{N_{glass} N_{glass} \cos\theta_t}{N_{air} N_{air} \cos\theta} \left( \frac{T_p - T_t}{2} \right)^2$$

Equation 3. Radiation power transmitted through glass, relative to angle of incidence.

$$\theta_t = \arcsin\left(\frac{\sin\theta}{N_{glass}}\right)$$

Equation 4. Transverse angle.

$$T_p = 2 \left( \frac{N_{air} \cos\theta}{N_{glass} \cos\theta + N_{air} \cos\theta_t} \right)$$

Equation 5. Parallel transmission coefficient.

$$T_t = 2 \left( \frac{N_{air} \cos\theta}{N_{air} \cos\theta + N_{glass} \cos\theta_t} \right)$$

Equation 6. Perpendicular transmission coefficient.

### **3.3.5.1.4 Insolation Function**

Within the insolation function, solar losses from refractions and module overlap are calculated to determine the actual solar flux incident on the CPV. This term in the program is given as energy in per cell (*EIPC*). The angle of incidence, calculated in the previous function is fed to the insolation function to determine the refraction at each transmissive interface. Using the same equations from the Glazing Attenuation section, above, the amount of solar radiation transmitted through the glass and air, before reaching the lens. By determining the refraction at each transmissive interface, the magnitude of direct normal radiance reaching the cell is determined. For a reference of the equations used in this process, please refer to the Glazing Attenuation section, above.

Next, the module overlap is calculated based upon the user defined vertical and horizontal cell spacing and solar tracking. A check routine is run to determine if shading is present at the given *AOI*. If clear, the check returns a value of 100% that is applied to the *EIPC* equation (below). If module overlap occurs, the percentage of shading is determined and the solar irradiance reaching the photovoltaic cell is discounted:

$$SELFISH = \frac{(HSPACE * VSPACE * COS(DNIAOI) * 0.9)}{LENS^2}$$

Equation 7: Equation to determine the percentage of module overlap.

(**SELFISH**) bases on the vertical (**VSPACE**) and horizontal (**HSPACE**) spacing, lens size (**LENS**), and the angle of incidence (**DNIAOI**). A value of 1 means there is no overlap, a value of 0 means there is complete overlap.

With the transmission through the layers and percentage of module overlap calculated, the Energy in per Cell (**EIPC**) is calculated using the EIPC equation.

$$EIPC = DNI * CELL^2 * MAG * g_{eff} * Fresnel * SELFISH$$

Equation 8: Energy-In-Per-Cell equation, used to calculate the maximum amount of solar energy reaching the cell before electrical and thermal conversion.

Where **EIPC** is energy in per cell, **DNI** is the magnitude of direct normal irradiance, **CELL** is the width of the photovoltaic cell, **MAG** is the concentration of the Fresnel lens on the PV cell,  $g_{eff}$  is the transmission efficiency through the transmissive layer, **Fresnel** is the concentrating factor, and **SELFISH** is the percentage the lens that are not overlapped.

With **EIPC** calculated, the amount of electrical and thermal power can be determined in the next function from the photovoltaic and heat transfer efficiency.

### **3.3.5.1.5 Photovoltaic and Heat Transfer Efficiency in the Conversion of Solar Radiation to Power Generations**

The energy in per cell (**EIPC**) is calculated in the last function in brought into the generation function to determine the electrical and thermal generation based on conversion efficiencies. From the **EVC** and **EVT** values calculated at the beginning of the code, the cell efficiency (**CELLEFF**) is determined with the maximum efficiency peak ( $E_{Peak}$ ) and temperature of the PV cell (**TPVGUESS**), which comes from the initial temperature of the water. Using equation:

$$CELLEFF = (E\_Peak * EVC) + (EVT * TPVGUESS)$$

Equation 9: Equation for determining the cell electrical conversion efficiency.

the cell efficiency (*CELLEFF*) is determined. *CELLEFF* is then multiplied by *EIPC* to determine electrical power generation at each cell.

$$POWER = EIPC * \left( \frac{CELLEFF}{100} \right)$$

Equation 10: Electrical power (*POWER*) generation based on energy in per cell (*EIPC*) and PV cell efficiency (*CELLEFF*).

$$EPOW = EPOW + POWER$$

Equation 11: After the power is calculated for one module, a For loop is run to sum up the values dependent on the number of cells in a vertical stack. This generated the electrical power for one stack (*EPOW*).

$$EPOW = EPOW * HSTACKS$$

Equation 12: The electrical power (*EPOW*) for one stack is multiplied but the number of stacks (*HSTACKS*) to determine the new *EPOW* for the entire array.

As the solar irradiance hits the cell, a percentage is converted to electricity, the remaining energy is converted into heat and absorbed by the cell.

$$HEAT_{IN} = EIPC * \left( \frac{100 - CELLEFF}{100} \right)$$

Equation 13: Amount of heat into the cell (*HEAT<sub>IN</sub>*) after a percentage is converted it electrical power.

The heat into the cell (*HEAT<sub>IN</sub>*) is the transferred to a thermal fluid that carries the heat away for the capture of heat for utilization in the building context. To determine this quantity a heat transfer equation is set up using the material properties and flow rate with the heat source of the PV cell.

$$T_{OUT} = T_{IN} + \left( \frac{HEAT_{IN}}{\dot{m} * C_p} \right)$$

Equation 14: Equation to determine the temperature of the fluid ( $T_{out}$ ) after the initial fluid temperature ( $T_{IN}$ ) flowing past the cell heat source ( $HEAT_{IN}$ ) with a user defined mass flow rate ( $\dot{m}$ ) and specific heat capacity ( $C_p$ ).

The heat subtracted by the fluid is then balanced with the heat at the cell to determine the new temperature of the cell.

$$T_{MEAN} = \frac{(T_{IN} + T_{OUT})}{2}$$

Equation 15: Averaging equation to determine the temperature of the cell ( $T_{MEAN}$ ) for the use of transferring more heat to a heat transfer fluid.

The transfer of heat between the cell and fluid is continued in a Do Until Loop that transfers the heat between the cell and fluid until they are the same temperature and possess no more heat to transfer. This process in the simulation produces idealized results for thermal transfer with the fluid. The amount of heat transfer from the cell to the fluid will not be 100 percent because the fluid must remain constantly flowing. Future advancement in heat transfer performance could have the potential to transfer almost all the heat captured. The transfer potential in the current simulation remains relevant as a projection of thermal potential. Future work will couple the ICSF simulation program with a more thorough heat transfer analysis for more accurate heat generation. When there is no heat left to transfer, the  $T_{OUT}$  variable is used to calculate the thermal power generation in the equation:

$$TPOW = HSTACK * \frac{T_{OUT} - T_{ORIG}}{R}$$

Equation 16: The thermal power generated (TPOW) is determined from HTF outlet temperature.

Original temperature of the fluid ( $T_{ORIG}$ ) is subtracted from outlet temperature, and divided by the heat loss factor ( $R$ ) determined at the beginning of the program. That value for a stack is then multiplied by the number or horizontal stacks to determine the total power of the array.

After the electrical and thermal power for the cell is generated, these values are inputs to the next cell in the stack. This process sums the electrical and thermal power generated by each series stack of ICSF cells. Each stack is then multiplied by the number of stacks to determine the generation for the entire array.

The entire process from AOI to Generation is then repeated for the next hour, until all hours of the year are calculated.

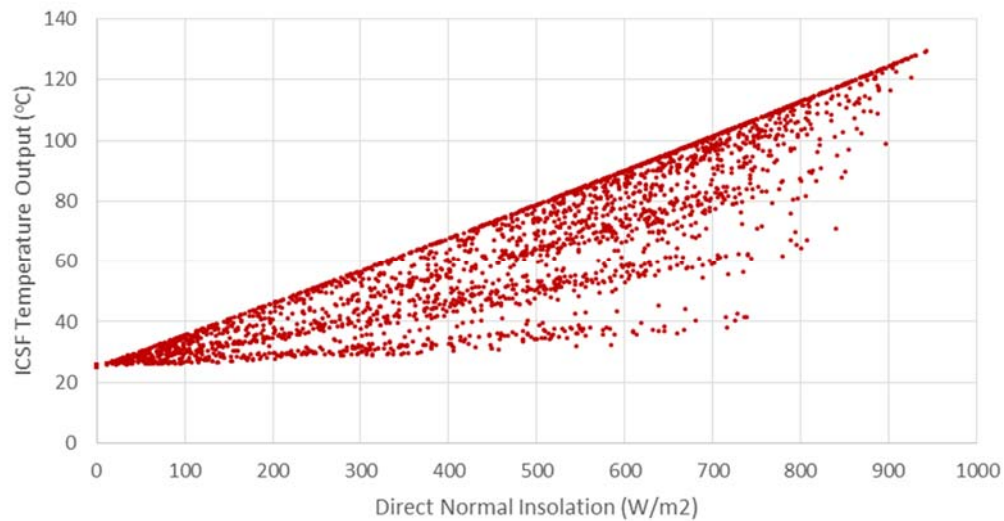


Figure 47. The relationship between incident direct normal insolation (from NYC TMY data) and ICSF temperature output for a stack of 15 modules from the ICSF simulation engine.

The visible Pareto front in the data represents the maximum efficiency of the modeled ICSF installation, which correlates to the times of day when the least module overlap occurs. (Hourly data, vertical façade, south facing, NYC, 24 module string.)

### 3.3.5.1.6 Simulated Electricity Production and Building Consumption Reduction

The electrical production of ICSF, is dependent on façade orientation and solar exposure. Accounting for electricity transmission and conversion losses, the total electricity produced can be applied to the building to offset consumption.

#### KWH OF NET DC POWER OUTPUT YEARLY FROM ICSF PER M2 OF ENVELOPE AREA

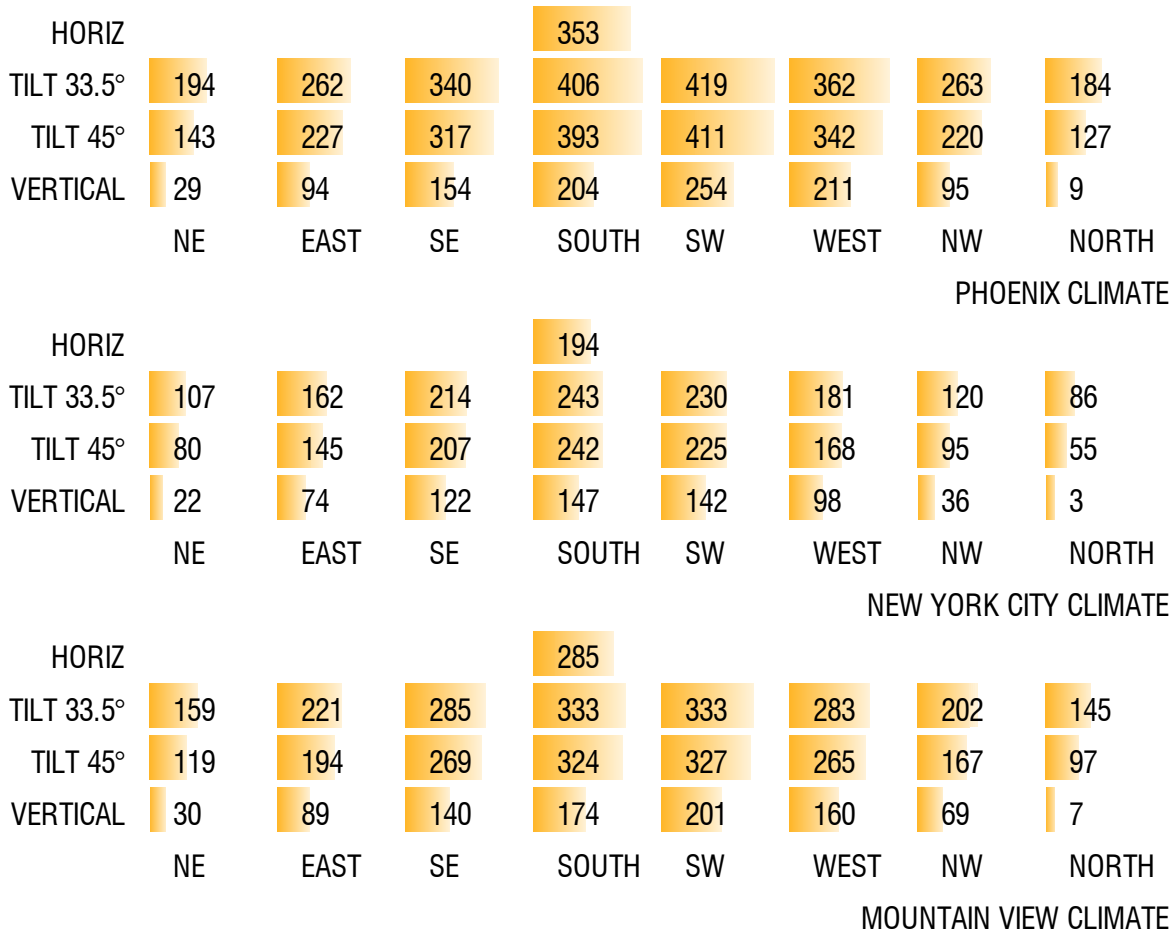


Figure 48. Electrical output of ICSF (kWh/m<sup>2</sup> of envelope area, yearly).

Summed over a period of one year, electrical output from ICSF is function of the orientation and tilt of the envelope element with which the unit is integrated. (Simulated in NREL System Advisor Model (SAM).)

### 3.3.5.1.7 Simulated Thermal Production and Building Consumption Reduction

The collection of thermal energy from ICSF is valuable for many reasons. After the generation of electricity at the PV cell, the remaining solar irradiance is converted to heat. The heat at a PV cell is often rejected to the surrounding environment but when concentrating, can be transferred to a thermal fluid as high grade heat. The thermal

energy captured by ICSF is energy that would have otherwise been solar heat gain into the space. The interception of solar heat gain reduces cooling loads in buildings by the percentage of heat that is taken away from the façade and adjacent zones. The heat, when concentrated and transferred to a thermal fluid, has the potential to be used in distributed sorption chillers for the generation of cooling. The capture and utilization of thermal energy is a valuable process capable of offsetting much (or all) of the cooling demands for a building. For more information on the conversion of heat to cooling please refer to Section 3.3.6 Thermal Energy Utilization Simulations for Internal Systems Applications, below. For case study results in a small, medium, and large office building in New York, Phoenix, and Mountain View, refer to Section 3.3.7

#### ***3.3.5.1.8 Comparison between ICSF Simulation and SAM Simulation***

System Advisory Model (SAM) is a program package designed by NREL to help advice in the performance and financial analysis of renewable energy systems. SAM is beneficial within this research as it contains a concentrating solar photovoltaic (CPV) module that allows the simulation of solar tracking arrays, such as ICSF. Using the CPV system module, ICSF could be simulated in various façade orientations with accurate concentration, cell efficiency, module overlap and maneuverability. This process helps verify the ICS simulation and find discrepancies to look for in future research.

Comparing the simulations provides insight into how the module overlap and tracking maneuverability of ICSF effects the electrical generation results. The ICS simulation uses a shading equation to determine the module overlap from the Fresnel lens. In other words, as the sun has a high solar altitude, the module lens above will block solar radiation from reaching the lens below. The SAM model implements this same method but possess harder range of motion stops. This means, that when the tracking reaches the point at which it can no move, due to adjacent module blocking, the array stops all generation. The ICSF simulation continues to generate electricity during the summer months, while the SAM model does not. The ICSF simulation uses the shading equation to determine the amount of radiation reaching the cells, which is very little, but should implement a harder stop to the generation due to the range of

motion limitations. Therefore, the ICSF simulation is over-reporting values at the beginning and ending of the day.

Glazing attenuation will influence how much solar irradiance actually reaches the high-efficiency photovoltaic cells. The ICSF simulation accounts for reflection of direct beam radiation at the double skin façade glass layers that houses the ICSF system and the lens material. At each transmissive layer, before the irradiance reaches the cell, a portion of energy is lost due to reflections on the layers. The ICSF simulation accounts for glazing attenuation but the SAM model does not. Meaning, that the output from SAM is over report by at least 9% due to Fresnel lens concentration efficiency on the PV cell and refraction.

Each model slightly overestimates the generation of electrical energy at the south facade. The SAM model informed the ICSF simulation by making it aware that the shading calculation may not be enough and the implementation of limits to the range of motion is required. When looking at the 45° roof-mounted array, the sum electrical generation of the SAM and ICSF simulations are very close, although the SAM model produces more power than the ICSF simulation in the low-sun portions of the year.

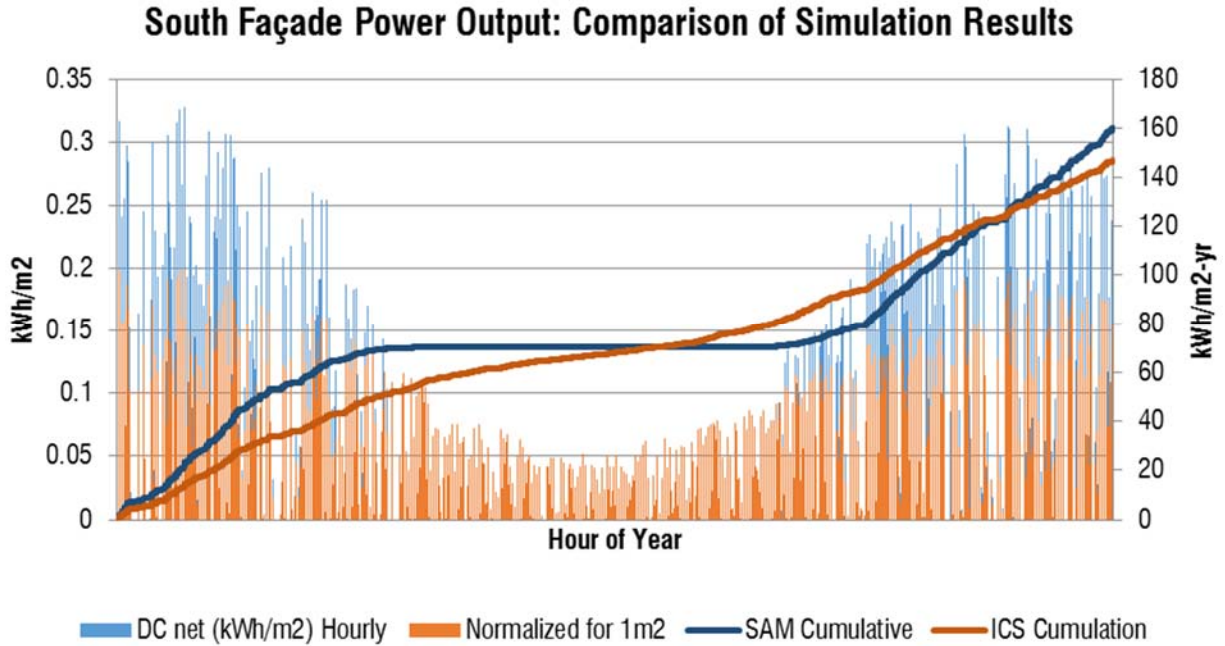


Figure 49. Comparison of simulated electrical generation between SAM and ICSF models for New York, NY.

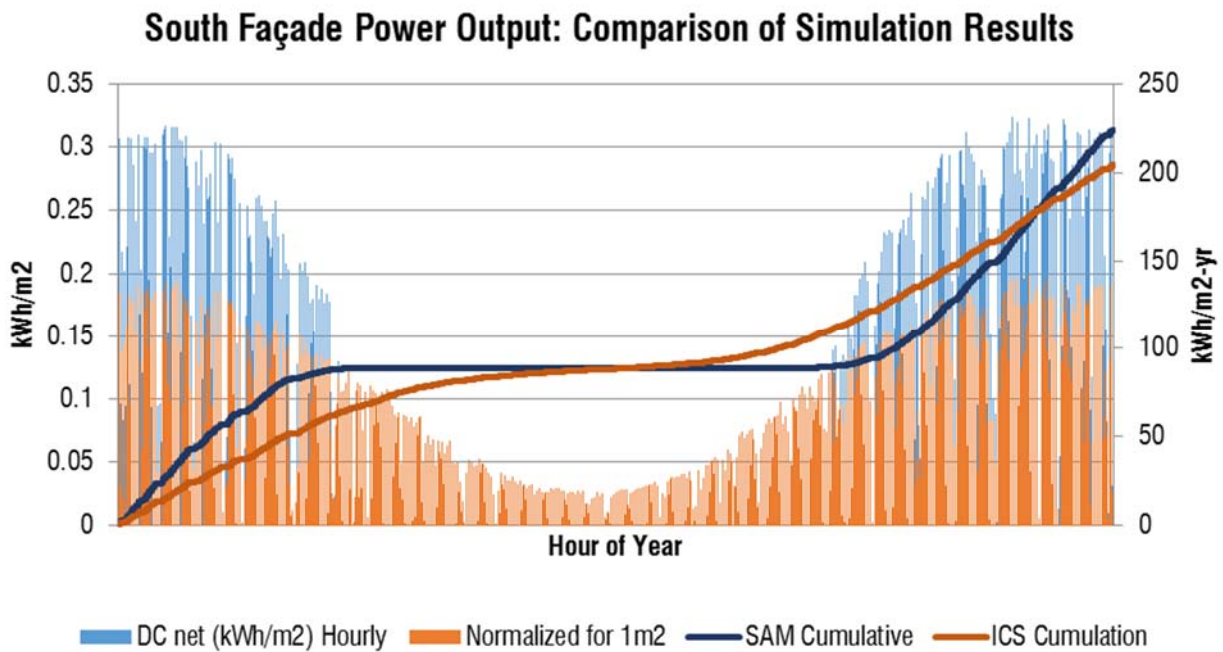


Figure 50: Comparison of simulated electrical generation between SAM and ICSF models for Phoenix, AZ.

### Roof Power Output: Comparison of Simulation Results

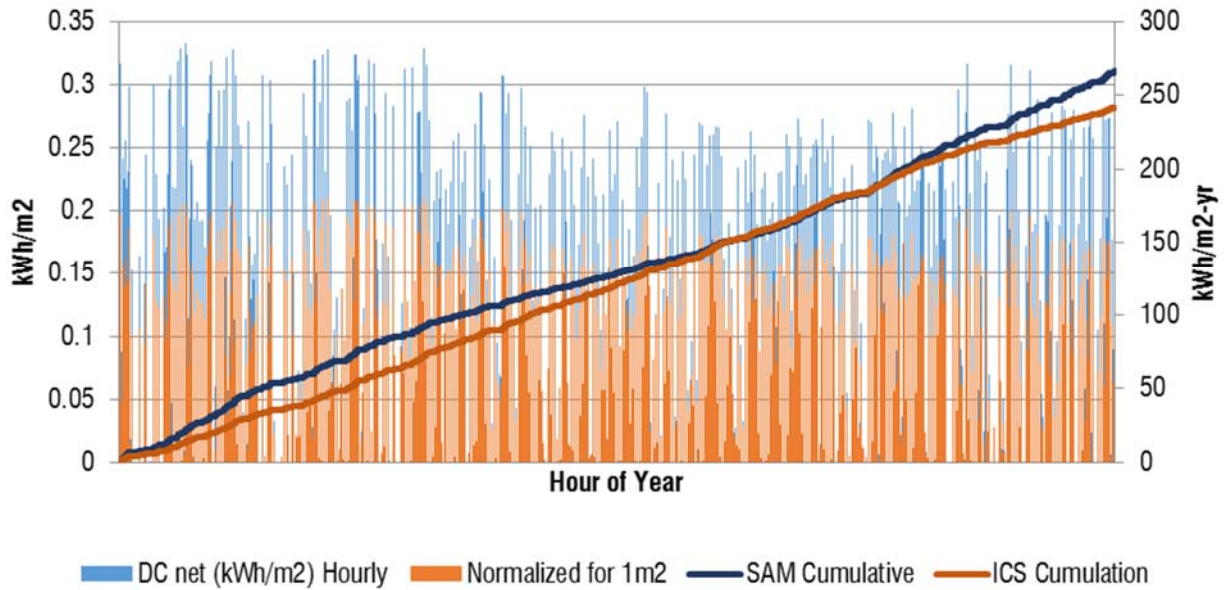


Figure 51: Comparison of simulated electrical generation between SAM and ICSF models for New York, NY.

### Roof Power Output: Comparison of Simulation Results

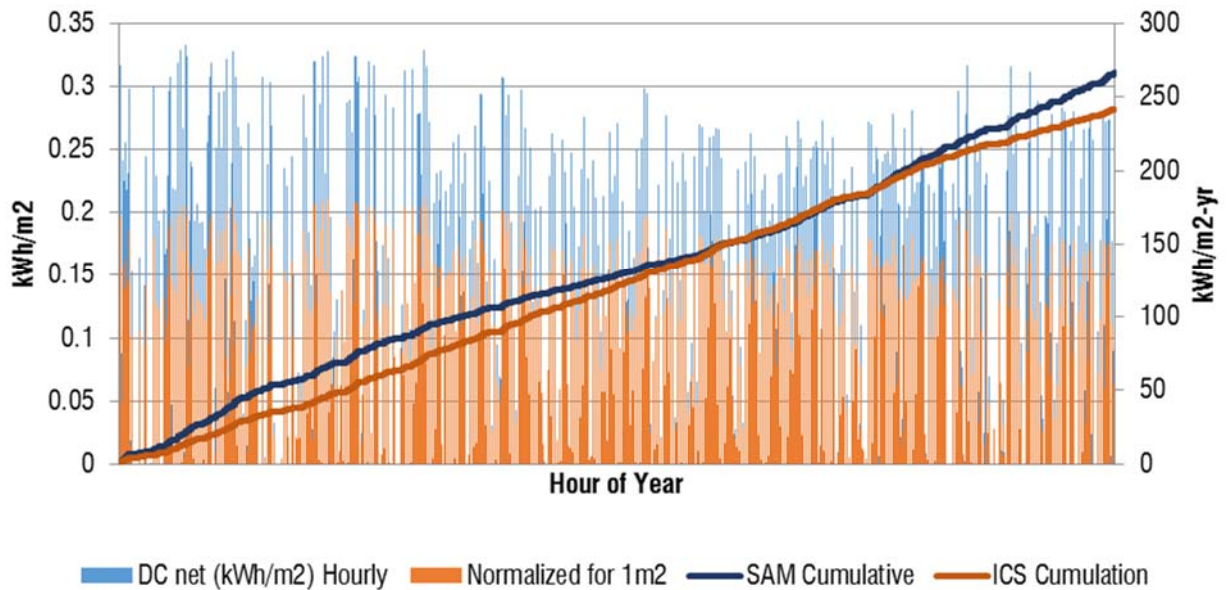


Figure 52: Comparison of simulated electrical generation between SAM and ICSF models for Phoenix, AZ.

### 3.3.5.2 Concentrator-Receiver Energy Balance

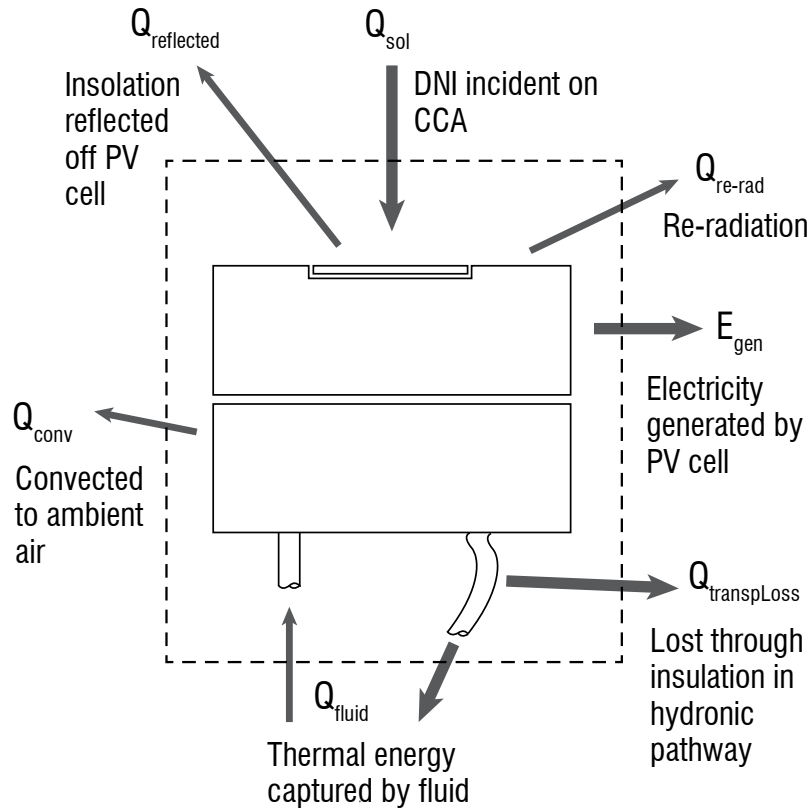


Figure 53. Thermal energy balance control volume of the hydronically cooled concentrator-receiver.

To characterize the thermal generation potential of the ICSF system, the energy balance at the concentrator-receiver module must be understood. The mechanisms of energy flow are described in Figure 54, with relevant parameters during an optimum operational state listed in Table 11.

Table 11. Sample conditions of concentrator-receiver steady-state thermal model.

Conservative estimates indicate that 25% of solar flux that reaches the CPV will be transferred to HTF under typical instantaneous operating conditions, although day-long efficiency would be higher (due to lower HTF temperatures during warm-up periods).

Term, Concentrator-Receiver Steady State Thermal Model	Value
HTF flow rate	1.9 ml/s
Thermal Resistivity of HX	0.15 K/W
Temperature of HTF at inlet	65 °C
Ambient Temperature	25 °C
Receiver Emissivity	0.95
Cell Reflectivity	0.05
Radiating Area of Receiver	0.005 m <sup>2</sup> 50 cm <sup>2</sup>
Convective Surface Area of Receiver	0.005 m <sup>2</sup> 50 cm <sup>2</sup>
Surface Convection Coefficient of Receiver	15.0 W/m <sup>2</sup> -K
Transport Tubing Overall HT Coefficient	0.2 W/K
DNI Input	35.7 W
DNI Penetrating Glazing	40.5 W
DNI Glazing-Exterior, best case	44.6 W
Steady State Temperature	66.75 °C
Steady State HTF Heat Gain	-11.6 W
Steady State HTF Temperature Gain	1.5 °C
Thermal Collection Efficiency (Relative to DNI Incident on Glazing)	26 %
Thermal Collection Efficiency (Relative to DNI Through Glazing)	29 %

A sensitivity study has been done of the thermal characteristics of the module's concentrator-receiver, indicating small convective and radiative thermal losses at the receiver, relative to electrical generation, losses in transport, and the heat captured in the HTF through the water block heat exchanger. As working fluid temperatures rise, thermal efficiency decreases, as insulation losses increase (see Figure 54). The nominal HTF inlet temperature is expected to be 65°C, to provide energy to the sorption chiller in its most efficient COP range.

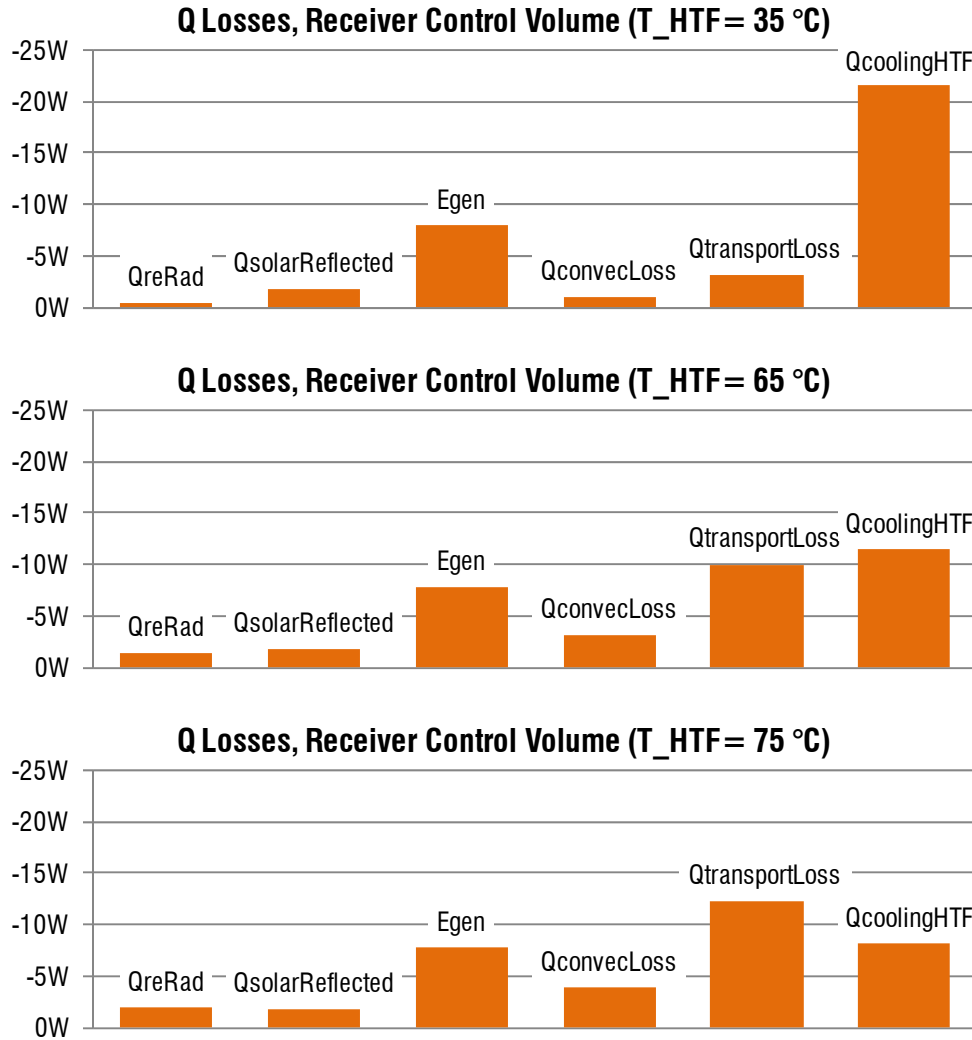


Figure 54. Energy losses of concentrator-receiver at steady state and operating temperature ranges. Thermal balance of concentrator-receiver at steady state indicates that under standard operating conditions (inlet HTF temperature = 65°C) thermal collection efficiency is 25%. Improving in-array insulation methods increases this performance.

The receiver control volume energy balance model includes both assumed values and empirically derived values. Electrical generation, insulation levels and transport mechanism conductivity were determined from observed experimental data (see Figure 55). Values for CCA reflectivity, re-radiation, and surface convection coefficient were assumed, conservatively, to err towards over-estimating the impact of these effects.

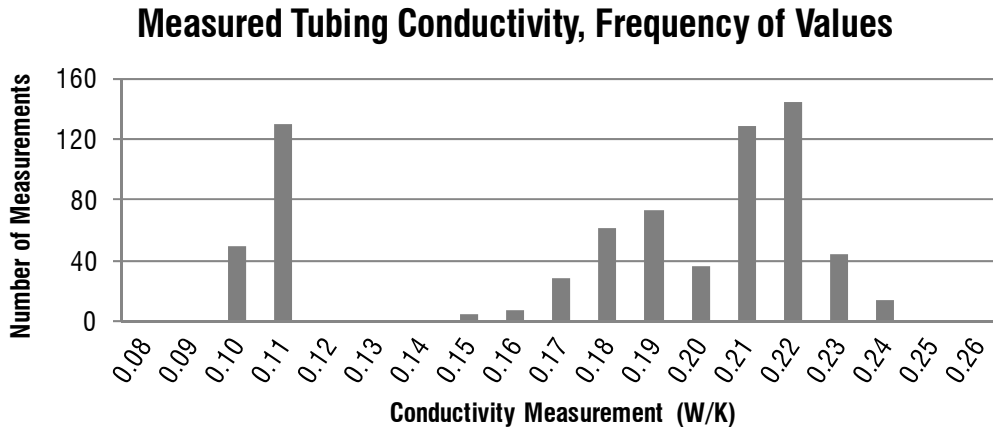


Figure 55. Measurements of thermal conductivity of tubing runs interstitial to module heat exchangers. Data taken suggests range of actual conductivity values, with UA=.24 W/K as upper boundary.

With reasonable parameters for the receiver energy balance model in place, observed performance of the ICSF prototype can be checked. For instance, lower-than-expected measured thermal gain in the working fluid lead us to inspect module heat exchangers, some of which had become fouled or un-glued from their respective CCAs. As a result, we have improved filtering and switched to a pasted (not epoxied) thermal junction between the water block and the CCA.

### 3.3.5.3 Concentrator-Receiver Steady State Heat Pipe Thermal Model

The thermal performance of a heat pipe mechanism for transporting heat out of the ICSF array has been briefly analyzed, as an alternative to the water-block heat exchanger for each module CCA. A heat pipe has the advantage of being potentially self-pumping: mass transport, and therefore heat transfer occurs without adding work to the system and attendant parasitic losses. Regarding thermal collection efficiency, a heat pipe mechanism would perform similarly to a hydronic loop, assuming the dimensions of both conduits types were roughly similar, as like-scale components would be insulated similarly. The heat pipe has the advantage of being somewhat defined performatively by the size of its condenser section. Since the condenser section would be out of the active region of the ICSF array, it can be made quite large, to facilitate heat transfer to the next leg of the collection system, whether that is another transport method, or a buffer for collected thermal energy.

It should be noted that the need for liquid recirculation likely demands a loop-type heat pipe design, which is specialized. Our industrial collaborator Thermacore has pioneered the production and application of specialized heat pipe types, including loop heat pipes, and we believe this topic to be a fruitful avenue of joint research with their development team.

### 3.3.5.4 Parasitic Losses Modeling

Cooling of CCAs in the current ICSF prototypes is done via coolant pumped through hydronic circuits that string individual modules together, most commonly in step with the modules in one physical array stack. Modeling of this power draw can be done with the relationship for incompressible pump energy (Equation 17), and Figure 56 describes a range of pumping conditions, with nominal rates for the current prototype highlighted.

$$P_h = \eta \dot{m} \rho g h$$

Equation 17. Incompressible pumping power.

Where  $P_h$  is pumping power,  $\eta$  is pump efficiency,  $\dot{m}$  is mass flow,  $g$  is gravitational acceleration, and  $h$  is pump head.

### Parasitic and Pumping Losses

		HTF flow per string (g/s)											
		0.5	0.8	1.1	1.4	1.7	2	2.3	2.6	2.9	3.2	3.5	3.8
Pressure Head	1m	12%	16%	<b>20%</b>	23%	27%	31%	35%	38%	42%	46%	50%	53%
	2m	18%	26%	<b>33%</b>	41%	48%	56%	63%	71%	78%	86%	93%	101%
	<b>3m</b>	<b>25%</b>	<b>36%</b>	<b>47%</b>	<b>58%</b>	<b>70%</b>	<b>81%</b>	<b>92%</b>	<b>103%</b>	<b>114%</b>	<b>126%</b>	<b>137%</b>	<b>148%</b>
	4m	31%	46%	<b>61%</b>	76%	91%	106%	121%	136%	151%	166%	180%	195%
	5m	37%	56%	<b>75%</b>	93%	112%	131%	149%	168%	187%	205%	224%	243%
	6m	43%	66%	<b>88%</b>	111%	133%	156%	178%	200%	223%	245%	268%	290%
	7m	50%	76%	<b>102%</b>	128%	154%	180%	207%	233%	259%	285%	311%	337%
	8m	56%	86%	<b>116%</b>	146%	175%	205%	235%	265%	295%	325%	355%	

Figure 56. Coolant pumping losses relative to electrical generation.

Current ICSF prototypes are cooled via coolant pumped to each module. Nominal parameters (3.2m head, 1g/s flow) results in 50% parasitic loss. Research underway in multiphase thermal transport at the module scale would negate pumping power, leaving negligible parasitic losses of motor drive and controls.

As the current research trajectory for ICSF is towards multi-phase thermal transport within the array (rather than hydronic transport), the building energy simulations undertaken in this period employ an assumption of nil pumping power.

Parasitic losses include the draw from servomotors and their controllers. As measured from the current prototype, with 24 modules in four stacks, the combined parasitic power draw (pump excluded) is 23W. Relative to the nominal module output of 12W, the parasitic losses are 8%. The losses are expected to decrease as module balancing is done in further design iterations and pre-loading of the pitch-axis servomotors is reduced. Due to this expected reduction, parasitic losses from the motors was neglected in building-scale simulations.

### ***3.3.5.5 Hydronic Thermal Transport Modeling***

To design the use of façade-sourced thermal resources, it is necessary to understand how heat can be successfully transported between systems. To this end a heat transfer model has been developed that models the individual components of the ICSF thermal collection strategy and generates expected operational states for a range of collector configurations.

Currently this hydronic transport tool overlaps in capability with both the ICSF output simulator and the concentrator-receiver energy balance model. In future work the various models will be linked under

#### ***3.3.5.5.1 Thermal Model Approach***

Figure 57 shows the heat transfer of ICSF Generation 8 with an equivalent thermal resistance diagram. It is important to note, only an order of magnitude for the heat losses is wanted from the model. Increasing the complexity of the simulation is extremely time consuming and meaningless after a certain point considering all the empirical correlation used, which are skewed by a significant margin of error. Considering the variability and the uncertainty of the experimental conditions, the initial thermal resistance diagram becomes simplified from treating radiation and surface contact thermal resistance as negligible.

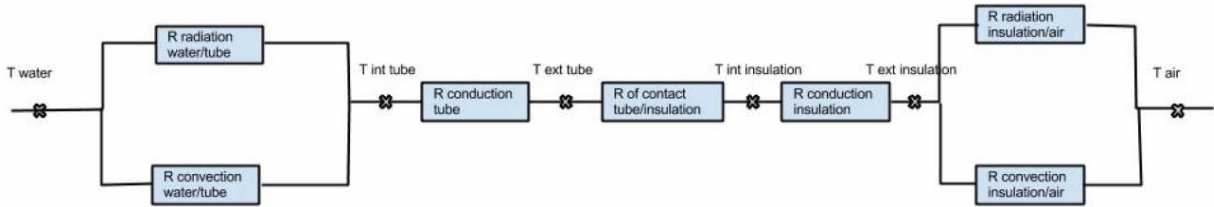


Figure 57: Equivalent Thermal Resistance of the Hydronic Distribution System.

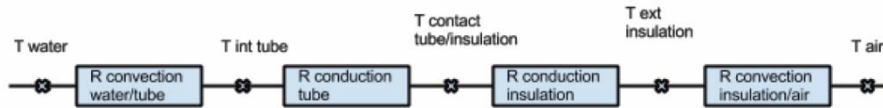


Figure 58: Simplified Model (Radiation and Contact Resistance removed).



Figure 59: Equivalent Thermal Resistance from combining series resistance.

The equivalent resistance expression from Figure 58:

$$R_{eqv} = R_{conv,i} + R_{cond,t} + R_{cond,i} + R_{conv,o}$$

Equation 18: Equivalent thermal resistance

The heat loss across a section of tubing can therefore be calculated by:

$$Q_{loss} = \frac{T_{water} - T_{air}}{R_{eqv}}$$

Equation 19: Heat loss for section on pipe.

### 3.3.5.5.2 Thermal Model Implications

Utilizing the model to determine best practices for distribution and storage of thermal energy have led to more efficient plumbing strategies for the ICSF Generation 8 hydronic systems. The silicon tubing network initially proposed for the array consisted of the tube lengths between modules to weave up the stack of collectors, through the module's supporting axis and back out to the receiver; resulting in ~1 meter of silicon

tubing between modules (Long Run). An alternative piping strategy was purposed to shorten the lengths between modules by going from one receiver directly to the next (Short Run). Figure 60 shows the comparison between the two piping approaches. From Figure 61; the temperature achieved after running the simulation for 5 hours is 72°C with the short run, and 50°C for the long run. Therefore, by shortening the tubing length there is a 44% percent improvement. Moreover, this modification leads an improved collection efficiency. At 25°C the simulated efficiency was 74.8% instead of 64.8%, and at 45°C it was 47.7% instead of 14%. This improvement is due to fact that reducing the tubing length will also reduce the surface area exposed to the air, which will then result in decreased thermal losses. Additionally, shortening the tubing length also represents an economic gain as 3 times less tubing is required.



Figure 60: Alternate coolant flow paths, short (left) and long (right).

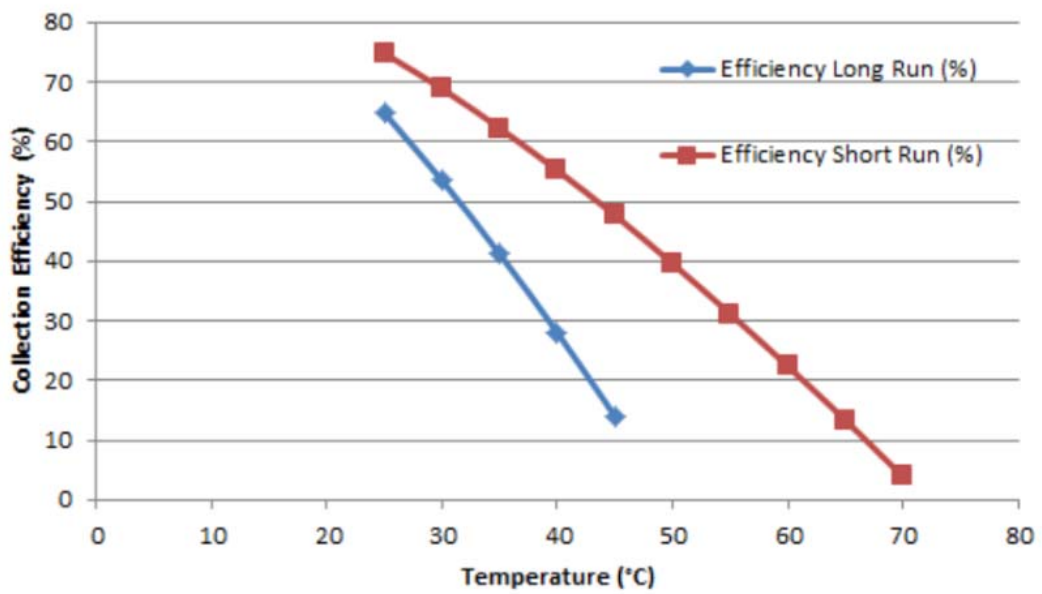


Figure 61: Collection efficiency relative to tank temperature for short and long coolant flow paths.

### **3.3.6 Thermal Energy Utilization Simulations for Internal Systems Applications**

#### **3.3.6.1 Cooling Capacity from ICSF**

With the power production characteristics of a façade-integrated concentrating solar collection system determined, the impact the system has on the cooling of a building can be extrapolated. Cooling capacity results from several functions of the concentrating façade, namely: the active energy collection which can be used to drive chiller processes, and the reduction in solar gain in perimeter spaces.

Thermal energy collected by the concentrating facade can be used to drive sorption chilling, or other heat engine-driven chilling. To model this, the thermal characteristics of small scale sorption chilling unit are modeled, and the thermal power output from the façade system simulation is applied as a power source in a step-wise fashion. For the sorption unit specifications, a commercially available small-scale adsorption chiller, the ACS 08 from SorTech AG is characterized.

Additional cooling capacity is represented by the interception of solar irradiation by the concentrating facade: energy produced, both thermal and electrical, can be subtracted from thermal loads in perimeter building zones adjacent to the enhanced envelope, given appropriate arrangement of factors in the model. The building simulated in this study has a façade that is almost entirely glazed, which is characteristic of modern commercial architecture, and the thermal loads in perimeter zones are largely due to insolation penetrating the glazing and heating interior space. Therefore, it is appropriate to model the interception and sequestration of those loads as direct subtractions from loads presented to the building's environmental control systems.

To supplement cooling capacity, the electrical power produced by the concentrating facade can be used to drive traditional vapor-cycle air conditioners. This is modeled using typical coefficients of performance for such units, and conversion efficiencies typical of electrical inverters that produce AC current from the DC output of the facade. In this simulation, the typical COP, set to 3.5, is increased by 1.0 to 4.5, to represent the

subtraction of electrical power that would otherwise be supplied to the building to power the air conditioning process, and must be compensated for by that process.

### 3.3.6.2 Adsorption Chiller Characterization

The SorTech ACS 08 adsorption chiller is modeled in this analysis via operational curves supplied by the manufacturer. The available curves relate coefficient of performance and output cooling power to heat rejection circuit temperature, and driving circuit temperature, given two performance envelope boundaries—one for high efficiency (“Eco”) mode, and another for high-capacity (“Power”) mode (Figure 62).

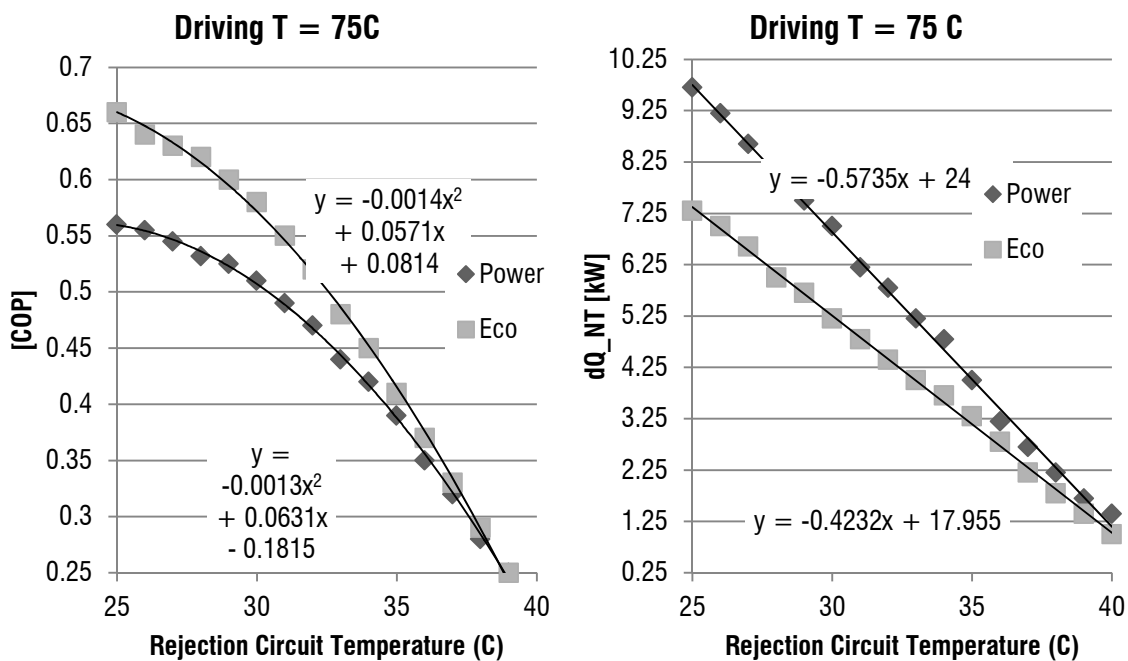


Figure 62. SorTech chiller performance curves.

At a given driving circuit temperature, the coefficient of performance and the capacity of the SorTech ACS 08 adsorption chiller are functions of rejection circuit temperature and operation state (Power or Eco). The curves provided by the manufacturer have been matched with equations for analytical purposes.

A nominal operating temperature for the driving circuit of 75C is assumed, which helps to reduce the indeterminate variable space of the SorTech operation. Further, the units are initially assumed to operate per their Eco mode curves. The drawbacks to these assumptions are economic: lower capacity and higher efficiency result in better energy use, which trades off against a possible increase in number of units that must be

installed to meet a given peak load condition. Other factors, including the overall energy available at a site, would realistically inform this decision.

SorTech AG supplies two sets of curves, corresponding to different chilled water output from the units. One set is calibrated to temperatures useful for fan coil hydronic transfer units; the second set is calibrated to higher chilled water output, which is typical when supplying cooling power to radiant ceiling panels. Radiant panels must be operated so that they don't approach dew point temperatures, for moisture control reasons, and therefore have less cooling capacity in a typical installation in each space. Given the relatively low loads resulting from ICSF incorporation in the envelope, it is appropriate to assume radiant panels are used to transfer cooling power to the zones, and therefore this set of SorTech performance curves, which model higher efficiency, can be used.

Given these constraints, the SorTech operation is modeled in conjunction with atmospheric conditions. It's determined that the nominal COP (roughly .65) can be maintained for most of the year in the NYC climate with infrequent application of the SorTech re-cooler's sprayer function, and in fact, leaving the re-cooler in dry operation all the time has negligible impact on overall cooling capacity. Real-time chilling (without utilizing some sort of re-cooling temperature storage) in Phoenix requires the evaporative function during most operational hours to maintain the nominal COP. In this simulation, for the Phoenix climate, the sprayers are set to engage when the COP would otherwise dip below 0.4, based on ambient dry bulb temperatures.

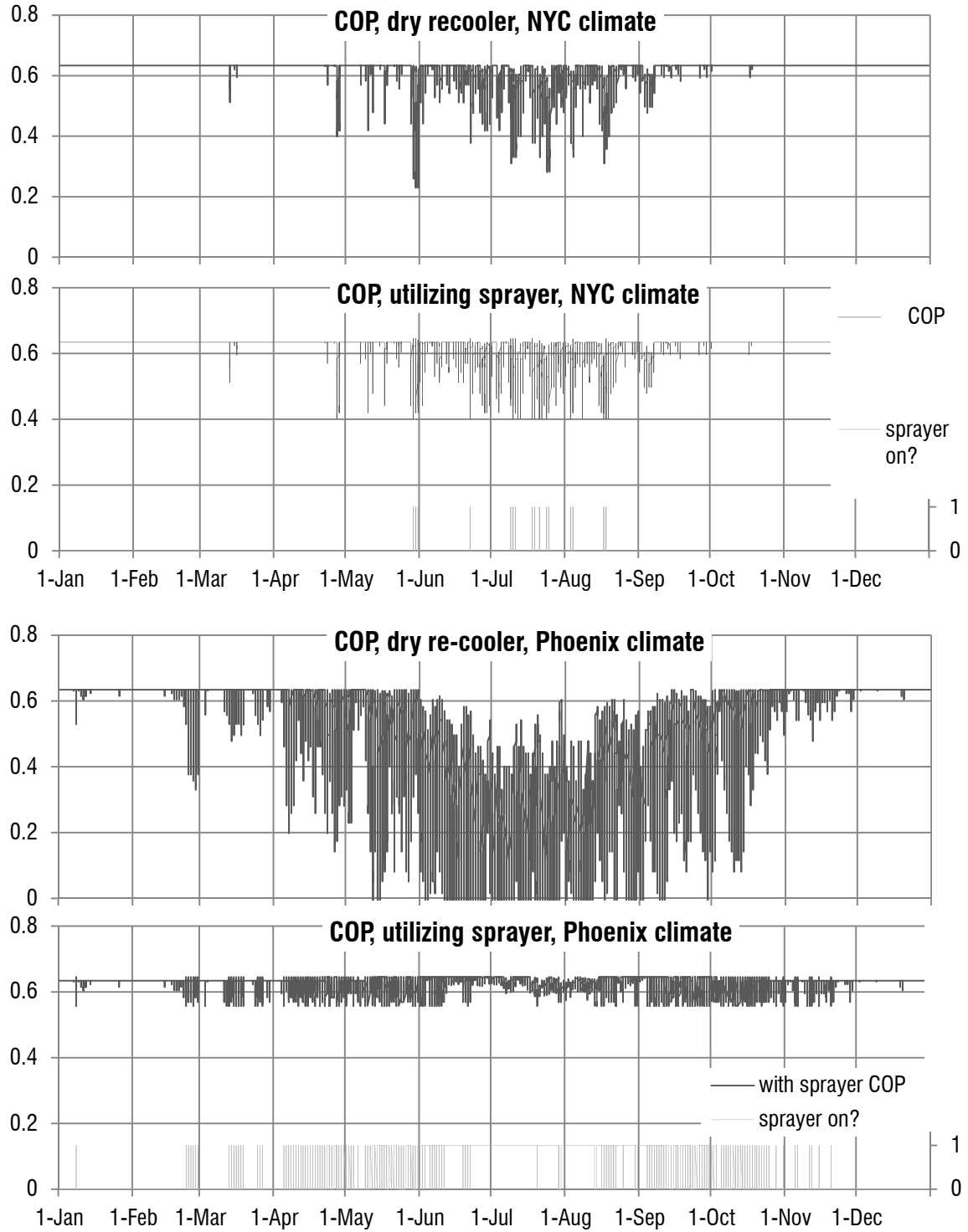


Figure 63. Chiller performance (COP) augmented with evaporative cooling.

The SorTech-supplied re-cooler incorporates a sprayer system. The operation described in this figure assumes that evaporative cooling kicks in when the COP dips below 0.4 if unassisted.

### 3.3.6.3 Calculations of System Performance and Sizing: Thermal Storage Sizing

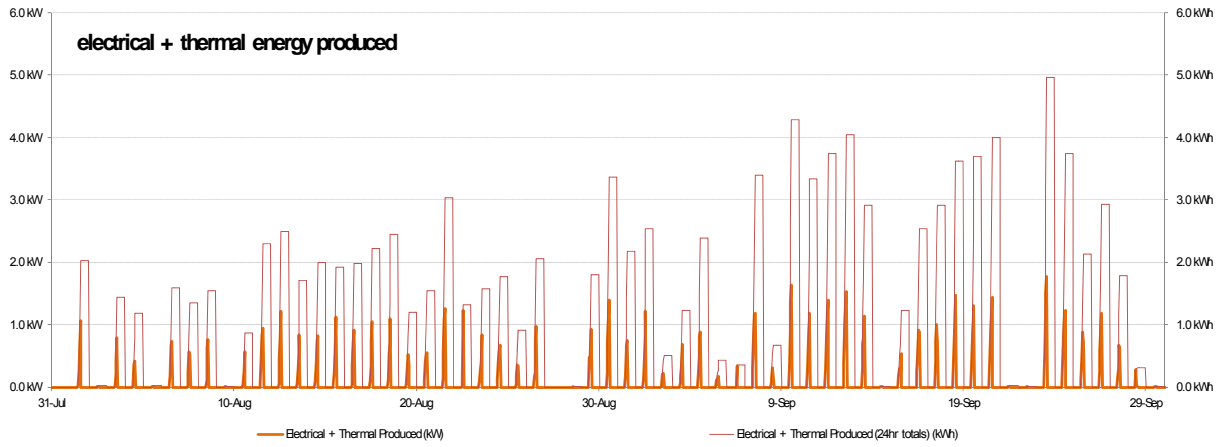


Figure 64. Energy produced by 5-bay ICSF system, hourly, and by daily totals.

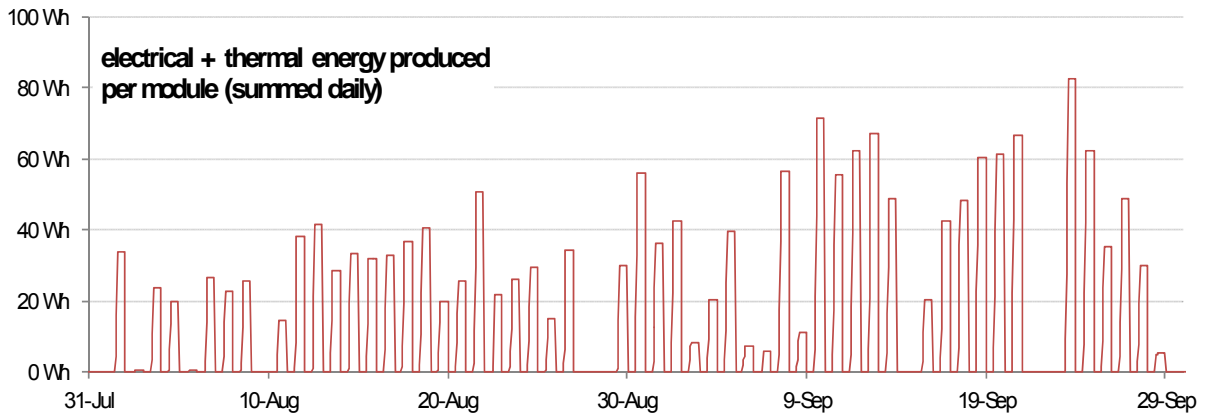


Figure 65. Per-module total energy output per day.

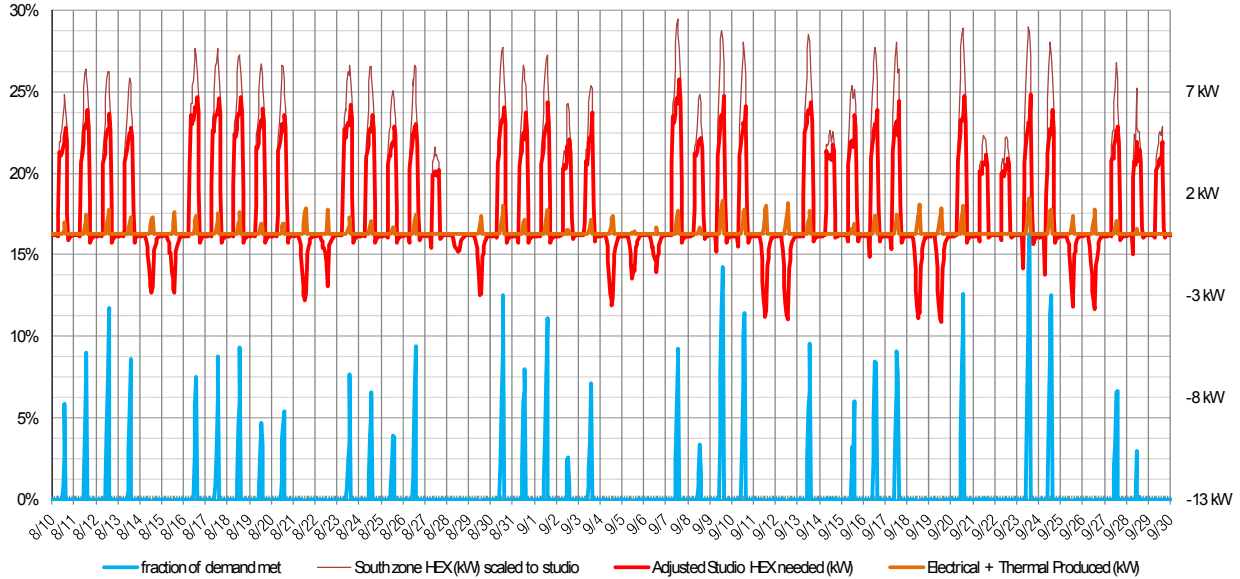


Figure 66. Relation of studio space cooling demand and ICSF production (hourly).  
Assumptions made for maximum gains, building shading and ICSF interception.

**Daily max T in buffer tank, relative to energy collected per day and volume of water in buffer system (in °C, assuming insulation losses in tank only)**

	(kWh)						
(liters)	1.00	1.31	1.72	2.25	2.94	3.86	5.05
30	44	52	63	77	96	120	152
39	38	44	53	64	78	97	121
51	33	38	45	53	64	79	98
67	29	33	39	45	54	65	80
88	26	30	34	39	46	54	66
116	24	27	30	34	39	46	55
152	21	24	27	30	35	40	47

**ASSUMPTIONS**

- u is constant, at value equivalent to steel at 130C in quiescent air, with 50mm insulation
- second calculation is done as simple fraction of max Q vs. max Q- losses.
- tank height = 3x diameter

Figure 67. Sizing of buffer tank vs. expected energy collected by ICSF.

**3.3.7 Case Study: Towards Energy-Positive Buildings Through a Quality-Matched Energy Flow Strategy**

To explore this concept, a medium-size office building was modeled with systems that include: a multifunctional envelope collector (characterized in previous studies), hydronic thermal storage and distribution at three temperature ranges, adsorption

chillers, and water-water heat pumps. As modeled, the collectors generated both electricity and thermal energy at high temperatures, while transmitting diffuse light and reducing unwanted solar heat gains and direct illuminance. The balance of systems satisfied cooling, heating, and hot water demands. Relative to the cooling-dominated baseline models, the revised models demonstrated greater annual and diurnal oscillation in heating and cooling demands, suggesting the effectiveness of the concept, and it is surmised that revised controls strategies would demonstrate additional energy savings through thermal storage and recuperation. Electrical consumption was modeled to decrease 71% in a humid-continental climate (New York City), and on-site net-zero electrical use was demonstrated in both a hot-desert climate (Phoenix) and in a dry-summer subtropical climate (Mountain View). Peak grid electricity demands decreased 6%, 28%, and 20% respectively. It is projected that with revised controls strategies and ground-source heat exchange, energy-positive behavior could be demonstrated.

#### ***3.3.7.1 Introduction: Framework for Valuing Climatic Energy Resources for Net-Zero and Net-Generating Buildings***

A great deal of energy can be sourced from a building's local climate, particularly from the sun. Across a range of climates, the exergy value of the insolation that falls on a medium-scale commercial building's envelope (roof and façade) far exceeds the building's own use (Table 12).

Table 12. Energy use intensity, per floor area, relative to incident insolation.

Medium-scale office building: 5000m<sup>2</sup>, three stories, south-oriented, ASHRAE 90.1-2013 standards.

<i>(in kWh/m<sup>2</sup>-yr)</i>	Incident Direct + Diffuse Insolation	Electricity Use	Electricity + Fuel Use
New York City (NYC)	820	92 (11%)	160 (19%)
Phoenix (PHX)	1130	127 (11%)	139 (12%)
Mountain View (MTV)	980	91 (9%)	120 (12%)

However, despite the abundance of climatic energy sources, net-zero energy building (NZEB) and energy-positive building (EPB) strategies are not currently widespread, and building-integrated strategies for harvesting and applying climatic resources—that are both architecturally and economically viable—are limited. For viability, besides being affordable, such strategies must be effective and efficient. To be successful, a solar collection and application strategy must maintain both the quality and exergy content of building-incident insolation while providing occupants with the conditions they value, such as the psychological connection to the greater world. By integrating selective solar cogeneration and daylighting with thermal energy storage and re-distribution, the Quality-Matched Energy Flow (Q-MEF) concept described here is such a strategy. By adopting this integrated strategy, increasing the resources available to a building on-site, NZEB and EPB projects could become more widespread.

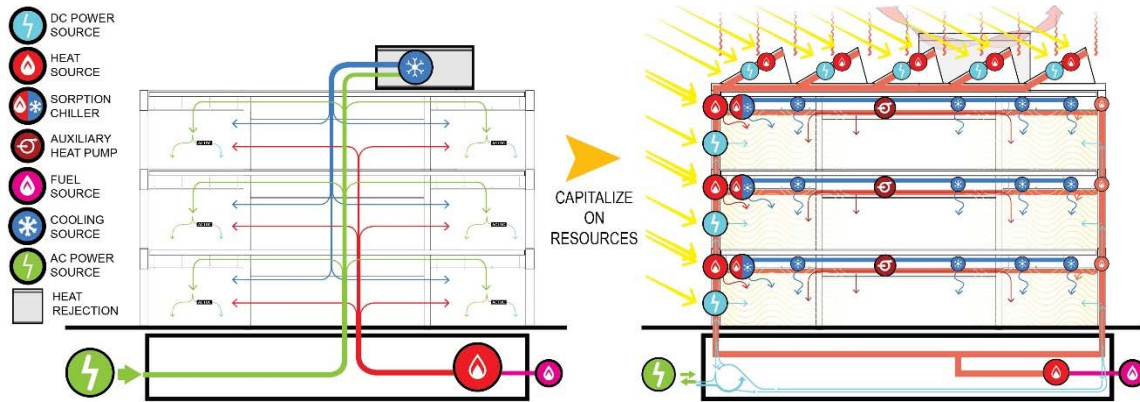


Figure 68. Transitioning from centralized systems (grid-source optimized) to distributed, integrated systems (climate-sourced optimized).

NZEB strategies typically follow a three-tier approach to energy efficiency: load reduction through careful design and morphology is foremost, followed by use of passive systems such as shading, and lastly the addition of active systems such as energy harvesting. Although load reduction is crucial, in contemporary architecture this approach has resulted in façade systems that supply good daylighting and ventilation but provide limited possibilities for energy harvesting.<sup>55,56</sup> Alternatively, active energy harvesting and exchange can be treated as a fundamental responsibility of the building envelope, and energy generation can be done while loads are reduced (as unwanted solar gain is redirected towards useful ends). The goal of envelope systems then becomes to redistribute the abundant light, heat, and power resources available at the building's envelope, transferring solar energy towards the building's demands, and when necessary, transforming incident solar energy into consumable forms. Q-MEF approaches this goal through distributed coolth storage and (thermally-driven) adsorption chillers, and a transparent, optically-concentrating cogenerating solar collector integrated into in a building's envelope design. The collector (which has been validated experimentally<sup>57</sup>) transmits diffuse irradiance for daylighting and views, and

<sup>55</sup> Briegleb, T. (Ed.). (1999). *Ingenhoven, Overdiek und Partner - High Rise RWE AG Essen*. (T. Kommerell, Trans.) (1st ed.). Birkhäuser Basel.

<sup>56</sup> Grinberg, M., Tai, C.-K. J., & Antia, P. (2013). NREL: Largest Net Zero Building. *ASHRAE Journal*, 55(9), 36–44.

<sup>57</sup> See Chapter 3.

strips out direct normal irradiance, either transforming the energy into electricity or collecting it as thermal energy. Rather than exacerbating cooling demands, insolation can therefore be used directly: electricity can power equipment, and thermal energy can drive the chillers and fulfill heating demands. The generated heating and cooling capacities can be stored and circulated through a building via thermally massive hydronic circuits, redistributing these resources as necessary, maintaining small but useful potentials (temperature differences), rather than immediately dispersing generated potential into the built environment, as with passive approaches to thermal mass control. In concept, an integrated system of the multifunctional envelope collector and thermal distribution can maintain, as much as possible, the quality of the solar resource (through daylighting), and the exergetic content, by collecting a high fraction of direct irradiance at elevated temperatures.

### **3.3.7.2 Methods: Precursor Models and Post-Processing**

To evaluate the effects of Q-MEF on a building's energy flows and consumption, a model was constructed by combining (through post-processing) precursor building energy models of a medium-scale commercial office building (generated in EnergyPlus<sup>58</sup>) with an analytical model of an active façade system (BITCoPT). The Q-MEF model was configured in two ways, analyzed in different climates, and compared to two baseline building energy model configurations. In addition to incorporating as inputs the two primary precursor models (BEMs and BITCoPT), the Q-MEF model incorporated functions representing the behavior of: hydronic thermal storage and redistribution, thermally-driven chillers, electrically-driven auxiliary heat pumps, a deep-mullion curtain wall cavity, and fan-powered air volume exchanges. The models and functions were integrated through post processing in time-step fashion, and basic controls schemes were devised to direct the flow of energy as necessary based on

---

<sup>58</sup> Crawley, D. B., Lawrie, L. K., Winkelmann, F. C., Buhl, W. F., Huang, Y. J., Pedersen, C. O., ... Glazer, J. (2001). EnergyPlus: creating a new-generation building energy simulation program. *Energy and Buildings*, 33(4), 319–331. [http://doi.org/10.1016/S0378-7788\(00\)00114-6](http://doi.org/10.1016/S0378-7788(00)00114-6)

system states in earlier time steps. Figure 69 is the Q-MEF model structure, showing incorporation of precursor models and time step functions.

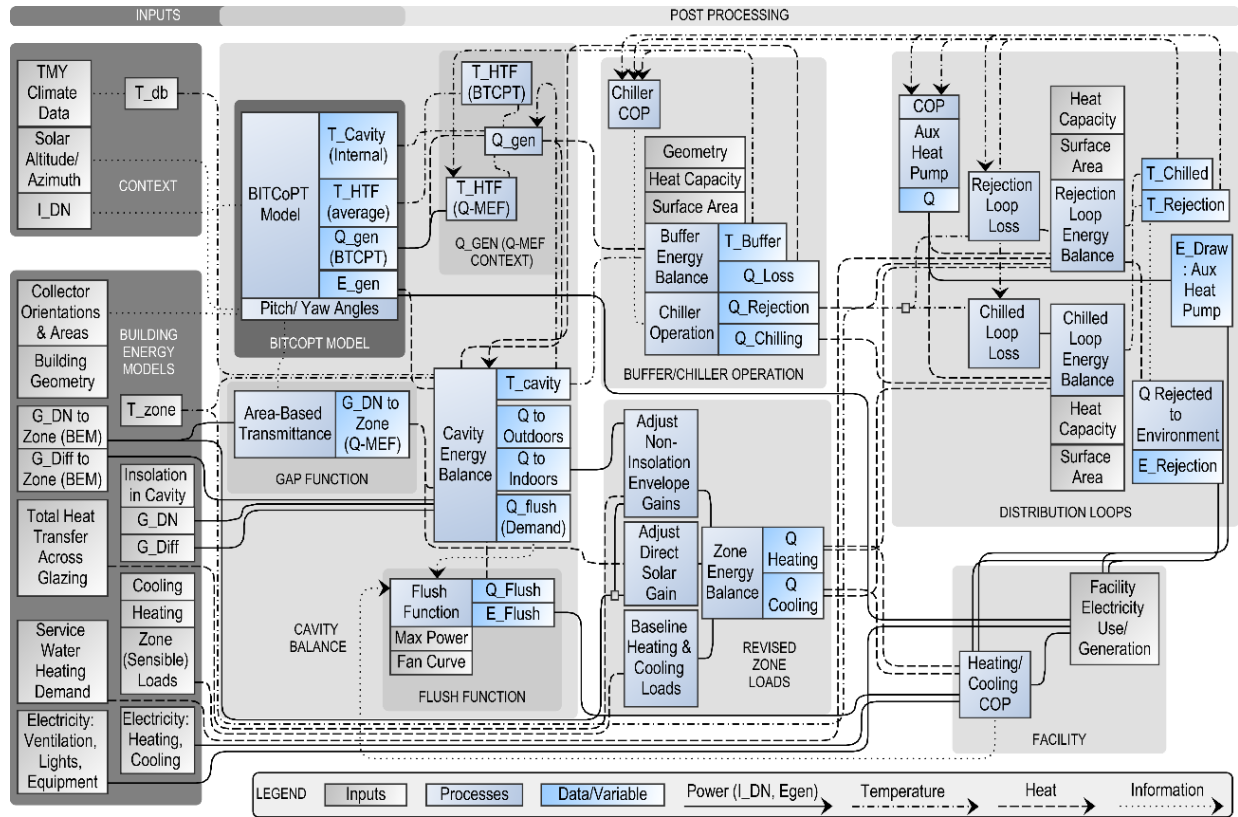


Figure 69. Q-MEF model, structure and variable flow.

The application of different modeling environments to generate the four studied configurations is shown in Figure 70.

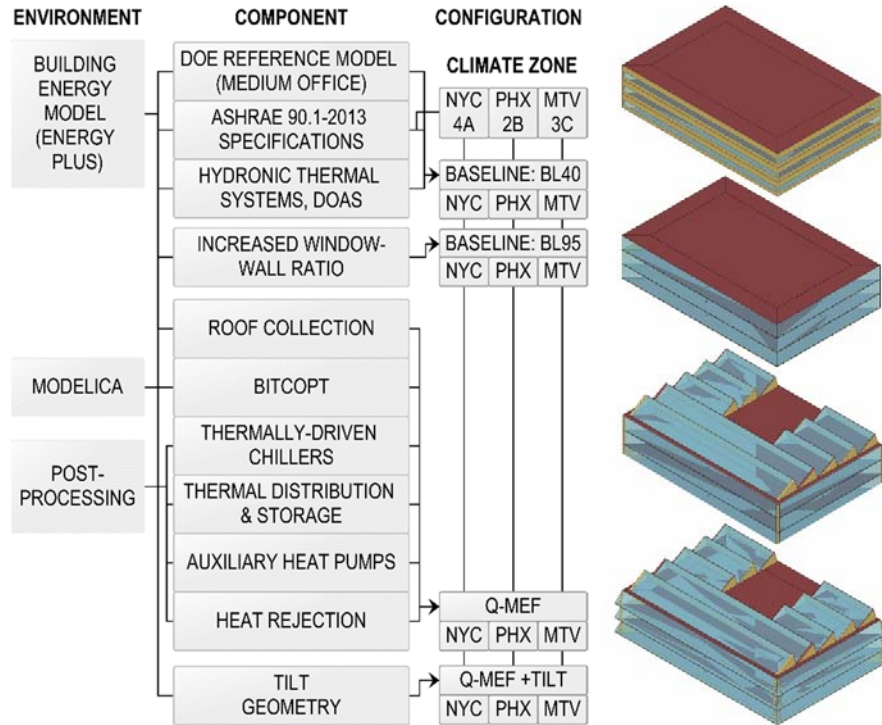


Figure 70. Building configurations and components from modeling environments.

### 3.3.7.2.1 Thermal Energy Strategy: Use and Redistribution

Under the Q-MEF rubric, solar thermal energy is concentrated and collected at the building envelope, passed through subsystems, applied to do work where possible, and eventually rejected to climatic sinks. In the modeled HVAC systems, heating and cooling capacity was developed by two mechanisms: by small-capacity sorption chillers distributed at the building's envelope, driven by collected thermal energy, and by auxiliary water-water heat pumps that supplemented the operation of the distributed chillers. In common with the baseline BEM, heat was distributed throughout the modeled building via two circulating hydronic loops. A heating loop (also used for heat rejection) was maintained at super-ambient or near-ambient temperatures, depending on the season. A chilled loop was maintained at sub-ambient temperatures. The two loops connected all the building's conditioned zones and envelope collection areas (Figure 71).

Although both baseline and Q-MEF models used dual hydronic circuits to distribute heating and cooling, there were differences in the systems employed. The baseline model employed a boiler for the heating loop and an electrically-driven, air-

cooled chiller for the cooling loop. In the Q-MEF model, the loops were thermally coupled with both sorption chillers and auxiliary heat pumps, so heat was pumped from the chilled loop to the heating (rejection-range) loop. The rejection-range loop additionally had an auxiliary boiler and a rejection circuit, which added or subtracted energy as necessary to keep the loop's temperature in target range. In the Q-MEF model, hydronic distribution was thermally massive, serving to source and sink energy both from the zone heating and cooling demands and from the sorption chillers that were driven by envelope-sourced thermal energy. The thermal network in the baseline systems addressed all zone heating and cooling demands in parallel. In the Q-MEF model zones were serviced sequentially, with systems on sub-loops that were serviced by circulator pumps, adding energy to or subtracting energy from the fluid thermal mass as it circulated through the loops (Figure 71). The circulation served to equalize loop temperatures, distributing heating and cooling capacity throughout a building.

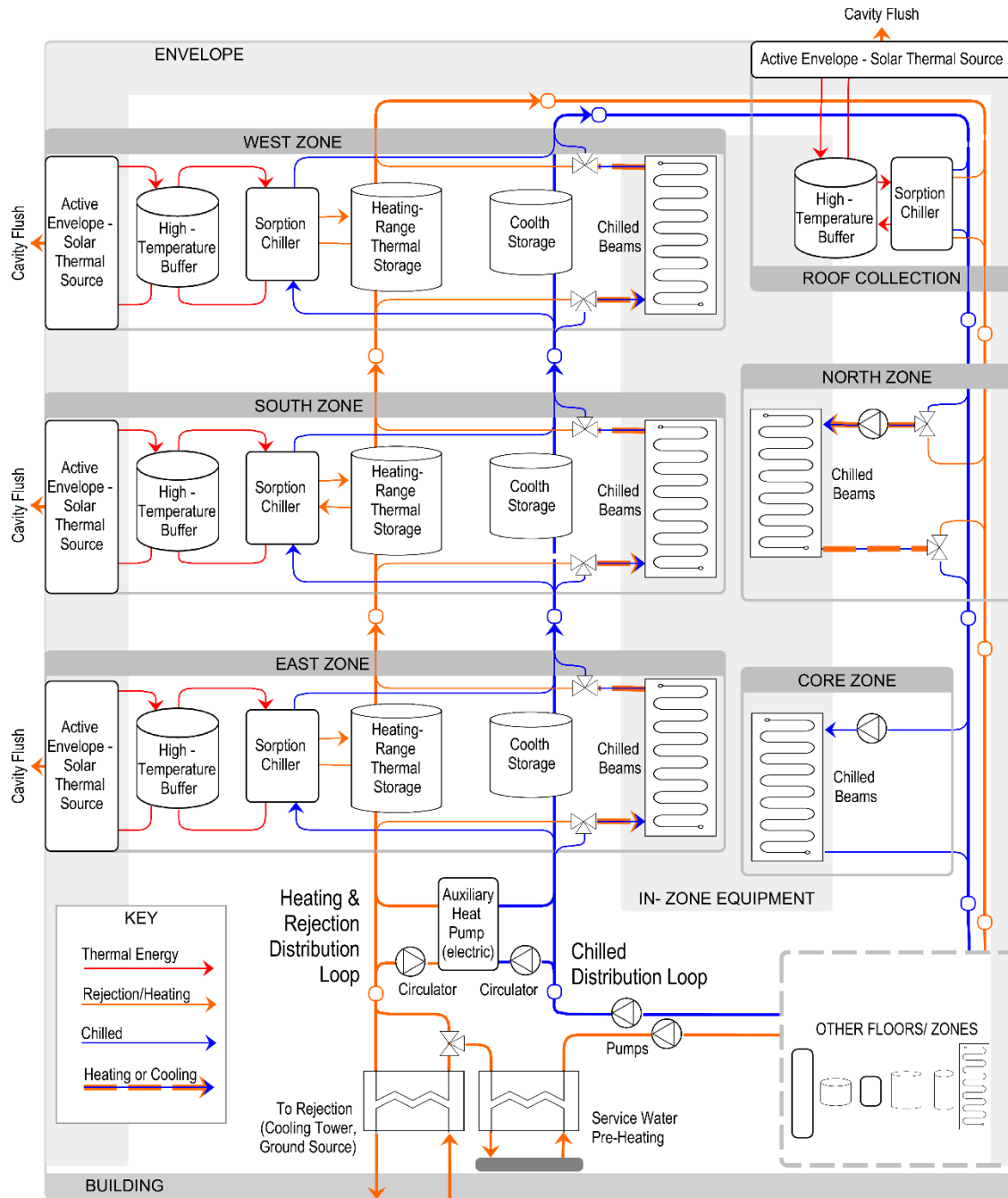


Figure 71. Plumbing schematic showing chilled and rejection-range distribution.

Storage or distribution applied at three temperature ranges. One floor shown; remaining floors arranged similarly.

In both the baseline and Q-MEF configurations, heating and cooling in a zone was modeled as transferring energy through baseboard units or chilled beams, from the rejection-range loop or to the chilled loop, respectively.

In the Q-MEF model, thermal energy collected by BITCoPT was used to drive sorption chillers and provide heat. The glazed areas of the precursor BEMs were defined to incorporate the effects of BITCoPT collectors.<sup>59</sup> In post-processing, each collector fed a thermal buffer tank, which in turn was plumbed to a chiller. When a buffer's temperature rose high enough to drive the connected chiller at a reasonable COP ( $COP_{chiller} \geq 0.5$ , requiring  $T_{buffer} \geq 60^{\circ}\text{C}$  or higher, depending on  $T_{rej}$ ), the chiller engaged, pumping heat from the chilled distribution loop to the rejection-range loop. In addition, if either the chilled loop became too hot or the rejection-range loop became too cold, the auxiliary heat pumps engaged, pumping heat in parallel to the thermally-driven chillers.

Pre-heating for service hot water demands was modeled to occur through a water-water heat exchanger, by subtracting energy from the rejection-range loop balance according to the difference between the water supply temperature reported in the BEM and the rejection-range loop temperature, less a  $2.0^{\circ}\text{C}$  approach (Figure 71). The quantity of pre-heating was subtracted from the boiler usage of the precursor BEM on a time step basis.

Pre-heating for the DOAS air intake was also modeled to occur through a water-water heat exchanger, by subtracting energy from the rejection-range loop balance according to the difference between the air supply temperature reported in the BEM and the rejection-range loop temperature, less a  $2.0^{\circ}\text{C}$  approach. The quantity of pre-heating was subtracted from the air heating coil usage of the precursor BEM on a time step basis.

By modeling envelope-integrated solar thermal collection with distributed thermal systems and circulating thermal mass, it was possible to represent the application of thermal energy both as a driving force (for sorption chillers, at high temperatures) and as useful heat (for zone demands and pre-heating), taking advantage of both the exergy and energy value of the collected energy.

---

<sup>59</sup> See Chapters 3 and 4.

### 3.3.7.2.2 Inputs: Multiple Climates

The Q-MEF model was analyzed in three climates that represent a range of situations and modes of operation for a building's systems (Table 13). New York City (LaGuardia TMY3 data) was chosen as an example of fluctuating climate conditions: the climate is continental and seasonally humid, with varying weather patterns and strong seasonal temperature swings. (Although the city of New York is dense, with many sites shaded by surrounding structures, this study parametrized climate context, not site, and no external shading was defined in NYC or other climates.) Phoenix, as an arid subtropical desert with high insolation, high mean temperatures, and large diurnal swings, was chosen to illustrate a strong solar resource. Mountain View is in a semi-arid Mediterranean climate with mild temperatures and a significant solar resource. TMY3 data was used to represent the climate conditions.

Table 13. Analyzed climate types.

Location	ASHRAE Zone	Climate Description	Degree Days (Base 10°C) CDD/HDD	Degree Days (Base 18.3°C) CDD/HDD	$T_{db(99\%)/T_{db(1\%)}$ (°C)
New York City	4A	Humid subtropical/ continental	2118/962	672/2557	31.8/-8.2
Phoenix	2B	Subtropical desert	5067/17	2532/523	42.3/5.2
Mountain View	3C	Warm-summer Mediterranean	2177/64	267/1196	28.7/3.7

### 3.3.7.2.3 Function: Thermal Energy Storage Elements

Two types of thermal energy storage elements (TES) were modeled: the high-range buffer tanks and the distribution loops. One buffer was defined for each solar collector. One cooling loop and one rejection-range loop were defined to service the building. Both TES types were defined to be well-mixed, rectangular tanks with a fixed height ( $h_{TES}$ ) and width ( $w_{TES}$ ). Thermal capacity was a function of TES volume, which (due to the fixed height and width) was defined by TES length ( $l_{TES}$ ). Length therefore varied per the requirements for the heat capacity for a TES:

$$C_{TES} = c_{p, TES} \rho_{TES} h_{TES} w_{TES} l_{TES(i)} \quad (20)$$

The TES exchanged heat in controlled fashion with the building's systems and in uncontrolled fashion with the interior environment, due to losses through their insulated surface areas. The TES energy balances were defined as:

$$C_{Buffer(i)} \frac{dT_{buffer(i)}}{dt_n} = Q_{gen, Facade(i)} + Q_{gen, Clerestory(i)} - Q_{loss(i)} - Q_{chiller, Draw(i)} \quad (21)$$

$$C_{loop, Chilled} \frac{dT_{loop, Chilled}}{dt_n} = \sum_{i=1}^{n_{zones}} Q_{loss(i)} - \sum_{i=1}^{n_{zones}} Q_{chiller(i)} + \sum_{i=1}^{n_{zones}} Q_{cooling(i)} - Q_{heatPumps} \quad (22)$$

$$C_{loop, Rejection} \frac{dT_{loop, Rejection}}{dt_n} = \sum_{i=1}^{n_{zones}} Q_{chiller, Rejection(i)} - \sum_{i=1}^{n_{zones}} Q_{loss(i)} - \sum_{i=1}^{n_{zones}} Q_{heating(i)} + Q_{heatPumps} - Q_{rej} \quad (23)$$

Because the loops interfaced thermally with all the separate occupied zones in a building, they were modeled not as continuous rectangular tanks but as a series of same-sized tanks, plumbed into a loop with insulated piping. A TES's specific heat  $c_{p, TES}$  was equivalent to the specific heat of the storage medium used ( $c_{p, HTF}$ ) as the volume of the balance of the tank materials was negligible. Losses were modeled as heat transferred across the TES boundary (tank walls) assuming insulation of 100mm of polyisocyanurate foam and negligible film coefficients on both interior and exterior surfaces, for an effective thermal resistance of  $R_{TES, wall} = 0.4W/m^2 \cdot K$ . The heat lost from the buffers transferred to the control volume of the curtain wall cavity in which BITCoPT was installed. The heat lost from the distribution loops transferred to the occupied zones. It was assumed that the pumping power required to equalize the temperature

between the storage elements in each loop was equivalent to the power provided by the equivalent circulation pumps in the contributing building energy model.

Buffer TES capacities were sized individually to maximize the yearly chilling work of their attached chillers. The distribution loop capacities were sized to minimize whole-building electrical use (Table 14).

Table 14. Thermal capacities of modeled thermal energy storage (NYC climate).

TES elements	Thermal capacity (kWh/K)	Allowable Temperatures
Buffers, East or West (3X)	0.9	Below 95°C
Buffers, South (3X)	1.4	Below 95°C
Buffer, Clerestory, front	4.9	Below 95°C
Buffer, Clerestory, balance	2.1	Below 95°C
Chilled loop	450	10 to 18°C
Rejection-range loop	583	$T_{out,db}$ to 35°C

#### **3.3.7.2.4 Building Energy Models as Baselines and Inputs**

Four building energy models were developed (using the Open Studio<sup>60</sup> interface for EnergyPlus<sup>61</sup>), which were used in two ways: directly, to define two baseline configurations, and as precursors to define two Q-MEF configurations. The first baseline, “BL40,” reflected the energy usage of the DOE medium office building prototype<sup>62</sup> with a 40% window-wall ratio. The second baseline, “BL95,” demonstrated a higher window-wall ratio of 95%, to demonstrate a fully-glazed curtain wall-type architecture. The third configuration demonstrated Q-MEF systems in a building similar to the BL95 baseline, with additional collector areas in tilted fractions of the model’s roof

<sup>60</sup> NREL/DOE. (2015, September). OpenStudio | OpenStudio. Retrieved November 30, 2015, from <https://www.openstudio.net/>

<sup>61</sup> Crawley, D. B., Lawrie, L. K., Winkelmann, F. C., Buhl, W. F., Huang, Y. J., Pedersen, C. O., ... Glazer, J. (2001). EnergyPlus: creating a new-generation building energy simulation program. *Energy and Buildings*, 33(4), 319–331. [http://doi.org/10.1016/S0378-7788\(00\)00114-6](http://doi.org/10.1016/S0378-7788(00)00114-6)

<sup>62</sup> Commercial Prototype Building Models | Building Energy Codes Program. (2014). Retrieved October 9, 2015, from <https://www.energycodes.gov/commercial-prototype-building-models>

area. The fourth configuration, “Q-MEF+Tilt,” demonstrated an envelope geometry revised to maximize solar gains (see Figure 70). Each energy model, whether it was used directly as a baseline or as a precursor to the Q-MEF model, was configured for three distinct climates (Table 13) per ASHRAE 90.1 (2013) building standards, resulting in a collection of twelve analyzed configurations.

Table 15. Model configuration parameters.

Model Configuration	40% Glazed	95% Glazed	Q-MEF	Q-MEF + Tilt
<b>Climates Modeled</b>	New York City, NY / Phoenix, AZ / Mountain View, CA			
<b>Geometry</b>	DOE Prototype: medium office	DOE Prototype: medium office	DOE Prototype: medium office + inclined clerestories	DOE Prototype: medium office+ inclined clerestories tilted facades
<b>Length (east-west)</b>			49.9m	
<b>Width (north-south)</b>			33.3m	
<b>Floors</b>			3	
<b>Floor to floor height</b>			3.96m	
<b>Perimeter zones depth</b>			4.57m	
<b>Total floor area</b>			4980m <sup>2</sup>	
<b>Envelope Specifications</b>				
<b>Wall U value (W/m<sup>2</sup>-K)</b>	0.204/0.251/0.223	0.204/0.251/0.223	0.429	0.429
<b>Roof U value (W/m<sup>2</sup>-K)</b>	0.223	0.223	0.223	0.223
<b>Façade glazing ratio</b>	40%	95%	95%	95%
<b>BITCOPT integrated</b>	NO	NO	YES	YES
<b>Glazing System</b>	to ASHRAE 90.1- 2013	to ASHRAE 90.1- 2013	deep-mullion with internal IGU	deep-mullion with internal IGU
<b>T<sub>vis</sub></b>	0.13/0.13/0.13	0.13/0.13/0.13	0.812	0.812
<b>SHGC</b>	0.40/0.25/0.25	0.40/0.25/0.25	0.764	0.764
<b>U-factor (W/m<sup>2</sup>-K)</b>	4.6/5.2/4.8	4.6/5.2/4.8	2.72	2.72
<b>Mechanical Systems</b>	to ASHRAE 90.1- 2013 with hydronic thermal distribution	to ASHRAE 90.1- 2013 with hydronic thermal distribution	Q-MEF specified distributed systems	Q-MEF specified distributed systems
<b>Plant(s)</b>	Heating boiler, SHW boiler, electric chiller	Heating boiler, SHW boiler, electric chiller	Envelope- integrated thermal collection, parallel adsorption chillers, auxiliary heat pumps + boiler	Envelope- integrated thermal collection, parallel adsorption chillers, auxiliary heat pumps + boiler
<b>system topology</b>	central plants, zone unit loops in parallel	central plants, zone unit loops in parallel	Primary heating and cooling distribution/ storage loops; secondary loops for plants, zones	Primary heating and cooling distribution/ storage loops; secondary loops for plants, zones
<b>Zone transfer units</b>			Chilled beams, hydronic baseboard heating	
<b>Heat rejection</b>	air-side rejection from chiller	air-side rejection from chiller	air-side rejection from heating distribution loop	air-side rejection from heating distribution loop
<b>Ventilation</b>	Dedicated Outdoor Air System (DOAS)			
<b>Lighting, Equipment</b>	up to 8 W/m <sup>2</sup> , up to 10 W/m <sup>2</sup> , scheduled			
<b>Daylighting controls</b>	Stepped dimming with centered zone sensor			

Simplifications were made to all configurations to the end of contrasting whole-building behaviors rather than characterizing specific systems. Sensible heating and cooling loads for the third and first floors were set equal to the equivalent zones on the second floor. This simplification was based on the observation that, in the precursor models, sum heating and sum cooling loads for the three zones that shared floor plan locations averaged slightly higher than the values for the second floor, meaning the simplification resulted in slight over-estimates of heating and cooling loads.

### ***Baseline Configuration BL40: Medium Office Building with Hydronic Systems***

The first baseline configuration (BL40) was a building energy model with no post-processing, based on the United States' Department of Energy Medium Office Commercial Reference, with ASHRAE 90.1 (2013) specifications.<sup>63</sup> The window-wall ratio was set to 40%. The baseline's HVAC systems were updated from the reference according to ASHRAE 189.1 recommendations, employing hydronic thermal distribution with zoned chilled beams and baseboard heating, with a Dedicated Outdoor Air System (DOAS). These changes slightly reduced the modeled energy use, relative to the DOE reference.

### ***Baseline BL95: Increased Window-Wall Ratio***

To represent current trends towards highly glazed facades, the second baseline configuration (BL95) was generated by increasing the window-wall ratio of the BL40 model to 95%. The glazing specifications and systems behaviors were held constant, though systems were re-sized (through the auto-sizing algorithms in EnergyPlus).

### ***Q-MEF Precursor BEM***

The precursor BEM to the Q-MEF configuration was created by modifying the BL95 BEM. Glazing specifications were changed to reflect the three-layer, deep mullion design of BITCoPT. The layers in the glazing construction were, from exterior to interior: a single glazing lite, a 0.359m deep air cavity, and an insulated glazing unit comprising a second highly-transparent lite, a 6mm air cavity, and a third lite. All the glazing was

---

<sup>63</sup> Commercial Prototype Building Models | Building Energy Codes Program. (2014). Retrieved October 9, 2015, from <https://www.energycodes.gov/commercial-prototype-building-models>

highly-transparent (Table 15) in contrast with the baseline models, in which transmittances were lower, to limit solar heat gain to the buildings' interiors.

The roof geometry of the precursor BEM was also modified. 80% of the flat roof area was replaced by a series of inclined wedges (referred to as clerestories), to model the inclusion of BITCoPT across that expanse (Figure 70).

### ***Q-MEF + Tilt Precursor BEM***

For the precursor BEM to the Q-MEF+Tilt configuration, the morphology of the Q-MEF BEM was additionally revised to increase the solar gain on the building (see Figure 70). At each floor the facades were tilted outward at 20°. The chosen angle balanced increasing solar gain through the exterior glazing, with minimizing the shade from one floor's tilted façade to the floor beneath.

### ***Modeling Daylighting***

As derivatives of the DOE reference model, all baseline and precursor BEMs employed daylighting controls. Daylighting algorithms in EnergyPlus modified interior lighting schedules per the illuminance levels at sensors from the daylight through envelope glazing. One sensor at 0.75m height was added in the center of each perimeter zone. The illuminance setpoint was 500 Lux and the lighting control type was chosen to be stepped. The controls did not respond to over-lit conditions, and glare conditions were not addressed by the energy-only method. Glare issues have been addressed in a previous study of the BITCoPT system,<sup>64</sup> indicating its effectiveness in reducing over-illumination caused by direct normal irradiance. In the prior study a reduction was noted in the room depth for which sufficient work-plane illuminance could be achieved, but the perimeter zone depth in this study, 4.57m, was shallower than that depth limit.

Precursor BEMs employed in this study did not include skylights, in keeping with the referenced DOE models. Daylighting from skylights would reduce the baseline

---

<sup>64</sup> Aly, M., Novelli, N., Shultz, J., Phillips, K., Andow, B., & Dyson, A. (2015). Daylighting Effect of Separating Direct and Diffuse Insolation with Facade-Integrated, Transparent Solar Collector. In *PLEA*. Bologna.

lighting electrical loads in the core of the third floor (which comprises 20% of the building's floor area), but would likely contribute net cooling loads due to solar gains. Although it is surmised that the zones' daylighting and thermal circumstances would improve with glazed roof expanses and installed BITCoPT, in this study the roof collection was treated as stand-alone equipment which did not interact (through lighting, or thermally) with the adjacent zones (in contrast to the vertical glazing expanses, for which light and thermal interactions were modeled).

### 3.3.7.2.5 Input: BITCoPT Envelope Cavity Model

A model of the BITCoPT<sup>65,66</sup> façade collector was integrated into the Q-MEF model, which contributes quantities for electrical generation ( $E_{gen}$ ), thermal collection ( $Q_{gen}$ ), and direct solar gain reduction based on inputs of climate data and envelope orientation. A constant efficiency ( $\eta_{conv}, E_{gen} = 0.96$ ) was applied to the BITCoPT model's electrical output ( $E_{gen,BCPMDL}$ ) to represent the transformation of BITCoPT's variable-voltage DC output to a useful form (constant-voltage DC for tying into to zone-level microgrids, or AC for tying into building-scale distribution).

The thermal collection output ( $Q_{gen,BCPMDL}$ ) was likewise modified to represent the heat transfer fluid inlet and envelope cavity temperatures in the Q-MEF model, which were distinct from those values in the contributing BITCoPT simulation, as the models were combined in post-processing:

$$Q_{gen[n]} = \frac{T_{HTF[n-1]} - T_{cav[n-1]}}{T_{HTF,BCPMDL[n-1]} - T_{cav,BCPMDL[n-1]}} (Q_{gen,BCPMDL[n]} - Q_{max,BCPMDL[n]}) + Q_{max,BCPMDL[n]} \quad (24)$$

where  $Q_{gen}$  was thermal power,  $T$  was temperature of the heat transfer fluid ( $T_{HTF}$ ) or cavity air ( $T_{cav}$ ), the subscript  $BCPMDL$  indicates values from the precursor BITCoPT model, and  $Q_{max}$  was the maximum possible thermal energy collection, assuming perfect insulation. Because the cavity temperatures in the Q-MEF model were held to lower temperatures than in the precursor BITCoPT model ( $T_{outd} < T_{cav} < 38^{\circ}\text{C}$ , and

<sup>65</sup> See Chapter 3.

<sup>66</sup> Novelli, N., Shultz, J., & Dyson, A. (2015). Development of a Modeling Strategy for Adaptive Multifunctional Solar Energy Building Envelope Systems. In *SimAUD*. Washington, DC.

$T_{cav,BCPMDL} = 45^{\circ}\text{C}$ ), the Q-MEF-modeled array lost more heat, and thermal collection efficiency was lower than that in the precursor model.

### 3.3.7.2.6 Function: Deep-Mullion Cavity Energy Balance

The building envelopes for the baseline and precursor models were modeled natively in EnergyPlus. In the Q-MEF configurations, the behavior of the deep-mullion curtain wall cavity (into which BITCoPT integrated) was represented by an energy balance in post-processing: thermal transfers across the glazing in the precursor BEMs were replaced by equivalent transfers as determined by this energy balance. One balance was performed for each zone or clerestory surface that contained windows, determining the energy and temperature changes in the cavities through time. The air in a cavity was assumed to be well mixed, with all components (air, BITCoPT support structure) at the same temperature. The energy balance comprised the transmittance of direct and diffuse solar energy into and out from the cavity, the thermal and electrical energy generated by BITCoPT, the heat transferred (via conduction and convection) across glazing surfaces with the two adjoining environments, the heat extracted from the cavity by a flushing function, and the heat lost from the high-range buffer. The balance was

$$\begin{aligned} \left( \sum m_{cav} c_{p,cav} \frac{dT}{dt} \right) &= G_{DN,cav} + G_{DN,ind} + G_{Diff,cav} + G_{Diff,ind} \\ &- Q_{gen} - E_{gen} \\ &+ Q_{cond,outd} + Q_{cond,ind} + Q_{cav,flush} + Q_{buffer,loss} \end{aligned} \quad (25)$$

where  $m_{cav}c_p$  refers to the cavity's thermal mass,  $G$  to transmitted solar power,  $DN$  to direct irradiance,  $Diff$  to diffuse irradiance,  $ind$  and  $outd$  to the indoor and outdoor environments,  $cond$  to non-irradiation thermal transfer,  $cav$  to the cavity,  $flush$  to the cavity flushing function (see section 0), and  $buffer$  to the high-range buffer TES. In addition to the twelve precursor BEMs, an alternative version of each was produced to facilitate modeling the BITCoPT cavity, using a glazing specification that represented only the exterior lite of the deep-mullion cavity. The alternate values for transmitted solar power (both direct and diffuse) were used as the insolation transmitted into the envelope cavity, while the values from the BEM with standard glazing specifications were used for insolation transmitted into the zone. For direct insolation only, this value

was further modified by the BITCoPT gap function (see section 0) to represent the collector's interception of the direct solar component.

Since the cavity balance function did not account for variations of temperature or fluid movement within (or external to) the cavity control volume, or heterogeneous masses, overall conductivity values between the cavity and adjacent environments were constant, whereas these relationships were variable in the precursor BEM. More accurate heat transfers would be expected from a cavity model that included convection, surface emissivity, material diffusivity, and thermal bridging effects, but the one-dimensional, steady state assumptions used here were deemed sufficient to contrast behavior between baseline and Q-MEF model configurations.

***Function: BITCoPT area-based gap transmittance***

The direct irradiance transmitted through the cavity to a building zone was modeled by multiplying the transmitted irradiance reported by the BEM by  $T_{gap}$ , a function that represents the collector's area-based transmittance of direct irradiance. When the solar vector is near to normal with the surface of an envelope region that incorporates a collector, insolation passes through the gaps between BITCoPT modules. As the solar vector moves away from envelope-normal and the collector modules track around pitch and yaw axes, the gaps decrease, falling to zero width at an excursion angle determined by the collector's geometry.  $T_{gap}$  was defined as

$$T_{gap} = (1 - c_{vert}) \left( \frac{\phi_{full} - \phi}{\phi_{full}} \right) (1 - c_{hz}) \left( \frac{\lambda_{full} - \lambda}{\lambda_{full}} \right) \quad (26)$$

where  $c_{vert}$  and  $c_{hz}$  were vertical and horizontal components of the fractions of envelope area filled by BITCoPT lens modules,  $\phi$  and  $\lambda$  were the rotations of the BITCoPT modules around their pitch and yaw axes, and  $\phi_{full}$  and  $\lambda_{full}$  were the respective threshold angles at which the gaps between lenses decrease to zero width when observed parallel to the solar vector. The floor for  $T_{gap}$  was set to 0: no direct irradiance was transmitted if the modules were rotated beyond the pitch and yaw thresholds.  $T_{gap}$  was applied to only direct insolation since, as modeled, BITCoPT does not attenuate diffuse insolation.

### **Function: Cavity Flushing**

A cavity flushing function ( $Q_{cav,flush}$ ) was implemented to simulate removal of heat from the BITCoPT cavity, to maintain the cavity temperature optimally relative to adjacent zone conditions. The cavity flushing function simulated a fan moving air between the cavity and the environment (Figure 72).

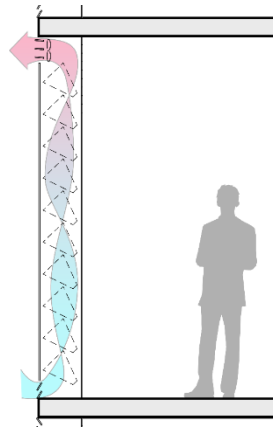


Figure 72. Modeled method of flushing excess heat from cavity.

Rather than optionally flushing to either the indoors or outdoors, as with currently operating ventilated curtain walls,<sup>67</sup> it was determined that, due to the prevalence of cooling loads in the model, flushing to the interior had negligible benefits. Therefore, flushing with outdoor air only was modeled, and the function remained decoupled from the building DOAS system.

Flushing was implemented both in the precursor BEM (as a window:Airflow property in EnergyPlus, with a constant volumetric rate of  $0.6\text{m}^3/\text{s}\cdot\text{m}$  and assumption of no fan power) and in post processing, wherein the maximum allowable cavity temperature was  $T_{cav,lim,high} = 40^\circ\text{C}$ , but if zone cooling demand was significant, the target temperature was set to the outdoor (dry bulb) temperature). The post-processing flushing function was modeled as:

---

<sup>67</sup> Briegleb, T. (Ed.). (1999). *Ingenhoven, Overdiek und Partner - High Rise RWE AG Essen*. (T. Kommerell, Trans.) (1st ed.). Birkhäuser Basel.

$$Q_{cav,flush(i)[n]} = K_{flush(i)} * C_{cav(i)} * (T_{cav[n-1]} - (T_{cav,target} + T_{cav,offset})) + K_{flush,IDN(i)}(I_{DN,cav(i)[n]}) \quad (27)$$

where  $K_{flush}$  was the proportional gain tuned for each zone,  $C_{cav}$  was the cavity thermal mass,  $T_{cav}$  was the cavity temperature,  $T_{cav,target}$  was set to either  $T_{outd,db[n-1]}$  or  $T_{ind}$  depending on heating demand, and  $T_{cav,offset} = 2^{\circ}\text{C}$  was used to establish a dead band, preventing the system from operating if heat removal would be inconsequential.  $K_{flush,IDN}$  was a separate gain constant used to add a fraction of the zone's direct insolation at the current-time step to the targeted flush rate. The fan energy required to flush the cavity ( $E_{flush}$ ) was determined assuming a constant pressure head (and therefore a constant power draw) multiplied by an hourly duty cycle. 100% of fan (electrical) power was assumed to be taken up by the airflow (as increased temperature).

These flushing controls maintained the cavity temperature close to the chosen target, minimizing unwanted non-insolation thermal transfer from the envelope cavity to the building's interior, and contributing energy to under-heated zone conditions.

### 3.3.7.2.7 Function: Revised Zone Thermal Balance

Each zone's sensible heating or cooling loads, were revised from those in the precursor BEM at each time step, according to the interception of direct normal irradiance, and local thermal storage leakages. The precursor simulations determined loads that would maintain thermal comfort in a zone based on air-temperature thermostats. The energy balance used to determine revised heating and cooling rates was:

$$HEX_{[n]} = HEX_{BEM[n]} - Q_{env,BEM[n]} - G_{DN,BEM[n]} + Q_{cond,ind[n]} + G_{DN,ind[n]} + Q_{chilled,loss[n]} + Q_{rej,loss[n]} \quad (28)$$

where at a given time step  $HEX_{BEM}$ ,  $Q_{env,BEM}$ ,  $G_{DN,BEM}$ , were the zone heating and cooling loads (heat extraction), non-solar thermal transfer across the glazing, and zone direct solar gain through glazing, respectively, from the precursor BEM.  $Q_{cond,ind}$  was the modeled thermal transfer with the BITCoPT cavity, and  $G_{DN,ind}$  was the direct solar gain

after BITCoPT interception. The  $Q_{chilled,loss}$ , and  $Q_{rej,loss}$  terms represented the contributions from the distributed TES elements.

In the Q-MEF configurations, cooling and heating loads in a zone were defined to be met, as they were in the baseline configurations, by circulating heat transfer fluid from the appropriate distribution loop through transfer units (chilled beams) in that zone. Heat transferred to or from a zone (per the revised zone thermal balance) was subtracted from the rejection-range distribution loop or added to the chilled distribution loop accordingly.

### 3.3.7.2.8 Function: Adsorption Chilling

Adsorption chillers were modeled by matching a solution surface to a manufacturer's COP data<sup>68</sup> relative to buffer, chilled, and rejection-range temperatures. Upper and lower limits are added to the function to keep the COP within the range of  $0 \leq COP_{chiller} \leq 0.56$ . The COP of the chiller was:

$$COP_{chiller} = a + bT_{chilled} + cT_{buffer} + dT_{rej} + eT_{chilled}^2 + fT_{buffer}^2 + gT_{chiller}T_{rej} + hT_{buffer}T_{rej} + iT_{rej}^3 \quad (29)$$

where  $T_{chilled}$  is the temperature of the chilled distribution loop,  $T_{rej}$  is the temperature of the rejection-range distribution loop, and  $T_{buffer}$  is the temperature of the high range buffer. The coefficients for the COP chiller function are shown in Table 16.

---

<sup>68</sup> Daßler, I., & Mittelbach, W. (2012). Solar Cooling with Adsorption Chillers. *Energy Procedia*, 30(0), 921–929. <http://doi.org/10.1016/j.egypro.2012.11.104>

Table 16. COP Chiller Function Coefficients.

Coefficient	Value
a	0.289
b	-0.025
c	0.005
d	0.016
e	-0.001
f	-0.145*10 <sup>-3</sup>
g	0.003
h	0.621*10 <sup>-3</sup>
i	-0.002

The chillers were controlled to draw energy from the thermal buffer with which they were paired when the buffer temperature exceeded a threshold ( $T_{buffer} > 60^{\circ}\text{C}$ ). Chillers were modeled to draw energy according to the excess in the buffer over the threshold, with no capacity limit and no dependence of COP on the fractional capacity, which represents multiple chillers ganged in parallel.

### 3.3.7.2.9 Function: Auxiliary Heat Pumps

Water-water heat pumps were incorporated in the thermal control strategy to maintain the temperatures of the chilled and rejection-range distribution loops within appropriate ranges. To control these heat pumps: if the chilled loop temperature was above its lower limit, energy was pumped from the chilled loop to the rejection-range loop either when the rejection-range loop became too cold or the chilled loop became too warm (see Section 0). The heat pump is modeled in steady-state, at a COP determined as a function of temperature lift, with functions sourced from Meggers et al.,<sup>69</sup> with an exergetic efficiency of 0.5 and  $COP_{HP}$  capped at 16.0:

$$COP_{HP} = 4.3 \times 10^{-5} (T_{lift})^4 - 5.02 \times 10^{-3} (T_{lift})^3 + 0.21956 \times 10^{-3} (T_{lift})^2 - 4.48 (T_{lift}) + 42.5 \quad (30)$$

---

<sup>69</sup> Meggers, F., Ritter, V., Goffin, P., Baetschmann, M., & Leibundgut, H. (2012). Low exergy building systems implementation. *Energy*, 41(1), 48–55. <http://doi.org/10.1016/j.energy.2011.07.031>

### 3.3.7.2.10 **Functions: Heat Rejection**

To prevent the rejection-range loop from getting too warm, heat removal from the loop to the outdoor environment was simulated by modeling a dry cooler, or fan assisted water-to-air heat exchanger. The heat removal function,  $Q_{rej,env}$  was:

$$Q_{rej,env[n]} = K_{rej} * C_{loop,rej} * (T_{rej[n-1]} - T_{rej,target}) \quad (31)$$

where  $K_{rej}$  was the proportional gain,  $C_{loop,rej}$  was the thermal mass of the rejection loop,  $T_{rej}$  is the rejection distribution loop temperature, and  $T_{rej,target}$  was the desired temperature set point. Like the function of the cavity flush fans (section 0), the fan energy required to remove heat ( $E_{rej,env}$ ) was determined by a constant power draw multiplied by an hourly duty cycle.

### 3.3.7.2.11 **Functions: Loop Temperature Controls**

The temperatures of the chilled loop ( $T_{chilled}$ ) was maintained by the activity of the adsorption chillers and auxiliary heat pumps. If  $T_{chilled}$  fell too low ( $T_{chilled} > 11.4^{\circ}\text{C}$ ) both the chillers and heat pumps were deactivated in the next time step (chillers were controlled to dump collected heat directly to the rejection-range loop). If the chilled loop temperature rose too high ( $T_{chilled} > 17.0^{\circ}\text{C}$ ), the auxiliary heat pump activated in the next time step.

The rejection-range loop temperature ( $T_{rej}$ ) was controlled by the activity of the auxiliary boiler, the auxiliary heat pump, and the heat rejection system. A target temperature  $T_{rej,target}$  was set, either to  $T_{out,db}$  (if heating demands were expected to be low) or to  $T_{rej} = 27^{\circ}\text{C}$ . If  $T_{rej}$  was low, the auxiliary heat pump was activated at the next time step; if the heat pump was unavailable, the boiler would activate. If  $T_{rej}$  was too high, the heat rejection system would activate, proportional to the difference between  $T_{rej}$  and  $T_{rej,target}$ . An additional check against the heat rejection COP ( $COP_{rej} > 3.0$ ) prevented operation when the temperature difference was small, effectively favoring night flushing of excess energy in the rejection loop. These controls together maintained the loop temperatures within useful bounds to provide cooling and heating to the zones, and heat rejection capacity for the adsorption chillers.

### **3.3.7.2.12 Utility Cost Metrics**

Costs for electrical use, capacity, and demand and gas use charges were computed with the EnergyPlus UtilityCost:Tariff function. Outputs were taken directly from simulation outputs for the baseline configurations, and scaled on an hourly basis for the Q-MEF configurations. Electricity costs were determined with monthly peak demand charges (\$17.00/kW for the winter and \$38.15/kW for the summer) and hourly energy charges (\$0.125/kWh on-peak and \$0.105/kWh off-peak), with surplus electricity generation net-metered at 100% of the current rate. The cost for natural gas was \$1.30 per therm.

### **3.3.7.3 Results & Discussion: Energy Metabolization**

Simulating revised systems of a medium-scale commercial office building according to the Q-MEF framework demonstrated implications for lighting demands, cooling and heating loads, peak demands, and net energy use.

#### **3.3.7.3.1 Daylighting Results**

With daylighting controls active in all configurations, modeled lighting power use decreased slightly in the configurations with greater glazing areas: BL95, Q-MEF, Q-MEF+Tilt (Table 17).

Table 17. Lighting loads under daylighting controls.

	<i>(in kWh-E/m<sup>2</sup>-yr)</i>	Lighting Loads
NYC	BL40	23
	BL95	20
	Q-MEF	20
	Q-MEF+Tilt	20
PHX	BL40	23
	BL95	19
	Q-MEF	19
	Q-MEF+Tilt	20
MTV	BL40	23
	BL95	19
	Q-MEF	19
	Q-MEF+Tilt	20

Because daylighting controls were modeled in the precursor BEMs, the controls did not respond to the reduction of direct irradiance due to BITCoPT. However, because prior daylighting and glare analyses of BITCoPT<sup>70</sup> resulted in sufficient illuminance through the same depth as the perimeter zones modeled in this study (4.5m), and other equipment (such as blinds) was not modeled to control for over-lit moments, it was determined that the daylighting behavior would translate from the precursor BEMs to the Q-MEF configurations.

Daylighting potentially has a great effect on the energy use profile of a building, but because of the complexity of daylighting analysis, which is highly contingent on occupant behavior,<sup>71</sup> it is hard to represent in simulation. It is possible that the daylighting energy benefits of BITCoPT are over-predicted, as cloudy moments would cause under-lighting. It is also possible that the benefits are under-predicted, as, during

<sup>70</sup> Aly, M., Novelli, N., Shultz, J., Phillips, K., Andow, B., & Dyson, A. (2015). Daylighting Effect of Separating Direct and Diffuse Insolation with Facade-Integrated, Transparent Solar Collector. In *PLEA*. Bologna.

<sup>71</sup> Reinhart, C. F. (2004). Lightswitch-2002: a model for manual and automated control of electric lighting and blinds. *Solar Energy*, 77(1), 15–28. <http://doi.org/10.1016/j.solener.2004.04.003>

brighter moments in the baseline buildings, occupants experiencing far more than 500 lux might deploy blinds and electric lighting.

#### **3.3.7.3.2 *Reduced Cooling Loads, Increased Heating Loads***

The incorporation of Q-MEF systems resulted in various responses in heating and cooling loads across the climate types, demonstrating the complex interconnections between envelope loads and building demands (Table 18).

Heating loads comprise the sum responses of modeled baseboard heating and DOAS preheating, while the cooling loads consist only of the modeled chilled beam responses.

Table 18. Yearly facility heating and cooling loads of twelve configurations.  
(Loads to be addressed by building thermal control systems).

<i>(in MWh-Q)</i>		Loads	
		Heating	Cooling
NYC	BL40	266	263
	BL95	364	346
	Q-MEF	388	274
	Q-MEF+Tilt	514	310
PHX	BL40	44	634
	BL95	78	959
	Q-MEF	167	729
	Q-MEF+Tilt	209	784
MTV	BL40	109	277
	BL95	174	357
	Q-MEF	316	261
	Q-MEF+Tilt	398	294

Due to the preponderance of cooling demands in the moderate climates, the heating increases were low (though not negligible) relative to total demands. The NYC climate showed sensitivity to glazing area and type, as the BL95 and QMEF cases showed marked changes in the total loads. Installation of BITCoPT (the Q-MEF case vs the BL95 case) resulted in significant reductions in cooling loads in all climates, although the Q-MEF+Tilt case did not decrease loads further. The difference in loads occurred mainly in the south, east, and west perimeter zones, where the decreased heat gain during direct solar conditions due to BITCoPT caused more frequent net-heating loads.

### **3.3.7.3.3 On-Site Thermal Collection and Use**

In addition to driving chilling processes, thermal energy collected by BITCoPT was applied to building demands for zone heating and SHW pre-heating (Table 19).

Table 19. Summary of thermal collection and heating applications.

<i>(in MWh-Q)</i>	Thermal Energy Collected	Zone Heating Loads	SHW Preheat	Heating Required (SHW, DOAS, Zone)	
NYC	BL40	-	266	-	330
	BL95	-	364	-	449
	Q-MEF	149	388	9	430
	Q-MEF+Tilt	151	514	9	488
PHX	BL40	-	44	-	64
	BL95	-	78	-	95
	Q-MEF	308	167	8	241
	Q-MEF+Tilt	348	209	8	141
MTV	BL40	-	109	-	136
	BL95	-	174	-	219
	Q-MEF	234	316	9	431
	Q-MEF+Tilt	244	398	9	345

Through the mechanism of the storage and rejection loop, collected thermal energy was applied to zone heating loads and SHW preheating (although due to the low demand in office-dominated buildings, the latter factor was small. Boiler (and fuel) usage was observed to increase in response to heating demands, despite net thermal collection in some cases exceeding net heating demands. This disparity indicates non-optimal behaviors in the thermal storage mechanisms, including mismatches between the times of collection and demand. This mismatch occurred largely over the annual cycle (Figure 73), indicating the usefulness of ground-source thermal storage, a function which was not implemented in the current Q-MEF model.

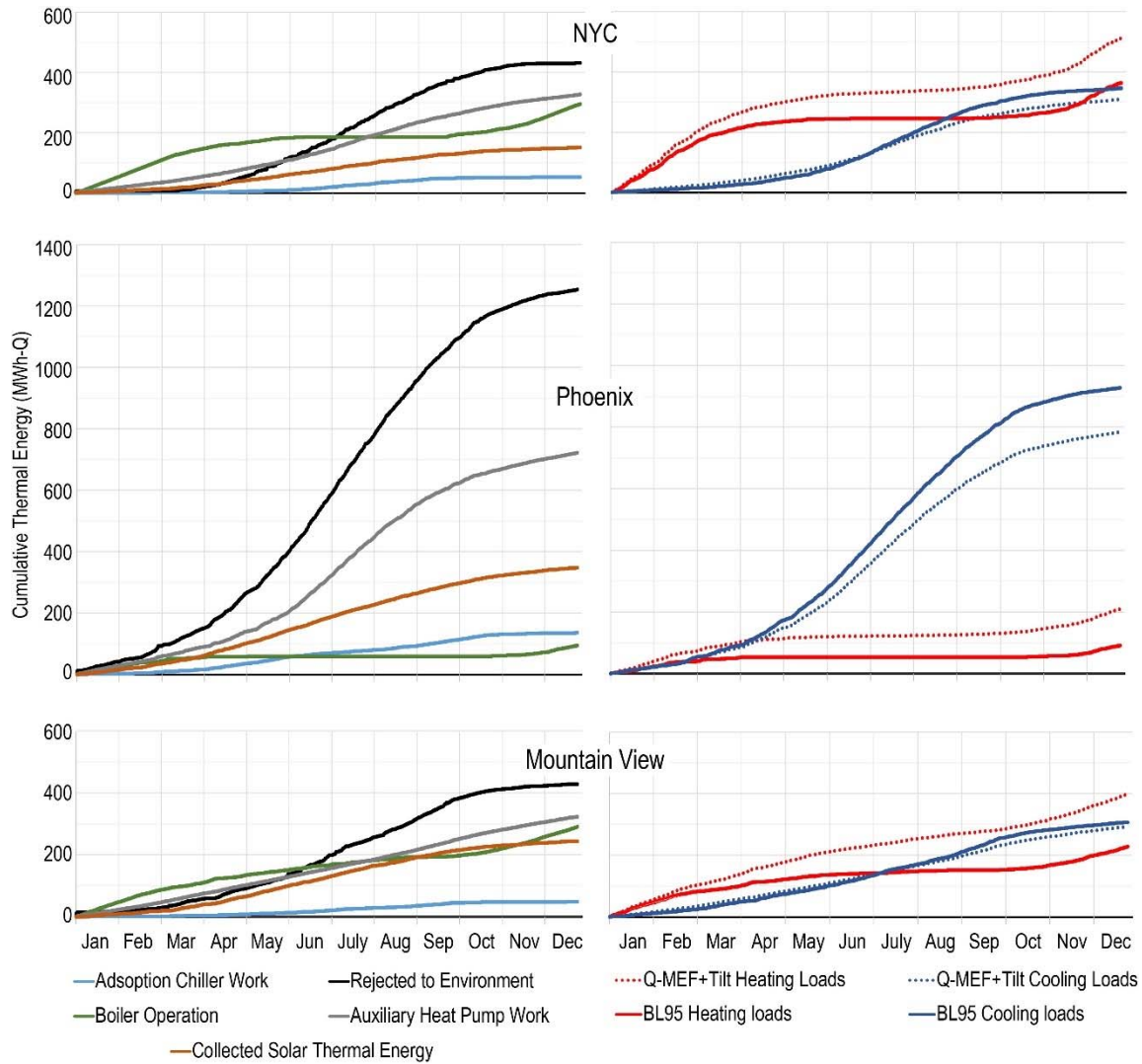


Figure 73. Thermal energy transfers, yearlong cumulative summary.

The disparity may also arise from a feature of the thermal distribution: because the rejection loop is used intentionally as both a heat source and a heat sink, its target temperature is at times sub-optimal for one purpose or the other. This is particularly true during transitional times of the year when heating and cooling demands are intermingled. More-responsive controls would be useful in reducing this conflict, though to address the underlying cause, systems would be revised. An additional loop could be implemented so that the dual purposes were separated, or stand-alone heaters, such as zone-scale low-lift heat pumps tied to the rejection loop could be implemented. The adsorption chillers could be modeled to run in reverse, although this would reduce the available cooling, and there is not generally a supply of driving heat when consistent

heating is demanded (cold, cloudy days). In building implementation, the first-cost of these options would be weighed against the long-term savings against energy use and other building performance criteria (thermal comfort, maintenance, lease value) that they would provide.

The increased heating and decreased cooling demands are notable because in internal load-dominated buildings with traditional systems, an imbalanced demand for cooling over heating reduces the effectiveness of ground-sourced heat exchange, which can be an efficient technology for providing thermal resources. Balancing net heating and cooling demands in a project therefore may broaden the applicability of ground-source heat exchange, and other mechanisms for buffering thermal energy.

### ***Solar Cooling with Adsorption Chilling***

Solar thermal energy, as collected by BITCoPT, was modeled to produce chilling work by driving adsorption chillers. This chilling work was additive to the passive reduction of cooling loads from reduced direct solar gains (Table 20), with the additional benefit of being dispatchable, since generated cooling capacity was initially stored in thermal mass of the chilled distribution loop.

Table 20. Solar cooling systems summary.

In Q-MEF configurations cooling loads are reduced and adsorption chillers offset fraction of remainder.

	<i>(in MWh-Q and % of net)</i>	Net Cooling Loads	Adsorption Chillers Work
NYC	BL40	263	-
	BL95	346	-
	Q-MEF	274	40 (15%)
	Q-MEF+Tilt	310	52 (17%)
PHX	BL40	634	-
	BL95	959	-
	Q-MEF	729	103 (14%)
	Q-MEF+Tilt	784	135 (17%)
MTV	BL40	277	-
	BL95	357	-
	Q-MEF	261	53 (20%)
	Q-MEF+Tilt	294	53 (18%)

Cooling loads in the Q-MEF configurations were demonstrated to be reduced relative to the BL95 configuration in the three chosen climates. The work done by modeled adsorption chillers further reduced the cooling response required from the balance of a building's systems (the auxiliary heat pump). The magnitude of collected thermal energy (Table 19) relative to loads suggests that more systems (such as night-flush controls and ground-source heat exchange) would be useful to perform more controlled storage and release of heat over both diurnal and annual cycles.

The amount of cooling power produced from solar energy was not sufficient to address 100% of modeled demands. Chilling processes operating at higher COPs might increase chilling work done, but as they would require higher driving temperatures, higher solar concentration ratios would be required to boost exergy collection and offset the greater losses that would be incurred in the thermal collection stage. This tradeoff was not explored here due to a desire to model water at standard pressure as the heat transfer fluid. The tradeoff would be a valuable exploration in future work, as the exergetic value of thermal energy increases with the temperature at which it is stored, enabling chilling processes which are both more efficient and less sensitive to rejection and chilled circuit temperatures. Higher collection temperatures could, in that way, reduce the difference between the target rejection loop temperature for chiller rejection and the target temperature for zone heating.

#### **3.3.7.3.4 Energy Use Profile Comparison**

Q-MEF simulations improved over the baselines according to all observed metrics—net electrical demand, net energy demand, and peak electrical demand (defined as the maximum observed electrical demands between noon and 5pm during the summer season). There were conditional exceptions: BL40 demonstrated the lowest peak demand of the NYC models, and the demand reductions of QMEF over BL40 were trivial. In both of these cases the reductions in electrical EUI was still significant. Results are summarized in Table 21.

Table 21. Summary: net energy use intensities, by demand type (kWh/m<sup>2</sup>-yr).

	Heating	Heating & Cooling	Ventilation	Lights	Equipment	Power Generated	Net EUI, Electrical	Net EUI, Total Site	Peak Electrical Draw
	kWh-Q/ m <sup>2</sup> -yr	kWh-E/ m <sup>2</sup> -yr	kWh/ m <sup>2</sup> - yr	kW-E					
NYC									
BL40	68	17	4	23	47	-	<b>92</b>	<b>160</b>	<b>139</b>
BL95	92	29	3	20	47	-	<b>99</b>	<b>191</b>	<b>156</b>
Q-MEF	86	26	3	20	47	-61	<b>36</b>	<b>121</b>	<b>151</b>
Q-MEF+T	98	26	4	20	47	-71	<b>27</b>	<b>124</b>	<b>147</b>
PHX									
BL40	13	47	9	23	47	-	<b>127</b>	<b>139</b>	<b>189</b>
BL95	21	72	12	19	47	-	<b>150</b>	<b>171</b>	<b>231</b>
Q-MEF	48	55	4	19	47	-106	<b>20</b>	<b>68</b>	<b>157</b>
Q-MEF+T	28	54	5	20	47	-125	<b>0</b>	<b>29</b>	<b>166</b>
MTV									
BL40	29	17	3	23	47	-	<b>91</b>	<b>120</b>	<b>133</b>
BL95	46	26	4	19	47	-	<b>96</b>	<b>142</b>	<b>164</b>
Q-MEF	86	31	4	19	47	-84	<b>18</b>	<b>104</b>	<b>133</b>
Q-MEF+T	69	26	5	20	47	-99	<b>-1</b>	<b>68</b>	<b>131</b>

Maximum on-peak electrical draw (during summer-season afternoons) was demonstrated to decrease with the application of the Q-MEF interventions in all climates, relative to BL95, and in the Phoenix climate, relative to both baselines.

The Q-MEF+T configuration demonstrated the highest generation and lowest net electrical and total site EUI across climates. Benefits were incremental over the straight Q-MEF configuration, which indicates the usefulness of further analysis comparing the marginal utility of the energy benefits with the marginal costs of increasing the complexity of the building's design.

### 3.3.7.3.5 Utility Cost Analysis

Annual energy cost savings were calculated for all configurations according to costs for electricity demand (kW), electrical supply (kWh) and natural gas supply (therms or kWh) (Figure 74, Figure 75, Table 22). Integration of Q-MEF systems generally decreased electricity and gas consumption costs, in some cases to near-zero, and demand costs were generally higher than in BL40 but lower than in BL95.

INTELLIGENT FACADES FOR HIGH PERFORMANCE GREEN BUILDINGS  
Property of Rensselaer Polytechnic Institute

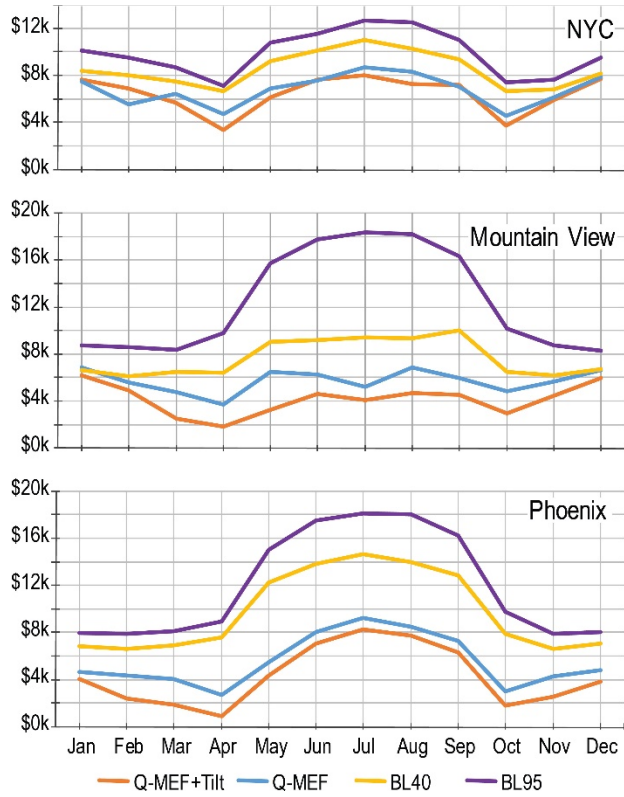


Figure 74. Utility costs, three climates, yearly.

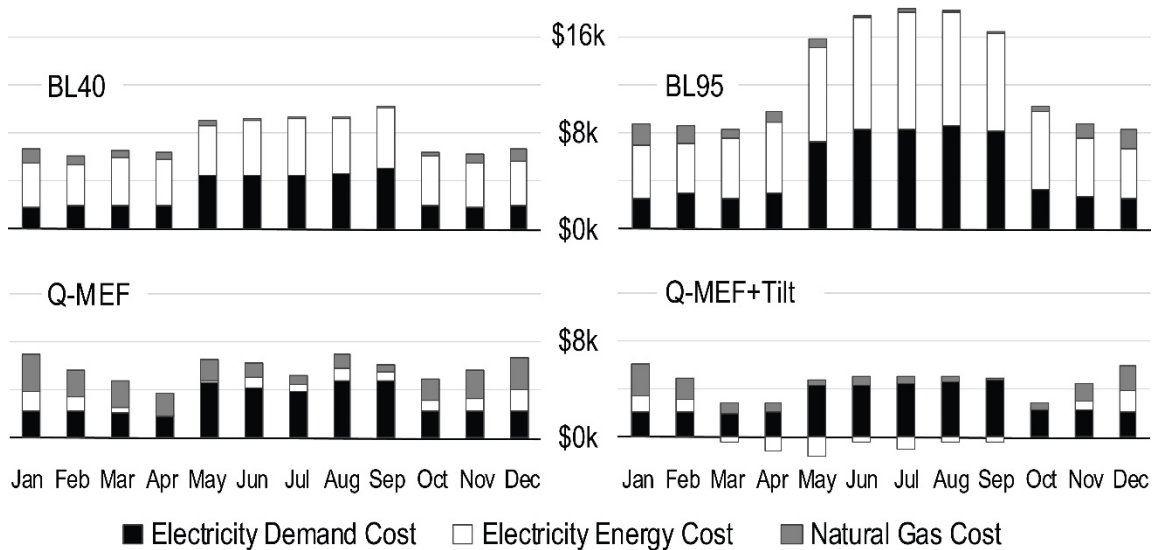


Figure 75. Utility costs breakdown, Mountain View, yearly.  
Net-meter benefits observed in summer, Q-MEF+Tilt case.

Table 22. Utility annual cost summary.

		Demand Charges	Energy Charges	Natural Gas Charge	Total Utility Cost	Savings over BL40	Savings over BL95
NYC	BL40	\$37,000	\$50,000	\$15,000	\$102,000		
	BL95	\$43,000	\$55,000	\$20,000	\$119,000		
	Q-MEF	\$39,000	\$20,000	\$22,000	\$81,000	\$21,000 (21%)	\$38,000 (32%)
	Q-MEF+Tilt	\$40,000	\$15,000	\$22,000	\$81,000	\$25,000 (25%)	\$42,000 (35%)
PHX	BL40	\$49,000	\$66,000	\$2,000	\$117,000		
	BL95	\$60,000	\$79,000	\$4,000	\$143,000		
	Q-MEF	\$43,000	\$12,000	\$11,000	\$66,000	\$51,000 (44%)	\$77,000 (54%)
	Q-MEF+Tilt	\$44,000	\$2,000	\$5,000	\$51,000	\$66,000 (56%)	\$92,000 (64%)
MTV	BL40	\$37,000	\$49,000	\$6,000	\$92,000		
	BL95	\$60,000	\$79,000	\$10,000	\$149,000		
	Q-MEF	\$37,000	\$11,000	\$22,000	\$69,000	\$23,000 (25%)	\$80,000 (42%)
	Q-MEF+Tilt	\$37,000	\$0	\$13,000	\$50,000	\$42,000 (46%)	\$99,000 (66%)

Observed in Table 14, Q-MEF resulted in increased fuel use consumption, but energy (fuel and electricity) consumption was reduced for all cases, relative to BL40 and BL95. The cost analysis demonstrates, however, that (due to the low cost of natural gas compared to electricity) annual energy charges were reduced in Q-MEF configurations.

Relative to the highly-glazed baseline (BL95), peak electrical draw was reduced for each Q-MEF configuration, resulting in lower demand charges. Compared to BL40, the demand charge for Phoenix was reduced, but New York City and Mountain View had similar demand charges.

In order to determine the financial costs vs benefits of Q-MEF, the utility savings would be weighed along with the expected changes in lease rates due to changes in the thermal comfort and desirability of occupied spaces, and the installation and maintenance costs for Q-MEF systems. These costs would be considered relative to the costs of the baseline configuration's mechanical systems, or other common systems such as Variable Air Volume HVAC, which incurs additional effects on a building project's value, such as reduced inhabitable room height due to the depth of duct work. The overall cost analysis of Q-MEF is highly contextual, due to the interaction of these factors and additional localized factors, such as capitalization rates expected on monies obtained to finance a project, which are in-part functions of perceived risk. A detailed

cost analysis is therefore usefully done at the scale of individual projects, and is outside the bounds of this study, which considered generalized circumstances.

### **3.3.7.3.6 Energy Use Ramifications**

The modeled application of the specific systems described in this study according to the Q-MEF strategy resulted, in simulation, in significant reductions in energy use in the three modeled climates. On-site net-zero electricity was demonstrated in different climates, a significant result for buildings as substantial as the chosen model. Additional modifications would likely show additional energy-use benefits: Although the baseline configurations were designed according to current minimum efficiency standards, they did not incorporate the full gamut of currently available high-performance building strategies, such as DOAS enthalpy recovery (important in high-humidity climates such as New York) or ground-source heat exchange (particularly useful in climates with steady cycles such as Phoenix). The application of these and other strategies would decrease the EUI of the baselines, and improve the EUI of the full Q-MEF implementations.

It should be noted that not all strategies considered useful in high-performance design are synergistic with Q-MEF. External shading devices, for example, are implemented in passive-driven designs to reduce solar gains on glazed façade areas. Q-MEF, however, in order to engage and metabolize available sources of energy and potential, intentionally internalizes these gains. The effects (Table 14) can appear as initial loads increases (particularly relative to the BL40 base case) but when processed by the building's thermal distribution network, the results are net benefits: decreases in both net energy use and peak demands. Although somewhat counter-intuitive from the passive design perspective, these effects develop from interacting with the solar resource simultaneously towards multiple ends.

A primary benefit to coolth storage systems is the reduction in peak demands on the electrical grid, and commercially-implemented systems that are financially beneficial are so in part due to this reduction.<sup>72</sup> The peak-load reductions simulated in this study, though significant, may not be fully indicative of the benefits to be expected from on-site

---

<sup>72</sup> Roth, K., Zogg, R., & Brodrick, J. (2006). Cool thermal energy storage. *ASHRAE Journal*, 48(9), 94–96.

coolth storage. This gap may be due to the simplified controls strategies employed in the Q-MEF model, which were chosen due to the exigencies of the post-processing modeling method. Further development of controls strategies has been shown to benefit thermal storage applications,<sup>73</sup> and might result in better utilization of the storage systems modeled in the Q-MEF configurations.

It might be noted that this study's simulations, the thermal collection efficiency of BITCoPT averaged lower than in precedent studies. This is due to the conflicting demands on the envelope cavity: It was determined that allowing the cavity temperatures to elevate (which reduces transportation losses in BITCoPT) had a net effect of increasing cooling demands in adjacent zones, and overall energy use in the building. This demonstrates how a building with Q-MEF is an example of a multiply coupled system of parallel modules that experience unique forcing functions. Optimizing overall objectives in such a system requires subordinating the peak performance of sub-systems. Given the increasing range of building technologies and analytical tools available for the design and analysis of the built environment, this type of result is to be expected.

#### **3.3.7.4 Summary**

To investigate a strategy of integrating multiple technologies into an ecosystem approach to architectural design, to the end of effectively using incident solar irradiance through a building's systems, simulations were done with a parametric group of building energy models. The models were assembled from a set of precursors: a set of building energy models, a model of an active envelope technology, distributed sorption chillers, hydronic thermal distribution and storage elements, water-to-water heat pumps, and ancillary systems. This systems strategy was described as a quality-matched energy flow (Q-MEF) network. Simulations of a 5000m<sup>2</sup>, three-floor office building demonstrated reductions in electrical use intensities of 70% over the baseline in a humid-continental climate and on-site net zero performance in arid subtropical and semi-arid

---

<sup>73</sup> Chen, Y., Galal, K. E., & Athienitis, A. K. (2014). Design and operation methodology for active building-integrated thermal energy storage systems. *Energy and Buildings*. <http://doi.org/10.1016/j.enbuild.2014.08.013>

Mediterranean climates. The magnitude of these figures suggests the utility of the multifunctional envelope technology employed, when integrated with systems which usefully process and distribute the thermal energy collected at the envelope. Heating and cooling loads were determined to be more balanced than in baseline models, indicating the utility of additional thermal storage technologies beyond those modeled in this study, and the possibility of energy-positive performance for this class of buildings.

### **3.4 Development of Integrated Optimized System Using Solar Energy for Electrical and Heat Applications**

To capitalize on the high-quality thermal energy that a system such as ICSF can generate, certain capabilities and organization are required of a building's thermal distribution systems. Specifically, systems must exist that store and release thermal energy at several specific temperatures, in order to synchronize resources with demands. Additionally, in order to minimize energy losses, systems that use or store high-quality generated heat must be located in-situ at the location of the thermal generation – the façade.

Required thermal storage and distribution capabilities are not novel, however, and as re-arrangements of existing technologies, are familiar in commercial office space.<sup>74</sup> Namely, hot-water and hydronic heating/cooling systems already contain the necessary components to capitalize on façade-generated resources: storage vessels, boilers, chillers, pressure modulation, piping distribution, and room transfer units.

The organization of building systems closer to the building's façade is, however, atypical relative to current as-built large building systems. The paradigm shift preferences smaller, multiply redundant components over larger centralized components. This distributed organization is more closely related to the layout of HVAC systems that have been retrofit into sub-divided commercial office towers, where individual lessees specify climate control systems relative to their own requirements.

---

<sup>74</sup> Further integration and development of the façade energy paradigm would optimize systems for climatic resource allocation (rather than for centralized fossil/grid power supplies), and component technologies will diverge from precursor building systems.

### **3.4.1 Localized Thermal Management and Onsite Energy Distribution**

Systems that use and manipulate heat in the built environment are organized according to the principles of heat transfer: masses exhibit heat capacities according to material properties and density, and energy flows between masses via convection, conduction and radiation. In order to maximize the thermal resource collected with an active façade, the work that can be accomplished must be measured against losses through insulation (which is designed to inhibit thermal transfer) and the parasitic losses of the work required to circulate mass in the thermal transport system. Minimizing the pumping power required to circulate heat transfer fluid (HTF) improves overall collection efficiency, as does minimizing the overall thermal conductivity of the thermal pathways. In the current ICSF prototypes, thermal collection is done with a hydronic system. In future iterations, heat pipes will be employed to leverage the advantages of latent energy transformations. Although employing heat pipes will negate the pumping power needed to circulate working fluid past individual modules, the efficiency of both methods is inversely proportional to the physical size of the thermal transport network, as longer pipe runs have proportionally greater surface area across which heat is lost. This relationship therefore preferences multiple, distributed applications: high-quality thermal energy collected at the façade is used at the façade for best efficiency.

### **3.4.2 Applications for Thermal Energy Captured at the Building Envelope**

Introducing Phase Change Material (PCM) into the high-temperature hydronic tank in the ICSF system theoretically improves the storage of high quality thermal energy by maintaining the working fluid at discrete temperatures. Most current research on PCM focuses on the material's ability to stabilize temperatures around thermal comfort for building occupants. We are investigating, however, how the same material properties that make PCM useful for buffering interior building temperatures could be appropriated to increase solar thermal collection efficiency. By absorbing thermal energy in the form of latent heat, the PCM allows the hydronic thermal buffer to remain at a nominal temperature while being charged or discharging thermal energy. This increases the collection efficiency of ICSF by minimizing the temperature difference between the

working fluid and the ambient air, and maintains the COP of a driven thermodynamic process by maintaining an optimal inlet temperature.

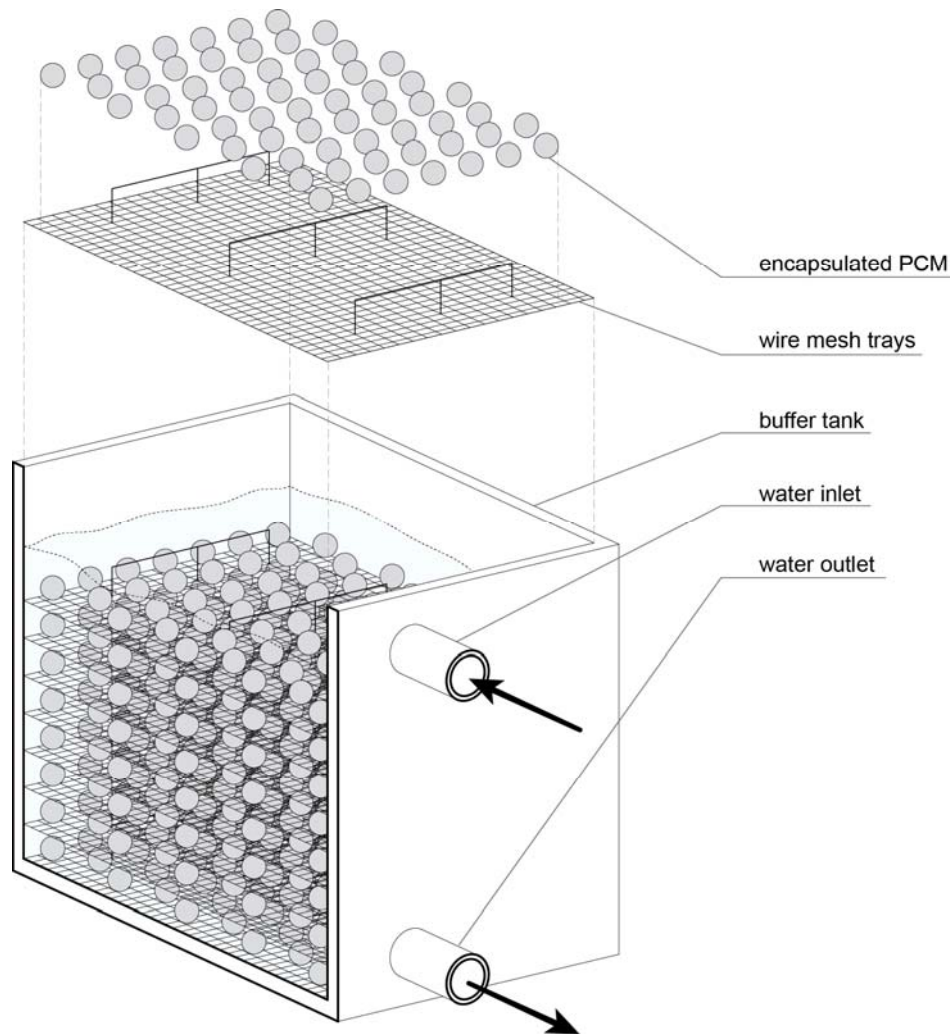


Figure 76. Schematic for introducing PCM to thermal storage buffer in ICSF.

### ***3.4.3 Passive Thermal Storage Techniques for Access to Thermal Energy According to Demand***

By classifying thermal resources according to tiers of potential, and distributing the storage of these resources throughout a building, maximal use of collected thermal resources can be attained. Interlinking distributed storage locations, such as with current-technology hydronic heating and cooling systems, enables heating and cooling capacity to be delivered where it is required in a building environment.

The three-tier strategy of thermal storage and buffering—sub-ambient for cooling capacity, super-ambient for heating, water preheat, and active rejection cooling, and high-grade for active chilling, dehumidification and ORC electrical generation—is identified as a flexible framework with which to maintain thermal energy at useful potentials. Applying higher-grade thermal energy as immediately as possible makes best use of the captured exergy, as this energy dissipates most drastically through time. In typical commercial building programs where a certain amount of cooling capacity is required on a daily basis, it is clear that directing high-quality energy directly to chilling processes makes best use of the resource. Cooling capacity is built up, by chilling the mass of water in a storage tank. This cooling power can be stored for a duration, and dispatched when heat gains increase and cooling loads arise. The sizing of storage is done in accordance with the modeled demands of a project, as influenced by program, building structural and systems specifications, and prevailing climatic conditions.

#### ***3.4.4 Applications for Electrical Energy Generated at the Building Envelope: Novel Techniques for Integrating Harvested Daylighting with ICSF with Bioresponsive Electrical Lighting***

In order to provide commercial building stock with its electrical requirements from on-site solar resources, it is essential that the daylighting strategies are fully synchronized with a highly efficient smart lighting system, such that the overall lighting loads can be optimally reduced. CASE is partnering with the Rensselaer Smart Lighting Engineering Research Center (ERC) to develop a series of integrated test beds within Rensselaer facilities in order demonstrate the full benefit of integrating daylighting from ICSF with emerging solid state lighting techniques that allow for unprecedented control over the basic properties of light, in order to allow building occupants to better support their natural circadian rhythms through daylighting, with the promise of a powerful range of associated health and well-being benefits, from better sleep cycles to the reduction of drug dependency and even reducing the risk of certain types of cancer. With our collaboration at the ERC, we are planning a demonstration at Rensselaer in 2014, which will be the first fully integrated daylighting/intelligent electric lighting system that goes beyond existing systems that are designed to self-calibrate with sensors and dimmers, to allow maximum use of available natural daylight into interior spaces.

Rather, by looking at lighting systems holistically (from integrated systems to the nanoscale characteristics of light generation and detection), we are looking at how to integrate a whole building energy-efficient lighting system that (1) "sees" *where* the light is going, and *what* it is doing, (2) communicates using light to send information and enable lighting information processing, and (3) has novel control systems that "think" about what the light needs to be doing to meet the expectations and requirements of people.<sup>75</sup>

#### **3.4.4.1 Project Overview: Realizing Energy and Health Benefits with Commercial Building Retrofits that Integrate ICSF with Emerging Smart Lighting Techniques**

Because buildings account for 41% (40 quadrillion BTU/year) of the primary energy consumption in the USA in 2010, there is a widespread opportunity to drive voluntary uptake of cost-effective efficiency measures in small commercial buildings, saving significant energy, costs and greenhouse gases, while dramatically improving the health and wellbeing of occupants, by providing an integrated retrofit of daylighting with Bioresponsive smart lighting. Energy efficiency retrofits are already considered to be among the most cost effective ways for the nation to reduce its energy use and carbon emissions in existing buildings; nevertheless, many technical, policy, financial, and business model challenges impede the uptake of rapid and scalable cost effective solutions that integrate a retrofit of the building envelope in concert with interior ECS. This project takes the proven model of a combined façade and lighting retrofit to another level of energy reduction and self-sufficiency, by providing all electricity requirements for the lighting scheme on-site through solar energy capture. Consumers and stakeholders in the market need consistent, accessible, and trusted information that provides sound technical information about the costs, benefits, and trade-offs of energy efficiency measures and services.

The project we are co-developing between CASE and the ERC is designed to drive increased uptake in the commercial building sector of energy efficient lighting solutions through an integrated plan that includes accessibility to transparent pricing and a proven

---

<sup>75</sup> Statement from the Director, Bob Karlicek, Rensselaer Smart Lighting ERC

distribution system coupled with bundling of financing, rebate and incentive packages, that fully realize the benefit of an integrated façade/lighting retrofit. It is focused on extreme energy efficiency measures that place value on high quality design and ultra-efficiency, workforce education, streamlined supply chain access, and bundles all information, tools, and guidance needed for building owners and managers to move forward with confidence. This effort expands on the partners' past efforts to develop a fully integrated nationally accessible solutions procurement system for intelligent integrated day/lighting strategies.

#### **3.4.4.2 Objectives of Integrated Retrofit Demonstration**

New LED lighting solutions, new daylighting strategies and integrated control systems for energy efficient illumination offer a geographically universal approach for large energy savings in new construction and existing commercial buildings. Today, significant and persistent technological, educational and market barriers make it very difficult for building owners and managers to specify, install and realize these significant energy savings through an integrated strategy. The Smart Lighting Engineering Research Center (ERC), Center for Architecture, Society and Ecology (CASE) and the Rensselaer Facilities Management group) in conjunction with Light Think University and Light Think Studios, Wiedenbach-Brown and Solid State Capital Services are creating an extremely innovative technical, educational and business platform designed to overcome these barriers. This project will provide consumers and stakeholders in the market with consistent, accessible and vetted technical information about the costs, benefits, and trade-offs of daylighting that is combined with energy efficient lighting and control solutions. The new sustainable, smart day/lighting system is targeted to outperform the most stringent energy code, ASHRAE 90.1 2010 by more than 80%. Together, by 'shading' with transparent materials that allow for access to views and diffuse daylighting, while with integrating lighting, will produce 20% or better total energy reductions for new or existing buildings from dramatic reductions in lighting loads. (NOTE: this figure is only from daylighting and lighting and does not include savings from reduced solar heat gain, or solar energy capture and distribution towards other

applications) This platform contains three key ingredients, which translate to these project deliverables:

1. ***Proof of Concept:*** Using university spaces typical of small commercial building types, this team will install ICSF, alongside state-of-the-art LED lighting systems integrated and building controls to demonstrate and document methods, products, installation practices and energy savings.
2. ***Building-type Application Guides:*** CASE will work with established LED lighting designers (Light Think Studios) and well-known lighting specialist, Wiedenbach-Brown, working in conjunction with Rensselaer's Smart Lighting ERC and the campus Facilities group, to establish a cost effective supply chain with prequalified suppliers and applications specific product and financing mechanisms (through Solid State Capital Services) to streamline the integration and installation of smart lighting in conjunction with high quality daylighting through ICSF with responsive light control systems at the lowest possible cost.
3. ***Functional Business Model:*** By creating exemplary university day/lighting solutions through on-site solar energy capture with extensive, web accessible application notes, documented energy savings, tested design methods, a cost effective product procurement client interface, installation guidelines and integrated financing services, a scalable, updatable platform for extending energy efficient solutions to other educational institutions, government buildings and commercial building owners throughout the United States will become available.

This strategy that has been developed by the ERC and CASE provides the commercial building sector with accessible, ultra-efficient day/lighting and customized control solutions, innovative in the demonstration platform and business model approach. The demonstration platform is the university campus, which is a microcosm of a range of small commercial building stock. Rensselaer Polytechnic Institute as a demonstration partner in this effort provides access to these prototypical small, commercial building

types for retrofits. By launching from an academic facilities base, development of educational collateral and an enlightened stream of future engineers, architects and business managers will help drive sustained growth through a wide commercial market place. The proposed solution will achieve over a 20% energy savings in new or existing buildings through integrated day/lighting and building illumination control solutions. (NOTE: This does not include additional savings from solar capture, heat gain reduction through ICSF) The composition of the energy saving plan consists of: lighting, plug load, cooling load, shading and daylighting.

The effort, as described above, would geographically begin in the Northeastern U.S., with concentrated efforts in research, design, development through the integration of lighting and building control systems in the establishment of proof of concept sites. These sites could be used to recruit additional sites to expand to the regional level, where the process continues with business model refinement through test, assessment and evaluation of the technology, demonstration sites, and web based client interface. Successful implementation and achievement of metrics at the regional level would lead to full scale national deployment, to include widespread partnerships, marketing campaigns and education and training to support the growing demand for accessible ultra-efficient solid state lighting and integrated building control solutions for commercial buildings including compliance and outperformance of the most stringent energy code, ASHRAE 90.1 2010.

#### ***3.4.4.3 Overview of Market/Commercial Viability***

The proposed strategy provides the commercial building sector with fully self-sufficient, on-site generated accessible, ultra-efficient day/lighting and control solutions and is innovative in its demonstration platform and business model approach. The demonstration platform is the university campus, which is a microcosm of a range of small commercial building stock. Rensselaer Polytechnic Institute as a demonstration partner in this effort provides access to these prototypical small, commercial building types for retrofits. By launching from an academic facilities base, development of educational collateral and an enlightened stream of future engineers, architects and business managers will help drive sustained growth through a wide commercial market place. The

target commercial building types and their campus equivalents, justify the initial local deployment, then subsequent expansion to the regional and national levels. A summary of a before and after installation comparison is shown in Table 24.

Table 23. Target Commercial Building Types and Campus Equivalents.

TARGET COMMERCIAL BUILDINGS AND UNIVERSITY CAMPUS EQUIVALENTS				
Education	Classrooms / Laboratories	Dormitory	Campus Store	Dining Hall
Small Hotel	Admin/ Conference Space	Rooms	Retail	Kitchen/ Hospitality
Office	Offices / Hallways	Midrise Apartment	Retail	Quick Service Restaurant

Table 24. Representative Before and After Installation Comparison.

BEFORE	AFTER
	
Single Source of Light	Multiple Sources of Light
Static intensity, color & distribution	Dynamic intensity, color & distribution
No flexibility of use	Flexibility of use
On/Off Switch	Dimming, Daylighting, Shading Controls
	Delivers 80% + lighting energy reduction

The proposed solution will demonstrate over a 30% energy savings in existing buildings through partial building retrofits that implement solar energy capture, heat

mitigation, integrated lighting and building illumination control solutions. The proposed business model has been developed explicitly to overcome the market barriers in the national deployment of an integrated lighting and building illumination control solutions provider service. The primary barriers addressed are discussed below.

### ***Achieving Credibility within the Marketplace***

Whom to trust for independent, reliable and appropriate to application product recommendations for innovative, emerging building products? For solid state lighting applications, here are more than 7,500 LED lighting products registered on DOE Lighting Facts alone to choose from. It is confusing and overwhelming. How do small business owners without any knowledge of lighting choose correctly? We all know that faced with too many choices leads to decision paralysis then nothing happens.

Small commercial business owners are busy with daily operations leaving little time to research and put in place integrated energy efficient measures. The ERC online platform featuring application specific “in-box-solutions” that has the right product, transparent pricing and financial services will make implementation easy, convenient and accessible.

Our online platform will help to remove the fear and instill confidence by showcasing demonstration projects utilizing the Application Guides, products, and services with real published costs. In addition, we are independent of manufacturers so, product selection will always be based on application performance.

### ***Market Channel and Cost***

It is not uncommon within the commercial lighting market channel to see between four to seven margin stacks. Beginning with the manufacturer’s representative who receives a commission, then adds overage to the manufacturer’s cost before pricing it to a wholesale distributor, next the wholesale distributor adds margin, then the electrical contractor puts margin on, then possibly the general contractor, designer or architect. This in many cases doubles or triples the original cost from the manufacturer.

Our online platform is committed to transparent pricing. We negotiate directly with manufacturers and then transparently add 15% for “Application In A Box” Solutions. We remove the margin stack and make these highly energy efficient solutions affordable.

### ***Accessibility***

There are many resources for “silo” information...a place for LED lighting, a place for daylighting, a place for best design practices, a place for rebates, and thousands of places for manufacturer products. They are all without specific, independently vetted product choices for everyday applications with transparent pricing. It makes the retrofit or new construction process unnecessarily complicated.

Our online platform will have in one, easy-to-find place have all the credible information needed to make informed decisions about design, product selection, control programming and implementation practices for electric lighting, daylighting, solar shading, lighting and plug-load controls for application specific projects. We take the complexity of system integration out of the buying equation.

Partnering with local utilities and local and regional organizations like the Chamber of Commerce, a city’s business development department and U.S. Green Building Council chapters we will create local word-of-mouth and motivate action.

#### ***3.4.4.3.1 Split Incentives and Multiple Stakeholders: Knowledge, Training and Experience***

Knowledge has not kept pace with technology. For example, most commercial buildings still lack, after more than twenty years, any type of day/lighting controls other than an on/off switch. Many electrical contractors don’t know how or like to install integrated lighting controls, most building owners don’t know to ask and many designers don’t want to get in the middle and risk responsibility. This is just one example of the lack of knowledge, training and experience that is needed to make 20% energy efficiency a reality.

The ERC program features not only offers online education modules but also a plan for classroom curriculum modules for both university settings and community colleges. It also will put together presentations for repeatable workshops.

### 3.4.4.4 Description of Impact

The proposed project's impact on overall energy savings is shown best in Table 25, identifying the breakdown of the components contributing to the potential overall US energy savings solutions. Please note that these figures *only* account for the added savings due to daylighting combined with smart lighting techniques, and do not account for energy savings due to other applications of ICSF, such as solar capture, heat gain mitigation, reduction in initial costs of HVAC equipment, etc.

Table 25. Proposed components of energy savings of LED smart lighting system integration (not including solar energy capture or solar heat gain mitigation from ICSF).

<b>ENERGY SAVINGS</b>	<b>% Reduction</b>	<b>Potential US Commercial Small Bldg kWh Savings<sup>1</sup></b>	<b>Reference for and/or calculation notes</b>
Lighting	16.10%	8.61x10 <sup>11</sup> kWh	DOE Building Energy Data Book, 2011
Plug load	2.50%	1.34 x 10 <sup>11</sup> kWh	New Buildings Institute Guidelines, 2012
Cooling load reduction	0.5% – 2.5 %	Max. 1.34 x 10 <sup>11</sup> kWh	DOE Building Energy Data Book, 2011
Shading	1.5% - 3.9%	Max. 2.09 x 10 <sup>11</sup> kWh	DOE Building Energy Data Book, 2011 Lutron Electronics Product Info, 2013
Daylighting	2% - 5% (building dependent, some studies give numbers as high as 24%, Not counted when shading used)	Max. 2.67x10 <sup>11</sup> kWh	Based on published daylighting energy savings estimates, kWh saved calculated from energy used by LED/controls systems during daylight hours
<b>Total</b>	<b>21% - 25%</b>	<b>1.61 x 10<sup>12</sup> kWh</b>	

<sup>1</sup> *Calculations to show potential savings in US, assumes 100% adoption in US Small, Commercial Building sector*

Lighting energy savings can be best demonstrated through reference to past lighting and controls solutions implemented by team member Light Think Studios as previously summarized in Table 25. Several specific examples are shown in which 80% - 90% lighting energy savings is achieved with over 95% installation of LED lighting. Plug load energy savings are achievable through the implementation of occupancy-based and or load-based plug load control systems<sup>76,77</sup>. Fully integrated into building control systems, plug load energy reduction can easily attribute for 2.5% energy reduction in commercial spaces. Cooling load reduction is a quantifiable byproduct of the installation of energy efficient LED lighting systems. Although geographically dependent for the total energy savings contribution, energy efficient lighting installations with reduced input wattage, reduces the amount of heat released by the lighting system, and therefore reduces the requirements of the air cooling system. The measurable contribution to the energy savings is calculated to be in the range of 0.5% - 2.5%, depending on geographic location<sup>78</sup>.

---

<sup>76</sup> Plug Load Best Practices Guide, New Buildings Institute.

<sup>77</sup> Acker, B., et al. "Office Space Plug Load Profiles and Energy Saving Interventions," ACEEE Summer Study on Energy Efficiency in Buildings, 2012.

<sup>78</sup> <http://www.lightsearch.com/resources/lightguides/hvac.html>

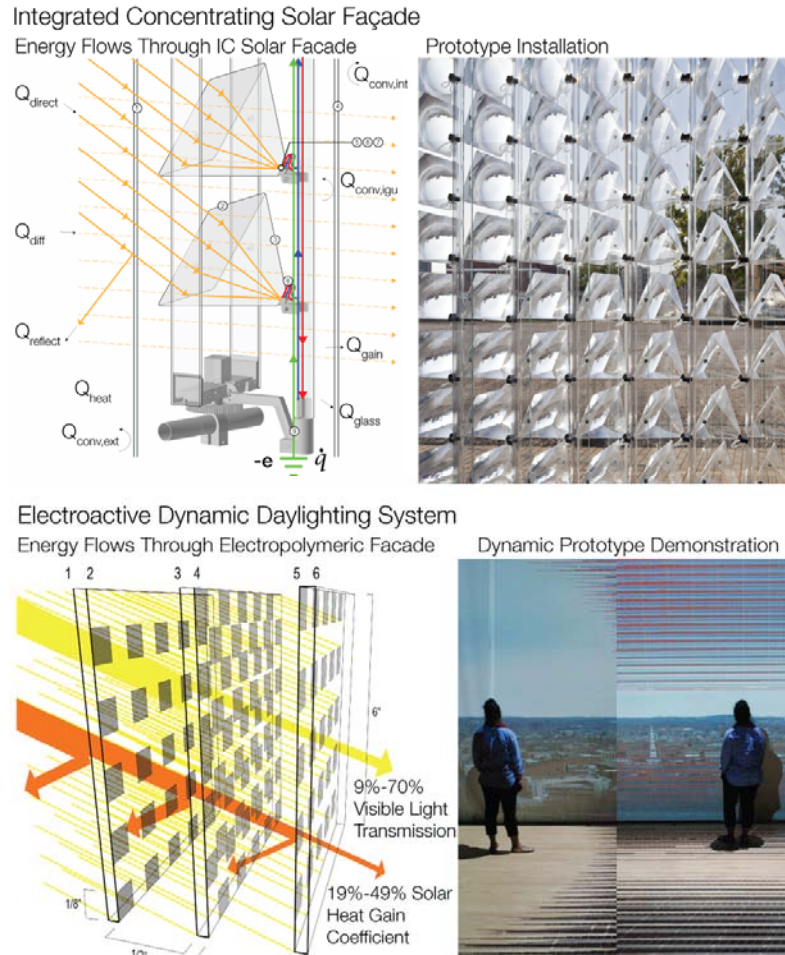


Figure 77. Comparison of daylighting performance: ICSF & Electroactive Dynamic Daylighting System<sup>79,80,81</sup>

Prior studies of light shelves, automated blinds, or switchable glazing, where façade daylighting technology is coupled with smart lighting controls to reduce lighting and cooling energy loads, show a potential to achieve up to 24% in electric lighting energy

<sup>80</sup> Krietemeyer, E., Smith, S., Dyson, A. (2011). Dynamic window daylighting systems: electropolymeric technology for solar responsive building envelopes. Proc. SPIE, 7976(1), 79763A.

<sup>81</sup> Andow, B., Krietemeyer, B., Stark, P.R.H., Dyson, A.H. (2013). Performance criteria for dynamic window systems using nanostructured behaviors for energy harvesting and environmental comfort. Proc. SPIE, 8692, 86923V.

savings.<sup>82,83</sup> Effective solar shading and daylighting strategies at the façade depend on the dynamic matching of available daylight with occupant demands for visual comfort. Conventional façade strategies, including light shelves, manual or automated blinds, fixed or automated louvers, and switchable glazing struggle to reduce building energy loads while improving visual comfort. Electrochromic windows are unable to precisely adjust to shifting solar geometries and intensities; with limited variability and control, they are unable to provide a specific response desired by the user, and their response time is generally considered too long. Furthermore, such existing dynamic glazing technologies block a large portion of usable daylight, limit clarity of view, while still being substantially limited in their control of heat gain, glare and visible transmission. The ICSF controls the direction and intensity of daylight, addressing contrast ratios and glare by directing diffuse daylight into the building and by tracking and intercepting direct beam daylight during periods of high illumination, effectively separating visible transmittance from solar heat gain. The benefits of daylighting associated with the IC Solar Façade technology are thereby coupled with energy harvesting (PV and heat capture); DC transfer to electrical applications; substantial reduction in solar heat gain; diffuse daylighting. The cumulative benefits of the ICSF will be characterized and compared with the operational benefits associated with other emerging and competing dynamic daylighting systems such as electroactive polymeric dynamic façade technology, which include: high user control within varying interior spaces; rapid switchability for more effective user control; real time control of the heat transfer properties of the IGU; alongside substantial value-added options for patterning, color and other visual effects and possibilities for information exchange. Coupling façade daylighting technology, LED lighting and lighting controls will provide additional contributions to total

---

<sup>82</sup> Leslie, R. P., Raghavan, R., Howlett, O., & Eaton, C. (2005). The potential of simplified concepts for daylight harvesting. *Lighting Research & Technology*, 37(1), 21-40. doi: 10.1191/1365782805li127oa

<sup>83</sup> Lee, E. S., DiBartolomeo, D. L., Klems, J. et al., (2006) "Monitored energy performance of electrochromic windows controlled for daylight and visual comfort," Annual Meeting of the American Society of Heating Refrigeration and Air-Conditioning Engineers. 112, 122-141.

energy savings in the 15% - 25% range for the targeted small commercial building sector.<sup>84</sup>

Applying the proposed integrated lighting and controls solution to a representative education building on a college campus, approximately 50,000 ft<sup>2</sup> in size, the annual energy savings estimated in Table 26 are expected.

Table 26. 50,000 ft<sup>2</sup> Education Building Annual Energy Savings Estimate

<b>Current Building Annual Energy Use</b>	<b>850,000 kWh</b>
Lighting & Controls savings	136,850 kWh
Plug load savings	21,250 kWh
Shading / daylighting savings	25,500 kWh
Cooling load savings	10,625 kWh
Reduced Building Annual Energy Use	655,775 kWh
Annual Energy Savings	194,225 kWh
Annual Energy Savings (%)	22.85%
Annual Carbon Emission Savings (metric tons)	137 MT

As shown above, the impact of the design solution can easily be tracked through energy savings audits conducted periodically on the buildings the designs are applied to. The impact of the business model can be tracked through monitoring the usage of the deployed website, by tracking and modeling the website activity such as application guide downloads, procurement tracking, service provider network reports. The 21% to 25% energy savings is expected across all target building types previously listed in Table 2, including Education, Small Hotel, Office, Retail, Quick Service Restaurant, and Midrise Apartments. Many small commercial building types could benefit from the proposed solution, with the exception of historic buildings. Based on available data, this

---

<sup>84</sup> Dyson, Anna H., Jensen, Michael K., and Borton, David N. (2010) Concentrating Type Solar Collection and Daylighting System within Glazed Building Envelopes. US Patent 7745723 B2.

solution has the potential to impact over 4.4 million (> 90%) commercial buildings (non-mall,  $\leq 50,000$  ft<sup>2</sup>) in the United States (CBECS 2003, Table B6).

#### **3.4.4.5 Analysis of Costs for Integrated Façade/Lighting Retrofits**

The business model in the proposed solution is innovative with integrated application research and design (improved lighting experience and quality with large energy savings), independent product vetting, transparent pricing, trusted distribution system, bundled financing, rebates and incentives joined with education, training and marketing campaigns. This approach is easily scalable as all solutions, application guides, and financial mechanisms are streamlined for online accessibility making it easy to scale from the initial local level through national deployment. As such, there is no standard solution to compare to. At best, we can provide a baseline comparison to a standard, renovation or remodeling effort involving a lighting and building control system in which products and services are identified and procured through a general contractor, where costs are difficult for the building owner to control. Alternatively, in the business model of the proposed solution, product and services solutions are purchased owner direct, guaranteeing a reduction of at least 2 margin stacks. In addition, product and service offerings will be bundled directly with financing, rebate and incentive options for the building owner. Depending on the size of the installation, the resultant cost savings are potentially significant and controllable by the building owner. The typical return on investment will range from immediate to five years.

#### **Approach to Project Risk**

The primary risks in the successful full scale implementation and national deployment of the innovative business model to provide new daylighting strategies, new LED lighting solutions, and integrated control systems for energy efficient illumination for large energy savings to existing commercial buildings owners include:

Risk 1: Convincing qualified vendors to bypass established distribution channels required by proposal model for product sales and on-line channel creation.

In the proposed business model, this is addressed through the execution of compelling, documented campus installations demonstrating revenue potential and

education students who are future designers and specifiers. The collaborating team includes significant experience and excellent reputations in the architectural, building engineering, and lighting industries.

Risk 2: Building skilled workforce needed for design and installation of advanced lighting/daylighting/controls

In the proposed effort, this is addressed with the execution of installations with educational collateral at universities that will have trickle down training potential. The collaborating team has a strong educational component with significant experience in educational outreach, which is paramount to the success of this effort and effectively minimizes this risk.

### 3.4.4.6 Deployment

Our proposed demonstrations include a definitive plan to transition from the research phase towards deployment as summarized below.

Table 27. Phases of ICSF Development

<b>PHASES OF DEVELOPMENT – Ultra-efficient day/ lighting solution for commercial buildings</b>	
<b>Research</b>	- Identify 10 most energy intensive spaces for comm. buildings
	- Application discovery research and field observations for each
	- Perform ROI, experience, energy, stewardship analysis
<b>Design for 80% Energy Reductions</b>	- Determine visual environment needs and energy allowances
	- Design integrated daylighting and electric lighting system
	- Integrated system - lighting, daylighting, shading, plug loads, and reduced HVAC loads related to inefficient lighting
	- Conduct vetting process for product specifications
	- Perform ROI, experience, energy, stewardship analysis
<b>Development</b>	- Design process and results Application Guides with
	- Website and demonstration sites/experience centers
	- Prioritize energy intensive zones with rebate infrastructure first

<b>Regional Deployment</b>	-	Investigate high-profile energy intensive commercial opportunities in various regions to deploy and showcase success stories
<b>Test/Validation Assessment</b>	-	People, energy, stewardship (including financial) metrics
<b>Design Refinement</b>	-	Assessment and evaluation of demonstration sites
	-	Continually review products for better performance
<b>National Deployment</b>	-	Partnerships (utilities, corporate, local community groups)
	-	Marketing campaign (website, social media, videos, collateral)
	-	Education and training (education modules)

The business processes, guides, demonstration sites, and all deliverable materials from this effort will be wholly produced in an environmentally safe manner in the United States. The path to self-sustainability includes revenue generation efforts, whereby the content and processes developed are integrated to develop interactive software applications which will be offered for license and/or subscription contracts paired with advertising and sales commission revenue through the web based interface.

#### **3.4.4.7 Target Markets**

The specific commercial buildings types (<50,000 ft<sup>2</sup>) targeted by this effort include:

- Education Buildings
- Hotels
- Office Buildings
- Retail Spaces
- Quick Service restaurants
- Midrise Apartments

Evaluating the market potential to support the scale up of the proposed innovative technical, educational and business platform to deploy energy efficient integrated solutions to the small commercial building space on the national scale shows steady, continued growth in the commercial building sector for the categories of number of buildings, floor space, and energy consumption. Table 6 below identifies the allocation of the targeted commercial building spaces with respect to number of buildings, floor

space, and energy consumption. These targeted building types include the top 3 in all categories substantiating that the proposed effort is targeting a well-defined commercial building market with the highest potential impact. Table 7 and Table 8 below show projection data for the entire commercial building sector for floor space and energy consumption.

Table 28. U.S. Commercial Building Types and Features, as percent of total.

<b>Building Type</b>	<b># of Buildings</b>	<b>Floor space</b>	<b>Energy Consumption</b>
Office	17%	17%	19%
Mercantile (Retail)	14%	16%	18%
Education	8%	14%	11%
Lodging	6%	7%	6%
Food Service	3%	2%	7%

*Source: Building Energy Data Book, 2011*

Table 29. U.S. Commercial Sector.

Projected Energy Consumption

<b>Year (Projection)</b>	<b>Total Energy Consumption (Quadrillion Btu)</b>
2010	18.3
2015	18.2
2025	20.1
2035	21.8

*Source: Building Energy Data Book, 2011*

Table 30. U.S. Commercial Sector Projected Floor Space.

Projected Floor Space	
<b>Year (Projection)</b>	<b>Total Floor Space (Billion ft<sup>2</sup>)</b>
2015	84.1
2020	89.2
2025	93.9
2030	98.2
2035	103

Source: *Building Energy Data Book, 2011*

The data provided above is further evidence that the projected growth of the commercial building market will support and need the proposed business model. Utilizing people-inspired design methods, solid-state lighting products, solar-shading, integrated smart lighting and plug controls, and renewable power sources will create sustainable and smart lighting systems achieving total building energy reductions of 20%. Creating an internet and app based platform for building owners will create easy access to application guides, educational modules, independently vetted product choices with links to DOE's Lighting Facts Label and website, transparent purchasing and financial services and local service providers. This seamlessly integrates the entire process for application specific implementation.

### **3.5 Building, Testing and Evaluation of Integrated System Using Solar Energy for Electrical and Heat Applications**

#### ***Prototype Tracking Improvements***

Regarding CPV design, the ICSF design continues to evolve a new approach to miniaturizing and distributing the essential components from concentrating systems into window assemblies. By taking advantage of the existence of the building structure, and proprietary optical designs, the over-design once required for (stand-alone) tracking mechanisms is no longer necessary. This addresses the principal problem that continues to plague the solar industry: the largest, and by far, most expensive component of any conventional high-concentration PV system is the tracker. In any high concentration system, tracking accuracy is paramount. In a laboratory setting, tracking accuracies within a few milliradians are possible. However, in the out of doors environment (such as solar PV farms), such numbers are rarely achieved with any system. When tested in 73 sites which were deemed as well suited to concentrator placement, the average wind speed during times of global normal insolation values of 975-1025 W/m<sup>2</sup> was measured at 4.5m/s.<sup>85</sup> This rather slow moving air mass, distributed over a large area results in a dramatic distortion of the tracking mechanism

---

<sup>85</sup> Kurtz, S. R. et al. Outdoor rating conditions for photovoltaic modules and systems. Solar Energy Materials and Solar Cells 62, 379-391 (2000).

and the attached concentrators. To increase the economic feasibility of the employment of high concentration systems, lens area is increased relative to tracker size. This results in even larger distortions. Even in large scale, model installations, with “perfect” tracking accuracy, angular deviations of greater than  $0.5^\circ$  were recorded along the aperture plane without significant wind loading.<sup>86</sup> In accurate optical models of common concentrator geometries, it has been shown that that  $0.5^\circ$  tracking error results in about a 10% drop in electrical output in average module geometries.<sup>87</sup> In more compact modules, in which the depth of the module, or effective focal length, compared to the characteristic lens width, the reduction in efficiency is much higher. This presents the essential trade-off that we are attempting with this system: inexpensive tracking assembly and motors, because we are using the building to brace the system against the wind for very large surface areas, however our module depth must be relatively small and our system tolerances far less forgiving than is typical within the building industry.

---

<sup>86</sup> Arboiro, J. C. & Sala, G. 'Self-learning tracking': A new control strategy for PV concentrators. *Progress in Photovoltaics* **5**, 213-226 (1997).

<sup>87</sup> Victoria, M., Dominguez, C., Anton, I., & Sala, G. (2009) Comparative analysis of different secondary optical elements for aspheric primary lenses *Optics Express* **17**, 6487-6492.

### 3.5.1 Generation 6 ICSF Prototype Experiments



Figure 78. ICSF Generation 6 working prototypes.

Generation 6 ICSF prototypes were installed at the Syracuse University Center of Excellence for operational, performance, and daylighting experimentation. Functional clarifications were made, informing 7<sup>th</sup> and 8<sup>th</sup> (current) generation prototypes.

#### 3.5.1.1 Generation 6 ICSF Prototype Description

Generation 6 of the ICSF prototype was a multi-scalar demonstration/installation at the Syracuse University Center of Excellence and took two primary forms. The first was a 64-module installation fully integrated into an IGU, and installed into the building façade. The functional purpose of this prototype was to demonstrate the system as an IGU integrated assembly, to demonstrate the quality of daylighting through the ICSF system, and to test the system tracking and alignment at a scale appropriate for integrating into the building façade.

The second form of ICSF Generation 6 installed was a mobile, 9-module, fully-instrumented testing array. The prototype was used for characterizing system effectiveness with the then-current optical design. The mobile array could be oriented in a vertical, horizontal, or inclined configuration, and oriented to any azimuth direction.

### **3.5.1.2 Generation 6 Assessment and Mechanical Issues to Address for Generation 7**

Operation and testing of the Generation 6 ICSF system brought to light several mechanical deficiencies in the system design that would need to be addressed in subsequent iterations.

- ICSF modules were overly constrained in the altitude axis when utilizing a rigid (glass) back tube as the altitude drive axis.
- Module assemblies needed to be more robust and various component connection details needed to be re-considered to include higher mating surface area or additional mechanical fasteners.
- Due to the design of the optical path, which included only a primary lens concentrating onto the PV cell, a prohibitively high degree of assembly precision and system tolerance was required to maintain all modules in proper alignment.
- The glued, two-piece metal heat sink with routed coolant channel failed to sustain required pressures.

### 3.5.2 Generation 7 ICSF Prototype Experiments

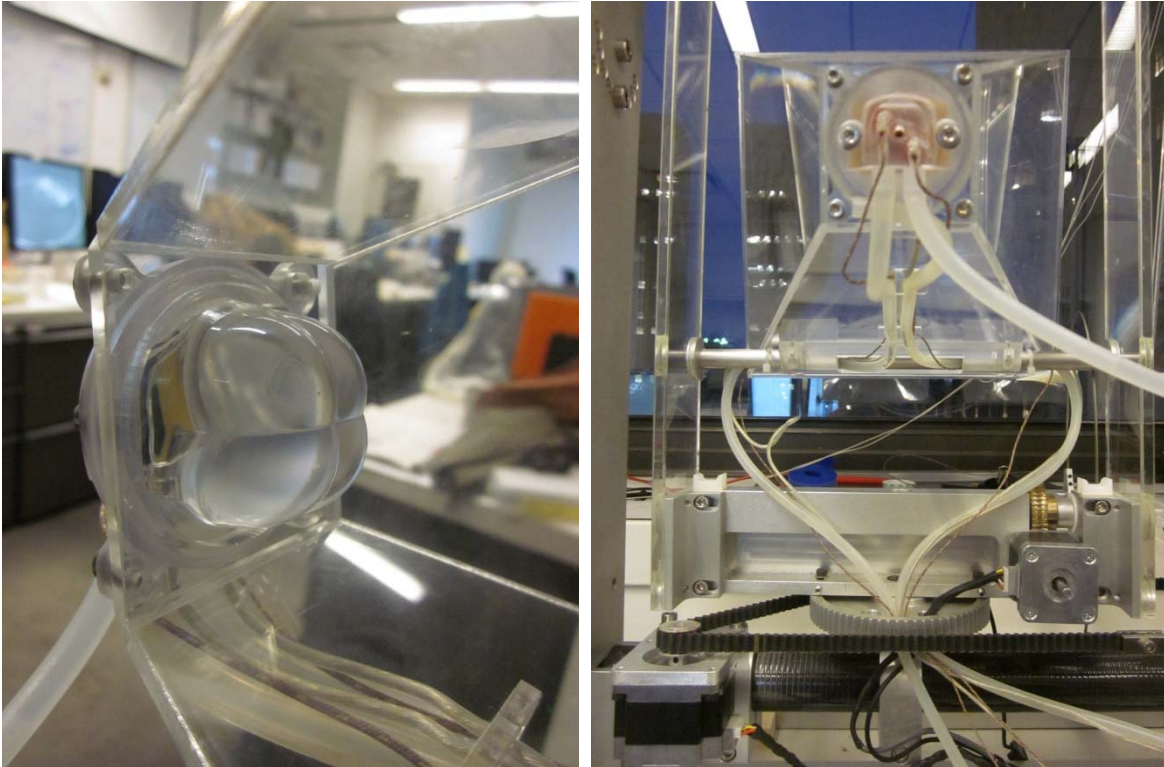


Figure 79. Secondary optical element and heat sink assembly in Generation 7 design.

#### 3.5.2.1 Generation 7 ICSF Prototype Description

Generation 7 of the ICSF system was designed and assembled between January and August 2011. The prototype is a 4-module array, mounted in an articulating aluminum frame to orient the array vertical, horizontal, or inclined in 20° increments. Revisions from the mechanical assemblies of Generation 6 include:

- A revised altitude drive assembly that eliminates the rigid back tube and alleviates over constrained altitude tracking was implemented. Altitude tracking is achieved via tension cable positioned at the front corner of each module.
- An optical train designed and provided by Light Prescriptions Innovators (LPI) for Opel Solar, that incorporates a primary PMMA optic lens, and a secondary glass lens mated to the PV cell. (See section 3.5.2.2 for further characterization of optical train.)
- Assembly and connection details for the system revised to address failures found in the Generation 6 prototype.

- A modified heat sink assembly to accommodate a higher flow rate through the system and better cooling of the PV cells. ICSF Generation 6 utilizes a modified copper pin matrix water block designed and manufactured by Swiftech for use in cooling computer CPU's. The performance characteristics of the water block assembly adequately meet the needs of the ICSF system.
- Discrete adjustment of individual modules, via set screw impingement upon the altitude axis tension cable, to adjust module pitch alignment.

### **3.5.2.2 Experimental Setup**

Tests of the Generation 7 ICSF were conducted on the premises of the Center for Architecture Science and Ecology (CASE), a Center of Rensselaer Polytechnic Institute (RPI), at 14 Wall St., Manhattan, NY in the later part of October 2012. During the reported tests, the conditions were exceptionally good for the evaluation of concentrators (DNI was quite high compared to AM 1.5 while scattered light was less.)

The ICSF employs both PV and material heating (in this case, H<sub>2</sub>O) for efficacious solar capture. The liquid water flowing behind the receiver (a multi-junction PV cell/ Au/Ni plated Al<sub>2</sub>O<sub>3</sub> substrate /thermally conductive adhesive (~.002" Arctic Silver® epoxy)/Cu 0.25mm pin matrix type heat sink) collects the power absorbed by the receiver which is not directly converted to electric power. Besides the thermal power collection, cooling has the additional effect of increasing the cell's electrical conversion efficiency. The power into the coolant can be productively employed via numerous methods (domestic hot water, refrigeration cycles, etc.; see Section 3.3.6.1) while the DC electricity is directly used in an inhabited structure for lighting and other DC loads such as computers and electronics. Both PV efficiency and heating efficiency are important in total capture efficiency. As such, both power absorbed by the coolant and produced by the cell are quantified during the test.

Change in coolant temperature was measured by insertion of 30 AWG fast response K type thermocouples into the inlet and outlet paths at the Cu heat sink. The analog voltage of the thermocouples was digitized by a thermocouple data acquisition module. The 24 bit National Instruments 9213 uses cold junction compensation and auto zero-ing in high resolution mode to achieve accuracy of +/-0.02°C or +/-0.06% at

30°C with a sample rate of approximately 4.5 samples/second. The coolant, tap water, was caused to flow through the heat sink by a FMI QD electric Lab Pump. The flow rate was measured by a Key Instruments GD 10810 flow meter. This instrument shows an accuracy of +/-3% of full scale (F.S.=565 ml/min,  $\text{error}_{\text{max}}$ : +/-16.95 ml/minute<sup>89</sup>). Electricity generation was measured by a programmable electronic load connected to the cell bus by soldered 18 AWG multi-strand, ultra-flexible Cu cables<sup>90</sup> (2m in length). The BK precision 8500 is an electronic load (power supply) that is programmed to evaluate peak power of the cell. The code, written in National Instrument's LabVIEW, adjusts voltage in increments of 5mV. The actual instrument measures current with an accuracy of +/-4.7% and voltage of +/-0.38% at these current and voltage levels. Evaluated at nominal values of peak power production, ( $j_{pp}$ =6.83A,  $V_{pp}$ =2.87V), this results in a potential error of +/-5.08% or +/-1.00W.

### **3.5.2.3 Optical Parameters and Module Assembly**

The modules of this test used optics designed by LPI, Inc. for Opel Solar. The optics of this test were purchased directly from LPI. They include a four quadrant PMMA Fresnel primary and a broad band A/R coated glass (B270) secondary. They have been designed for high concentration (>600X  $C_g$ ). In our case, we cropped the primary to achieve a  $C_g$  close to 500X. This is closer to the optimum efficiency of the cell. The cells of this test were produced by Spectrolab. The Spectrolab C3MJ+ cell was tested at close to 38.6% This value was verified by us using the focused ( $\sim f/10$ ) Cermac (Perkin Elmer) ultra-high pressure Xe lamp at the equivalent of a little greater than 300 suns at AM 1.5. We were able to measure cell efficiency within in two percentage points of 38% but as the field of the nominally collimated lamp is not very flat (greater than 30% increase over average on the perimeter) this measurement is useful for cell qualification, but not indicative of on-sun performance. The Spectrolab measurements

---

<sup>89</sup> Change in water density as a function of temperature was disregarded over the small change in temperature.

<sup>90</sup> Series resistance was measured using a 4 wire measurement to determine if the potential drop across the 18AWG wires introduced a significant error. It was determined that the 18AWG is large enough to introduce a negligible potential drop.

of their cell show a fairly flat response of the cell beyond 200 to 500X. Assuming that this is correct, we have, also, assumed that the cell efficiency should be close to 38.6% at 500X. The cells were coupled through index matching silicone (Dow Corning Sylgard 184) to the secondary. The two part silicone was de-aerated after base/catalyst mixing and after filling the vacancy between the cell surface and the back surface of the SOE. Irradiance on the lens of the module was measured by Hukseflux DR01 WRR pyrheliometer. This reference instrument shows the second largest potential error of +/- 1.0% to the composite errors in measurement.

### 3.5.2.4 ICSF Generation 7 Efficiency and Observations

The efficiency of a module is calculated with values in Table 31 (brackets denote worst case).

Table 31. Observed module efficiency (Electrical + Thermal), Generation 7 prototype.  
 Data collected October, 2012.

<b>Variable</b>	<b>Value (Lower Bound)</b>	<b>Value (Upper Bound)</b>
Incident direct normal radiation	882W/m <sup>2</sup>	817W/m <sup>2</sup>
DNI per Module	53.0W	49.1W
Measured output at PP	10.9W	11.0W
<b>Electrical Efficiency</b>	<b>20.6%</b>	<b>22.3%</b>
Water flow rate	0.7ml/s	0.9ml/s
Temperature change	8.74°C	9.14°C
Power change in water	25.6W	32.9W
<b>Thermal Efficiency</b>	<b>48.3%</b>	<b>67.0%</b>
<b>Total Efficiency</b>	<b>68.9%</b>	<b>89.4%</b>
Lens area	0.0601 m <sup>2</sup>	

The total collection efficiency calculation shows a close approach to the optical efficiency of the optical train which is a little bit better than 86%.<sup>91</sup> Of immediate note,

<sup>91</sup> Benitez, P., Minano, J., Zamora, P., Mohedano, R., Cvetkovic, A., Buljan, M., ... Hernandez, M. (2010). High performance Fresnel-based photovoltaic concentrator. *Optics Express*, 18(S1).

though, is the ratio of electrical efficiency to total efficiency, which should be very close to the cell efficiency (somewhat reduced because of the lack of conversion beyond the lowest energy junction which composes a small but significant part of the irradiance on the receiver) is not at the level at which it should be. It was discovered, post-test, that the effective focal length of the primary was about 25mm longer than was described in a model delivered by the manufacturer (this was a communication error between the scientists) resulting in an irradiated area quite a bit larger than the cell's active area; however, the light did fall onto the alumina substrate which was coupled to the Cu heat sink. We have, since, measured the assembly tolerances associated with axial and radial displacements from optimum. Through that measurement, we have redefined our assembly procedure and are pleased to report that ordinary mechanical assembly procedures result in theoretically optimum efficiency; that robotic/optical feedback assembly is not required for maximum bias towards direct electric conversion while still maintaining optimal overall efficiency Figure 80 shows one of two DR01 pyrhemeters currently in our employ on the same fixture used for assessing assembly tolerances as well as verifying reproducibility and quality of calibration of the pyrhemeters.

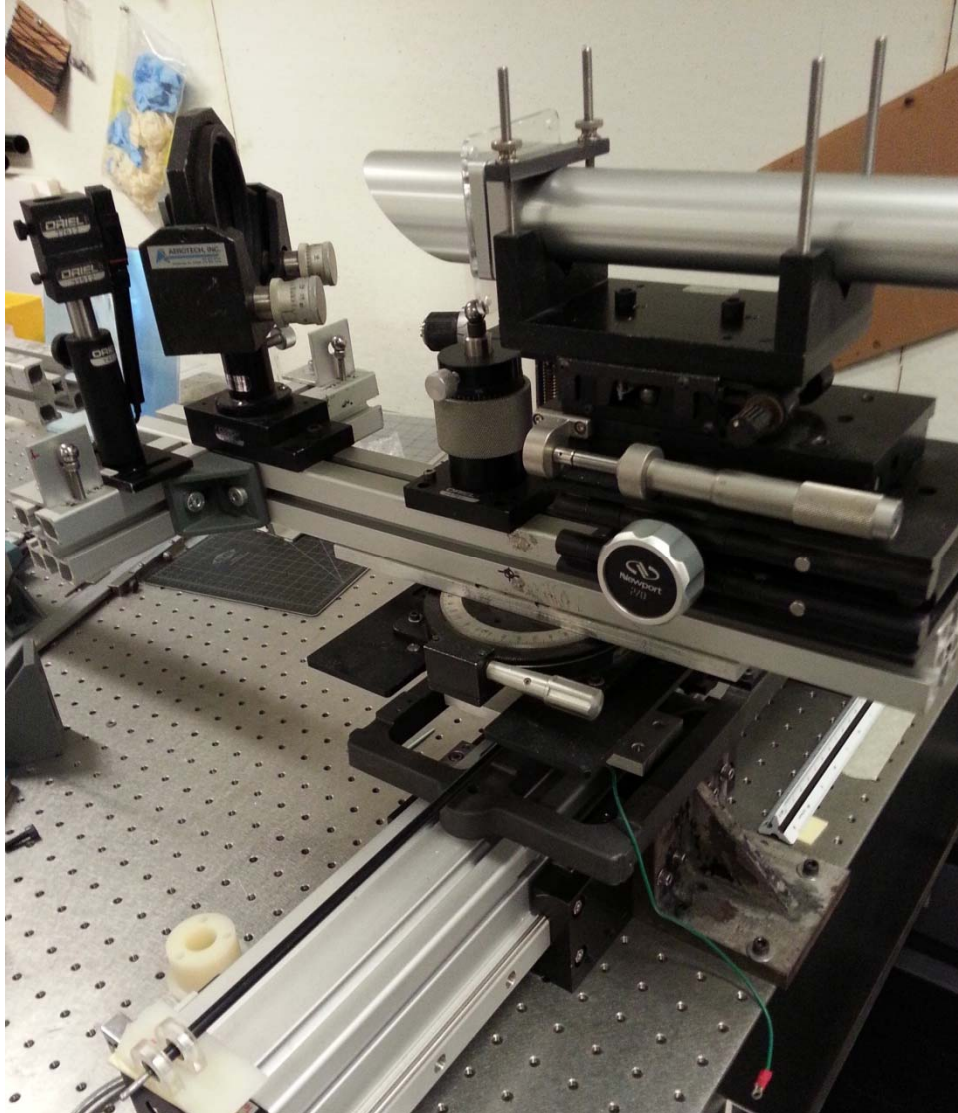


Figure 80. Pyrliometer mounted to measure sensitivity to flux.

This picture shows the degrees of freedom used in measuring the design and assembly latitude of the receiver to POE. In this case, the Hukseflux DR01 pyrliometer is mounted to view the filtered Xe arc lamp shown in Figure 81. The results of the assembly latitude with these optics is very encouraging and shows that ordinary two place (metric) or three place (imperial) machining tolerances in parts allows perfectly acceptable optical path alignment alleviating the need for closed loop robotic assembly.



Figure 81. Re-calibration of pyrheliometers.

During data collection in December 2012, while deploying two same-model pyrheliometers side by side, discrepancies were noticed in signal voltages. The pyrheliometers were re-calibrated against a known reference provided by the manufacturer (Hukseflux).

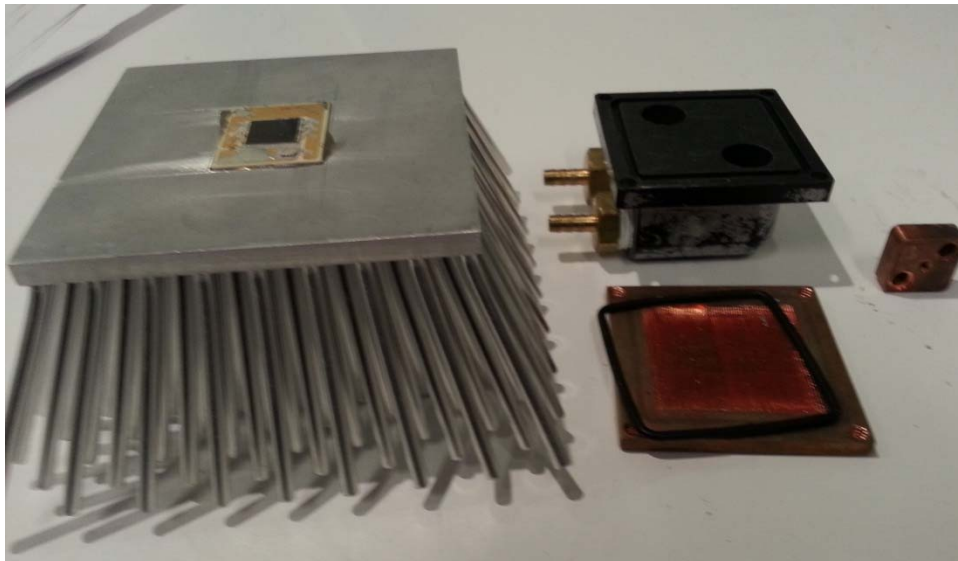


Figure 82. Potential heat sink designs.

Multiple heat sink options, providing equivalent cooling capacity, were explored for on the Generation 7 prototype, resulting in the optimized solution in Generation 8 (the heat sink of which is pictured far right).

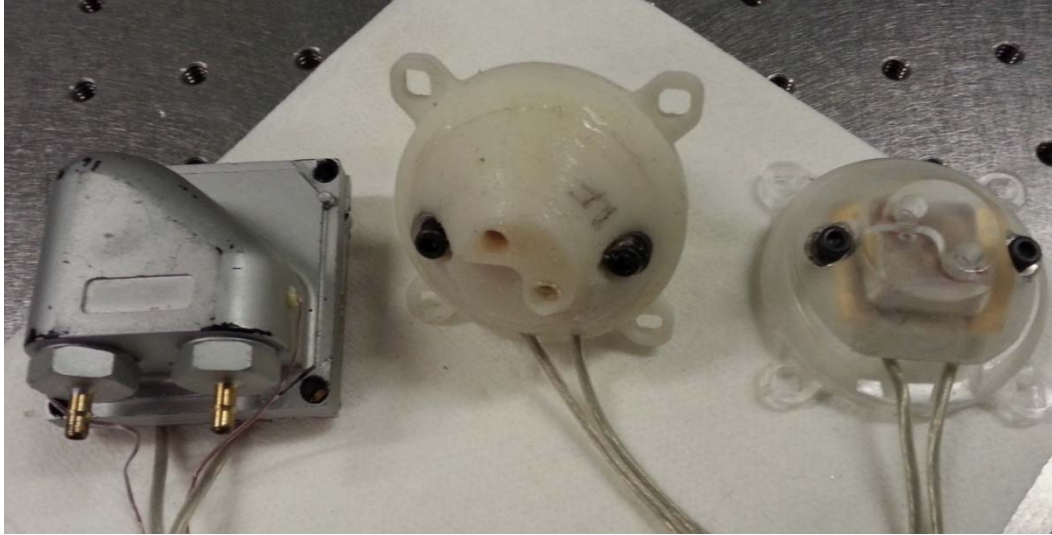


Figure 83. ICSF receiver and heat sink evolution.

Receiver and heat sink design updated from Generation 7 to Generation 8 designs. From left to right: Modified Swiftech MCW80 water block, a 3D-printed prototype which cradles the ICSF-specific copper heat sink, and the machined beta prototype housing to the final polycarbonate housing which includes a monolithic flow path (the hose barbs and fluid path are all contained in a single piece, reducing potential leaks).

### **3.5.2.5 Generation 7 Assessment and Design Issues to Address for Generation 8**

Experimental results and operational feedback from ICSF Generation 7 led to re-design of some components in preparation for a larger scale demonstration of the ICSF (Generation 8). System components deemed necessary for reconsideration/revision include:

- Re-consideration of azimuth drive mechanism to reduce cost and perception of system complexity.
- Stepper motors and required controllers are highly specialized and expensive equipment when considering an increase in scale from 4 modules to 72 modules (Generation 8 prototype)
- Revision of module geometry to reflect determination of optimal focal length.
- Further revision and refinement of altitude adjustment to allow for finer resolution adjustment.
- Heat sink is oversized relative to CCA, by 4.6 times. (Swiftech heatsink is 49.6mm square, and the CCA dimensions are 25.5mmx21mm)

### 3.5.3 Generation 8 ICSF Prototype Experiments

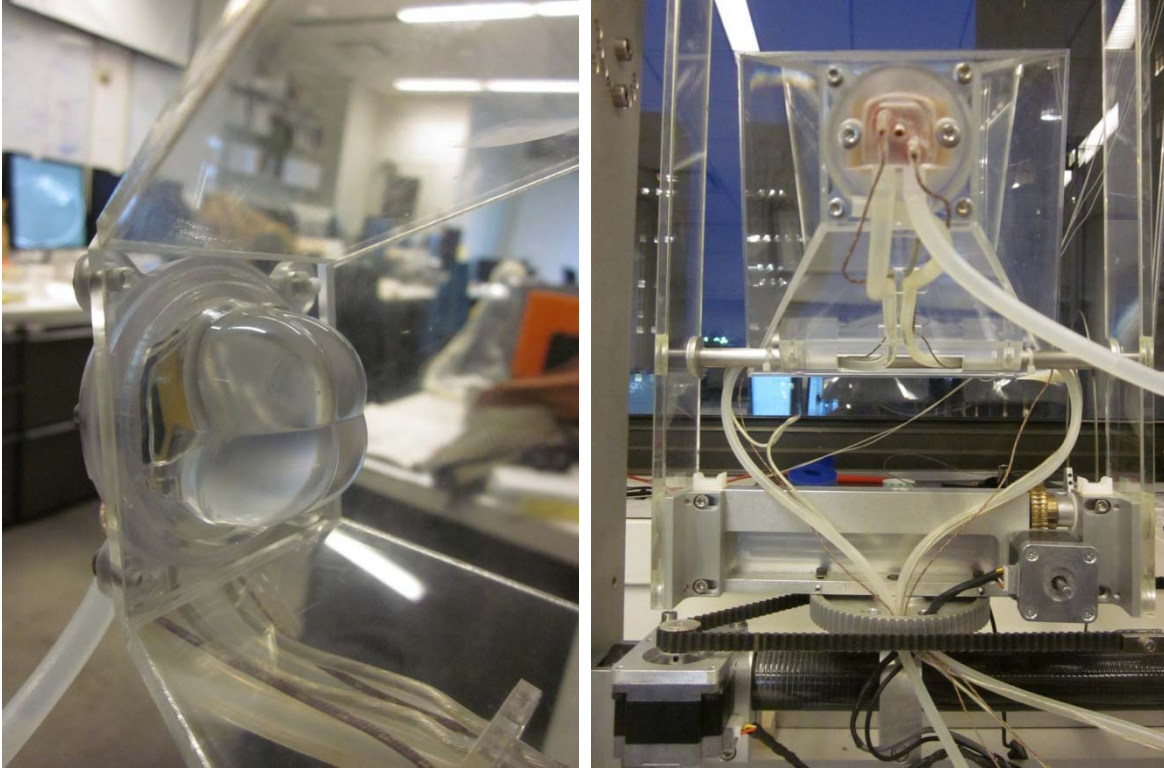


Figure 84. Secondary optical element and heat sink assembly in Generation 7 design.

- Summary of Progress
- Integration of ICSF with thermal collection and transport system.
- Sorption chilling balance-of-system design finalized and in-process
- Updated ICSF servo and feedback-based tracking method with improved components cost and parasitic power draws
- Improved tracking accuracy tolerances
- Dozens of hours of ICSF prototype operation completed.

The Generation 8 ICSF prototype is currently under construction and characterization, with operation and data collection during the fall of 2013. The array is implemented at the building scale, occupying several square meters of southwest-facing window area available at the CASE studio in Manhattan, New York. Partially installed now, a total of 72 working modules will be installed in three window bays: three bays of

four stacks, and six modules per stack. Two bays will be plumbed to provide full thermal effects of the technology; the third bay will comprise modules with passive heat sinks, to characterize an alternative ICSF installation.

### **3.5.3.1 Improvements to ICSF from Generation 7 to Generation 8**

Generation 8 incorporates changes which make the experimental rig more characterizable and robust including:

- The tracking actuators are lower-cost servos and driver/amplifiers, rather than the steppers and stepper controller design of the last two generations.
- Spacing along the optical axis has been adjusted to compensate for beam convergence that was characterized in experiments during the summer of 2012 as part of Generation 7 testing.
- The heat sink and heat exchange module has been updated with an application specific assembly that reduces fixturing error, losses relative to differential contact areas, and overall receiver profile.
- Commercially-available DC-DC converter/MPPT modules, sourced through a co-development agreement with eIQ, will be used to maximize electrical output from the array.
- HTF circuits are constructed largely from PEX, a familiar system in the building industry.
- A drag linkage assembly was selected over the belt drive assembly used in Generation 7
- The ICSF system will be eventually connected to Sorption chilling equipment balance-of-system design and demonstration

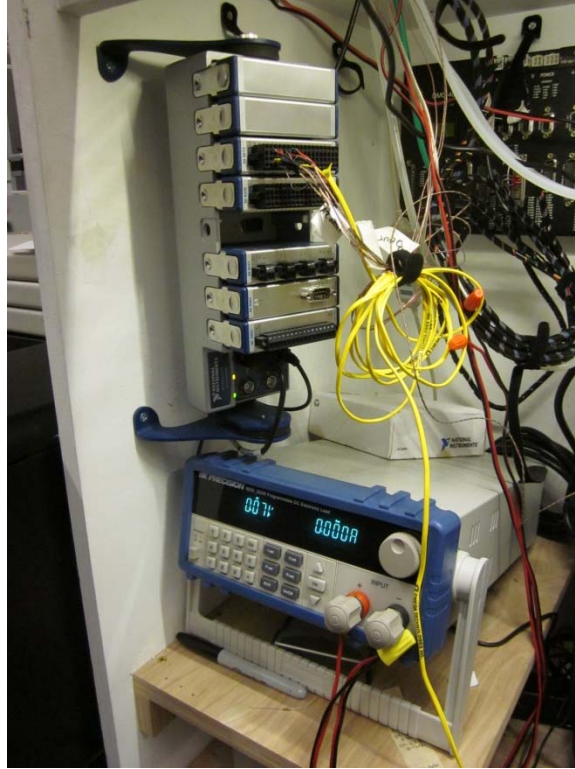


Figure 85. Balance of system measurement and control hardware for Generation 7.  
Shown: National Instruments data acquisition system, BK electronic load, Galil stepper controller/amplifier.



Figure 86. Trailing end of Generation 8 tracker stacks.  
Toothed timing belt mechanism from Generation 7 replaced with drag link. Design selected to reduce perceived complexity and substantially reduce material costs (due to fewer gears).

### 3.5.3.2 Generation 8 Tracking Control System

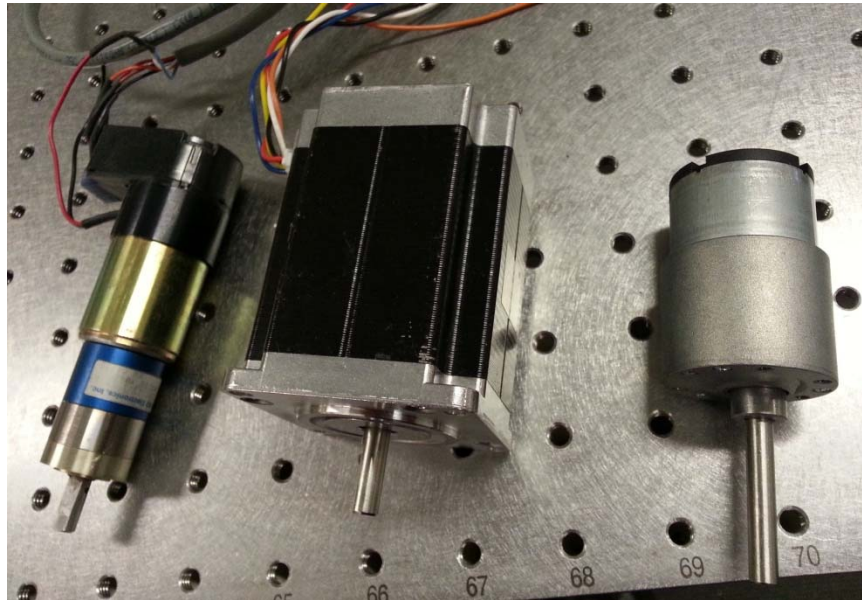


Figure 87. Motor specification evolution, past and current tracker design.

The ultra-high precision, zero backlash geared brushless servo motor cum quadrature optical encoder (about \$250) was replaced with the lower torque hybrid open loop micro stepping stepper motor (about \$48) and, finally, with the brushed DC geared servo motor with very low backlash (the backlash is compensated for with constant direction loading) commodity motor (about \$6). All motors, in their installation, allow tracking errors that result in less than the 1% optical loss that the authors feel is an acceptable tradeoff. The final motor operates closed loop with a 14 bit, single turn, low cost (commodity) angular encoder mounted on a representative module in each vertical stack ensuring sub-milliradian accuracy. Not only are the motors and the accompanying encoders commodity items, but the motor control has shifted from overly feature rich servo and stepper controllers (~\$600/axis) to extremely low cost (~\$6/axis), high performance solutions designed for simple motion control that is similar to the current control code.

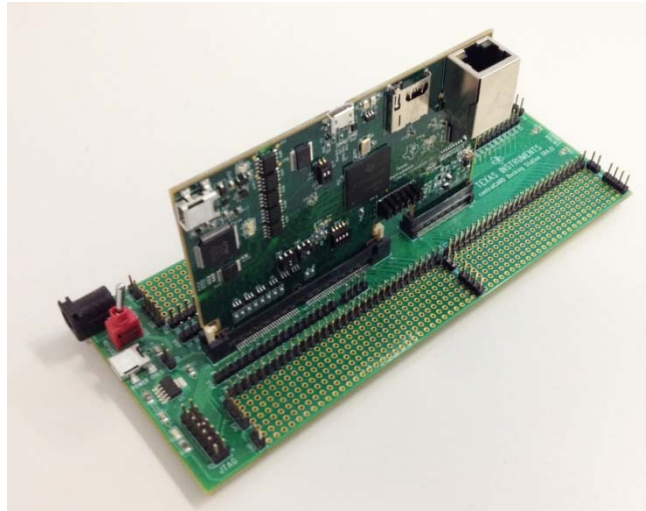


Figure 88: Tracking Embedded Controller: Concerto F28M36PX MCU (on dev board).  
Multi-processor TI Concerto Controller used to translate a multi-axis position vector (determined through ICSF control interface) into array motion.

### **3.5.3.3 Selection of Microcontroller (MCU)**

The Texas Instruments Concerto dual-subsystem microcontroller (MCU) was selected as the motor controller for the ICSF tracking system because of its independent processors dedicated to communication (M3-Cortex) and real-time control (C28-C2000). Since current building system controllers incorporate elements of both control and communication, the Concerto is an appropriate choice for future integration into built environments. Additionally, this embedded controller selection is applicable for scaling up for industrial level designs because it can establish 'Control Area Networks' (CANs), and has integrated Ethernet MAC protocol capabilities; both of which are industry standards for building system controller communication. The MCU can also configure up to 8 pairs (16 total) of output pins to perform pulse width modulation (PWM); the method to control the DC drive motors. Typically, 2 sets of PWM pins are needed to control a DC motor; one for each direction of rotation. By employing an external H-bridge motor driver, only one PWM channel is required to set the duty cycle and an auxiliary output pin (non-PWM) can then set the direction. This allows for control of 16 independent motors as compared to the original case of 8 motors without the external H-bridge. Only one MCU is needed because the ICSF research experiment has 15 axes of control.

### **3.5.4 Experimental Investigation of a Building Envelope-Integrated, Transparent Concentrating Photovoltaic and Thermal Collector**

Sustainability depends on improving the built environment's energy use, since buildings consume one-third of energy produced in industrialized countries. Transformative energy strategies, however, face technological, economic, and conceptual hurdles. To explore new affordances in metabolizing solar energy, a Building envelope-Integrated, Transparent, Concentrating Photovoltaic and Thermal collector (BITCoPT) was developed. BITCoPT optically separates diffuse and direct insolation, maintaining lighting and exergetic qualities: diffuse light is transmitted for illumination, while direct insolation—which is typically moderated by a commercial building's envelope to control glare and cooling loads—is converted to electricity and thermal energy. A full-scale BITCoPT prototype was tested in conventional installation, and array efficiencies of 25% (exergy) and 43% (energy) were observed relative to direct normal irradiance transmitted through exterior glazing. Increasing the heat transfer fluid inlet temperature to 75°C negligibly impacted exergetic efficiency, indicating suitability for driving active thermal processes. Observations showed good agreement with modeled results. In simulation (with projected enhancements to optics, cell type, and exterior glazing) cogeneration efficiency increased to 41% (exergy) at 62 °C, and 73% (energy) at 60°C. Observed and projected results suggest power generation would be significant relative to energy use in small and medium-scale commercial buildings, indicating BITCoPT might broaden opportunities for on-site net-zero and energy-positive architecture.

#### **3.5.4.1 Methods: Technology, Model, and Prototype Description**

##### **3.5.4.1.1 BITCoPT Technology Description**

As an instance of an envelope-integrated climatic energy metabolization strategy, BITCoPT comprises an array of actively tracked, concentrating collector modules that transform insolation into electricity (via photovoltaics) and thermal energy (via a hydronic heat transfer circuit). The modules are suspended in columns (or “stacks”) in the cavity of a deep-mullion curtain wall cassette (see Figure 89).

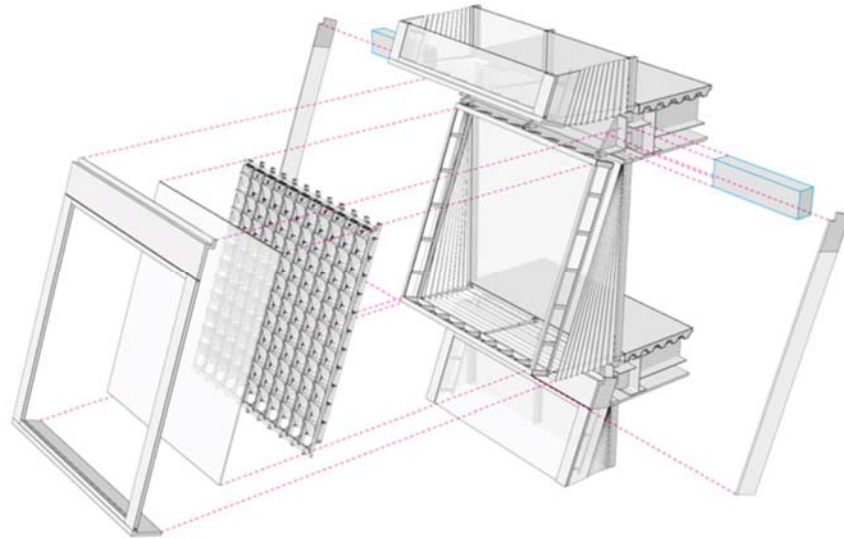


Figure 89. Cassette assembly (exploded view). Façade installation shown with 20° tilt and glass infill.

Image: Ryan Salvas, CASE

The cassette comprises the rain screen assembly and thermal envelope of a building and acts as the wall infill or the roof (as in an atrium). The cassette can also be tilted (Figure 89). The functional area of the cassette can be constructed of glass, or other transparent materials such as ETFE. The exterior glazing is highly transparent, to transmit solar energy to the collector modules, while the inner glazing's transparency and thermal conductivity would be specified to the intentions for the occupied space interior to the cassette. The cassette cavity is sealed against uncontrolled infiltration from both outdoor and indoor environments, but would be serviced by air handling systems to exchange cavity air, or in the case of an ETFE construction, to maintain the pressure of the envelope. The array itself is mainly constructed from transparent components so that building occupants have views to the exterior much as they would through other glazed envelopes (see Graphical Abstract and Figure 90).

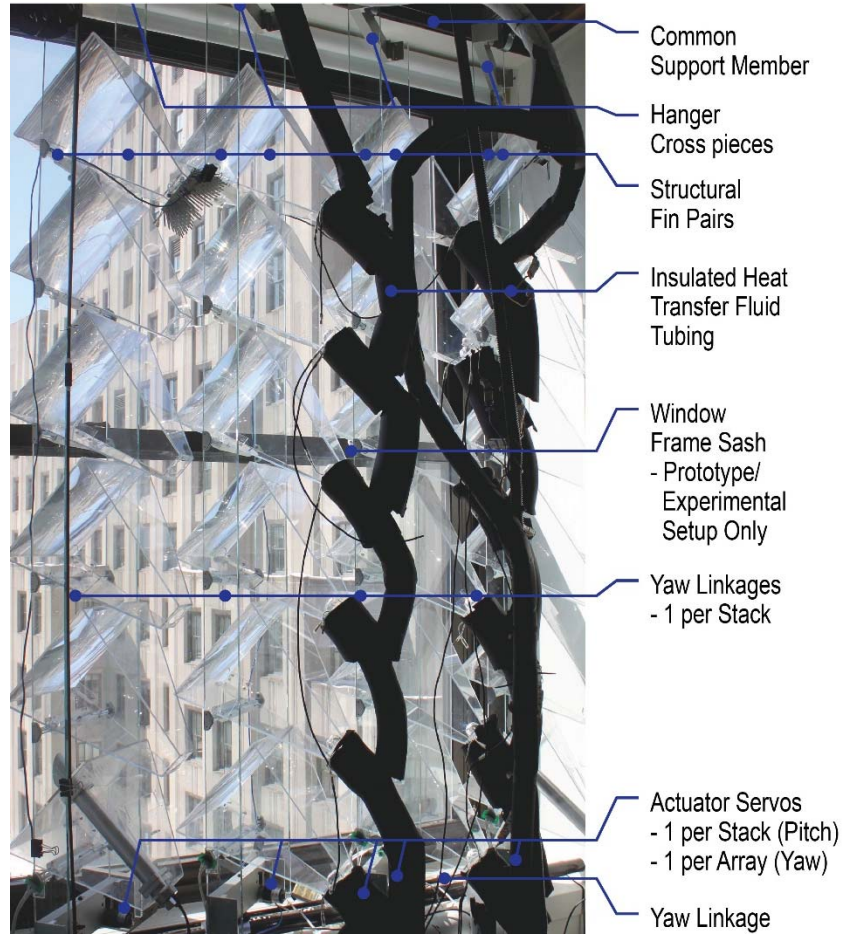


Figure 90. Installed BITCoPT prototype (photograph).

Shown: arrangement of modules into stacks and array, transparency.

### ***Prototype Construction: Concentrator Module, Stack and Array***

In the module, the fundamental unit of BITCoPT, direct irradiance is concentrated by an achromatic, non-imaging lens set onto a concentrator photovoltaic (CPV) cell. The CPV converts a fraction of the irradiance to electrical power, leaving the balance available for thermal collection via a liquid cooled heat exchanger mated to the back of the CPV. The heat transfer fluid circuit services one or more stacks of modules in series, transferring collected energy to a thermal reservoir.

The BITCoPT module can be considered two sub-assemblies (Figure 91).

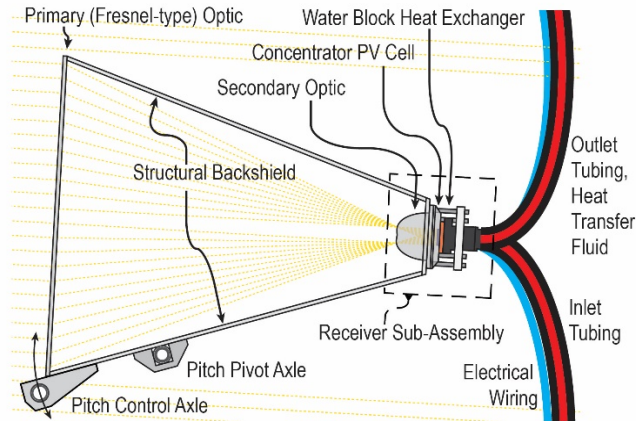


Figure 91. BITCoPT prototype module components.

The first sub-assembly is comprised of the primary optic, structural back shield, and axle attachment points. The second sub-assembly (the “receiver”) is comprised of the secondary optic, CPV, water block heat exchanger, and fixturing.

Modules are grouped into stacks that reach the height (or span the breadth) of a cassette; stacks are repeated horizontally to fill the cassette’s area. A stack consists of a pair of glass fins between which the module axes are fixed to form a ladder-like structure. The fin pairs are attached to a hanger cross piece which rotates on an axle. The axles of each stack are suspended from a common support member that spans the width of one array (Figure 90). Although BITCoPT is designed to function in all orientations, the prototype was installed in a vertical window (Figure 90).

Modules are actively tracked according to the angle of incidence ( $\theta_{AOI}$ ) between the solar vector and the envelope-plane normal vector. The array moves with two degrees of freedom: the modules pitch around their horizontal axes, and the stacks yaw around their vertical axes. A whole-array linkage rotates the stacks in unison while separate linkages rotate each stack’s modules in unison (Figure 90).

### ***Optical Prototype Design: Point-Focus, Two-Element Concentrator***

Direct irradiance is concentrated onto a module’s CPV through a two-element Köhler-type integrator lens assembly, a lens design that, with high tolerance for off-axis

illumination, reduces the requirements on the array's alignment mechanisms.<sup>92</sup> The lenses are fixed relative to the CPV by the back shield. The gap between the secondary optic and the CPV is filled with an index-matched silicone elastomer. The lens' geometric concentration ratio is  $X_{opt} = 615$ , and  $f/\# = 0.87$ , here defined as the ratio between the diagonal of the primary optical element (POE) and the CPV. The POE is formed from PMMA, while the secondary optical element (SOE) is formed from BK7.

### **Electrical Generation: Multi-Junction Concentrator Photovoltaics**

Direct insolation is converted to electricity by an individual multi-junction concentrator photovoltaic cell (CPV) in each module. In the prototype the CPV (Spectrolab C3MJ CCA100<sup>93</sup>) is a triple-junction cell of  $A_{CPV} = 1.0\text{cm}^2$ , mounted on an alumina back plane in parallel with a bypass diode. The CPV's rated efficiency is a function of temperature ( $T_{CPV}$ ) and effective concentration ratio  $X_{eff}$  (see section 0). Nominally,  $\eta_{CPV} = 38.5\%$  at  $X_{eff,CPV} = 615$  and  $T_{CPV} = 25^\circ\text{C}$ . At  $T_{CPV} = 95^\circ\text{C}$ , the upper bound of the experimental temperature range,  $\eta_{CPV} = 34.9\%$ .

For the projected model setup, a generalized CPV is assumed based on current multi-junction technology<sup>94</sup> with a nominal performance spec and applied temperature coefficients for short-circuit, open-circuit, and fill factor<sup>95</sup>.

### **Concentrated Thermal Collection: Hydronic Circuit**

In the prototype, commercially-available microprocessor coolers (Swiftech Model MCW30) were used for cell to fluid heat exchange. As the thermal resistance of these exchangers ( $R_{WBHX,proto}$ ) was not readily available it was determined empirically.

---

<sup>92</sup> Benitez, P., Minano, J., Zamora, P., Mohedano, R., Cvetkovic, A., Buljan, M., ... Hernandez, M. (2010). High performance Fresnel-based photovoltaic concentrator. *Optics Express*, 18(S1).

<sup>93</sup> Spectrolab. (2011). C3MJ\_CCA100 data sheet.

<sup>94</sup> Dimroth, F., Grave, M., Beutel, P., Fiedeler, U., Karcher, C., Tibbits, T. N. D., ... Schwarzburg, K. (2014). Wafer bonded four-junction GaInP/GaAs//GaInAsP/GaInAs concentrator solar cells with 44.7% efficiency. *Progress in Photovoltaics: Research and Applications*, 22(3), 277–282. <http://doi.org/10.1002/pip.2475>

<sup>95</sup> Peharz, G., Ferrer Rodríguez, J. P., Siefer, G., & Bett, A. W. (2011). Investigations on the temperature dependence of CPV modules equipped with triple-junction solar cells. *Progress in Photovoltaics: Research and Applications*, 19(1), 54–60. <http://doi.org/10.1002/pip.987>

Customized heat exchangers have been designed for BITCoPT, and although they were not employed in this prototype, the projected model setup incorporates performance curves (provided by their manufacturer) that relate thermal resistance ( $R_{WBHX,proj}$ ) to fluid flow rate ( $\dot{V}_{HTF}$ ).

Fluid flow in the cassette is distributed by an inlet manifold to parallel branches of modules, merging in an outlet manifold. In the experimental prototype, the twelve operational modules were joined in series.

Thermal energy is collected in a fluid reservoir tank adjacent to BITCoPT from which fluid would be circulated to supply the various hypothetical demands of a building's systems (Figure 92).

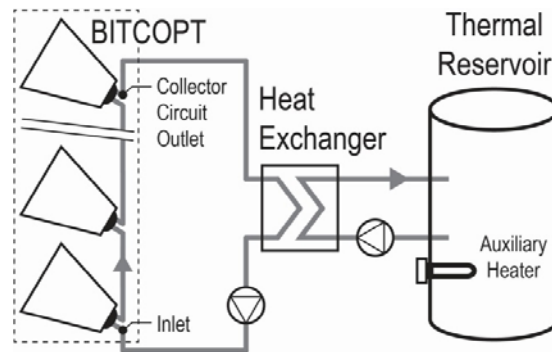


Figure 92. Thermal collection scheme: hydronic circuits, heat exchanger.

Two hydronic circuits linked through cross-flow heat exchanger transfer thermal energy from BITCoPT to reservoir (with auxiliary heater).

### **Wall and Roof Integration: Modular Envelope Cassette**

Although BITCoPT is designed to operate with a ventilation-controlled cavity behind highly-transparent glazing, the prototype was installed in a bay (an open cavity) behind a double-hung window with insulated glazing units (IGUs) to the exterior (Figure 90). The prototype is, therefore, exposed to the conditioned interior space, rather than sealed within a cassette. The prototype is constructed with 24 modules: four stacks of six modules each. The two middle stacks are active collectors, for a total of twelve active modules. To reproduce the intended shading conditions for the active collector modules in the central stacks, all four stacks are tracked during operation.

### 3.5.4.1.2 Analytical Model Details

The analytical model of BITCoPT, described in an earlier study,<sup>96</sup> is a quasi-steady state, lumped-capacitance representation of relevant physical relationships. Energy balance equations are solved at discrete time steps. Key relationships are highlighted here, as are differences between the prototype and projected model setups. The model was used in two ways. First, a set of parameters in the prototype model setup was tuned to correlate with data from the experimental prototype output, as per the earlier study, to verify array behavior. Second, a different set of parameters was updated to project the performance of the prototype under revised circumstances.

### Model Inputs and Outputs

To evaluate the prototype model setup and to extrapolate the projected model setup, the relevant variable inputs and outputs of the analytical model of BITCoPT are described in Table 32.

Table 32. Inputs and outputs of active envelope model.

Model Inputs	Prototype/Projected Setup
BITCoPT orientation (tilt, cardinal direction)	Vertical, 40° West of South
BITCoPT module and stack configuration	Two stacks of six modules (twelve modules in series)
BITCoPT pitch and yaw angles	Measured/calculated
Solar position	Calculated
Direct normal irradiance ( $I_{DN}$ )	Measured at BITCoPT, modified by $F_{POE}$
Diffuse irradiance ( $I_{diff}$ )	Uncontrolled
Module shading function ( $F_{POE}$ )	Simulated, measured
Heat transfer fluid inlet temperature ( $T_{HTF,in}$ )	Controlled with heater/ thermostat (25 to 85°C)
Heat transfer fluid flow rate ( $\dot{V}_{HTF}$ )	Controlled, measured
Outdoor dry bulb temperature ( $T_{outd}$ )	Uncontrolled
Cavity temperature ( $T_{cav}$ )	Uncontrolled, measured
Reference Temperature ( $T_{ref}$ )	$T_{ref} = 20^{\circ}\text{C}$
Model Outputs	
Electrical generation (net: $E_{gen}$ , efficiency: $\eta_{Egen}$ )	Measured/simulated
Thermal collection (net: $Q_{gen}$ , efficiency: $\eta_{Qgen}$ )	Measured/simulated

<sup>96</sup> Novelli, N., Shultz, J., & Dyson, A. (2015). Development of a Modeling Strategy for Adaptive Multifunctional Solar Energy Building Envelope Systems. Presented at *SimAUD*. Washington, DC.

Cogeneration exergetic efficiency ( $\epsilon_{cogen}$ )	Measured/simulated
Heat transfer fluid outlet temperature ( $T_{HTF,out}$ )	Measured/simulated

### Solar Input Quantities

Multiple measurements of insolation and irradiance are referenced in determining the performance of BITCoPT, as described in Table 33.

Table 33. Insolation quantities defined.

Variable	Description, Equation	Unit
$I_{DN}, I_{diff}$	Building-independent direct normal and diffuse irradiance (source: weather data) <sup>97</sup>	W/m <sup>2</sup>
$G_{DN,POE}$	Direct normal solar power incident on collector:	W
	$G_{DN,POE} = I_{DN} T_{glaz,\theta} A_{POE} \sum_{i=1}^n F_{POE}$ (32)	
$G_{DN,CPV}$	Solar power incident on a module CPV:	W
	$G_{DN,CPV} = I_{DN} T_{glaz,\theta} A_{POE} \eta_{opt} F_{POE}$ (33)	

The direct irradiance incident on the collector's primary optics  $G_{DN,POE}$  (inside the exterior glazing) was the reference for efficiency in the prototype model setup.  $T_{glaz,\theta}$  is the transmittance of the exterior glazing to direct flux (refer to section 0).  $A_{glaz}$  is the area of the cassette's glazing.  $A_{POE}$  is the area one primary Fresnel lens optic (constant at  $A_{POE} = 0.0626\text{m}^2$ ).  $F_{POE}$  is the unshaded fraction of the primary optic, a function of array pitch and yaw, which varies across modules based on their location within the BITCoPT array (refer to section 0).  $G_{DN,CPV}$  is used in the receiver energy balance and incorporates the optical concentration efficiency (refer to section 0).

Due to uncertainties in the assembly of the prototype's modules, the optics' transmission efficiency ( $T_{opt,proto} = 57\%$ ) was determined empirically (and averaged across all modules) for the prototype model setup. For the projected model setup, the theoretical optics' efficiency ( $T_{opt,proj} = 88.6\%^{98}$ ) was applied.

<sup>97</sup> NREL. (2009). NSRDB: 1991- 2005 Update: TMY3. Retrieved May 26, 2011, from [http://rredc.nrel.gov/solar/old\\_data/nsrdb/1991-2005/tmy3/](http://rredc.nrel.gov/solar/old_data/nsrdb/1991-2005/tmy3/)

<sup>98</sup> Benitez, P., Minano, J., Zamora, P., Mohedano, R., Cvetkovic, A., Buljan, M., ... Hernandez, M. (2010). High performance Fresnel-based photovoltaic concentrator. *Optics Express*, 18(S1).

### **Environmental and System Temperatures**

The BITCoPT prototype's rates of thermal energy collection and loss were affected by the temperature of the cassette cavity air and of the heat transfer fluid. The heat transfer fluid source temperature was controlled at the thermal reservoir and measured at the inlet to the first module and the outlet of the last module. All thermal losses were to the air in the bay, the temperature of which was measured.

### **Insolation Flux through Cassette Glazing**

BITCoPT is designed to function within a glazed cassette in a curtain wall assembly; therefore, the optical properties of the interior and exterior glazing were modeled. Transmittance of direct insolation ( $T_{glaz,\theta}$ ) is attenuated by particulate soiling, optical scattering, and Fresnel reflections at the boundaries between non-index-matched transparent materials. Transmittance was modeled by

$$T_{glaz,\theta} = \left(1 - \frac{R_{sfc}}{\cos \theta_{AOI}}\right) \left[\left(1 - \frac{c_{scatt} x_{lite}}{\cos \theta_{AOI}}\right) \left(1 - \frac{2R_{Fres}}{1 + R_{Fres}}\right)\right]^{n_{lites}} \quad (34)$$

Where  $R_{sfc}$  is the attenuation from particulate soiling on the first glazing surface and  $c_{scatt}$  is the coefficient of scattering in the glass material.  $R_{Fres}$  is the Fresnel reflectance from one surface (polarization independent),  $x_{lite}$  is the glazing thickness, and  $n_{lites}$  is the number of glazing lites. Fresnel reflections were modeled with Schlick's approximation:<sup>99</sup>

$$R_{Fres} = R_0 + (1 - R_0)(1 - \cos \theta_{AOI})^5 \quad ; \quad R_0 = \left(\frac{n_{air} - n_{glaz}}{n_{air} + n_{glaz}}\right)^2 \quad (35)$$

where  $R_0$  is the reflectance at normal ( $\theta_{AOI} = 0^\circ$ ) while  $n$  is a material index of refraction ( $n_{air} = 1.0$  and  $n_{glaz} = 1.53$ ). To model the transmittance of diffuse radiation, the solar heat gain coefficient (SHGC) is used. Parameters for all glazing instances in both prototype and projected model setups are given in Table 34.

---

<sup>99</sup> Schlick, C. (1994). An Inexpensive BRDF Model for Physically-based Rendering. *Computer Graphics Forum*, 13(3), 233–246. <http://doi.org/10.1111/1467-8659.1330233>

Table 34. Glazing loss parameters.

Parameter	Prototype Glazing	Projected Glazing
$R_{sfc}$	0.030	0.0
$c_{scatt}$ (1/mm)	0.0221	0.0075
$x_{lite}$ (mm)	3	6
$n_{lites}$	2	1
SHGC	-	0.88

Glazing properties were determined empirically and analytically. For projected glazing instances,  $c_{scatt}$  was derived from manufacturer’s data.<sup>100</sup> To inform the prototype model setup, the solar transmittance of the existing double-pane window was measured ( $T_{glaz,proto} = 0.69$  at  $\theta_{AOI} = 35^\circ$ ).  $R_{sfc}$  is derived from  $T_{glaz,proto}$ . To represent transmittance in the projected model setup, the exterior glazing was modeled as a single thickness of low-iron glass. The interior glazing was modeled as an insulated glazing unit with a low transmittance to limit indoor solar gains.

### **Module Shading Non-Uniformity**

Each module’s primary optic undergoes shading from the cassette’s frame, external objects such as other buildings, or adjacent modules (or “overlap”). The shading due to overlap reduces direct insolation available to the modules’ CPVs, roughly, per the cosine of the solar-cassette angle of incidence. These shading effects are modeled using a geometric ray tracing simulation. To determine  $F_{POE}$ , the fraction of a primary optic that remains unshaded (and consequently the irradiance available to the CPV), a distinct look-up table was generated for each distinct shading condition within the BITCoPT array. Modules at the edges of an array are shaded, on average, 10% more than modules in the central field condition of the array, due to shadows cast by the cassette frame.

For the projected model setup, because of the long horizontal length of a typical commercial building façade, it can be assumed that a BITCoPT array is at least 12

---

<sup>100</sup> Guardian Ultrawhite and Clear materials, Retrieved from <https://glassanalytics.guardian.com/PerformanceCalculator.aspx>, July 1, 2015.

stacks wide. Given the projected stack height of ten modules and 10% increase in shading at the array edges, the edge shading effects cause a 2% decrease in solar power available relative to a field-condition-only assumption. Therefore, to simplify modeling for the projected setup, it is assumed that all modules in the projected model setup exhibit the central, field condition.

To model the shading conditions for the prototype and prototype model setup, due to the limited size of the window bay and the crosspiece of the window's sash frame, geometric ray-tracing was used to generate a unique shading condition and look-up table for each of the twelve operational modules (Figure 93).

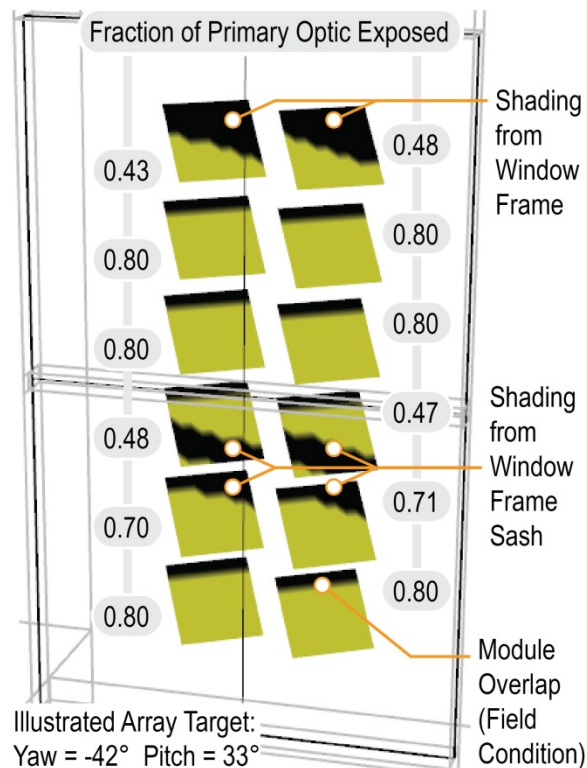


Figure 93. Simulation of angle-dependent shading conditions ( $F_{POE}$ ).  
 Each module in prototype model setup has a unique  $F_{POE}$ .

### **Energy Balances: Module Receiver, Arrays**

An energy balance of a module's receiver sub-assembly was performed to determine the thermal energy collected and lost. The control volume is shown in Figure 94.

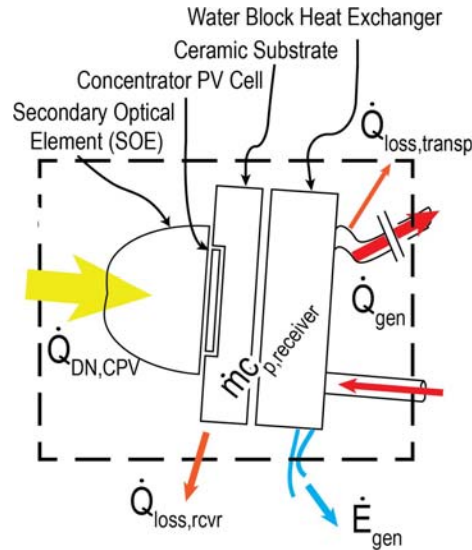


Figure 94. Control volume for energy balance at module receiver.

The energy balance is as follows:

$$mC_{p,rcvr} \frac{\partial T_{rcvr}}{\partial t} = G_{DN,CPV} - E_{gen} - Q_{gen} - Q_{loss,rcvr} - Q_{loss,transp} \quad (36)$$

where  $mC_{p,rcvr}$  is the receiver thermal mass,  $T_{rcvr}$  is its temperature, and  $Q_{loss,rcvr}$  and  $Q_{loss,transp}$  are loss terms for the receiver body and hydronic transport tubing. Because the changes in system state and inputs were slow relative to the time constant of the receiver's thermal mass, steady-state operation was assumed and the thermal mass of the receiver was treated as a lumped capacitance.

The energy balance of the array and chosen sub-arrays was the sum of the module energy balances. In each stack the HTF inlet of a module is connected to the HTF outlet of the previous module. In the prototype, the two physical stacks (six modules each) were connected in one series branch with an additional length of insulated tubing, for which an additional heat loss term ( $Q_{loss,transp}$ ) was included in the array energy balance.

### **Electrical Generation Efficiency**

In the prototype model setup, the CPV's electrical conversion efficiency was represented by a multivariable regression of the manufacturer's data:<sup>101</sup>

$$\eta_{CPV} = \frac{E_{gen}}{G_{DN,CPV}} \quad (37)$$

$$\eta_{CPV,proto} = 0.364 + 5.0 \times 10^{-4} (52.5 - (T_{CPV} - 273.15)) + (1.997 \times 10^{-6}) (X_{eff,CPV} - 627.5) \quad (38)$$

Electrical efficiency is insensitive to irradiance on the CPV, varying less than 1.0% over the functional range  $35W \leq G_{DN,CPV} \leq 90W$ . The irradiance (and therefore CPV electrical efficiency) is variable, however, and expressed as an effective concentration ratio  $X_{eff,CPV}$  relative to the solar power incident on the CPV area from the AM1.5 reference solar spectrum:

$$X_{eff,CPV} = \frac{G_{DN,CPV}}{G_{DN,CPV,AM1.5}} \quad (39)$$

$X_{eff,CPV}$  therefore incorporates direct normal irradiance, solar angle of incidence, transmission efficiencies, and the geometric and optical concentration ratios.

For the projected model setup, a nominal cell efficiency was determined from published data<sup>102,103</sup> to be  $46.0\% \pm 2.2\%$  at  $22.5^\circ\text{C}$  and 508X. The area of the sample reported in the literature would increase from  $5.2\text{mm}^2$  to  $118\text{mm}^2$  ( $10.9\text{mm}$  square), in order to experience a nominal concentration factor, given the BITCoPT lens design. The nominal efficiency in this study was therefore de-rated to  $\eta_{CPV,nominal} = 42.0\%$ , to account for the reduction in active area and absorption effects of the larger leads required to drain current from the larger cell, and the increased shading (from the increased lead

<sup>101</sup> Spectrolab. (2011). C3MJ\_CCA100 data sheet.

<sup>102</sup> Dimroth, Frank, Matthias Grave, Paul Beutel, Ulrich Fiedeler, Christian Karcher, Thomas N. D. Tibbits, Eduard Oliva, et al. "Wafer Bonded Four-Junction GaInP/GaAs//GaInAsP/GaInAs Concentrator Solar Cells with 44.7% Efficiency." *Progress in Photovoltaics: Research and Applications* 22, no. 3 (March 1, 2014): 277–82. doi:10.1002/pip.2475.

<sup>103</sup> Green, M. A., Emery, K., Hishikawa, Y., Warta, W., & Dunlop, E. D. (2016). Solar cell efficiency tables (version 47). *Progress in Photovoltaics: Research and Applications*, 24(1), 3–11. <http://doi.org/10.1002/pip.2728>

height) of the extreme angle rays from the large-aperture optics. The nominal efficiency was modified with temperature by applying linear thermal coefficients for short circuit current, open circuit voltage, and fill factor:

$$\eta_{CPV,proj} = \eta_{nominal,C4J} * [1 - (1 - k_{sc})(1 - k_{oc})(1 - k_{FF})(T_{CPV} - T_{CPV,nominal})] \quad (40)$$

where the thermal coefficient for the short circuit current is  $k_{SC} = 0.1\%/K$ , for the open circuit voltage is  $k_{OC} = -0.14\%/K$ , and for the fill factor is  $k_{FF} = -0.18\%/K$ . The change in  $\eta_{CPV}$  with incident flux was neglected, as most energy was produced during time steps with strong irradiance, meaning the effective concentration ratio did not vary greatly.

### ***Thermal Collection and Transport Behavior***

Thermal energy collected by a BITCoPT module, stack, or array was determined by

$$Q_{gen} = \dot{V}_{HTF} \rho_{HTF} c_{p,HTF} (T_{HTF,out} - T_{HTF,in}) \quad (41)$$

where  $\dot{V}_{HTF}$  is the volumetric flow rate of the heat transfer fluid ( $m^3/s$ ),  $\rho_{HTF}$  is the fluid density,  $c_{p,HTF}$  is the fluid specific heat, and  $T_{HTF}$  refers to the outlet and inlet fluid temperature of the module, stack, or array. Specific heat and density were assumed constant at  $c_{p,HTF} = 4.190 \text{ kJ/kg-K}$  and  $\rho_{HTF} = 974.9 \text{ kg/m}^3$ , corresponding to an average fluid temperature of  $75^\circ\text{C}$ .<sup>104</sup>

The resistance to heat flow across the water block heat exchanger ( $R_{WBHX}$ ) was determined through two distinct methods for the prototype and projected model setups. For the prototype model setup, with  $Q_{gen}$  known, the temperature difference across the water block was measured, comparing the temperature measured at the CPV-water block mating surface ( $T_{CPV}$ ) to the mean temperature of the fluid in the heat exchanger ( $T_{HTF,LMT}$ ):

$$R_{WBHX,proto} = \frac{T_{CPV} - T_{HTF,LMT}}{\dot{V}_{HTF} \rho_{HTF} c_{p,HTF} (T_{HTF,out} - T_{HTF,in})} \quad (42)$$

<sup>104</sup> Incropera, F., & DeWitt, D. (1996). Fundamentals of Heat and Mass Transfer (4th ed.). New York, NY: John Wiley.

The water block thermal resistance was determined to be  $R_{WBHX,proto} = 0.90^{K/W}$  and  $0.70^{K/W}$  at  $\dot{V}_{HTF} = 1.5 \cdot 10^{-6} \text{ m}^3/\text{s}$  and  $3 \cdot 10^{-6} \text{ m}^3/\text{s}$ , respectively. For the projected model setup, in which the customized heat exchanger was modeled, a regression of the manufacturer's data<sup>105</sup> describing  $R_{WBHX}$  relative to mass flow was applied:

$$R_{WBHX,proj} = 0.2487((10^6)\dot{V}_{HTF})^{-0.773} \quad (43)$$

Thermal losses at the collection stage (from the insulated receivers) and the transport stage (from the hydronic tubing) were modeled as separate transfers across bulk resistances,  $R_{rcvr}$  and  $R_{tubing}$ . Values for  $Q_{loss,rcvr}$  and  $R_{rcvr}$  were determined by combining the overall energy balance equation with the losses at the receiver:

$$Q_{loss,rcvr} = \frac{(T_{rcvr} - T_{cav})}{R_{rcvr}}; \quad R_{rcvr} = \frac{1}{UA_{rcvr}}; \quad Q_{loss,transp} = \frac{(T_{HTF,LMTD} - T_{cav})}{R_{tubing}} \quad (44)$$

### **Parasitic Losses**

Two parasitic electrical losses are inherent in BITCoPT: tracking servo motors and pumps. In an installation, these would represent a small fraction of the generation output. The servo motors might consume an average of  $E_{par,trk} = 2.5\text{W}$  per ten-module stack, based on a maximum torque of 4Nm required to lower a stack from a pitch angle of 75°. Energy expended for fluid pumping would be accounted for by summing the pressure losses across the water block heat exchangers, the hydraulic head (assuming a vertically-oriented array), and the friction losses in piping and fittings. This loss might be on the order of  $E_{par,pump} = 1.8\text{W}$  per stack. In this analysis, however, the output of the array (and calibration of the model's results) was the primary objective, and tracking power and pumping losses were not considered in the results.

### **Sub-Arrays for Cogeneration**

Because the modules in the prototype experienced heterogeneous shading conditions and generating behavior, three different sub-arrays were considered. The homogeneously shaded, co-generating sub-array (C6, C3, C2, B6, B3, B2:  $n_{modules,cogen,homo} = 6$ ) was measured to determine electrical performance. The

---

<sup>105</sup> Valenzuela, J. (2011). Mikros heat sink 10x10mm CP Test Data.

homogeneously shaded, fully-instrumented sub-array (C6, C3, C2:  $n_{modules,cogen,homo,FI} = 3$ ) was measured to determine cogeneration in the field condition. Since this set was small (with higher measurement uncertainty), the full array (C6, C5, C4, C3, C2, C1, B6, B5, B4, B3, B2, B1:  $n_{modules,hetero} = 12$ ) was also analyzed for total output, even though not all modules were generating both electrical and thermal power. This full array, with heterogeneous cogeneration and shading conditions, was the basis for the calibration of model parameters.

### **Energy and Exergetic Collection Efficiency**

The primary performance metric for BITCoPT is cogeneration exergetic efficiency ( $\epsilon_{cogen}$ ): the fraction of solar exergy converted to either collected thermal exergy or electricity. Energy efficiency ( $\eta_{cogen}$ ) is likewise important, as not all a building's systems or demands require high-temperature heat sources. Exergy efficiency is designated by  $\epsilon$ , while  $\eta$  is energy efficiency.

Efficiencies were determined relative to the solar power available on the primary optics, which is calculated from the shading matrices and the direct normal irradiance measured in the cassette cavity. For the prototype setup, efficiencies were calculated for the homogenous sub-array:

$$\eta_{Egen,proto} = \frac{E_{gen}}{G_{DN,POE(n=6)}} \quad (45)$$

$$\eta_{Qgen,proto} = \frac{Q_{gen(n=3)}}{G_{DN,POE(n=3)}} \quad (46)$$

$$\eta_{cogen,proto} = \eta_{Egen,proto} + \eta_{Qgen,proto} \quad (47)$$

To project the efficiency of the BITCoPT prototype in an installation-type setting, the projected model setup was run with the experimentally measured input conditions and building site orientation. This projected cogeneration efficiency of the prototype setup was calculated as:

$$\eta_{cogen,proj} = \frac{E_{gen,proj} + Q_{gen,proj}}{G_{DN,POE(n=10)}} \quad (48)$$

Exergetic collection efficiency ( $\epsilon_{cogen}$ ) is a ratio relating thermal, electrical, and solar exergy quantities.  $\epsilon_{cogen}$  was defined relative to different baselines for prototype and projected model setups:

$$\epsilon_{cogen,proto} = \frac{Ex_{Egen,proto} + Ex_{Qgen,proto}}{\psi_{sol} G_{DN,POE,proto}} \quad (49)$$

$$\epsilon_{cogen,proj} = \frac{Ex_{Egen,proj} + Ex_{Qgen,proj}}{\psi_{sol} G_{DN,POE(n=10)}} \quad (50)$$

To determine exergy collection, the exergy to energy ratio of solar irradiance was assumed constant at  $\psi_{solar} = 0.933$ .<sup>106</sup> Exergy content of generated electricity is equivalent to its energy content ( $Ex_{Egen} = E_{gen}$ ).<sup>107</sup> Collected thermal exergy was defined as the power that can be drawn from a system as it is brought to equilibrium with a heat reservoir at a reference temperature, which accounts for entropy generation:<sup>108</sup>

$$Ex_{Qgen} = \dot{m}_{HTF} c_{p,HTF} \left( T_{out} - T_{in} - T_{ref} \ln \left( \frac{T_{out}}{T_{in}} \right) \right) \quad (51)$$

The reference temperature of  $T_{ref} = 20^{\circ}\text{C}$  was chosen. By considering both the exergetic and energy efficiencies of a building-integrated solar collection system, a more complete picture is drawn of the system's benefits than if considering either metric alone, as both the quality and quantity of collected energy are useful (for both driving processes and heating) in the built environment.

#### 3.5.4.1.3 Experimental Prototype Details

To characterize the behavior of the BITCoPT prototype, it was operated over a period of two months, installed in the southwest-facing window of a commercial office tower in New York City, behind a double-hung window fitted with double-pane glazing. The site is partially shaded from buildings to the south and southwest so the daily

<sup>106</sup> Petela, R. (2003). Exergy of undiluted thermal radiation. *Solar Energy*, 74(6), 469–488. [http://doi.org/10.1016/S0038-092X\(03\)00226-3](http://doi.org/10.1016/S0038-092X(03)00226-3)

<sup>107</sup> Dincer, I., & Rosen, M. A. (2005). Thermodynamic aspects of renewables and sustainable development. *Renewable and Sustainable Energy Reviews*, 9(2), 169–189. <http://doi.org/10.1016/j.rser.2004.02.002>

<sup>108</sup> Suzuki, A. (1988). General theory of exergy-balance analysis and application to solar collectors. *Energy*, 13(2), 153–160. [http://doi.org/10.1016/0360-5442\(88\)90040-0](http://doi.org/10.1016/0360-5442(88)90040-0)

collection period occurred in the early afternoon. Data from three days in 2015 were analyzed: February 19, March 20, and March 23.

Data were collected on the flow rate and temperature of the heat transfer fluid, the air temperature in the cavity, electrical generation, direct irradiance, and the shaded fractions of the modules' primary optics. The experimental prototype was outfitted with sensors as detailed in Figure 95 and Figure 96.

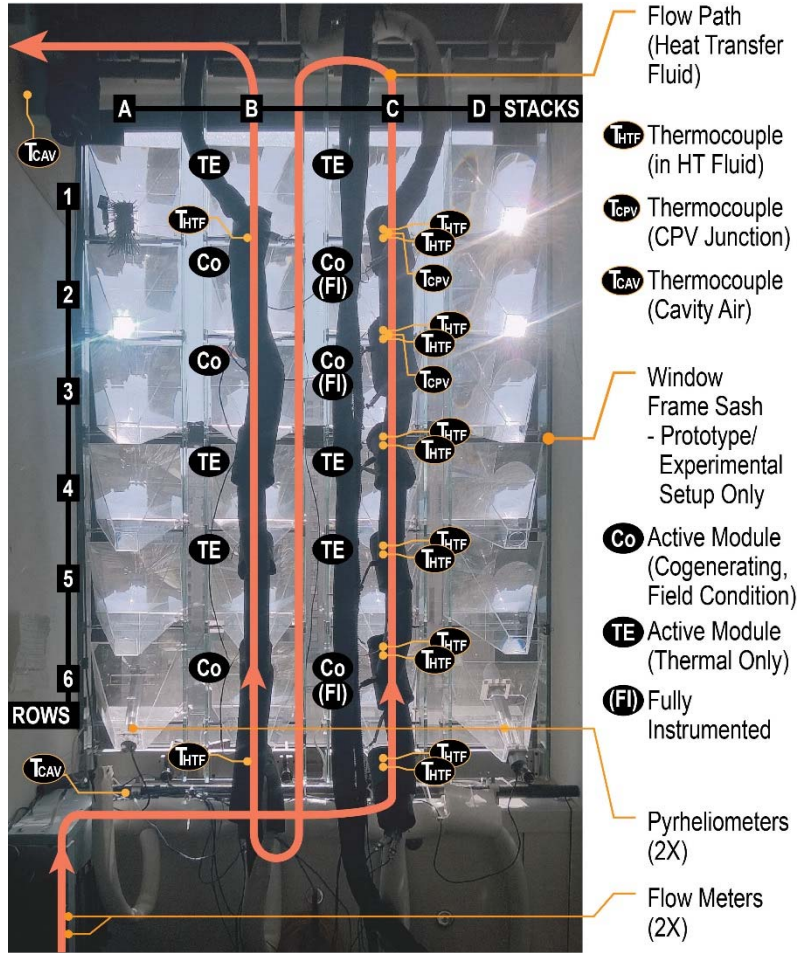


Figure 95. BITCoPT prototype as tested, with sensor placements.

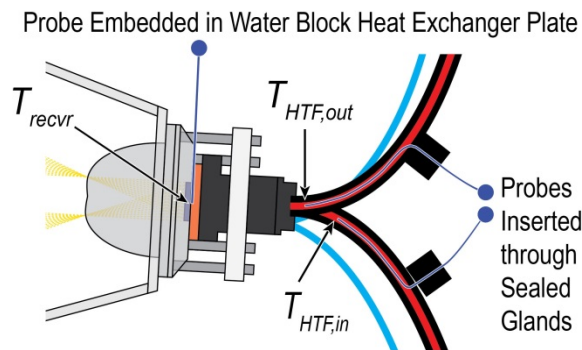


Figure 96. Experimental setup: thermocouples installed at module receivers.

### Measuring Electricity Generation

Electricity generation was measured from six modules that experience a similar shading field condition, as shown in Figure 95. Electrical power generated by the serial string of modules was measured by sinking power to an electronic load (BK Precision

8500). The string's maximum power point (MPP) was maintained to within  $\pm 0.1V$ . The measured modules were connected in series. 12AWG or larger copper wire was used to minimize voltage drop in the module circuit.

### ***Measuring Thermal Collection***

Fluid temperature increases and flow rates were measured both for individual modules and for the branch of twelve modules that included the two six-module stacks. To measure the temperature rise due to individual modules, fluid temperatures were measured at the water blocks' inlets and outlets (Figure 96). These thermocouples were installed on the six modules in the third stack and the first and sixth modules of the second stack (Figure 95). The temperature rise from the branch of modules was taken to be the difference between the temperature at the inlet of the first module in the branch and at the outlet of the last module. The tubing that connected the heat exchangers was insulated with low density neoprene foam ( $k_{insul} = 0.0372$  at  $32^{\circ}C$ ) to a minimum thickness of 18mm.

Heat transfer fluid flow rates were measured with float-type volumetric flow meters (Porter F150-B125-60). To mitigate measurement error, flow rates and floats were picked so that, for typical rates ( $\dot{V}_{HTF} = 1.5 \cdot 10^{-6} \text{ m}^3/\text{s}$ ), readings were at half-height or higher on their scales and the temperature rise across the branch was large relative to the measurement error stack-up. In the projected setup, the thermal resistance across the modeled heat exchanger increases with flow rate. In the prototype, however, varying flow rates had little effect on thermal collection, likely due to the high flow capacity of the commercial water block heat exchangers used, which would result in laminar-only flow for all tested flow rates.

Fluid temperatures were measured with thermocouple probes inserted into the flow through packing glands (Figure 96). The thermocouples were T-type, ungrounded, and in 1mm diameter stainless steel probe sheaths. At selected modules, additional temperatures were taken at the mating surface between the water block heat exchanger and the CPV (Figure 95 and Figure 96). The ambient air temperature in the window bay cavity ( $T_{cav,proto}$ ) was measured with bare, ungrounded K-type thermocouples in free air, in two locations: in the upper and lower corners of the bay and at the foot of the bay at

the outlet of a fan coil unit that supplies tempered air (part of the laboratory's HVAC system).

The thermal collection circuit is documented in Figure 92. In the experimental prototype, flow in the collector circuit was driven by a positive-displacement pump (Pentair pump GCBN23V) at a constant speed. Pressure was modulated by means of a bypass branch with a needle valve control. Flow passed through a liquid/liquid plate heat exchanger before returning to the pump, and a separate fluid circuit joined the second side of the heat exchanger (in counter-flow) to the reservoir tank, containing 10kg of water (or 42kJ/K heat capacity). The tank was fitted with an auxiliary 1kW heating element, modulated by a thermostat, which maintained the collector circuit inlet temperature to within  $\pm 0.5^{\circ}\text{C}$  of the chosen set point. The reservoir circuit was pressurized with a low-head, high-flow circulator (Bell and Gossett NBF-220, 0.12hp). Both circuits were fitted with necessary expansion, bypass, and fill mechanisms.

### ***Data Acquisition***

Data acquisition was performed on a PC through an interface developed in the LabVIEW environment. Logged measurements are noted in Table 41. All measurements were taken and logged automatically, except for the flow rates, which were periodically read at the flow meters and logged through the interface.

### ***Tracking and Monitoring Control***

The prototype was controlled by software developed in the LabVIEW environment. The software determines a yaw target for the array and pitch targets for each stack based on the solar vector, the orientation of the array in space, and alignment trims for each axis. The solar vector was calculated using NREL's solar position algorithm.<sup>109</sup> Axis targets were sent to an embedded motion controller (which controls the servo-encoder feedback relationship) via serial communication. Targeting was performed open loop, without a sun position input signal. Alignment was verified during prototype operation, however, by periodically adjusting the pitch and yaw trims around the

---

<sup>109</sup> Reda, I., & Andreas, A. (2004). Solar position algorithm for solar radiation applications. *Solar Energy*, 76(5), 577–589.

calculated target vector and observing the maximum power generation relative to the trims.

### **Steady-State Definition**

Data were collected during steady-state operation. The steady state is defined as any period when the time derivative of a given temperature rise is small relative to that rise:

$$\frac{d}{dt}(T_{HTF,out} - T_{HTF,in}) \leq c_{ss,HTF} T_{HTF,in}; c_{ss,HTF} = 0.026 \text{ } 1/s \quad (52)$$

Steady-state does not refer, specifically, to the stability of the system's inputs but to the lack of change in state of one part of the prototype relative to another part. Some fluctuations in input signals result in retarded transient system behavior due to low heat transfer fluid flow rates and high heat capacities. Gradual shifts in inputs do not, however, disrupt steady-state behavior below the following threshold:

$$\frac{d}{dt} G_{DN,POE} \leq c_{ss,GDN} G_{DN,POE}; c_{ss,GDN} = 0.10 \text{ } 1/s \quad (53)$$

### **Uncertainty Characterization**

Measured results were characterized by analyzing the propagation of uncertainty, assuming no covariance between measurements.<sup>110</sup> Table 35 lists the uncertainties for the measured values in the experiment (FS indicates full-scale reading, with values shown in parentheses).

---

<sup>110</sup> Moffat, R. J. (1988). Describing the uncertainties in experimental results. *Experimental Thermal And Fluid Science*, 13-17.

Table 35: List of Uncertainties.

Parameter	Uncertainty (Absolute or Relative)
$\dot{V}_{HTF}$	$\pm 5\%$ FS $3.5 \times 10^{-6}$ m <sup>3</sup> /s
$c_p$	$\pm 1\%$ 4190 J/kg-K
$\rho_{HTF}$	$\pm 1\%$ 974.9 kg/m <sup>3</sup> <sup>111</sup>
$T_{HTF}$	$\pm 0.5^\circ\text{C}$ <sup>112</sup>
$V_{gen}$	$\pm 0.05\% + 0.025\%$ FS (120V) <sup>113</sup>
$I_{gen}$	$\pm 0.2\% + 0.15\%$ FS (30A) <sup>113</sup>
$I_{DN}$	$\pm 1.2\%$ <sup>114</sup>
$F_{POE}$	$\pm 3\%$

\*FS: full-scale reading (FS value in parentheses)

#### 3.5.4.1.4 Projected Model Setup Details

By informing the analytical model with results from operating the prototype, a projected model setup was developed to extrapolate BITCoPT's behavior in a configuration that might be expected in an installation. This setup involved two areas. First, parameters and functions were modified that govern the behavior of certain components (glazing types, concentrating optics efficiency, water block thermal resistance, shading, and stack geometry), as noted in the Technology Description (section 0) and Model Description (section 3.5.4.1.2). Second, the collector's geometry was generalized as one stack, ten modules tall. It was assumed the modules were centrally located in the BITCoPT array, as described in section 0. The single stack of ten modules occupies a façade area of 0.958 m<sup>2</sup>.

---

<sup>111</sup> Incropera, F., & DeWitt, D. (1996). *Fundamentals of Heat and Mass Transfer* (4th ed.). New York, NY: John Wiley.

<sup>112</sup> Omega. (2008). Revised Thermocouple Reference Tables. Retrieved July 13, 2015, from [www.omega.com](http://www.omega.com).

<sup>113</sup> BK Precision. (2014). 85xx Datasheet. Retrieved July 13, 2015, from [https://bkpmedia.s3.amazonaws.com/downloads/datasheets/en-us/85xx\\_datasheet.pdf](https://bkpmedia.s3.amazonaws.com/downloads/datasheets/en-us/85xx_datasheet.pdf)

<sup>114</sup> Hukseflux. (2015). DR01 pyrhelimeter. Retrieved July 13, 2015, from <http://www.hukseflux.com/product/dr01-pyrhelimeter>

#### **3.5.4.2 Results: Model Validation, Prototype and Projected Efficiencies**

Data from the operational prototype were interpreted to fulfill three objectives: to evaluate the analytical model's predictive capacity, to determine the prototype's energy and exergetic cogeneration efficiencies, and to project the performance of BITCoPT as it might be installed. To evaluate the model's predictive capacity, the prototype's measured operating outputs were compared to outputs of the prototype model simulation, given four measured inputs: direct normal irradiance, heat transfer fluid temperatures, fluid flow rates, and cavity air temperatures. These measured inputs were consequently used as inputs to the projected model setup, and projected exergetic efficiency was compared to the behavior of the prototype.

#### **3.5.4.3 Model Validation with Prototype Data**

Modeled results were compared to measured results from the testing site in New York, NY, with the experimental array configured as shown in Figure 95. Three collection periods over three days were considered. The periods of data collection were limited to one hour or less due to the shading from buildings to the south of the installation. Values were determined for four parameters of interest in the prototype model setup by minimizing the root mean square error (RMSE) relative to the measured samples mean between four measured and modeled signals. The parameters of interest were: optical efficiency, water block thermal resistance, the heat transfer coefficients for the receiver-cavity loss and loss through tubing insulation. The quantitated signals were: electrical generation ( $RMSE_{E_{gen}} = 6.3\%$ ), thermal generation ( $RMSE_{Q_{gen}} = 4.3\%$ ), CPV temperatures, and the fluid temperatures at tubing inlets and outlets.

Energy collected from all twelve modules, relative to direct irradiance measured at the primary optics and heat transfer fluid inlet temperature, is shown in Figure 97 (both measured and modeled quantities).

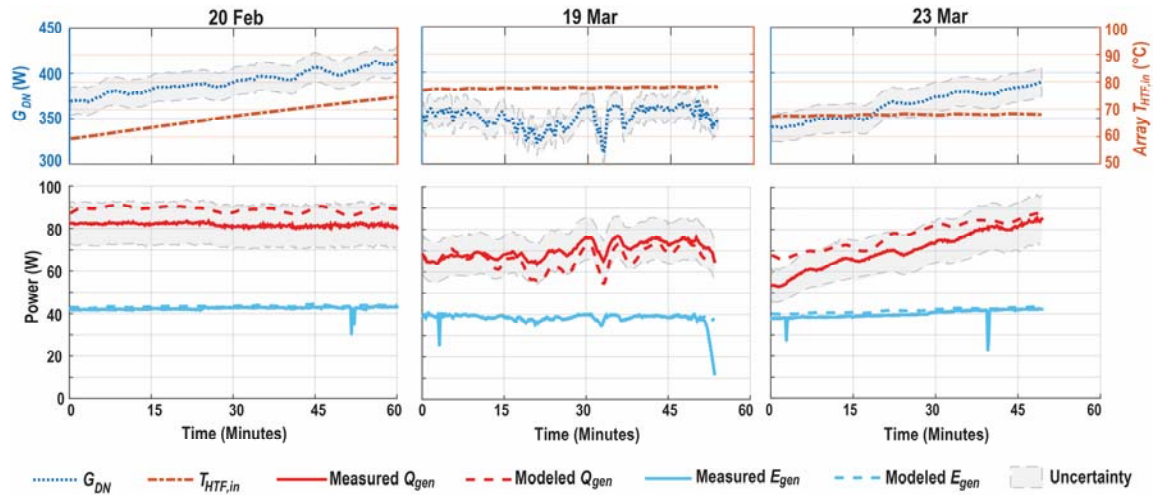


Figure 97. Observed prototype power generation.

Solar power incident on twelve modules, inlet fluid temperature, electricity generated (from six modules), thermal energy collected (from twelve modules) during three reporting periods.

The electricity generated by the six active modules was relatively constant at  $E_{gen} \cong 40 \pm 0.7W$ . Modeled  $E_{gen}$  tracks observed  $E_{gen}$  with some over-prediction during the early part of the March 23<sup>rd</sup> data.  $Q_{gen}$  in the February 20<sup>th</sup> data remained relatively constant as two conditions shifted in counteracting ways during the collection period. Shadows cast from the window frame and sash decreased on the primary optics of the thermal-only modules, a shift which increased the insolation available for collection. Inlet temperatures likewise increased (as controlled by the auxiliary heater), a shift which decreased the energy efficiency of collection. Because the decrease in shading was not significant on the six cogenerating modules, electrical output remained stable. In the March 19<sup>th</sup> data both  $E_{gen}$  and  $Q_{gen}$  tracked the measured irradiance, which, due to intermittent cloudiness, varied over the collection period. It should be noted that while the typical target flow rate during these periods of data acquisition is  $\dot{V}_{HTF} = 1.5 \cdot 10^{-6} \text{ m}^3/\text{s}$ , the flow was increased to  $\dot{V}_{HTF} = 3.0 \cdot 10^{-6} \text{ m}^3/\text{s}$  on March 19<sup>th</sup> to reduce the risk of boiling. Although the modules tested in the prototype were neither contiguous (split over two stacks) nor homogenous (either cogenerating or thermal-only), the corroboration between measured and modeled outputs demonstrated that the model can represent the behavior of this system with a simplified set of energy transfer equations.

### 3.5.4.4 Experimental Energy and Exergetic Collection Efficiency

Energy and exergetic cogeneration efficiencies were determined from prototype operation for the homogeneous sub-arrays (Figure 98).

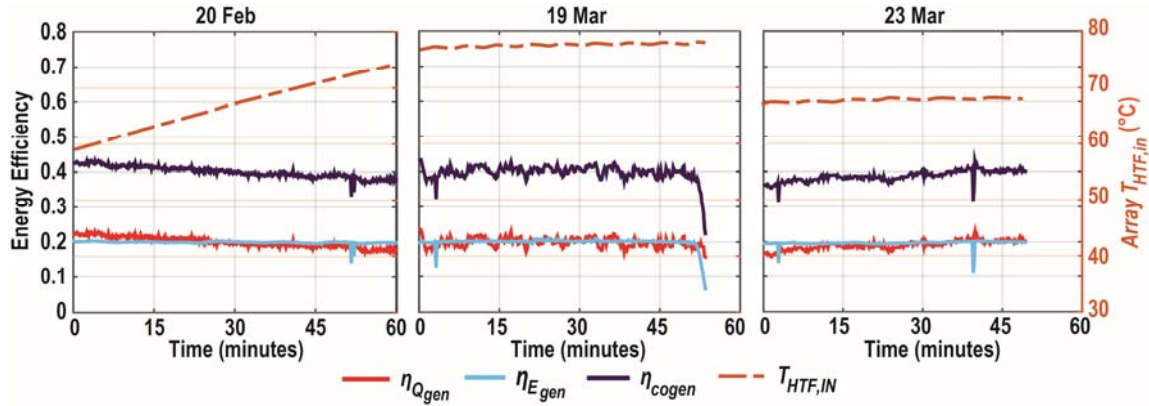


Figure 98. Energy efficiencies (measured) of homogeneous sub-array.

The peak cogeneration energy efficiency was  $\eta_{cogen,proto} = 43.3\% \pm 9.1$ , relative to module-incident direct solar energy ( $G_{DN,POE}$ ). This peak output occurred at the lowest measured inlet temperature of  $60^{\circ}\text{C}$ , which is suitable for service water heating as well as sorption chilling, albeit at a limited COP. Thermal collection was nearly equal to electrical collection efficiency at lower inlet fluid temperatures, peaking at  $\eta_{Qgen,proto} = 22.1\%$  at  $59^{\circ}\text{C}$ . Over the three reporting periods, cogeneration  $\eta_{cogen,proto}$  was reliably between 35% and 40% ( $\eta_{Egen,proto} \cong 20\%$  and  $\eta_{Qgen,proto} \cong 15\%$  to 20%).

The peak exergetic efficiency  $\varepsilon_{cogen,proto} = 25.1\% \pm 3.8\%$  occurred in the February 20<sup>th</sup> data at  $T_{HTF,in} \cong 60^{\circ}\text{C}$  (Figure 99).

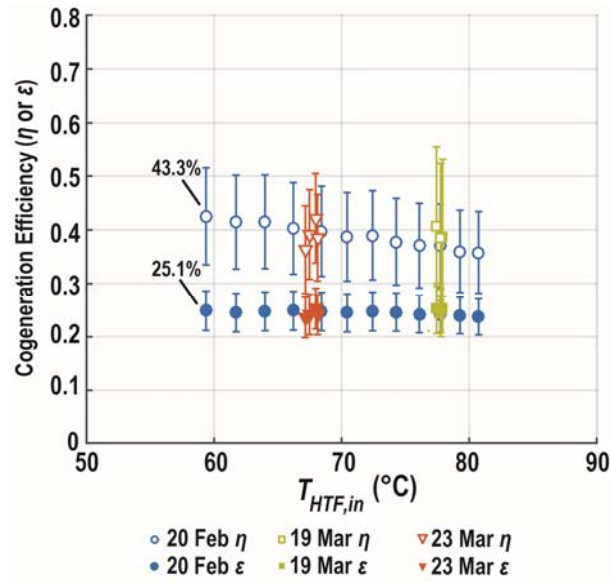


Figure 99. Observed cogeneration efficiencies  $\eta_{cogen}$ ,  $\epsilon_{cogen}$ , for homogenous modules (functions of  $T_{HTF,in}$ ).

The homogeneous value describes the output of the fully-cogenerating sub-array. The response curve of exergy output vs fluid temperature has a broad peak, varying less than 1% over the 20°C range of measured temperatures. The March 19<sup>th</sup> data were less well-represented by the model than the other two data sets; this outcome was expected since the flow rates during that collection period were functionally higher.

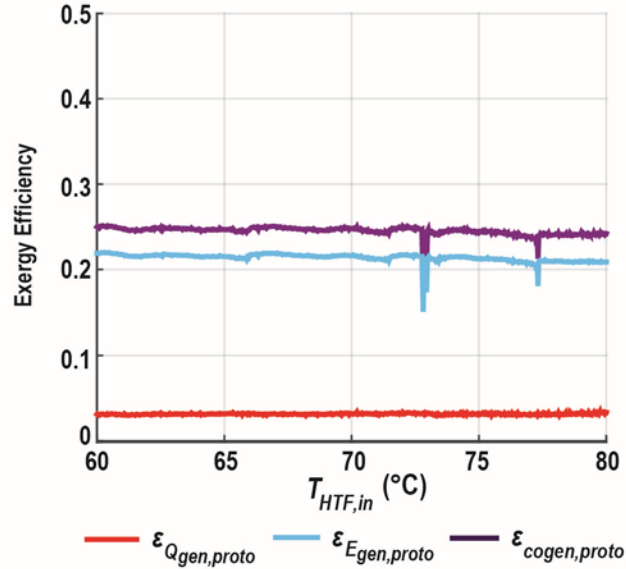


Figure 100. Exergetic efficiencies for homogenous sub-array on February 20<sup>th</sup>.  
 Inlet temperature increased monotonically with time in data set.

Contributions for  $\epsilon_{cogen,proto}$  from  $\epsilon_{Egen,proto}$  and  $\epsilon_{Qgen,proto}$  are shown in Figure 100 relative to inlet fluid temperature. There is a relatively flat response for  $\epsilon_{Qgen,proto}$  between 60°C to 80°C, while  $\epsilon_{Egen,proto}$  slightly diminishes over the same period.

### 3.5.4.5 Projected Energy and Exergetic Collection Efficiency

To investigate the exergetic efficiency to be expected if BITCoPT's design was optimized, the conditions measured from experimental data were input to the projected model setup (Figure 101). The setup includes revisions that represent nominally-efficient, low scattering optics, low-scattering glazing, current-generation CPVs, and appropriate heat exchangers (see the Analytical Model Description, section 3.5.4.1.2).

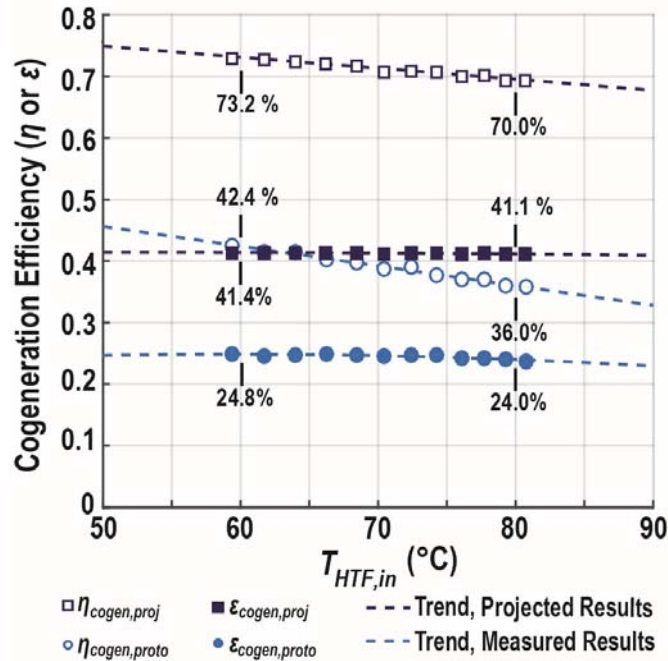


Figure 101. Observed and projected cogeneration energy and exergetic efficiencies.

With the projected model setup, simulated energy cogeneration efficiency increased to  $\eta_{cogen,proj} = 73.2$  at the lower bound of analyzed temperatures,  $T_{HTF,in} = 60^\circ\text{C}$  (Figure 101). The projected maximum exergy efficiency both increased and occurred at a higher heat transfer fluid temperature,  $\epsilon_{cogen,proj} = 41.4\%$  at  $62^\circ\text{C}$ .

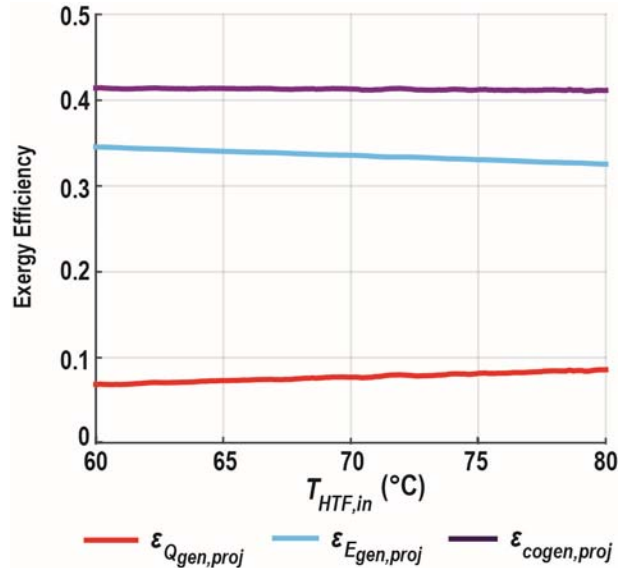


Figure 102. Exergetic efficiencies for projected setup, February 20<sup>th</sup> input data. Inlet temperature increased monotonically with time in data set.

From Figure 102, the exergetic efficiency tradeoff between projected model electrical and thermal exergy is more noticeable than the observed case (Figure 100). The projected model is more sensitive to temperature as potential electrical production decreases from  $\epsilon_{Egen,proj} = 35\%$  to  $32\%$  with higher collector temperatures, while  $\epsilon_{Qgen,proj}$  increases from  $6\%$  to  $9\%$ .

#### 3.5.4.6 Discussion: Ramifications of Experimental and Projected Results

As seen in section 3.5.4.5, the projected maximum exergy efficiency  $\epsilon_{cogen,proj}$  improved over the experimental results, suggesting improvements could be made to the current prototype. In the measured data, the flat response of exergetic collection to operating temperature correlates to the tradeoff between increasing potential and increasing losses, indicating the prototype is operating near its own local optimum. The trends indicate that the prototype is operating beyond its optimum temperature while the projected model might increase in efficiency with increased temperature, albeit with a flat response, as mentioned. Increasing the effectiveness (insulation) of the thermal collection system would be expected to increase the exergetic efficiency, shifting the maximum to a higher temperature.

In the projected results, cogeneration exergy is greater than the electrical-only exergy that would be expected at lower cell temperatures, if the trend of Figure 102 is followed back to 35°C and 45°C, a nominal range for passively cooled CPV modules. This was determined in precedent studies<sup>115</sup> to be true for opaque systems; these results suggest this benefit extends to a transparent system, which permits the diffuse solar energy to be used for daylighting, and collects only the direct solar component. Due to the projected nature of the analysis and uncertainty in the prototype results, further experimentation could be done to explore this possibility.

#### **3.5.4.7 Summary**

To develop deeper capabilities for buildings to collect and utilize solar energy, a prototype of a Building envelope-Integrated, Transparent, Concentrating Photovoltaic and Thermal solar collector (BITCoPT) has been investigated by comparing an analytical model of its behavior to empirical data. BITCoPT, conceived out of recognition for the need for building envelopes to interact with external and interior environments in more complete and complex ways, is designed to provide daylighting (by transmitting diffuse daylight) and transform direct irradiance into electricity and thermal energy at high exergetic efficiency. The prototype demonstrated exergetic cogeneration array efficiency of 25.1% and energy cogeneration array efficiency of 43.3% relative to direct irradiance that penetrates the envelope's exterior glazing layer.

The model demonstrates good predictive capacity for the cogeneration output of BITCoPT. The model was used to explore further the technology's energy and exergetic collection efficiencies, demonstrating, in simulation, projected cogeneration array efficiencies of 73.2% (energy) at 60°C, and 41.4% (exergy) at 62°C. Additionally, exergetic efficiency was demonstrated to be sustained at elevated temperatures that are suitable for driving heat engine processes. With the analytical model in place, future investigations can be done into the behavior of broader building systems strategies that

---

<sup>115</sup> Pathak, M. J. M., Sanders, P. G., & Pearce, J. M. (2014). Optimizing limited solar roof access by exergy analysis of solar thermal, photovoltaic, and hybrid photovoltaic thermal systems. *Applied Energy*, 120, 115–124. <http://doi.org/10.1016/j.apenergy.2014.01.041>

incorporate BITCoPT. In concert with providing daylighting, views to the exterior, and cooling load reductions, BITCoPT could generate electricity and thermal energy at a magnitude significant to a commercial building, enabling net-zero or energy-positive operation. Results of experiments with the prototype, modeled output, and extended simulations are presented and discussed.

### ***3.5.5 PHASE III: Assessment of Research Field of Inquiry***

Modern strategies for solar collection place value on system simplicity over maximum possible power generation, creating solutions that generate electricity over a narrow band of time during the solar day. This creates two problems. The first problem is these systems produce little energy over the course of the day relative to their cost, and in many conditions will never recover first costs.

Secondly, because they are not dynamic and not considered as part of a fully integrated system, these static photovoltaic systems create problems of heat accumulation, reflective glare, and daylight reduction, even when they are not producing any electricity. A more efficient strategy based on alpine buttercup bio-mimetic processes would be to create a dynamic solar tracking system that performs multiple functions in response to a fluctuating solar resource. By not responding dynamically, new problems are created that may outweigh the benefits of the system's initial intents.

The perceived complexity of the ICSF is a liability that needs to be massaged with greater simplification and reduction of parts within the ongoing DFM process. However, with more than 50% reduction in parts over the last two iterations, the system has achieved a tremendous degree of robustness and lowered tolerances, such that with the right manufacturing partners within the supply chain, it can achieve low initial costs (projected at \$150/ft<sup>2</sup>, which results in a projected cost-payback period that is comparable to other technologies with far less power and functionality once they are paid off.

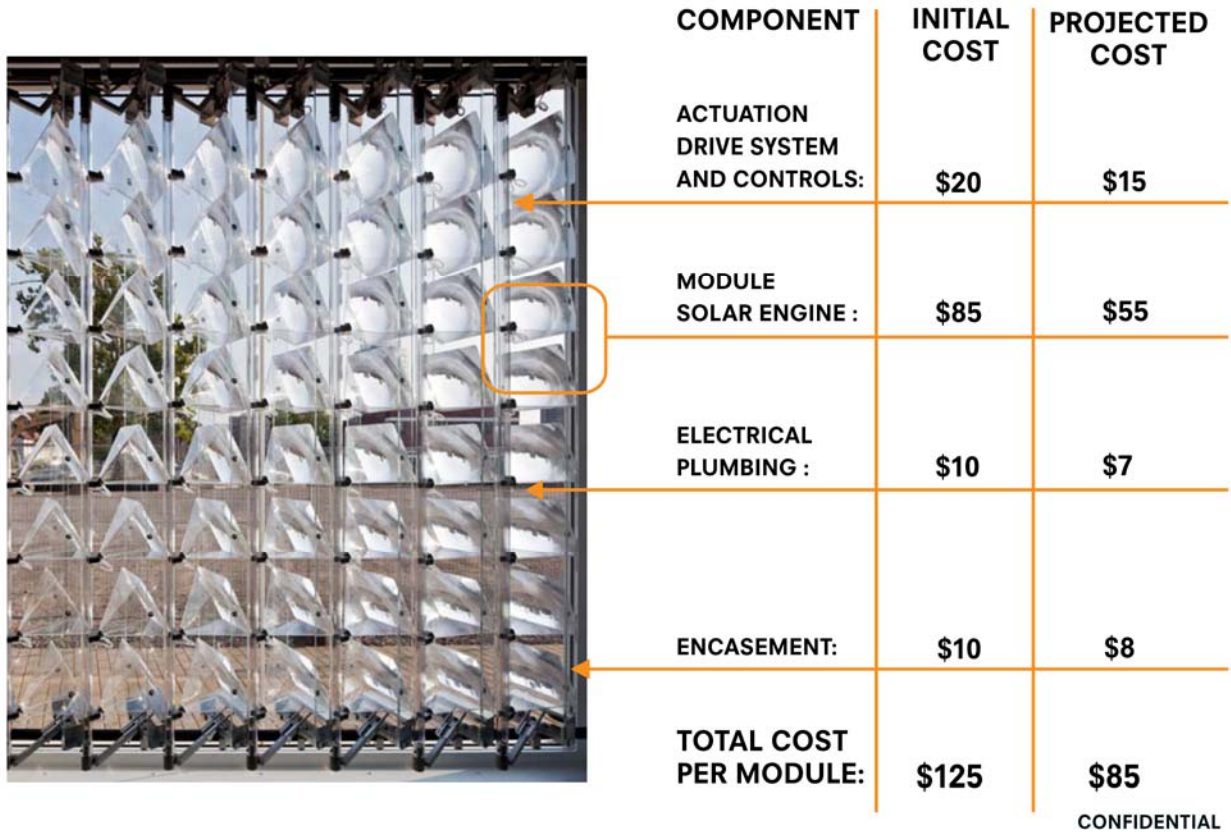


Figure 103. Projected Price Per Module for Mass Produced ICSF.

### 3.5.5.1 Moving Beyond the Existing Market Driven Metrics of ‘Installed Cost versus Energy and Cost Payback’ Periods

Perhaps the most innovative achievement of the ICSF system in terms of a potential market breakthrough is to couple architectural and social values (daylighting, views, heat and glare mitigation) with energy generation, thereby overcoming the static market metrics that tie initial costs to cost payback periods.

With conventional energy saving technologies, in the mind of many building owners, the choice of incorporating a new energy producing technology falls squarely on its payback period. The integration alludes to other associated factors that would aid in reducing payback periods, such as improved worker productivity due to increased access to daylight and thermal comfort, as well as integration with phase change material for thermal storage to offset HVAC loads. However, building owners will need convincing beyond the conventional monetary metrics of a more complex mixture of quantitative and qualitative outputs.

To this end, there are different expectations placed on payback periods which may dictate what market envelope integration should be targeted towards. For example, a small office will commonly require a one year payback on investment for energy savings and production and will rarely accept more than a two-year payback, unless energy costs are a substantial fraction of the building's total cost. A large office or building application, on the other hand, would expect between ten and twenty percent real return on an investment, and provided it is producing a moderate amount of energy, it would normally the same discount rate to investment for energy conservation, allowing it to undertake more advanced conservation measures requiring higher capital investment.

Making matters even more complex is the localized thermal and electric production and whether the tenants of a specific floor achieve the benefits of energy conservation and production. The decision by building owners in favor of distributed benefits would be increased tenant rent on areas of the facade that produce on average the most peak energy associated to the specific associated program. Increased revenue through special value rental floors would decrease the cost payback period as the increased rent would go directly toward paying back the system. And the tenants, because they have a vested interest in the performance of their system, would conserve more energy and try to optimize their programmatic energy requirements to sync with the output of the facade. Further social and system payback projections will be tested as to find the point where real estate, economics, and social science overlap to benefit all potential parties.

### **3.6 Overall Assessment for Future Research and Development for this Area of Inquiry: Implications for Envelope and Thermal Transfer Integration and Optimization Strategies for Building Integrated Solar Energy**

#### ***3.6.1 Integrating Device Scale Finite Element Analysis with Building Energy Modeling Methods for the Adaptation of Future Energy Systems in a Double Skin Façade***

The building envelope, one of the most important yet misinterpreted components of achieving energy self-sufficient buildings, is tasked with the challenge of controlling

drastically changing qualities of temperature, sunlight, wind, and moisture all while maintaining a constant desired interior condition.<sup>116</sup> In traditional building science, it is common practice to insulate and glaze the exterior envelope in the hope to reject environmental energy flows and reduce cooling and heating loads.<sup>117</sup> This method cuts occupants off from quality environmental conditions like sunlight and air, while underutilizing the available envelope area for energy capture.<sup>118</sup> By integrating the envelope with energy transformation technology, like ICSF, the envelope no longer rejects natural energy flows but, instead, captures, stores, and transports energy away from the envelope for the reduction of energy, supply of desirable climatic variables, and utilization of energy in building systems.<sup>119</sup>

Dynamic double-skin facades provide a potential to meet future energy reduction qualifications<sup>120</sup> but, to meet long term energy codes, require an intervention of energy capture and transformation technology. Current energy modeling software lack the ability to account for all the benefits to the whole building when combined with an integrated concentrating solar façade.<sup>121</sup> Current methods to investigate the best possible configuration for the reduction of energy usage is through a method of linking various simulation results together.<sup>122</sup> This process, although effective, is afflicted with

---

<sup>116</sup> S.E. Selkowitz, E.S. Lee, O. Aschehoug. "Perspectives on Advanced Facades with Dynamic Glazings and Integrated Lighting Controls."

<sup>117</sup> Krarti, Moncef. *Energy Audit of Building Systems: An Engineering Approach*. 2nd ed. Boca Raton, FL: CRC, 2011. Print.

<sup>118</sup> AN ICS CASE PUBLICATION WOULD BE GREAT HERE.

<sup>119</sup> Dyson, A., Ngai, T., & Vollen, J. (2011). Characterizing the Problem: Bioenergetic Information Modeling. BIM in Academia. New Haven, CT: Yale School of Architecture.

<sup>120</sup> Hensen, Jan, Ph.D, Martin Bartak, and Frantisek Drkal, Ph.D. "Modeling and Simulation of a Double-Skin Façade System." *ASHRAE Transactions: Symposia* 108.2 (2002): n. pag. Print.

<sup>121</sup> Hensen, Jan, and Roberto Lamberts. *Building Performance Simulation for Design and Operation*. Abingdon, Oxon: Spon, 2011. Print.

<sup>122</sup> Krarti, Moncef. *Energy Audit of Building Systems: An Engineering Approach*. 2nd ed. Boca Raton, FL: CRC, 2011. Print.

bulk assumptions and the software's slow adaptation of energy capture technology and integrated systems into the program's functionality.<sup>123</sup>

By running advanced simulation models of a double-skin façade, with integrated concentrating solar, empirical formulas will be implemented into building energy simulation software to characterize the behavior between climatic energy flows and the result on the building, in a computationally feasible method.

Standard practice procedures in building energy reduction, using energy modeling, will be outlined with regards to advantages and limitations. Previous methods for linking external simulations to EnergyPlus will be considered for their potential into modeling the building envelope as a transformation mechanism of climatic energy flows. To explore advanced energy capture technology, a finite element (FE) model will be designed for the analysis of Integrated Concentrating Solar (ICS) within a double-skin façade. Finite Element analysis is a technique that discretizes a problem, of an otherwise difficult to solve differential equation, into a series of small pieces (or finite elements) that are individually solved to reach an approximate solution of the exact solution.<sup>124</sup> The energy model planned couples computational fluid dynamics (CFD) and ray tracing (radiation)<sup>125</sup> with incremental, user defined parameters to test every possible outcome of variation in the system.

The methods for simulating the energy flows will be looked at from two scales: building scale, whole building simulation will be applied to solve the problem from a systems' performance simulation; and, device scale, finite element models will be simulated to explore how the energy flows are transformed at the individual devices. The project provides the opportunity to link models that inform one another from different scales to produce results that would otherwise not be possible to achieve in their individual context.

---

<sup>123</sup> Hensen, Jan, and Roberto Lamberts. *Building Performance Simulation for Design and Operation*. Abingdon, Oxon: Spon, 2011. Print.

<sup>124</sup> Hughes, Thomas J. R. *The Finite Element Method: Linear Static and Dynamic Finite Element Analysis*. Mineola: Dover Publications, 2000. Print.

<sup>125</sup> *AcuSolve Command Reference Manual*. Mountain View: ACUSIM Software, Inc.; 2008.

The connection of energy flow behavior between the device and building scale, will provide insight into how the envelope equations in building simulation needs to be integrated with more advanced formulas to simulate future energy capture systems. When accounting for the device physics (FE model) in building simulation, the limitations of adapting future energy transformation systems into building simulations will become clear by the lack of specificity in the envelope physics. When accounting for whole building simulation in FE modeling, the complexity of the FE results will limit the ability to simulate an entire building using the advanced modeling methods. To provide the best results, the coupling of scales (models at each) will provide insight into the whole building energy behaviors, while following accurate physics of energy transformation at the building envelope. Outlining a framework across a wider range of technologies and application, increase the potential of the advanced envelope modeling method to impact a greater range of building applications.

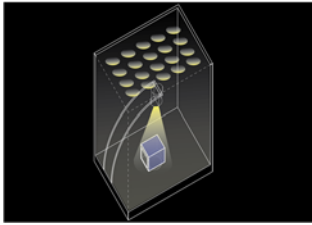
An understanding of the interconnected energy flows at the building envelope will be evaluated using a double-skin finite element (FE) analysis with Integrated Concentrating Solar (ICS); coupling CFD and radiation models.<sup>126</sup> From the FE analysis, empirical formulas will be generated to represent the interconnected energy flow behaviors, without large computer loads and costs. Recommendations for future building simulation software will be made by integrating empirical envelope formulas (from the FE model) with existing whole building energy modeling software (EnergyPlus). The resultant software would more accurately represent the interconnected physics and allow the simulation of advanced energy capture technology within a building energy simulation, without adding computational intensity.

### **3.7 Requirements for Ongoing Research**

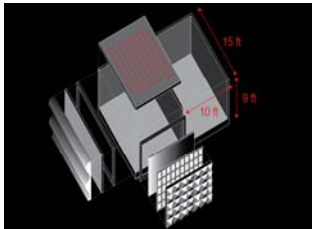
---

<sup>126</sup> Hughes, Thomas J. R. *The Finite Element Method: Linear Static and Dynamic Finite Element Analysis*. Mineola: Dover Publications, 2000. Print.

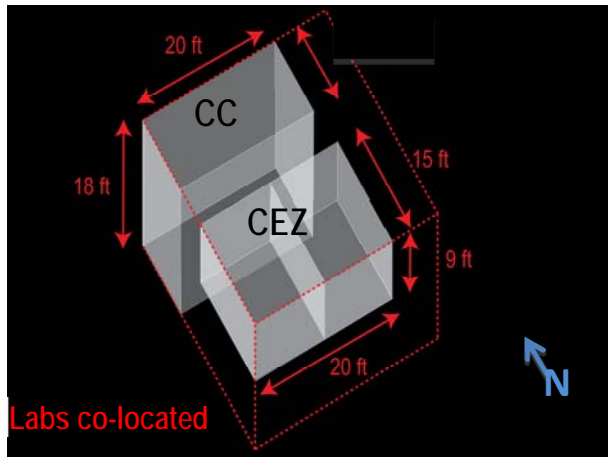
### 3.7.1 Proposal for Low-Cost Solar Simulator



LAB 1: Chamber Climate Simulator (CCS) reproduces a gamut of diverse climate and environmental phenomena



LAB 2: Controlled Envelope Zone (CEZ) reconfigurable roof/wall cassettes and independent environmental control



This laboratory would enable unprecedented investigations into the coupled, multivariate systems that characterize the built environment.

The 2 laboratories operate at two overarching scales: the chamber scale and the full/building scale

Figure 104. Testing facility with co-located labs that accelerates scale-up from 'hotbox' testing to integration within building.

To resolve the current seasonal, time, and space constraints faced by our research team, CASE proposes to build a multi-purpose solar simulator. Solar simulators generally fall into one of two categories; scientific and weathering. The weathering simulators, as their name implies, are used for simulating long term exposure of targets for understanding bleaching, polymerization, de-polymerization, etc. through direct effect (photochemical) or through indirect effects like thermal (catalyst enhancement, thermal expansion, etc.) Usually, the photons from the source in the weathering simulator are grouped into a few categories (e.g., UVA, UVB, violet-green, green-red, NIR, IR). The spectra in each category, often, only loosely match the filtered black body curve of the solar spectrum incident on earth. As such, the source(s) of the weathering

spectrum can show strong discontinuities across the summed spectrum. For example, a good weathering simulator could be constructed entirely of LEDs with augmentation by a W lamp. Also, as most materials tested under weathering tests are rough (on a wavelength scale), the incident angle of the incoming light is only of minor importance.

Scientific solar simulators have more onerous specifications. They are classified by three parameters, with an A,B, or C graded assigned to each parameter. The three parameters are: deviation from solar spectrum, spatial constancy of irradiance (usually just “constancy of irradiance” which describes how spatially uniform is the incident light on the irradiated plane immediately above the surface) and temporal constancy of irradiance (how much the spectrum and power change with time). Most often for an AAA or BAA type of simulator, the irradiance delivered to the plane of irradiance is also collimated to a large degree; a very important quality for testing many devices such as PV concentrators, solar hot water collectors, shades, etc. With the rather small tolerance acceptable for such simulators, multiple sources are exceedingly difficult to implement and, therefore, the most efficacious solution is to use a single high power source which adequately mimics the spectrum desired (in this case, the solar spectrum). The single sources that can achieve this is limited to two types, Xe and metal halide type of lamps. Both of these lamps can easily be temporally stabilized through their ballasts. The spatial delivery (constancy of irradiance and collimation) are functions of the lamp and the associated optics. Essentially, there are two methods to achieve collimation. The first is to simply remove all un-collimated light through a baffling collimator which is a very long tube (in comparison) with the size of the illumination area. The second is to employ optics (reflective, refractive or both) to achieve collimation. Due to conservation of etendue, achieving excellent collimation via the second method of a large source is not possible leaving the terribly inefficient method of baffling or baffling in combination with the second, optical, method. This is the case with extended sources such as metal-halide lamps. For efficacious solar simulators, then, that have all of the properties desirable for simulation of irradiance, the Xe short arc lamp is really the only solution. Of course, these are tremendously expensive. For a commercial system capable of pure class A performance AND

collimation on the order of only  $1^\circ$  the costs are on the order of \$75000. These systems need to be ganged to irradiate areas larger than 100mm by 100mm.

There are very few systems that sit between the weathering simulator and the scientific simulator. For our testing, pure class A performance is not necessary: time averaging is acceptable as response times of the elements is orders larger than the spatial/temporal deviations (due to convection currents in the arc area and ballast response times), with very large areas of irradiance and macroscopic affects (those that are on an order much larger than the wavelength) and relatively low resolution requirements spatial averaging is also acceptable. This leaves only collimation and spectrum, which, as we noted before can only easily be achieved via Xe.

CASE has designed and is currently fabricating our own simulator. This simulator is based on a 7kW short arc Xe lamp. The geometry of the structure is simple: the lamp is placed at the focus of a large plastic Fresnel lens, the lamp is held at the focus via water cooled electrodes, behind the lamp (along the same optical axis) sits a water cooled first surface aluminum<sup>127</sup> spherical mirror. Although this geometry is excellent for optical collimation of a short arc, it is not at all perfect, especially as the light reflected by the mirror travel back through the arc substantially diminishing the life of the lamp. The most common method, and the most efficacious, is to put the arc at the focus of a first surface aluminum parabaloid. These parabaloids are usually either solid aluminum or deposited on substrates. While simple to fabricate on small scales, they are immensely expensive on larger scales. For a power supply, we shall not require expensive high frequency ballasts (in fact, it is quite common to run Xe lamps on DC for solar testing). This is another departure from the hyper-expensive class A systems.

The most common method of simulating atmospheric conditions is to place a thin layer of water in the ray path. This is easily done with quartz sheets or other minimally absorptive materials such as ETFE. This provides the filtering of humidity (IR). If further scattering is required, another ETFE layer can be added. While the ETFE has a small

---

<sup>127</sup> Aluminum is required as most metals plasma frequency is well into the violet range and, therefore, do not reflect ultraviolet well or at all. The first surface is not required if the aluminum is on a quartz superstrate. However large quartz superstrates are exceeding expensive.

degree of haze (about 2-3%) in its best state, that can be modified easily by roughening the surface through plasma etching. (This is quite common.)

CASE will be making use of the high current power supplies available to us through RPI saving a substantial amount of money.

CASE has designed and is fabricating the effective relative solar movement mechanics using a combination of source movement in tandem with movement of a reflective system. The movement, effected through motors, will be controlled numerically through a personal computer running LabVIEW code implementing NREL's solar position algorithm.

### 3.7.2 Phase Change Material Incorporation and Sizing

Table 36. Decision matrix for optimal mass of PCM in ICSF/VTR system.

To store immediately-generated coolth, roughly .7kg of a phase-changing material is required to store one module's daily output, and less than 1% of stored energy is lost daily. (If storing high-grade thermal energy, 1.5 kg of PCM serves one module's daily output, and ~10% of collected energy is lost daily).

Quantities and Constants	Scenarios				Notes
	100 % PCM (latent)	Combo 1 50%	Combo 2 30%	All Water (sensible) 0%	
Percent PCMs by volume	100%	50%	30%	0%	
Tank in-out delta T				8	°C this number is a big assumption
thermal storage capacity	184			33,456	kJ/kg Heat of fusion of PCM, and heat capacity * temperature delta for water
Density	1690			1000	kg/m3
specific thermal storage capacity	310.96			33.456	kJ/liter
specific thermal storage capacity	310,960	172,208	116,707	33,456	kJ/m3
Number of Modules		80			
ICSF input per day, max per module		80			Wh 80Wh is what the Hptx sim says, and a quick calc (shown below) says we could hope for 120Wh
Maximum storage required for 24 hours		23.0E+6			J 18e6 J is the high point of estimated collection for Aug-September for the whole in-studio ICSF
Storage method volume fraction	70%	100%	92%	92%	assumed amount of storage volume given to actual media (as opposed to transport channels and such)
total Volume for 24hr storage	0.106	0.134	0.215	0.749	m3
total Volume for 24hr storage (l)	105.85	133.79	214.58	748.55	liters
required PCM mass for 24 hour storage	125.22	62.61	37.57	0.00	kg
Tank diameter	0.5	0.5	0.5	0.5	m
Tank height	0.63	0.68	1.09	3.81	m
Surface area	1.25	1.46	2.11	6.38	m2
Ambient Tout		22			°C
Storage Tin	75	79	79	83	°C
Delta T across insulation	53	57	57	61	°C
Rate of heat loss	23	29	41	134	W
Hours analysed		24			
Heat lost	2.0E+6	2.5E+6	3.6E+6	11.6E+6	J
Polyiso R value		0.97			m2-K/ W-in
Max heat loss	8.55%	10.75%	15.49%	50.16%	
Insulated dia	0.61	0.65	0.65	0.61	m
Insulated height	0.79	0.83	1.25	3.96	m
Insulation thickness	3	3	3	3	in
formatting key:		(constants)	(parameters)	(outcomes)	

## 4. Appendix

### A. Tracking Control System

#### A.1 Hardware

##### *Magnetic Rotary Encoders (Position Sensors)*

AMS AS5048 magnetic rotary encoders are used for angular positioning of the solar array. The sensors have 14 bit resolution ( $1/16384$ ), which translates to an angular resolution of  $0.02^\circ$ . By measuring the sensor output while the array is stationary, the steady-state error can be characterized. To determine this error, a sample size of 1000 measurements were observed and fitted to a normal distribution Figure 105. For  $\pm 3\sigma$  or 99.7%, the positional error is calculated to be  $0.05^\circ$ . This is within the  $1^\circ$  optic concentration alignment tolerance.

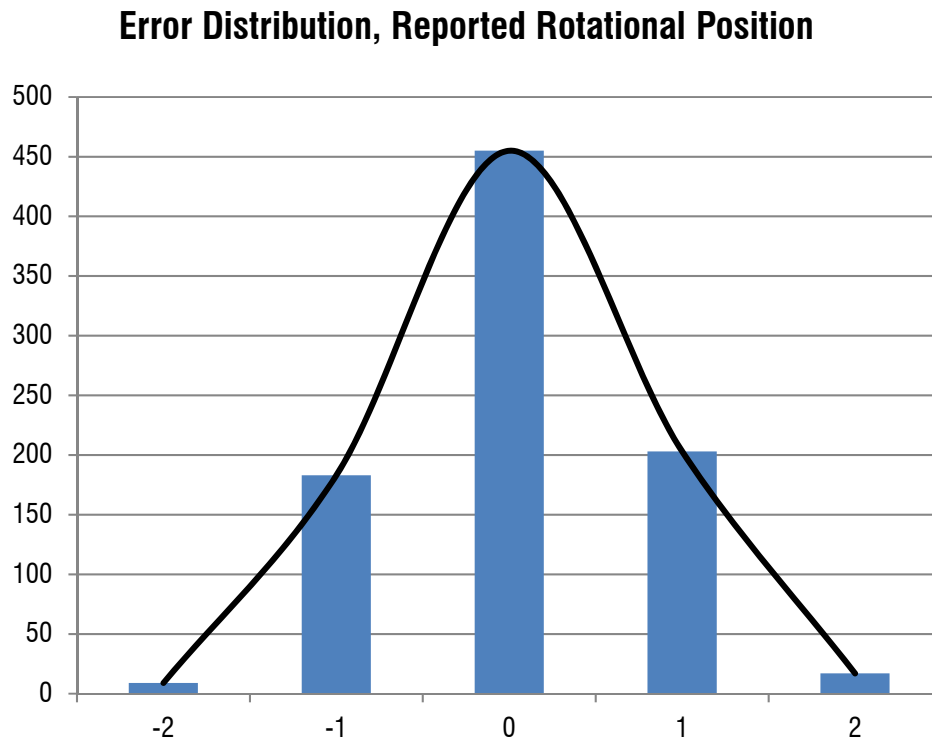


Figure 105: Distribution of rotational feedback steady state error from mean ( $n = 1000$ ).

### ***DC Drive Servo Motors***

The ICSF solar array comprises 24 modules, (4 stack of 6 modules each) with five axes of control (1 yaw and 4 pitch). One motor per array controls the yaw position of the modules, for tracking the Sun's azimuth position. Each stack has a motor to set the pitch angle for tracking the Sun's altitude.<sup>128</sup>

Servo motors (12VDC) were selected for the current tracking system, as opposed to stepper motors (as in the last two iterations), in order to prove feasibility of a cost effective design. With a feedback system connecting rotary encoders and the DC motors, similar performance characteristics to stepper motors are achieved. The geared motors chosen have a high torque, low speed characteristic which result in an over-damped system response. Figure 106 shows the response from a step input for an altitude/pitch control motor. The control system is given a TARGET position that is 10° from an initial starting position. The Y axis is shown in the 14 bit resolution scale where  $ERROR = TARGET \text{ position} - CURRENT \text{ position}$ . Feedback control continues to run the motor until the module reaches the TARGET position or, as perceived from the controller, the ERROR becomes zero.

---

<sup>128</sup> The direct yaw-azimuth and pitch-altitude relationships apply for vertically installed ICSF arrays. The relationships are modified through a rotation matrix for tilted or horizontal arrays.

### Tracking Servos Step Reponse

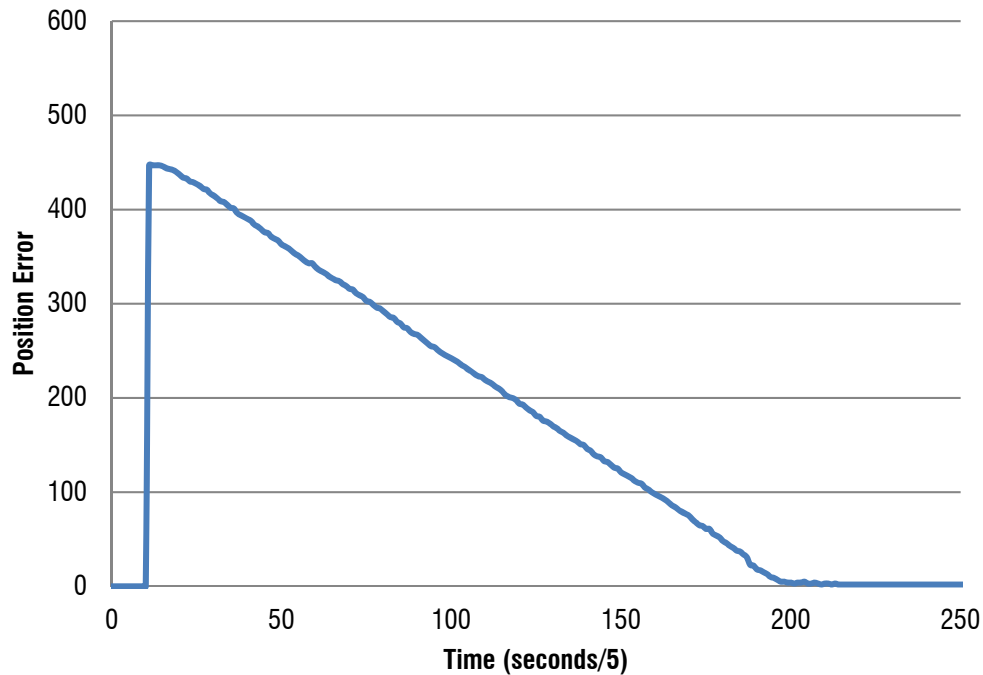


Figure 106: Tracking servos step response to an introduced position change.

Shown: Effects of velocity ramp (at T = 10) and proportional gain (at T = 200). Position overshoot is negligible with tuned PD values.

## A.2 Software

### Control Strategy

The ICSF array is targeted via a combination of solar tracking algorithms, manual inputs, and positional checks, currently implemented in LabVIEW on a PC. The NREL SPA (Solar Position Algorithm) is used to generate a real-time solar vector relative to earth-surface coordinates. Manual override of this target can be selected to drive the array to positions other than sun-aligned. Checks are performed to ensure the array isn't driven towards physically damaging orientations.

## ICSF TRACKING CONTROL SYSTEM

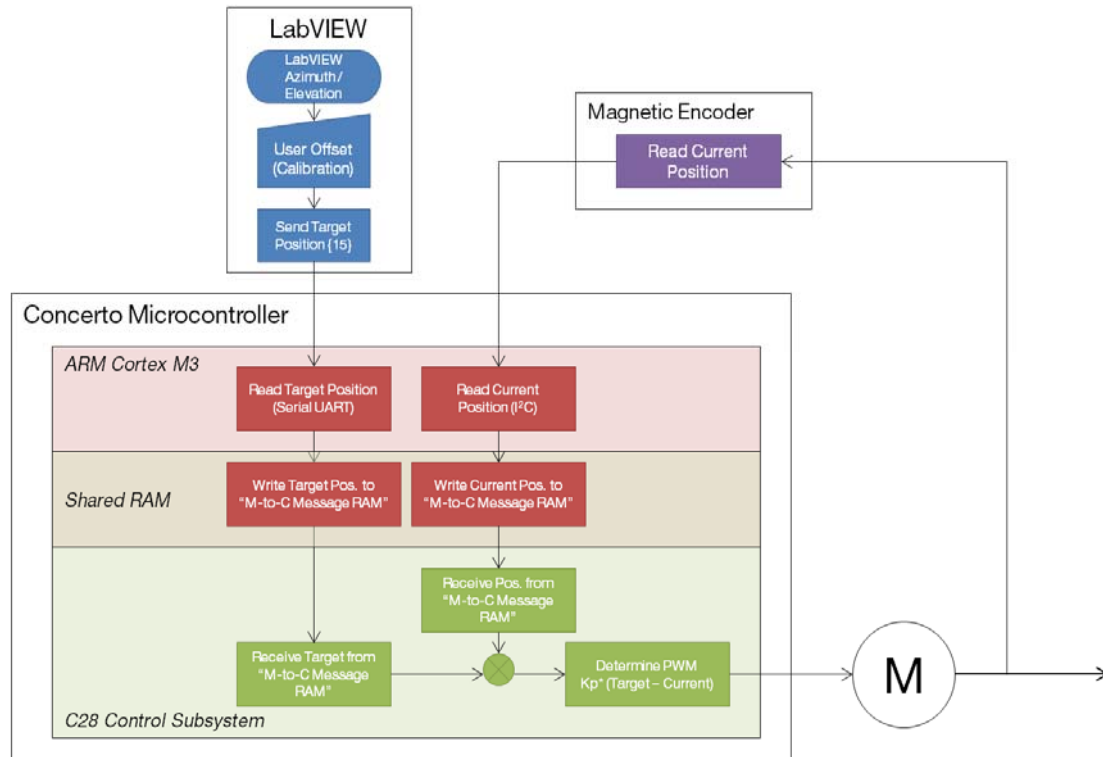


Figure 107. ICSF Control System flow chart.

The generated array target vector is communicated to the M3 embedded controller which performs PID control of the driving servo motors. (PC and M3 communicate via UART/serial communication.) The CURRENT array position is determined from encoders is transferred to the controller via I2C communication protocol. Both the TARGET and CURRENT values are then sent to the C28 via IPC. The C28 computes an ERROR where  $ERROR = TARGET - CURRENT$ . The ERROR is multiplied by a gain ( $K_p$  or proportional control) to generate a PWM duty cycle for current supplied to the drive servos. PID controllers are normally used for similar applications because they are versatile feedback compensators, but no integral (I) or derivative (D) control is needed because the system is over-damped and responds effectively to proportional (P) control.

### ***Description of M3 Control***

After initialization, the program idles in a "While(1)" loop until either one of two conditions. The first priority is the UART/serial interrupt. Whenever LabVIEW writes data to the serial port, the M3 will halt operation and read these TARGET position values. The second priority is the timer interrupt which is used to trigger the I2C read sequence in order to determine the modules' position. An embedded function then averages 10 reads per axes of control to compute the CURRENT positions. An IPC event flag is finally triggered to send the TARGET and CURRENT positions to the C28 processor.

### ***Description of C28 Control***

After initializing, the CURRENT positions of the modules are set as the TARGET positions in order for the array to remain stationary until proper commands are sent from LabVIEW. The program will wait in a "While(1)" loop until the interrupt service routine (ISR) is triggered, which occurs at a rate of 20 Hz. The program will read the CURRENT and TARGET positions from the M3 and will then set the PWM channels based on the ERRORS. The system will only move when an enable flag is set by the user.<sup>129</sup>

### ***Control Algorithm***

$$\begin{aligned} \text{PWM Setpoint} &= K_p * |\text{TARGET} - \text{CURRENT}| \\ \text{if PWM Setpoint} > 9900 \text{ then } \text{PWM Setpoint} &= 9900 \\ \text{PWM Duty Cycle} &= \frac{\text{PWM Setpoint}}{10,000} \end{aligned}$$

Figure 108. Tracking servo PID control pseudocode.

A proportional gain (Kp) of 1200 was found to be effective for controlling the array. The steady-state error of  $\pm 2$  when multiplied by Kp=1200 leads to a PWM duty cycle of 24%, which is not enough overcome the starting torque of the 12 VDC motors. When a target position is just outside this limit, the resulting PWM duty cycle of 36% energizes the motors enough to start rotation. A high saturation limit is added to set the maximum duty cycle to 99%. Because the system is naturally over-damped, overshoot is not an issue.

---

<sup>129</sup> This feature is included in order to ensure a human operator is monitoring the system. Going forward, the control program will become more autonomous and require less user interaction.

#### **4.1.1.1.1 Ramp Control**

Ramp control was added to smooth system response from the steady-state error. Although approximately 99% of the position sensors reads are within  $\pm 2$  units of the true position, an error of 3 or greater can sometimes be observed. These values cause the array to over respond or briefly jump out of position. By incorporating a ramp control algorithm, the system takes multiple cycles to get to the intended PWM duty cycle as opposed to setting the PWM duty cycle instantaneously after the error calculation. This is referred to more specifically as 'ramp-up control' because it modifies the system response to takes a series of continuously increasing step to reach the intended duty cycle. Therefore, if an error of 3 or greater is encountered as a result of steady-state error, on the first cycle through the code the duty cycle will begin to be increased incrementally, but then on the next iteration when the steady-state error will most likely return to the  $\pm 2$  distribution region, the PWM duty cycle returns back to the idle state of ~0-24%.

```
if (CURRENT PWM Setpoint – PREVIOUS PWM Setpoint) ≥ 100
    then PWM Setpoint = PREVIOUS PWM Setpoint + 100
    else PWM Setpoint = CURRENT PWM Setpoint
```

Figure 109: Tracking servo PID control psuedocode.

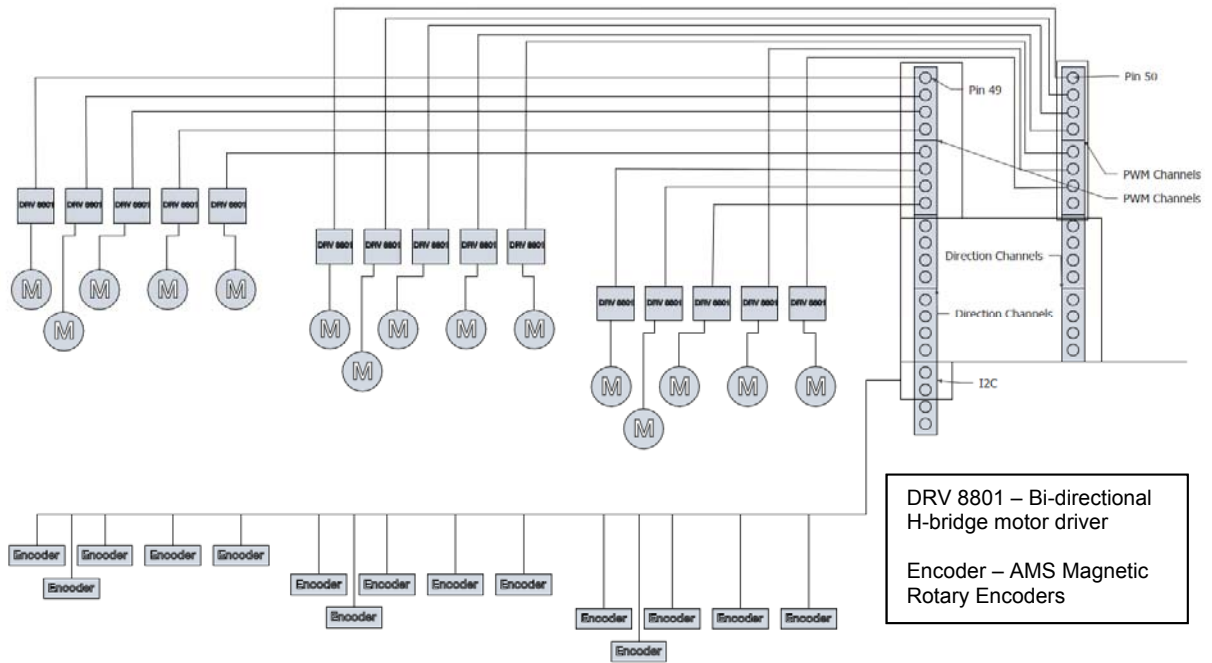


Figure 110: ICSF Control System One-Line Schematic.

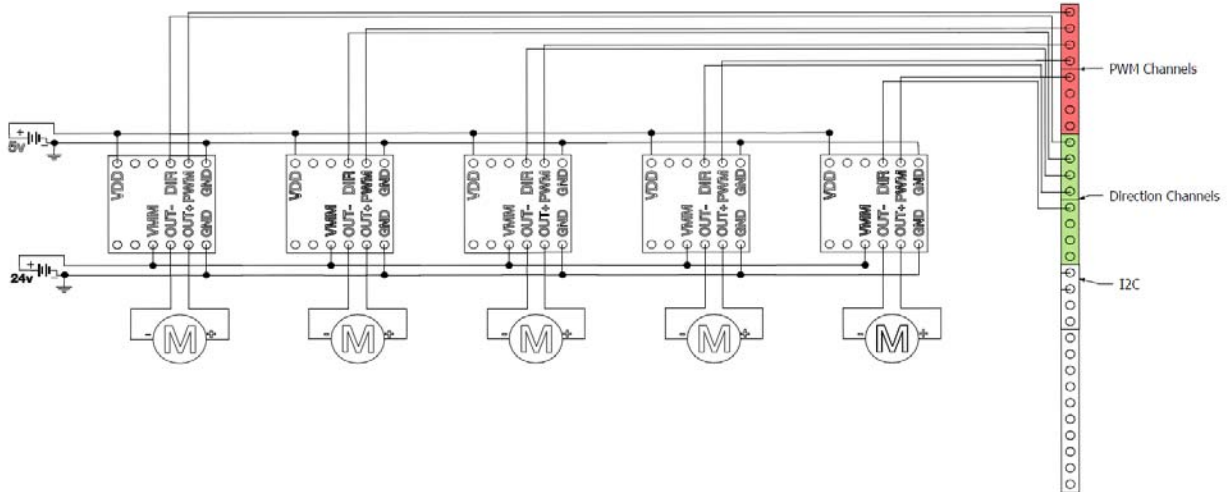


Figure 111: Circuit Diagram for Bi-Directional H-Bridge servo motor drivers.



Figure 112: Fabricated Motor Control Board to House Motor Drivers.

## B. ICSF Simulation Details

Table 37. Front panel of original ICSF simulation developed at CASE/Rensselaer (constructed in Microsoft Excel). (3 pages)

Simulation incorporates physical, thermal, electrical, and fluid characteristics to simulate energy output and interception of ICSF module. Current expanded simulation is an expansion of this original work, with revised optical characteristics.

<b>System Inputs</b>			
<b>USER INPUT VALUES</b>		<b>AM or PM</b>	
<b>Operating Conditions</b>			
Latitude	40.00 degrees	(latitude)	0
Time (minutes past midnight)	1440.00 minutes	(time)	
Day of year (Jan 1 = 1)	10	(day)	
Normal to building face - NS line angle (0 = south facing wall)	0.00 degrees	(gamma)	
Tilt angle of incident surface (90 = vertical, 0 = horizontal)	40 degrees	(intilt)	
Amount of light	100 percent	(light)	
Direct normal insolation	0 W/m <sup>2</sup>	(Gbeam)	
Diffuse horizontal insolation (=Gd)	0 W/m <sup>2</sup>	(Gdiffuse)	
Solar concentration	623 suns	(concentration)	
Light transmission through Fresnel lens	85 percent	(efflens)	
Light transmission into PV cell	95 percent	(effpv)	
Number of PV cells	1 units	(cells)	
Convective surface area of PV cell (smaller)	0.0001 m <sup>2</sup>	(areapv_v)	
Conductive surface area of PV cell (bigger)	0.000104 m <sup>2</sup>	(areapv_d)	
Decrease in PV cell efficiency with temperature	-0.76 %/C	(thermloss)	
Coolant mass flow rate	2 kg/s	(mdotf)	
Outside air velocity	0 m/s	(velo)	
Temperature of outside air	25 C	(Tout)	
Temperature of inside air	25 C	(Tin)	
Temperature of inlet water	25.0 C	(Tf)	
Image shape factor (square image = 1, circular image = 0.63)	1	(sf)	
Reflectivity of heat sink surface	0.5	(effhs)	
Diffuse light transmission through outer glass	96 percent	(effdiff_o)	
<b>Thermal Properties</b>			
Outside window thermal conductivity	0.3 W/mK	(kout)	
Inside window thermal conductivity	0.3 W/mK	(kin)	
PV cell thermal conductivity	148 W/mK	(kpvc)	
Heat sink thermal conductivity	237 W/mK	(khs)	
Epoxy thermal conductivity	8.2 W/mK	(ke)	
<b>Module Geometries</b>			
Outside window thickness	0.005 m	(thout)	
Inside window thickness	0.005 m	(thin)	
PV cell thickness	0.0001 m	(thpv)	
Heat sink side length	0.03 m	(lhs)	
Heat sink thickness	0.01 m	(thhs)	
Thickness of epoxy between PV cell and heat sink	0.0001 m	(the)	
Width of microchannels	0.001 m	(wmc)	
Depth of microchannels	0.002 m	(dmc)	
Distance between microchannels	0.001 m	(dmc)	
Length of microchannels	0.02 m	(lmc)	
<b>Panel Geometries</b>			
Vertical distance between units	0.24 m	(wlens)	
Horizontal distance between units	0.24 m	(hlens)	
Distance between wall and pivot point	0.10 m	(plens)	
Length of armature	0.15 m	(llens)	
Depth of window space	0.20 m	(slens)	
Percentage of window coverage	50 percent	(coverage)	
Brick (or alternate material) wall thickness	0.3 m	(thb)	
<b>INITIAL CALCULATIONS</b>			
<b>Operating Conditions</b>			
Light transmittance through outer glass	0.0 percent	(t_glass)	
Amount of light shaded by adjacent lenses	100.0 percent	(effshade)	
Efficiency of PV cell at 25 C at given concentration ratio	37.0 percent	(effelec)	

INTELLIGENT FACADES FOR HIGH PERFORMANCE GREEN BUILDINGS  
Property of Rensselaer Polytechnic Institute

<b>Thermal Properties</b>		
Water density	997.90 kg/m <sup>3</sup>	(rhof)
Water specific heat	4177.95 J/kgC	(shf)
Water absolute viscosity	8.72E-04 kg/ms	(muf)
Water thermal conductivity	0.61 W/mK	(kf)
Outside air thermal conductivity	0.026 W/mK	(ko)
Outside air density	1.18 kg/m <sup>3</sup>	(rhoo)
Outside air specific heat	1007.24 J/kgK	(sho)
Outside air absolute viscosity	1.83E-05 kg/ms	(muo)
Brick (or alt. material) thermal conductivity	2.30 W/mK	(kb)
Brick absorbtivity	0.63	(alphab)
Inside air thermal conductivity	0.026 W/mK	(ki)
Inside air density	1.18 kg/m <sup>3</sup>	(rhoi)
Inside air specific heat	1007.24 J/kgK	(shi)
Inside air absolute viscosity	1.83E-05 kg/ms	(mui)
Window air thermal conductivity	0.026 W/mK	(ka)
Window air density	1.18 kg/m <sup>3</sup>	(rhoa)
Window air specific heat	1007.24 J/kgK	(sha)
Window air absolute viscosity	1.83E-05 kg/ms	(mua)
<b>System Geometries</b>		
PV - heat sink assembly CONVECTIVE surface area	0.0021 m <sup>2</sup>	(areahs_v)
Heat sink CONDUCTIVE surface area (PV cell not included)	0.000904 m <sup>2</sup>	(areahs_d)
% PV - heat sink assembly convective surface that is PV	4.76% percent	(Cpv)
Area of windows per module	0.03 m <sup>2</sup>	(areawin)
Number of microchannels	14	(numc)
Surface area of microchannels	1.40E-03 m <sup>2</sup>	(areamc)
Area per module	0.0576 m <sup>2</sup>	(aream)
Corrected building angle	50 degrees	(beta_c)
Total area	0.0576 m <sup>2</sup>	(areat)
Lens area	0.65804375 ft <sup>2</sup>	
electric	0	
thermal	1.06176E-07	
<b>Major Calculations</b>		
Aspect ratio	2	(Arhx)
Fully developed Nusselt number in rectangular channel	3.41125	(Nu)
Friction aspect ratio	15.661375	(fRe)
Hydraulic diameter of microchannel	0.002 m	(hymc)
Microchannel Reynolds number	131089.85	(Re)
Heat transfer coefficient of outside air	15.0 W/m <sup>2</sup> C	(hout)
Heat transfer coefficient of inside air	15.0 W/m <sup>2</sup> C	(hin)
Heat transfer coefficient of window air	15.0 W/m <sup>2</sup> C	(ha)
Heat transfer coefficient of coolant	1295.8 W/m <sup>2</sup> C	(hf)
<b>Energy Flow Resistances</b>		
Outside air - module convection resistance	1.157 K/W	(Rconv_o)
Outside window R-value	0.350 Km <sup>2</sup> /W	(Rgo)
Inside air - module convection resistance	1.157 K/W	(Rconv_i)
Inside window R-value	0.350 Km <sup>2</sup> /W	(Rgi)
Brick (or alt. wall material) R-value	0.130 Km <sup>2</sup> /W	(Rb)
Wall insulation R-value	2.600 Km <sup>2</sup> /W	(Rinsul)
Window air - module convection resistance	1.157 K/W	(Rconv_a)
Window air - heat sink convection resistance (approx)	31.746 K/W	(Rconv_hs)
Window air - PV cell convection resistance	666.667 K/W	(Rconv_pv)
PV cell conduction resistance	0.006 K/W	(Rcond_pv)
PV-heat sink interface resistance	0.001 K/W	(Rinterface)
Heat sink conduction resistance	0.047 K/W	(Rcond_hs)
Coolant convection resistance	0.551 K/W	(Rconv_f)
U-value of brick and insulation	0.011 W/K	(Uw)
U-value of inside glass	0.082 W/K	(Ug)
Interior wall conduction resistance	10.772 K/W	(Rcond_i)
<b>Total Resistances</b>		
Between window air and outside	8.391 K/W	(R_1)
Between window air and inside	13.087 K/W	(R_2)
Between PV - heat sink assembly and fluid	0.599 K/W	(R_3)
Between PV - heat sink assembly and air	31.746 K/W	(R_4)

INTELLIGENT FACADES FOR HIGH PERFORMANCE GREEN BUILDINGS  
Property of Rensselaer Polytechnic Institute

<b>Heat Exchanger/Coolant Calculations</b>				
Minimum heat capacity rate for heat exchanger	8355.893	W/K	(Cmin)	
Number of Transfer Units	0.000		(NTU)	
Effectiveness of heat exchanger	0.000		(effex)	
Friction factor in microchannels	0.000		(f)	
Fluid velocity in microchannels	71.579	m/s	(velmc)	
Pressure drop across microchannels	3817.7	N/m <sup>2</sup>	(deltaP)	
<b>Energy Flows</b>				
Diffuse solar power into system	0.0	W	(Qdiff)	
Direct insolation reflected	0.0	W/m <sup>2</sup>	(Greflected)	
Direct solar power captured by each lens (with shading)	0.0	W	(Qdirect)	
Direct solar power not captured by each lens (with shading)	0.0	W	(Qheat)	
Energy convection to exterior of building	0.0	W	(Qconvo)	
Energy convection to interior of building	0.0	W	(Qconv)	
Energy transmitted through lens	0.0	W	(Qlens)	
Energy reflected off PV - heat sink assembly	0.0	W	(Qreflected)	
Energy convected off PV - heat sink assembly by air	0.0	W	(Qloss)	
Energy incident on brick	0.0	W	(Qbrick)	
Energy absorbed by brick	0.0	W	(Qabsorb)	
Energy convected off brick to interior	0.0	W	(Qbin)	
Energy convected off brick to window space	0.0	W	(Qbout)	
Energy transmitted through interior glass	0.0	W	(Qgain)	
<b>Thermal Results</b>				
Temperature of PV cell	25.0	C	(Tcell)	
Temperature of air in window	25.0	C	(Tair)	
Temperature of brick wall	25.0	C	(Tb)	
Temperature of outlet water	25.0	C	(T_2)	
PV efficiency after temperature correction	37.0	percent	(efftherm)	
Energy convection to fluid	0.0	W	(Qfluid)	
Electric power output from PV	0.0	W	(P)	
Required pumping power	7.65E+00	W	(pump)	
Heat gain to building	0.0	kW/100 m <sup>2</sup>	(gain)	
<b>Solver Constraints</b>				
Control Volume 1 (complete system - one module)	-1.0E-06		(CVone)	
Control Volume 2 (PV - heat sink assembly)	0.0E+00		(CVtwo)	
Control Volume 3 (brick wall)	-1.5E-15		(CVthree)	
Must Equal	0.0			
Projected PV cell temperature	25.0		Tcellp	
<b>Direct Insolation transmitted</b>				
Direct Insolation transmitted	0.0	W	Qdir	
<b>Losses</b>				
<b>Reflection Losses</b>				
Declination	-22.09	degrees	(declination)	
Hour angle of the sun	540.00	degrees	(hour)	<b>Corrected</b>
Solar Altitude	-72.09	degrees	(alpha_s_)	## (alpha_c) <-- Building tilt angle
Solar Azimuth	171.89	degrees	(gamma_s_)	## (gamma_c)
Angle of incidence between sun's rays and outer face of façade	122.09	degrees	(theta)	
<b>Shading Losses</b>				
Length of lens	0.25	m	(dlens)	
Maximum angle	81.07	degrees	(alens)	
Vertical shadow length across lens	0.38	m		
Horizontal shadow length across lens	0.33	m		
Shadow on lens from above	0.0623	m <sup>2</sup>	(vshadow)	
Shadow on lens from side	0.0000	m <sup>2</sup>	(hshadow)	
<b>Overall System Efficiency</b>				
Total incoming sun power	0.0	W	(intotal)	
Total electrical power produced	0.0	W	(electtotal)	
Total thermal energy captured	0.0	W	(thermtotal)	
Total system efficiency	#DIV/0!	percent	(eff)	
<b>Perfect Insolation Calculation</b>				
omega	180		(omega)	
Cos(theta)	-0.95	-54.518		
Gbeam* (input from climate)	1000			
New Gbeam	0			

### C. ICSF Module Heat Sink Specifications

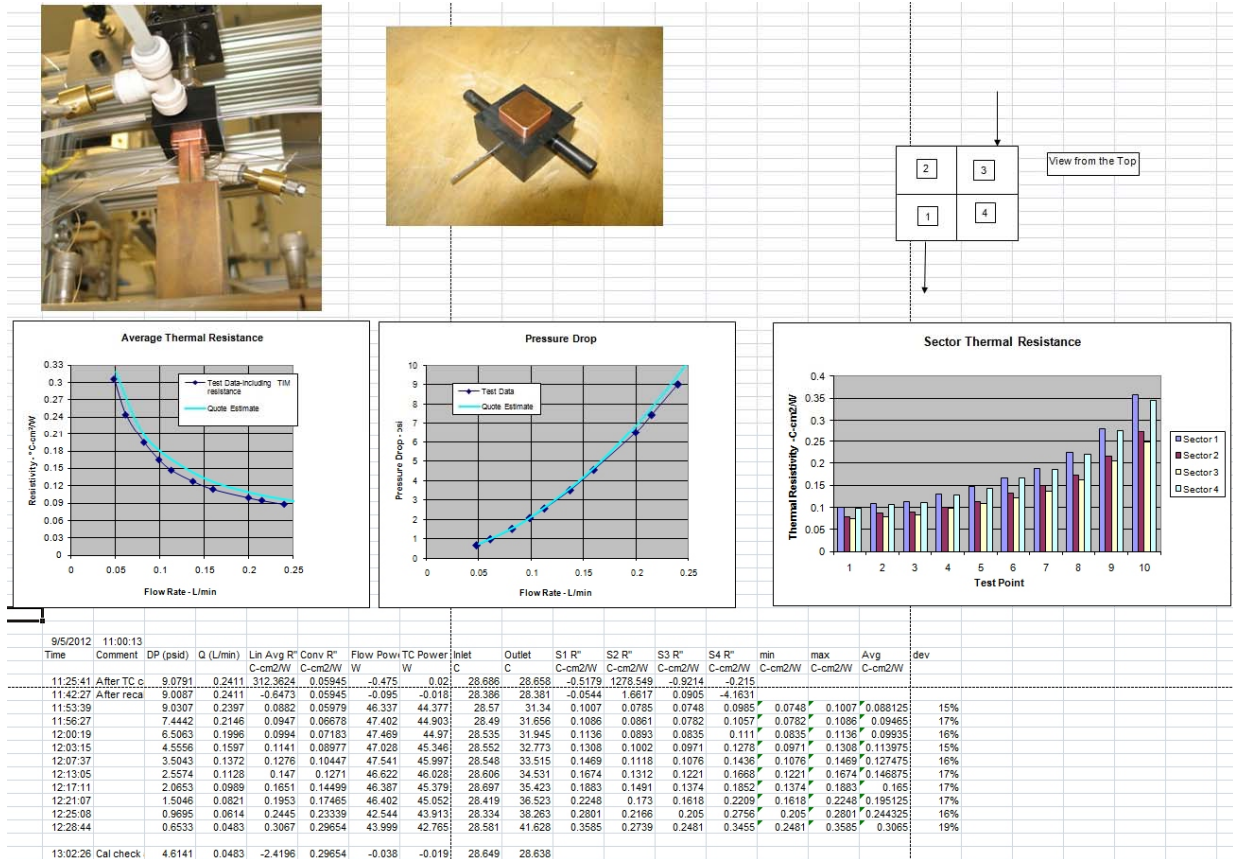


Figure 113. Datasheet provided by Mikros, characterizing heat sink in Generation 8 module.

## D. Electrical Distribution Efficiency Characterization

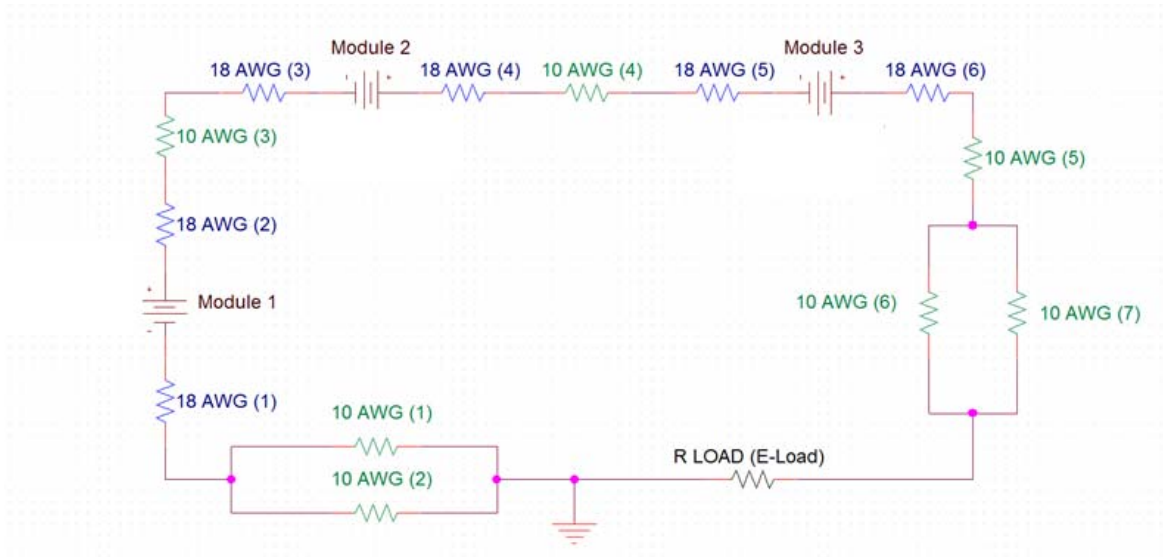


Figure 114. Circuit Diagram for Electrical Transmission Efficiency Calculation. Voltage drop was measured and calculated for 3 modules connected in series.

### CALCULATED VOLTAGE DROP

#### Resistance Properties (Ohms/kft)

Ni-Cu 18 AWG 6.770  
Cu 10 AWG 0.999

#### CURRENT (amps)

3.29 CLOSED

#	Wire Description	Material	Gauge	Length (ft)	Resistance (Ω)	Vdrop = I*R	%
1	10 AWG (1)	Copper	10	17.02	0.017	0.028	30%
2	10 AWG (2)	Copper	10	17.02	0.017	(above in parallel)	
3	18 AWG (1)	Ni -Cu	18	0.21	0.001	0.005	5%
4	18 AWG (2)	Ni -Cu	18	0.25	0.002	0.006	6%
5	10 AWG (3)	Copper	10	1.04	0.001	0.003	4%
6	18 AWG (3)	Ni -Cu	18	0.21	0.001	0.005	5%
7	18 AWG (4)	Ni -Cu	18	0.19	0.001	0.004	5%
8	10 AWG (4)	Copper	10	1.02	0.001	0.003	4%
9	18 AWG (5)	Ni -Cu	18	0.21	0.001	0.005	5%
10	18 AWG (6)	Ni -Cu	18	0.13	0.001	0.003	3%
11	10 AWG (5)	Copper	10	1.06	0.001	0.003	4%
12	10 AWG (6)	Copper	10	16.56	0.017	0.027	30%
13	10 AWG (7)	Copper	10	16.56	0.017	(above in parallel)	

<b>TOTAL Vdrop (Volts)</b>	<b>0.09</b>	<b>100%</b>
----------------------------	-------------	-------------

$$V_{Total} = (\# \text{ of Modules}) * V_{mp}$$

$$\eta_{elec.} = \frac{V_{Total} - V_{Drop}}{V_{Total}}$$

$$\eta_{elec.} = 1 - \frac{V_{Drop}}{V_{Total}}$$

\*Vmp = 2.65V  
\* # of Modules = 3

<b>η elec. - OPEN</b>	<b>98.8%</b>
-----------------------	--------------

Figure 115. Calculated Voltage Drop for 3 Modules in Series.

## **E. Electrical Power Pricing**

Estimations were done for the monetary savings provided by integrating BISCf into a 5000m<sup>2</sup> office building for three locations and their local tariff schedules. The three examined locations were New York City, Mountain View, and Phoenix. The utilized tariff schedules were selected for their appropriateness for the building type and hour-independent pricing structure.

The cost of the electrical power consumed in a building has three main factors: service fees, tariffs based on the energy, and tariffs based on maximum power demand. This analysis considered only the energy and demand tariffs, since inclusion of BISCf would not affect a building's service fees.

Surplus electrical power generated from BISCf was assumed to be sold back to the utility at a 1:1 rate. Although net-metering policies in the United States are not currently universal in buying back electricity, in other countries electricity is bought back at higher prices than centrally-produced power.

Data at an ideal resolution would contain hourly building power consumption and ICSF power production data for an entire year. This analysis involved a limited dataset, necessitating an assumption for summer vs. winter pricing. The fraction of the year's energy consumption used during summer and winter rate periods (priced differently) was apportioned according to building heating and cooling loads, for which monthly data was available. In Phoenix 73% of the cooling loads occurred in the during the summer rate period (May-October), compared to 59% for Mountain View.

In analysis of the moments of peak electrical consumption for a 5000m<sup>2</sup> office building in the three studied climates, the power benefits provided from ICSF typically push the building into net-generating territory. Assuming that a peak-period demand of 0kW would be unreasonable to the utility providers, and in absence of hourly data, the peak power demands of the buildings using ICSF systems were assumed to be 20% of the baseline peak monthly power demands.

Table 38. Electricity Service Costs (simulated), baseline building vs. building with ICSF strategies.

	Baseline Costs			Costs with BICSF Strategies			Savings
	Energy	Demand	Total	Energy	Demand	Total	
Mountain View, CA	\$68,841	\$18,446	\$87,287	\$1,922	\$3,689	\$5,612	94%
New York City, NY	\$123,195	\$47,543	\$170,738	\$105,469	\$9,509	\$114,978	33%
Phoenix, AZ	\$82,239	\$19,343	\$101,583	-\$1,145	\$5,141	\$3,996	96%

## F. BICSF Façade Retrofit Analysis

### ***Proposed Retrofit Façade Assembly and Installation***

The design of a retrofit building integrated dynamic curtain wall strategy should learn from the failures of curtain walls in the past. The design should be take into account material choices, so as to mate materials that react similarly to thermal deviation. The design should not rely on a single line of defense to prevent thermal and air infiltration, and should account for multiple paths of redundancy. The design should be highly resistant to degradation, and in the case of inevitable failure, easy to replace failed components. The design should allow for future integrations, for the ability to plug into new technologies without costly facade system overhauls or redesigns.

### ***Assembly Process***

The facade panel has to be of a box window assembly as to appropriately house the ICSF system and all of its performance specific requirements, including control of particulate matter, a thermally monitored cavity, and an ultra-transparent outer lite. The box window structural frame can be completely constructed of lightweight aluminum, as the entire ICSF system only weighs a total of 300 pounds. The heaviest piece will be the outer lite of glazing which is cantilevered off at a varying distance from the structural connection to the building. The all-aluminum cage built around the perimeter of the box window will be constructed to structurally bring the load of the outer lite of glazing back where it can be distributed and transported in multiple locations to the slab. The manufacture and assembly of the entire box window enclosure will be fully completed

within a factory assembly line, minimizing the requirement for field work. It is desirable to prefabricate the entire box window assembly similar to the process of manufacturing a unitized curtain wall. Complete assemblies, with inner and outer glass leaves installed, can be lifted into place in one step. The units will be self-contained box windows with air intake and exhaust ports for cavity ventilation and to minimize the accumulation of particulate within the cavity.

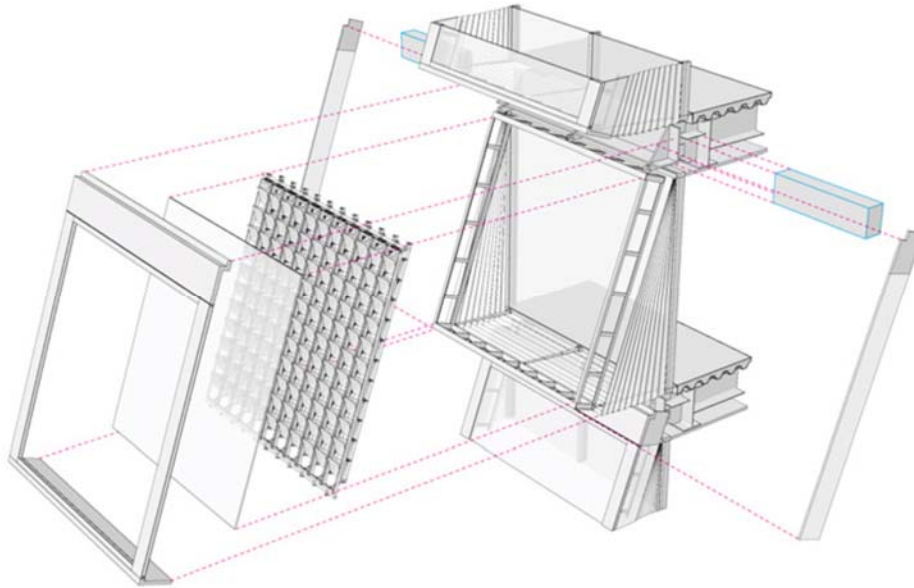


Figure 116: Facade Retrofit Exploded Component Axonometric (ICSF installation at 15 tilt)

### ***Installation Process***

The first and second generation of installed curtain walls (built between 1950 and 1980), of which will make up the majority of retrofits, contain glazed spandrel panels that conceal the structural connection of the facade to the slab. The old spandrel panel will be discarded in the retrofit process to allow access to the structural tiebacks. The new double skin box window supplies a new head spandrel which contains enough room for the installation of required climate specific systems for thermal and electric connection to building systems, as well as localized conversion units such as mini-absorption chillers. The head unit also houses the structural connection of the entire facade panel, meaning that the entire box window is "hung" from the top slab. If the existing structure allows, the head unit of the new double skin box window will attach

directly to specially designed dead load anchors which provide three axis of tolerance and can be adjusted to allow the new box window to fit exactly to the pre-existing opening. The old curtain wall glazing and framing will be recycled if possible along with all associated seals, gaskets, and insulation.

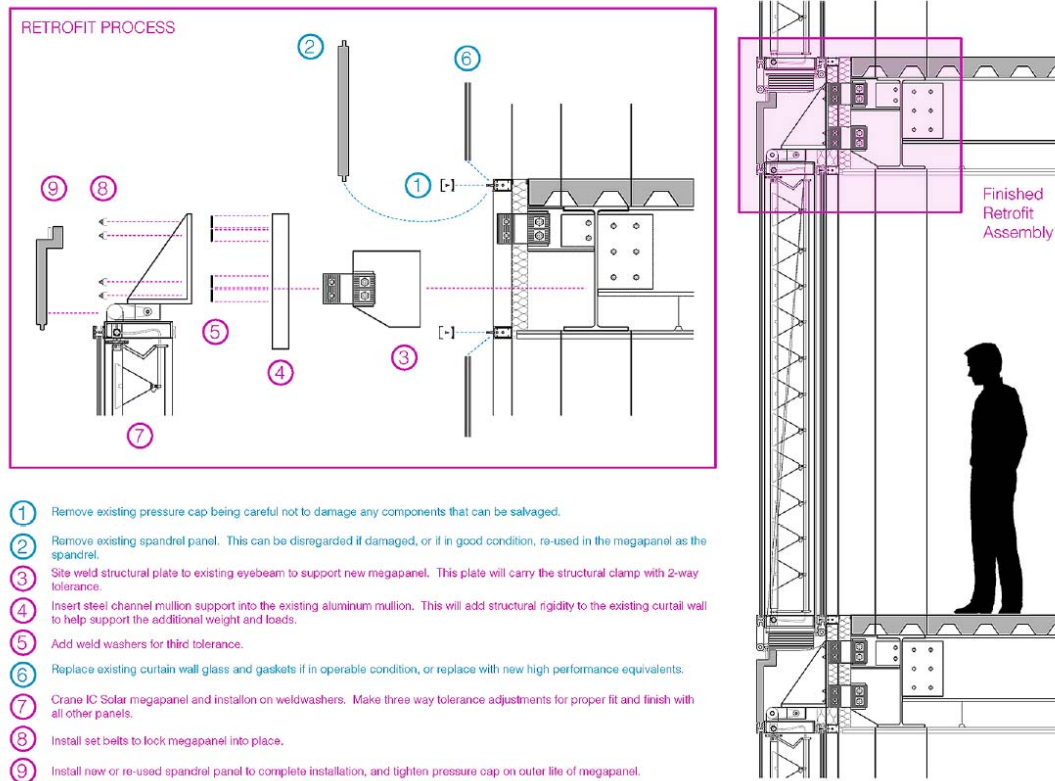


Figure 117: Installation of ICSF Mega-panels onto Existing Curtain Wall Conditions (Vertical Orientation)

### ***Curtain Wall Retrofit Case Study***

A 200,000 square foot office tower outside of Mayport, Florida required its twenty year old façade replaced after the silicone seals failed and began allowing air and water infiltration. At the same time, its large air conditioning system needed renovation to renew the moving parts and replace the ozone depleting CFC refrigerant. Analysis performed by a subcontracting firm revealed that converting the renovation to a whole system approach could dramatically improve comfort, quadruple energy efficiency, and cost about the same as normal renovations. According to the analysis, more energy efficient glazing, deep daylighting, and efficient lights could reduce the cooling load by

85%. The reduction in cooling loads would make the replacement cooling equipment three-fourths smaller than the original system, four times as efficient, and \$200,000 cheaper, a sum large enough to pay for the other improvements<sup>130</sup>. The annual energy bill would then fall by 75%, or by \$1.10 per square foot per year, at least ten times the competitive rent difference in the local market. The fourfold energy efficiency improvement would cost approximately the same as the curtain wall renovation with far better amenity, aesthetics, and resale.

### ***Problem with Current Retrofit Strategies***

The Florida case study represents the link between interior and exterior performance, and how the upgrading of the façade allows for the possibility of more efficient internal thermal comfort systems. The logic makes sense as a combined strategy, using energy savings over existing HVAC system to payback the cost of the retrofit of the curtain wall, however, where the new HVAC system pays for itself in energy savings, the curtain wall begins to degrade as soon as it is installed. Based on the material failures and assemblies predicated on material performance, the dependence on existing curtain wall technology is a losing thermal battle. The payback periods of simply a retrofit curtain wall will likely never fully payback on investment, and the cost saving by coupling it with modified HVAC systems will eventually decrease as the retrofit façade begins to leak thermal energy again, as the previous failed curtain wall did before.

A potential solution to the immediate depreciation of repeated curtain wall retrofit, as many architects and engineers have discovered, is the incorporation of energy collection devices and products into the façade, adding a level of multi-functionality to the curtain wall and incorporating the supplemental cost benefit of energy production as a deciding factor in retrofit.

---

<sup>130</sup> Davies, Russell, Simpson Gumpertz Heder Interview, 2008.

## G. ICSF Test Bed: Sheikh Khalifa Medical City, Abu Dhabi, UAE

### *Project Description*

#### Sheikh Khalifa Medical City (SKMC)

Total Area: 266,369 m<sup>2</sup>

Location: Abu Dhabi, UAE

Latitude: 24.4705104827881 North

Longitude: 54.3663597106934 East

Project North: 50.154 West of True North

Program: Multi-functional medical facility campus with retail, office, patient rooms, surgical suites, and medical support spaces.

#### General Hospital Lobby

Location: Part Plan 11; (21-26,E'-H")

Total Area: 861.29 m<sup>2</sup>

Occupied Area: 628.49 m<sup>2</sup>

ICSF Area: 647.24 m<sup>2</sup>; 144 Cartridges; 5,184 modules

Program: Main campus lobby, waiting area, reception



Figure 118. SKMC Hospital City



Figure 119: SKMC Hospital Entrance



Figure 120. SKMC General Hospital Lobby with transparent ICSF roof modules that bathe the interior space with cool diffuse daylight and allow for a clear view to the sky while removing solar heat gain and glare from the space.

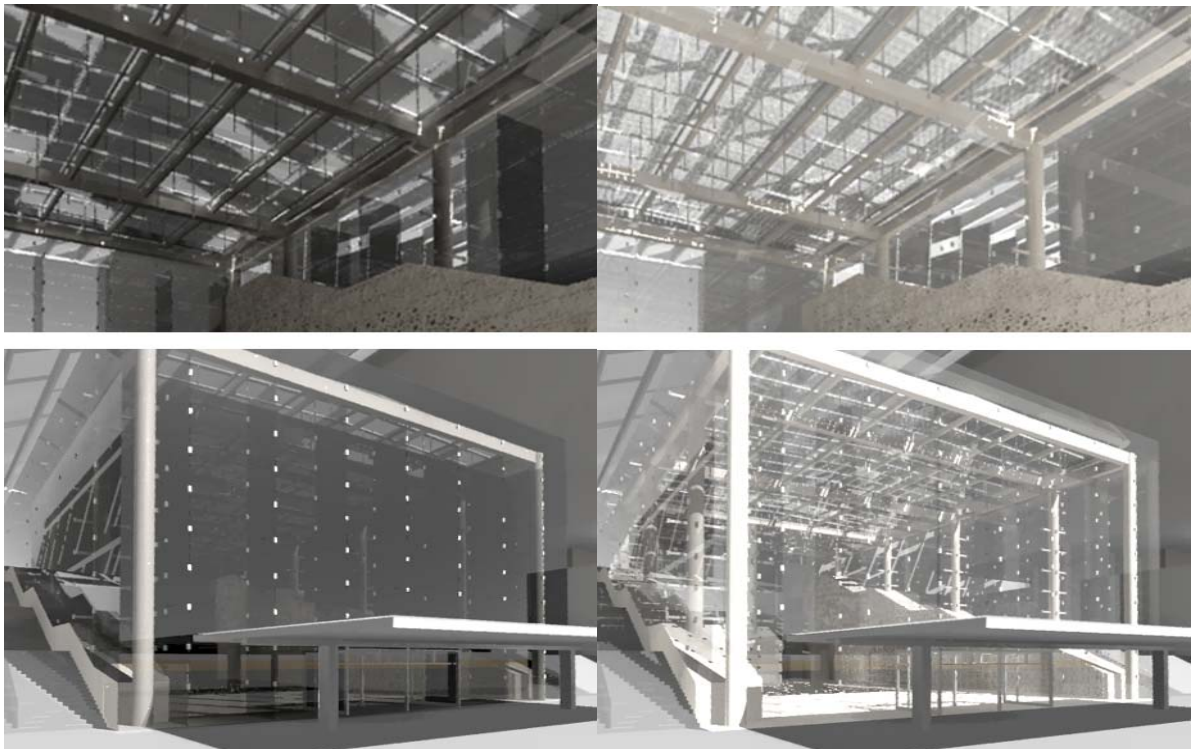


Figure 121. General Hospital Lobby, with and without active façade intervention. opaque roller blinds & tinted glass impede views while allowing heat to permeate occupied space. (left) Lobby with clear glass & ICSF that absorbs the heat and glare with clear modules allowing for access to views and daylight. (right)

### ***Design Problem***

Due to the intensity of the sun and severe temperatures, the harsh climate of Abu Dhabi places extreme demands on glazed building envelopes to control solar heat gain while providing visible clarity. The General Hospital Lobby, the main entrance to the Sheikh Khalifa Medical City, is intended to be an open, transparent, transitional space with an inviting visual lightness and views to the exterior, but is anticipated to have problems controlling glare for visual comfort and controlling solar heat gain for cooling load reduction. Conventional responses, which include retractable roller blinds or heavily tinted glazing, are used to reduce glare or heat gain, but do so at the cost of visible clarity. The application of shading devices or tinted glazing would result in a façade that limits views from the interior or appears dark and opaque from the exterior, contradicting the intent for the main entrance and first impression to be a bright, inviting transition into the hospital city.

Implementation of ICSF into the glazed roof of the General Hospital Lobby is anticipated to improve visual comfort by reducing glare and reduce the cooling loads by reducing the solar heat gain, while renewably generating electricity to be fed into the hospital city grid. The multi-function benefits of ICSF are anticipated to reduce glare by 28-51%, reduce the cooling power demand in the space by 10-41% and generate 35-61 MWh per year of electricity, while preserving a highly transparent and visually open design for the reception of hospital visitors.

### ***Modeling Enhancements of Visual Comfort through Glare Reduction, Clarity of Daylight and Views to the Exterior***

The current all-glass design of the lobby is anticipated to have a substantial impact on visual comfort due to the high solar resource climate, high transmission glazing, and light colored, moderately reflective interior finishes, with the potential for negative impacts on discomfort and disability glare in particular. A daylighting modeling tool was developed and seven simulation models were run to evaluate the effectiveness of ICSF against, and in combination with, other typical countermeasures for reducing glare including roller blinds and lower transmission glazing. Given the all-glass design of the

lobby, the occurrence of glare is highly dependent on three factors which are independent of individual glare mitigation countermeasures: 1) the high solar resource climate with high atmospheric radiative forcing, 2) the reflectance of interior finish materials, and 3) differing glare mitigation treatments between roof and wall surfaces. Additionally, glare in the context of a lobby program requires modification of the glare metric in order to account for a higher glare tolerance based on ambulatory freedom and an adherence to the original transparent, visually open design. Eliminating glare for a 100% window-to-wall ratio construction in the Abu Dhabi climate is untenable without disruptive design changes.

### ***Daylighting and Visual Clarity Model - Approach***

The Daylight Glare Probability metric (DGP) is an empirical approach to predicting the probability that an occupant will experience discomfort glare, and is based on vertical eye illuminance ( $E_v$ ), glare source luminance ( $L$ ), the glare source solid angle ( $\omega$ ), and the glare source Guth position index ( $P$ ). The DGP metric shows a strong correlation with human subjects' response regarding glare perception (Wienold, 2012). The DGP metric substantially outperforms other glare prediction metrics under daylit architectural scenes such as the Daylight Glare Index (DGI), the CIE Glare Index (CGI), Visual Comfort Probability index (VCP), and the CIE Unified Glare Rating (UGR), which were developed primarily for the lighting and auto industries and therefore focus on electric sources of light. The equation for calculating DGP is shown below with DGP < 0.35 corresponding to *Imperceptible Glare*, 0.35 < DGP < 0.4 corresponding to *Perceptible Glare*, 0.4 < DGP < 0.45 corresponding to *Disturbing Glare*, and 0.45 < DGP corresponding to *Intolerable Glare*:

$$DGP = 5.87 * 10^{-5} * E_v + 9.18 * 10^{-2} * \log\left(1 + \sum_i \frac{L_{s,i}^2 * \omega_{s,i}}{E_v^{1.87} * P_i^2}\right) + 0.16$$

Equation 54. Daylight Glare Probability

## Daylighting and Visual Clarity Model - Results

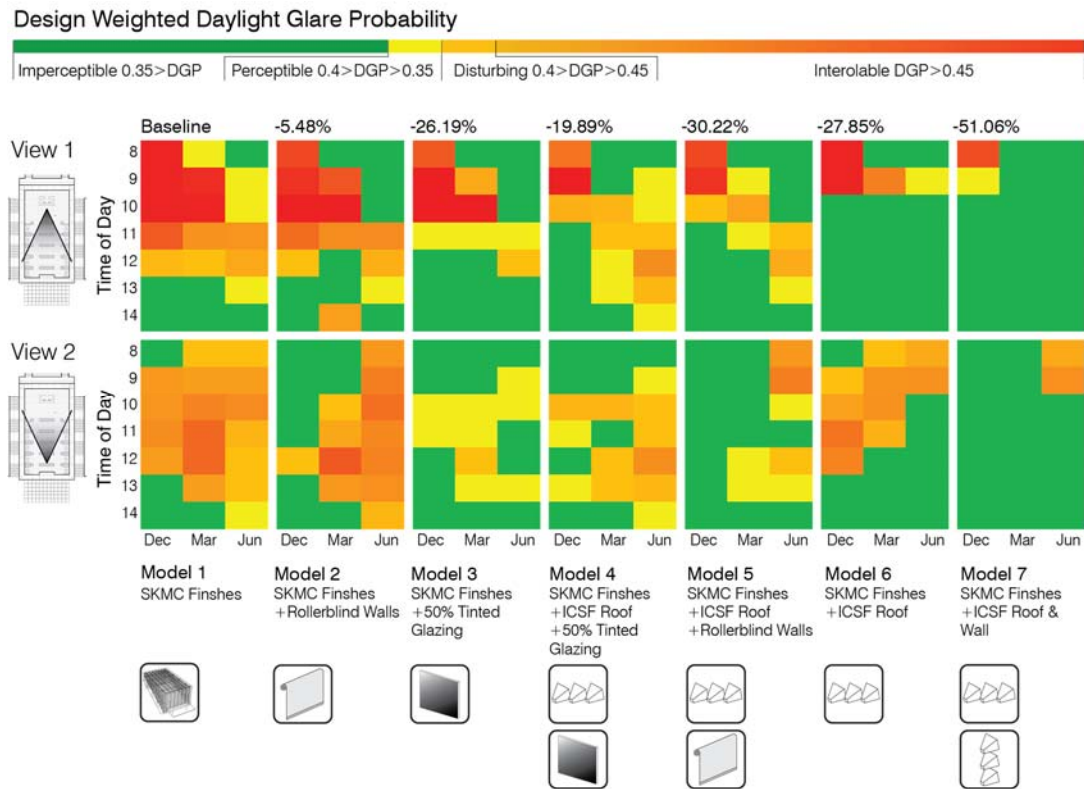


Figure 122. Design Weighted Daylight Glare Probability Matrix showing the progressive reduction in glare resulting from the integration of ICSF in the SKMC lobby.

The 7 simulation models are summarized for two station points exiting (View 1) and entering (View 2) the lobby along with percent reduction in design weighted glare totals. ICSF on the roof (Model 6) and on the roof and entrance wall (Model 7) show the greatest improvements in visual comfort while maintaining the transparent design.

Seven simulation models were run to evaluate the effectiveness of ICSF against, and in combination with, other typical countermeasures for reducing glare in the lobby space including roller blinds and lower transmission glazing. Substantially tinted glazing (Model 3), on the order of 50% transmission, is found to reduce a design weighted glare probability by 26.19% when compared to the baseline (Model 1), yet interferes with the openness of the space, reducing the quality of receiving visitors, particularly when viewed from outside during daylight hours when the glass will appear opaque black (see Figure 121). ICSF roof installation with 73% transmission glazing (as specified, Model 6) reduces the design weighted glare probability of the space by 27.85% while maintaining

views into and out of the space, and preserving the highly transparent design. The modest improvement in glare in Model 6 is due to the relative imbalance between the ICSF ceiling and unmitigated wall luminance, inducing glare through high adjacent contrast. Adding ICSF to the south-east facing entry wall in combination with the ICSF roof installation (Model 7) reduces adjacent contrast and results in a design weighted glare probability reduction of 51.06%.

### ***Building Test Beds: CASE and SOM Calibration***

One of CASE's foundational philosophies is to bridge the gap between academia and professional practice through shared work spaces in order to foster the cross-pollination of ideas. By combining multi-institutional and professional office research and development resources, the boundaries of environmental performance in urban building systems on a global scale are being tested with actual building projects as test beds. This unique opportunity, special to only a handful of centers in the world situates CASE at the forefront of next generation building technologies research. Other research projects in developments at CASE outside of the Dynamic Façade area of inquiry also have future test beds in many of SOMs architectural projects.

Future work being proposed for ICSF including post-occupancies assessments would be far more thorough and justifiable at the building test scale as oppose to continued analysis in a lab setting. Many of the daylighting benefits discussed, while having associated metrics, for the most part have been qualitative arguments. Occupant surveys and interviews would provide valuable feedback to the experience of habitants next to ICSF, and finally *shed light* in a quantitative manner (e.g. increased worker productive) on the improved spatial qualities of natural daylight that ICSF is able to offer to the built environment.

## 5. Publications and Patents

### 5.1 Publications and Patents

#### ***Relevant Publications that were partially supported by this award***

##### ***Published***

Aly Etman, M., Novelli, N., Schultz, J., Phillips, K., Andow, B. and Dyson, A. (2015).

Daylighting Effect of Separating Direct and Diffuse Insolation with Facade-Integrated, Transparent Solar Collector. In: PLEA.

Dyson, A., Phillips, K., Shultz, J., Vollen, J., Gindlesparger, M. and Novelli, N. (2014).

High Efficiency Solar Building Envelopes for Integrated Delivery of Environmental Control Systems. In: OSA, p. AF2P.4. Available at:  
[http://www.opticsinfobase.org/abstract.cfm?URI=CLEO\\_AT-2014-AF2P.4](http://www.opticsinfobase.org/abstract.cfm?URI=CLEO_AT-2014-AF2P.4)

Novelli, N., Shultz, J. and Dyson, A. (2015). Development of a Modeling Strategy for Adaptive Multifunctional Solar Energy Building Envelope Systems. SimAUD.

##### ***Upcoming / Pending Publications***

Novelli, N., Phillips, K., Shultz, J., Derby, M., Stark, P., Jensen, M. Craft, J. and Dyson, A (2016). Experimental Investigation of a Building Envelope-Integrated, Transparent Concentrating Photovoltaic and Thermal Collector (UPCOMING). *Solar Energy*

Novelli, N., Phillips, K., Shultz, J., Derby, M., Stark, P., Jensen, M. Craft, J. and Dyson, A (2016). Full-Scale Modeling of a Building Envelope-Integrated, Transparent, Concentrating Photovoltaic and Thermal Collector (UPCOMING). *Energy and Buildings*

Novelli, N., Phillips, K., Shultz, J., Aly, M., Vollen, J. and Dyson, A. (2016). Towards energy-positive buildings through a quality-matched energy flow strategy (UPCOMING). *Applied Energy*.

Shultz., J., Zaide, D., Novelli, N., Phillips, K., Dyson, A., and Oberai, A. (2016) A Method for Modeling Building Integrated Energy Capture Technology (UPCOMING). *Energy*

***List of Relevant Patents that were developed during the grant award period***

***United States Provisional Patent: 62/351,596***

Title: A unitized modular building system that captures, transforms, stores, and redistributes ambient energy resources in order to supply required energy quantity and quality in real-time for NetZero energy buildings.

Inventors: Anna H. Dyson, Nicholas E. Novelli, Jason O. Vollen, Peter R.H. Stark, Michael K. Jensen.

iEdison record: 6910301-14-0005

## 6. Computer Modeling Descriptions

### 6.1 Computer Modeling Description

Most of the modeling efforts highlighted in this document were completed in Visual Basis in order for simulation results to be more accessible for visualizing findings in Microsoft Excel. These results could also then be used in conjunction with building energy modeling results through a post-processing work flow in order to determine the effects of incorporating a building with the ICSF technology. This modeling workflow is referred to in the document as the ***HelioOptix Simulation Engine***.

Later modeling efforts realize that while the previous mentioned methods is able to give adequate feedback on the potential energy generation for the ICSF system, its approach is limited in its ability to interface with building energy models. A more comprehensive and accessible approach leverages emerging techniques in multi-physics modeling known as co-simulation. Using co-simulation, building energy models can trade information with sub models - such as models of ICSF – that are solved independently with coupling through discrete domains. A simulation environment, Modelica, which has purported extensibility and ease of co-simulation through the functional mock-up (FMI) standard was used to develop a modeling strategy for Adaptive Multifunctional Solar Energy Building Envelopes Systems, such as the ICSF system. This model is referred to as the ***Modelica Model***. The Modelica modeling efforts are extensible covered in the attached publications.

## 6.2 HelioOptix Simulation Engine Model Description. (2012)

### 6.2.1.1 Simulate ICSF Performance

In order to extrapolate the known operative characteristics of ICSF into a larger context, a model of the collection system has been constructed. We use the simulation engine, written by Peter Stark and Steve London at HeliOptix and based on an earlier model developed at CASE, and append updated hydronic distribution characteristics which account for thermal losses in the balance of the cooling network.

### ***Stark/HeliOptix Simulation Engine***

The simulation engine developed by Peter Stark and HeliOptix is used to predict performance for ICSF in a matrix of situations. The engine is a consolidated update of an earlier model developed at CASE, the details of which can also be found in the Appendix.

Table 39. HeliOptix simulation engine input and output variables.

The engine is a consolidation version of an earlier model developed at CASE.

<i>HeliOptix Simulation Engine</i>	
<i>Inputs</i>	<i>Outputs</i>
Climate Data (TMY2 or TMY3 in .epw format)	DNI (from climate data)
Fresnel Lens Width	Array Coolant Output Temperature
CPV Cell Width	Electrical Power Output (W, hourly)
F#	Thermal Power Output (W, hourly)
Fresnel Lens Material	
Vertical Module Spacing	
Horizontal Module Spacing	
Window Area	
Modules per Stack (Modules in Thermal Series)	
Number of Stacks (calculated automatically)	
Front Glass Pane Refraction Index	

### 6.2.1.2 Glazing Attenuation

As the sun impinges on the outer glass surface of a building, a fraction of the radiation is reflected from the surface, according to the angle of incidence between the surface

normal and the solar rays. This effect must be accounted for in a consideration of the amount of energy expected to pass through ICSF. Although the effect results in lowered input to the solar modules, here it is modeled as an affected output, a function of the incident angle between the surface normal of the outer glazing and the solar rays. This attenuation due to exterior glazing is accounted for in the HeliOptix simulation engine (Equation 55 through Equation 58), and variables used in the calculation are explained in Table 40.

$$P = \frac{N_{glass} \cos\theta_t}{N_{air} \cos\theta} \left( \frac{T_p - T_t}{2} \right)^2$$

Equation 55. Radiation power transmitted through glass, relative to angle of incidence.

$$\theta_t = \arcsin\left(\frac{\sin\theta}{N_{glass}}\right)$$

Equation 56. Transverse angle.

$$T_p = 2 \left( \frac{N_{air} \cos\theta}{N_{glass} \cos\theta + N_{air} \cos\theta_t} \right)$$

Equation 57. Parallel transmission coefficient.

$$T_t = 2 \left( \frac{N_{air} \cos\theta}{N_{air} \cos\theta + N_{glass} \cos\theta_t} \right)$$

Equation 58. Perpendicular transmission coefficient.

Table 40. Variables in calculation of glazing attenuation.

<i>Glazing attenuation variable</i>	<i>Symbol</i>	<i>Value</i>
Transmitted power	P	
Index of refraction, air	N <sub>air</sub>	1
Index of refraction, glass	N <sub>glass</sub>	1.5
Angle of incidence	θ	
Transverse angle	θ <sub>t</sub>	
Transmission coefficient, parallel	T <sub>p</sub>	
Transmission coefficient, perpendicular	T <sub>t</sub>	

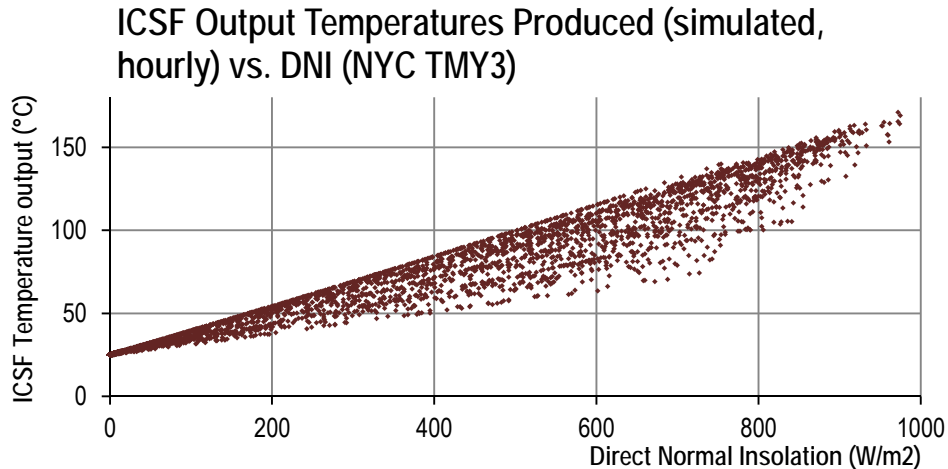


Figure 123. The relationship between incident direct normal insolation (from NYC TMY data) and ICSF temperature output from HeliOptix simulation engine.

The visible Pareto front in the data represents the maximum efficiency of the modeled ICSF installation, which correlates to the times of day when the least module overlap occurs. (Hourly data, vertical façade, south facing, NYC, 24 module string.)

### **6.2.1.3 Adjustments to HeliOptix Engine Output**

In order to more accurately describe the thermal output from ICSF, an additional thermal calculation is mapped onto the output from the HeliOptix model. The loss of heat in the hydronic transfer circuits impacts the overall thermal power efficiency of ICSF, as well as the maximum temperatures that can be produced. By characterizing the fluid and thermal flows, as well as the insulation method for the hydronic connections, these heat losses can be gauged and incorporated into the model. This comparison is shown in Figure 124.

### ICSF Output Temperatures Produced (simulated with hydronic losses, hourly) vs. DNI (NYC TMY3)

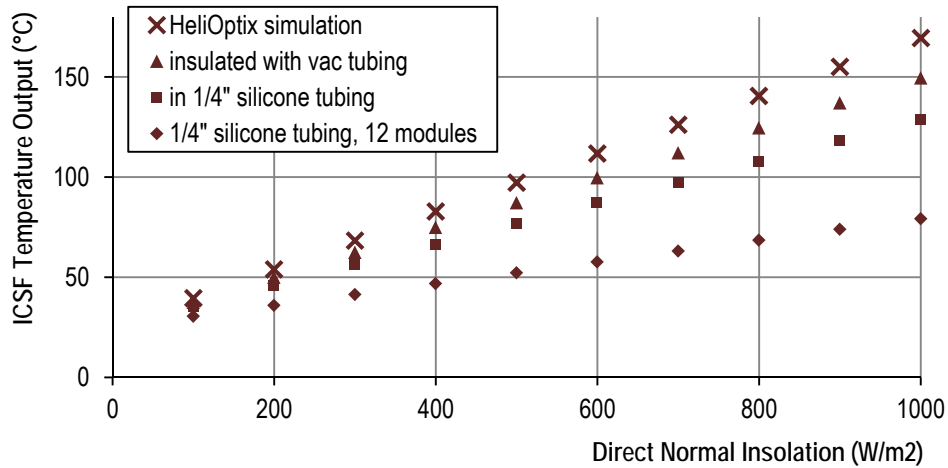


Figure 124. Simulated ICSF installation output temperatures.

Temperatures are adjusted for hydronic losses expected in silicone tubing and vacuum-insulated coolant circuits (24 modules modeled in series). 45% thermal efficiency from empirical data factored in. Proposed active-pulled vacuum tubing increases insulation effectiveness.

As seen in Figure 124, the maximum temperature output from the array scales linearly, at a rate dependent on the method used to simulate the output, and the array configuration. These scaling factors are used to alter the output from the HeliOptix simulation, assuming that the vacuum-insulated tubing will be used.

### ICSF Output Temperatures Produced (simulated with vacuum insulated tubes) vs. DNI (NYC TMY3)

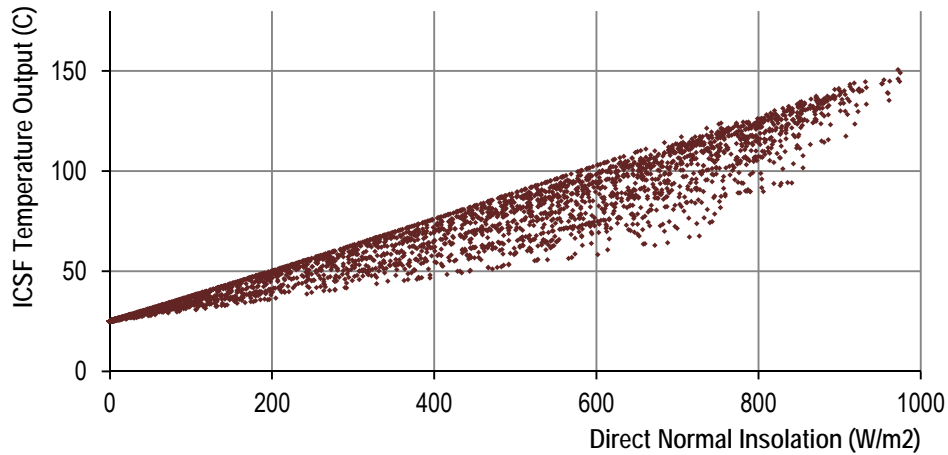


Figure 125. Simulated ICSF Output Temperatures, relative to hourly DNI data, for NYC climate. Heat loss effect of hydronic cooling circuit simulated with vacuum-insulated tubing.

### ICSF Power Gain per Stack, including insulative losses (silicone tubing, 6-module stack)

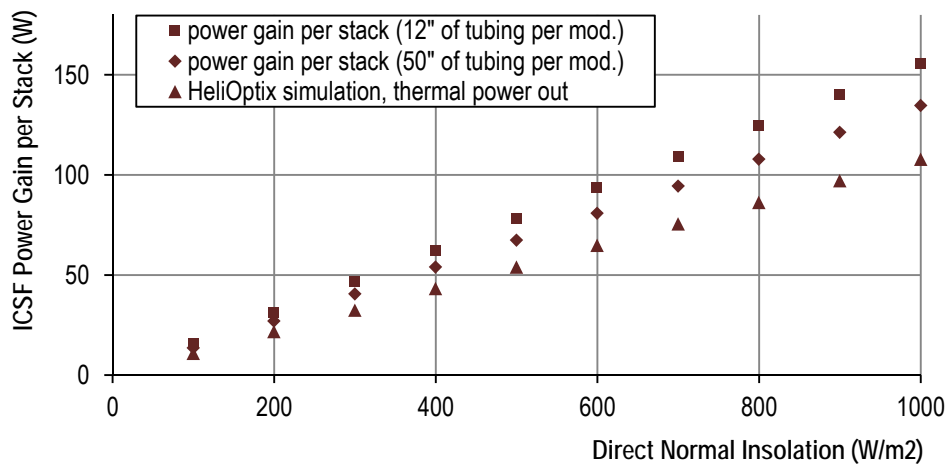


Figure 126. Simulated thermal energy gains from a 6 module stack, given short- and long-tubing configurations, and HeliOptix simulation output, for reference.

### **Simulated Electricity Production**

The electrical production of ICSF, is dependent on orientation.

KWH OF NET DC POWER OUTPUT YEARLY FROM ICSF PER M2 OF ENVELOPE AREA

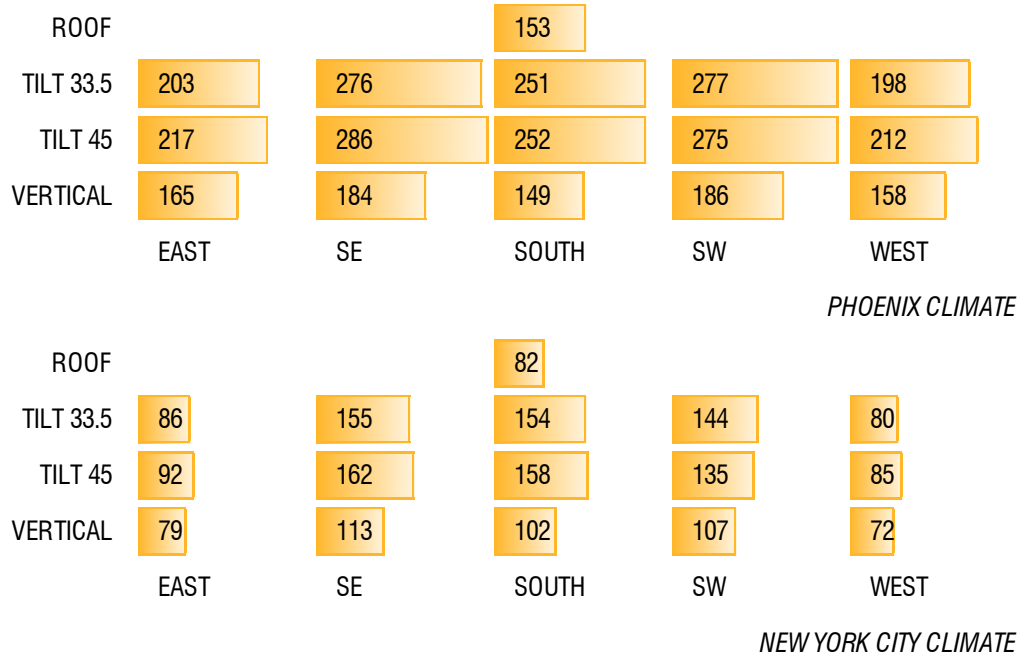


Figure 127. Electrical output of ICSF (kWh/m<sup>2</sup> of envelope area, yearly).

Summed over a period of time, electrical output from ICSF is function of the orientation and tilt of the envelope element with which the unit is integrated. (Simulated in NREL System Advisor Model (SAM).)

**Thermal production**

An inference must be made to extrapolate ICSF thermal production from the simulation data. Based on empirical data (exemplified in Figure 128), ICSF steady-state thermal collection is understood to vary in scalar fashion with the DC output.

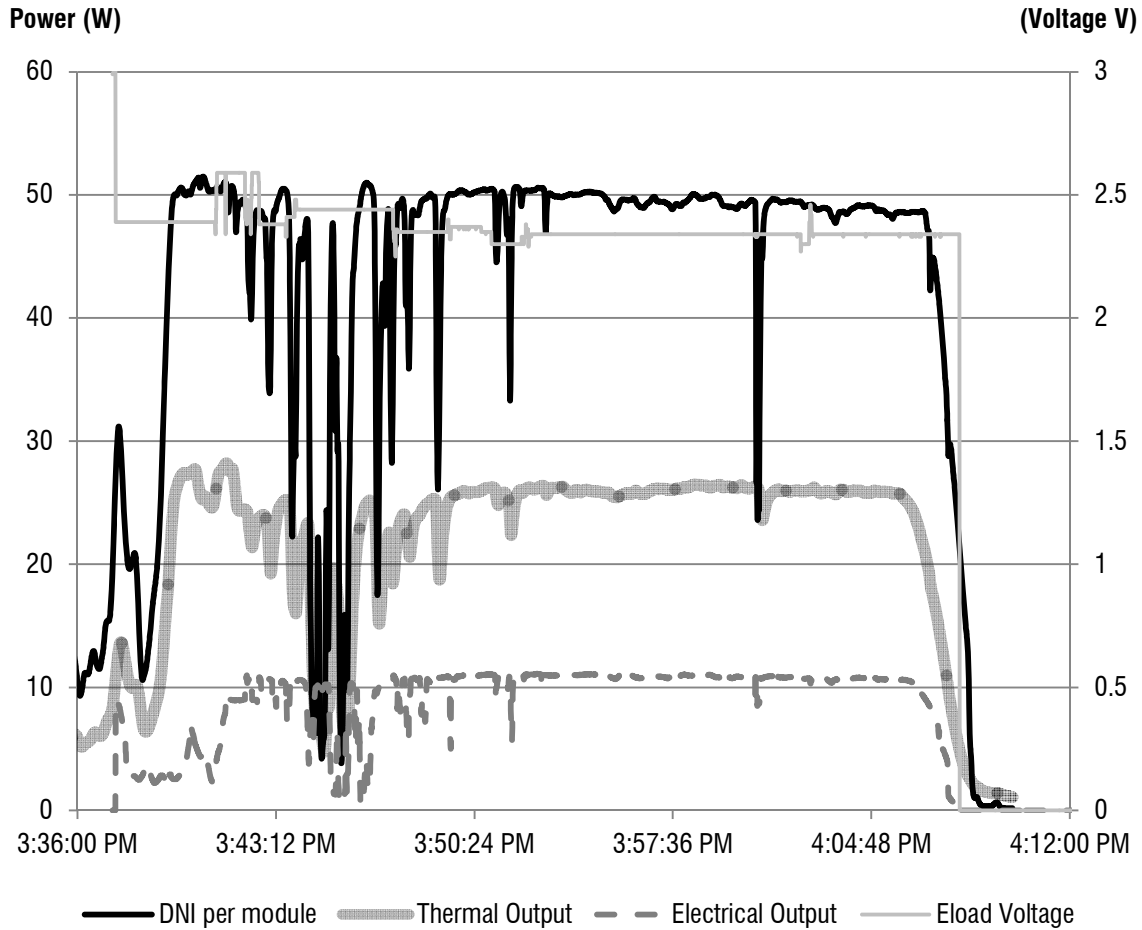


Figure 128. Data collected from ICSF module.

Data shows relationship of incoming beam solar radiation, module thermal and solar output, and module voltage (fixed by electronic load testing apparatus).

### ***Simulated Thermal Power Production***

Extrapolating based on this assumption of perfect insulation, the empirically-observed scalar correlation between DC output and thermal gains, and the simulated DC generation, thermal production across a parametric matrix of climates and envelope orientation is done, seen in Figure 129.

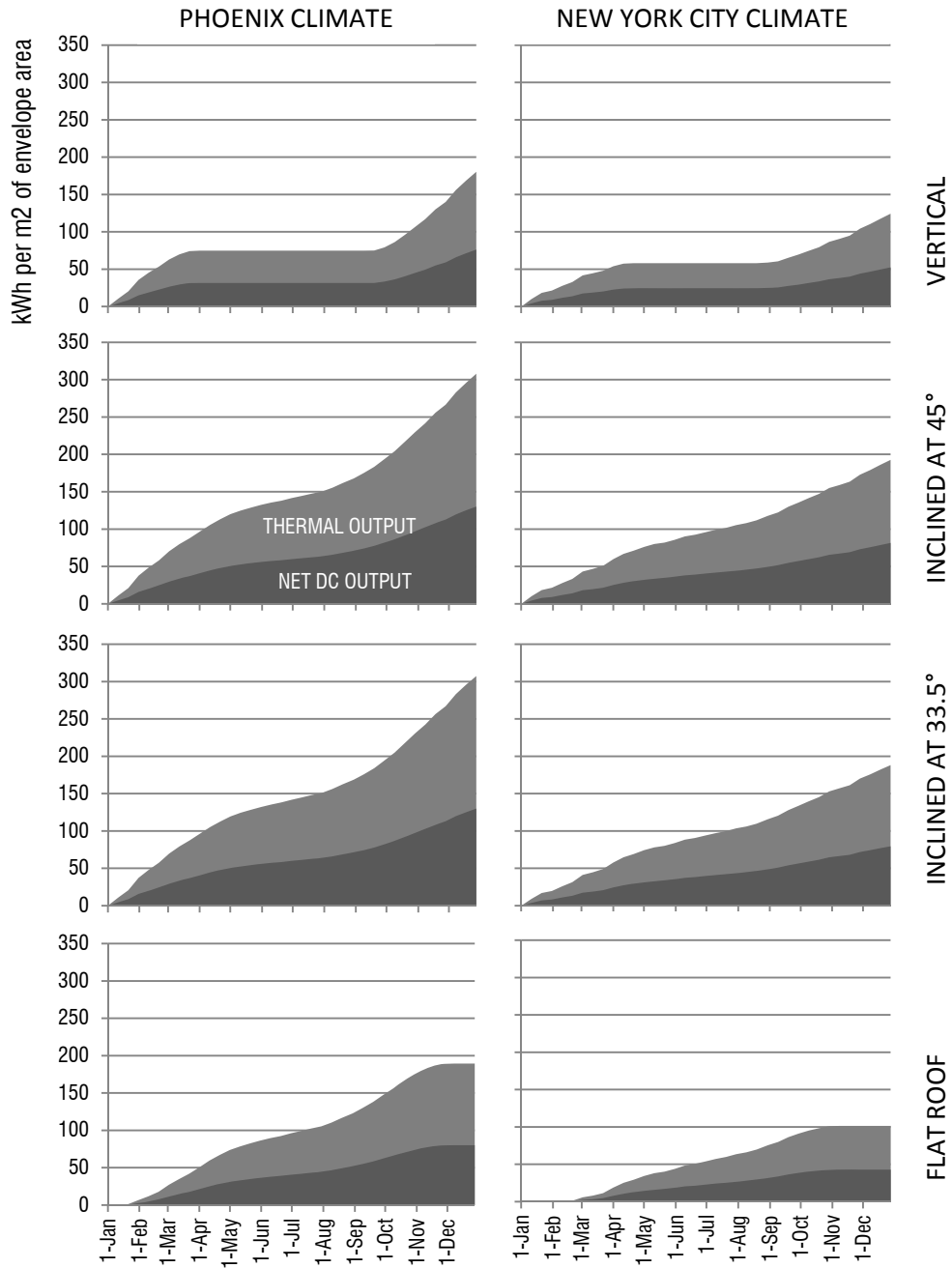


Figure 129. Thermal energy and net DC electricity production from installed ICSF. Differences are shown according to climate characteristics and envelope surface orientation. The orientations of all surfaces are towards due south.

### ***Cooling Capacity from BICSF***

With the power production characteristics of a façade-integrated concentrating solar collection system determined, the impact the system has on the cooling of a building can be extrapolated. Cooling capacity results from several functions of the concentrating façade.

Thermal energy collected by the concentrating facade can be used to drive sorption chilling, or other heat engine-driven chilling. To model this, the thermal characteristics of small scale sorption chilling unit are modeled, and the thermal power output from the façade system simulation is applied as a power source in a step-wise fashion. For the sorption unit specifications, a commercially available small-scale adsorption chiller, the ACS 08 from Sortech AG is characterized.

Additional cooling capacity is represented by the interception of solar irradiation by the concentrating facade: energy produced, both thermal and electrical, can be subtracted from thermal loads in perimeter building zones adjacent to the enhanced envelope, given appropriate arrangement of factors in the model. The building simulated in this study has a façade that is almost entirely glazed, which is characteristic of modern commercial architecture, and the thermal loads in perimeter zones are largely due to insolation penetrating the glazing and heating interior space. Therefore it is appropriate to model the interception and sequestration of those loads as direct subtraction from loads presented to the building's environmental control systems.

To supplement cooling capacity, the electrical power produced by the concentrating facade can be used to drive traditional vapor-cycle air conditioners. This is modeled using typical coefficients of performance for such units, and conversion efficiencies typical of electrical inverters that produce AC current from the DC output of the facade. In this simulation, the typical COP, set to 3.5, is increased by 1.0 to 4.5, to represent the subtraction of electrical power that would otherwise be supplied to the building to power the air conditioning process, and must be compensated for by that process.

### Adsorption Chiller Characterization

The Sortech ACS 08 adsorption chiller is modeled in this analysis via operational curves supplied by the manufacturer. The available curves relate coefficient of performance and output cooling power to heat rejection circuit temperature, and driving circuit temperature, given two performance envelope boundaries—one for high efficiency (“Eco”) mode, and another for high-capacity (“Power”) mode (Figure 62).

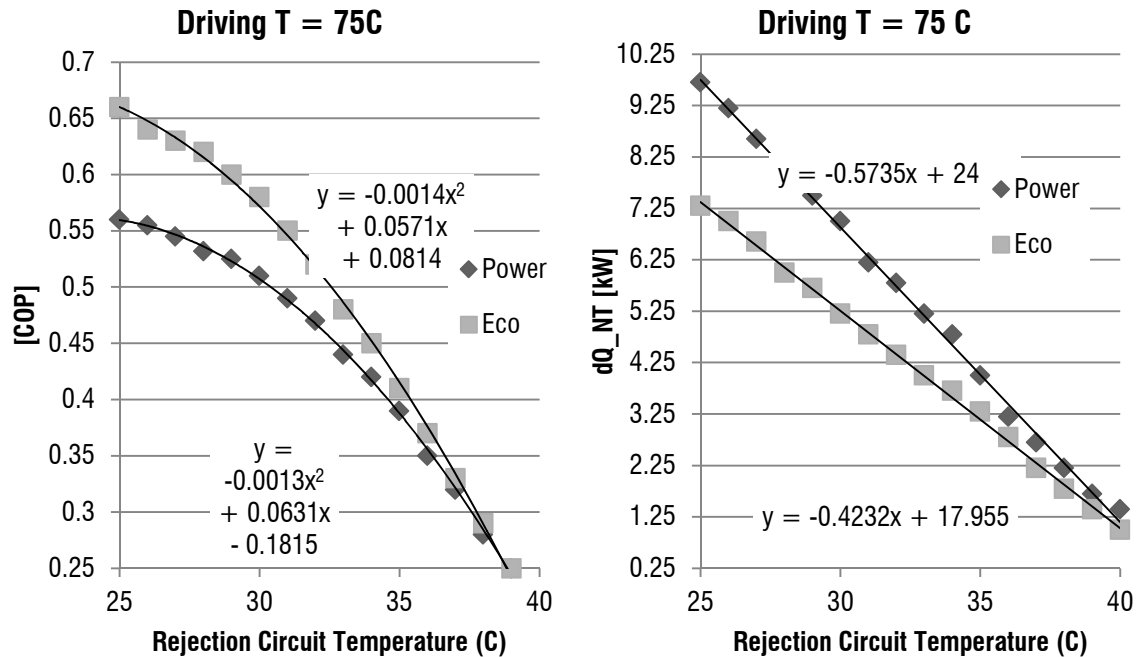


Figure 130. Sortech chiller performance curves.

At a given driving circuit temperature, the coefficient of performance and the capacity of the Sortech ACS 08 adsorption chiller are functions of rejection circuit temperature and operation state (Power or Eco). The curves provided by the manufacturer have been matched with equations for analytical purposes.

A nominal operating temperature for the driving circuit of 75C is assumed, which helps to reduce the indeterminate variable space of the Sortech operation. Further, the units are initially assumed to operate according to their Eco mode curves. The drawbacks to these assumptions are economic: lower capacity and higher efficiency result in better energy use, which trades off against a possible increase in number of units that must be installed to meet a given peak load condition. Other factors, including the overall energy available at a site, would realistically inform this decision.

Sortech AG supplies two sets of curves, corresponding to different chilled water output from the units. One set is calibrated to temperatures useful for fan coil hydronic transfer units; the second set is calibrated to higher chilled water output, which is typical when supplying cooling power to radiant ceiling panels. Radiant panels must be operated so that they don't approach dew point temperatures, for moisture control reasons, and therefore have less cooling capacity in a typical installation in a given space. Given the relatively low loads resulting from ICSF incorporation in the envelope, it is appropriate to assume radiant panels are used to transfer cooling power to the zones, and therefore this set of Sortech performance curves, which model higher efficiency, can be used.

Given these constraints, the Sortech operation is modeled in conjunction with atmospheric conditions. It's determined that the nominal COP (roughly .65) can be maintained for most of the year in the NYC climate with infrequent application of the Sortech re-cooler's sprayer function, and in fact, leaving the re-cooler in dry operation all the time has negligible impact on overall cooling capacity. Real-time chilling (without utilizing some sort of re-cooling temperature storage) in Phoenix requires the evaporative function during most operational hours to maintain the nominal COP. In this simulation, for the Phoenix climate, the sprayers are set to engage when the COP would otherwise dips below 0.4, based on ambient dry bulb temperatures.

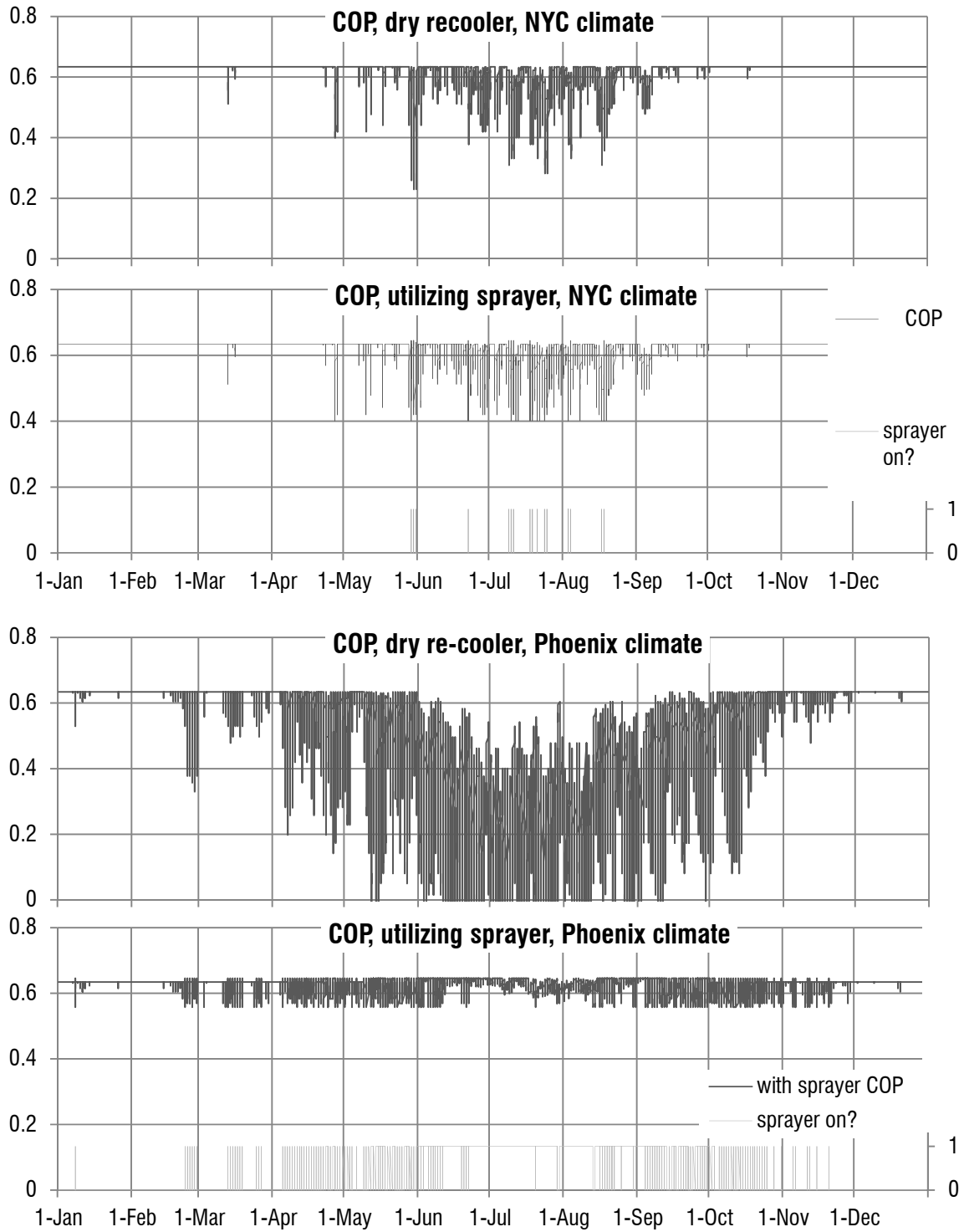


Figure 131. Chiller performance (COP) augmented with evaporative cooling.

The Sortech-supplied re-cooler incorporates a sprayer system. The operation described in this figure assumes that evaporative cooling kicks in when the COP dips below 0.4 if unassisted.

#### **6.2.1.4 Steps to Model BICS-Supplied Cooling Capacity in Building Setting**

- Start with baseline heat extraction rate, hourly, over one year, required in the modeled building.
- Use south perimeter zone of a middle floor of the simulated building, as it demonstrates the highest and most fluctuating heat extraction rate.
- Subtract the net energy production of ICSF from the baseline heat extraction rate.
- Assume an installation of ICSF that replaces the available glazed area of one floor's worth of the south building façade.
- Evaluate ICSF on a basis of the system's output per area of envelope area.
- Assume that the hydronic system includes enough thermal capacity to store cooling energy that is generated when it is not actively needed, such as during weekends when thermostat set points can be elevated. This energy can then be applied to consequent cooling loads.
- Include sorption chilling capacity.
- Assume thermal energy produced by ICSF is available to chillers.
- Calculate chillers' COP based on current outdoor dry bulb temperature, including an approach offset of 2°C.
- Set a floor on the re-cooling circuit temperature according to the lower limits of Sortech's published performance curves (25°C).
- The number of chiller units required can be calculated from the published nominal capacity and the amount of thermal power supplied by ICSF.
- Include sorption chilling capacity of a portion of assumed ICSF installed on building roof area.
- Assume ICSF on roof is inclined at a nominal 33.5° towards south.
- The roof installation of ICSF available to power this cooling load is equivalent to a third of the total roof area, as the south zone accounts for a third of the floor plate cooling requirements, divided by the number of floors in the building (10).

- Apply electrical power from ICSF to heat extraction rates based on nominal vapor cycle COP of 3.5+1 (as explained earlier).
- Include electrical air conditioning capacity from power supplied by assumed roof installation of ICSF.

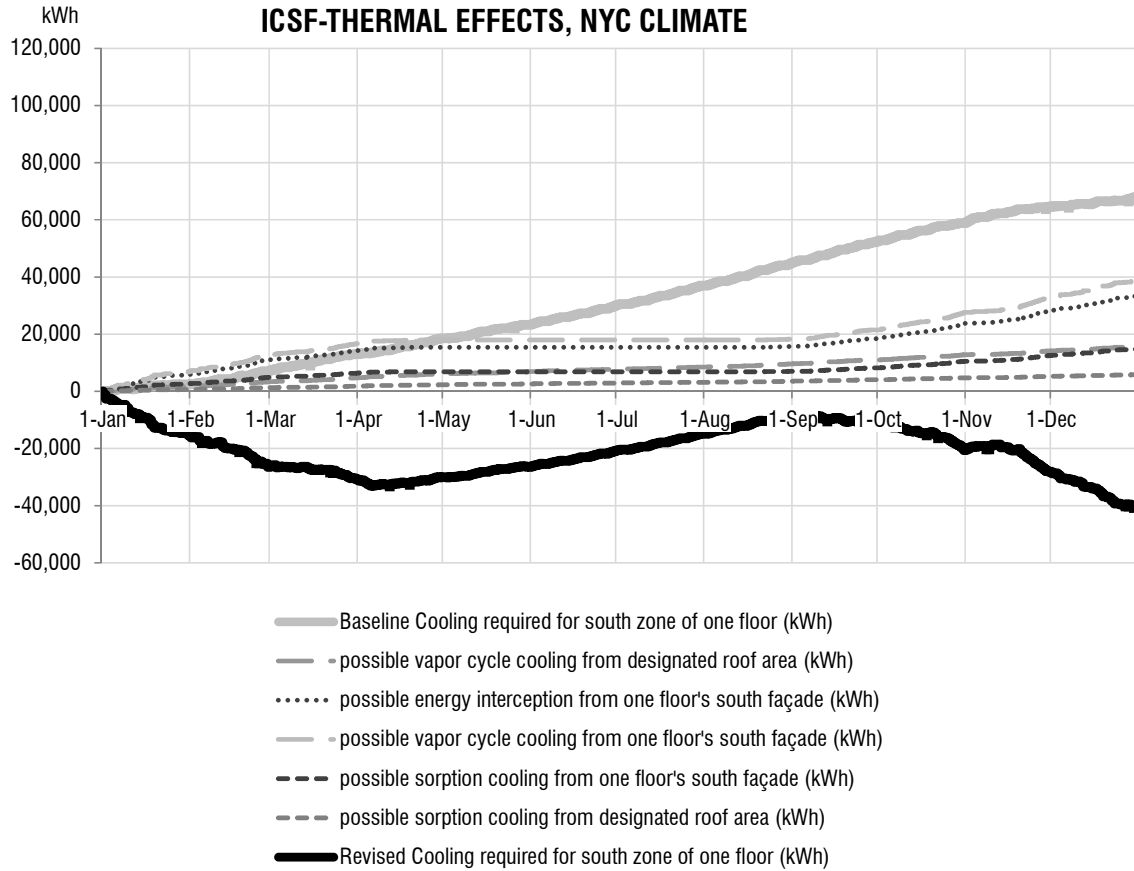


Figure 132. Cumulative effects of ICSF on the thermal loads, NYC climate.

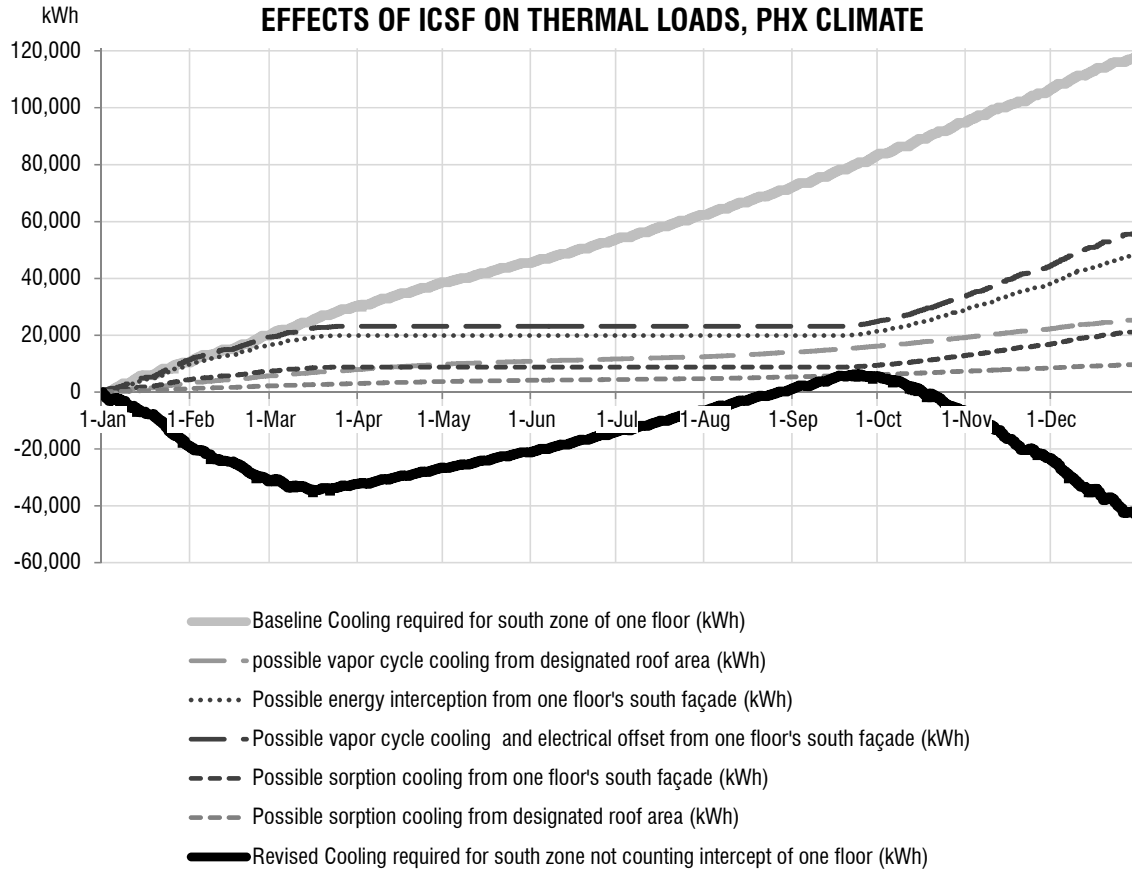


Figure 133. Cumulative effects of ICSF on the thermal loads, Phoenix climate.

### **Solar Cooling Analysis Results**

The integration of ICSF to a building’s south perimeter zone’s thermal control systems has distinct effects on the thermal load profile. Over the course of a year, in either Phoenix or New York climates, more than enough cooling capacity is generated to offset the cooling loads that remain after the interception effects of ICSF. Baseline cooling loads in south zone of the chosen building architecture are roughly constant over the course of the year. This results from the trading-off of insolation loads on the façade (higher during low-sun winter months) with compensation for ambient outdoor temperatures (higher during warmer months). For the late fall through early spring the ICSF-augmented system generates a surplus of capacity. During the warmer months, the available solar input drops off, and consequently the solar-powered system is overtaxed.

A solution to this overtaxing lies in building geometry. Referring back to ICSF capacity through a range of envelope surface orientations (Figure 127), it's seen that yearly ICSF capacity is strongest when the system is installed on surfaces angled away from cardinal directions, and additionally on tilted surfaces. Designing buildings with this in mind would result in improved warm-season cooling capacity. Alternatively or conjointly, the incorporation of longer-term cooling energy storage in building design would improve the cooling energy requirements similarly. The indicated erasure of cooling loads, however, over the course of the year, is a substantial result from the activation of the building envelope through integration of ICSF. The surplus of cooling power can be used for other purposes: the electrical energy is universally useful in a commercial building context (where its application still results in a net reduction of cooling loads, by reducing demands for externally-generated power). Excess generated thermal energy might be applied to other tasks, such as generation of more electrical power through processes such as low-pressure Rankine cycles.

### **6.3 Description of ICSF Modelica Model Development of a Modeling Strategy for Adaptive Multifunctional Solar Energy Building Envelope Systems**

*Note: the following write-up was presented at the Symposium on Simulation for Architecture and Urban Design (SimAUD) conference in 2015. A new acronym, BITCoPT was developed to describe the Integrated Concentration Solar Façade Technology for this paper. BITCoPT stands for building-integrated, transparent concentrating photovoltaic and thermal collector (BITCOPT) system. For a copy of the publication please see the appendix or attached supporting documents.*

#### **Abstract**

To achieve significant progress towards global targets for clean on-site energy self-sufficiency within the building sector, the integration of adaptive high efficiency solar collection systems into building envelope systems could offer broad additional benefits beyond power generation, such as: daylighting, hot water heating and purification, thermal comfort control, energy use reduction through lowered lighting and cooling loads, and tie-ins to direct current (DC) microgrids. Dramatic system efficiencies could be achieved with multifunctional envelopes by coupling to building systems to respond to fluctuations in weather and building use patterns. The development of active building envelope systems is impeded by current modeling workflows which do not provide adequate feedback or facilitate rapid design iteration within the context of building energy modeling (BEM). A simulation environment, Modelica, has purported extensibility and ease of co-simulation through the functional mock-up (FMI) standard. This environment is evaluated here through the development of a model for a novel multifunctional building envelope system, with concentrating photovoltaic and thermal collectors (BITCOPT) that incorporates multiple active and passive energy strategies simultaneously, while providing architectural benefits such as increased transparency and connection to views. The model is calibrated with measured data from an experimental prototype and is used to extrapolate the system's theoretical power

generation and energy efficiency effects. The simulation environment did indeed facilitate extensible model construction, encouraging future work to be pursued in co-simulation of the model with BEM via the FMI standard. The model structure, correlation to measured data, extrapolated results and future work are described here.

## Introduction

As the building sector is responsible for 40% of primary energy use in the United States [10], it would be beneficial to evolve buildings into carbon-neutral systems that effectively exploit on-site energy resources and promote human health and well-being. Active envelope strategies have been identified as a promising route towards the development of these benefits while managing both program and environmental fluctuations at multiple time scales [9,19], however no building-integrated energy harvesting strategy currently exists that both meets environmental performance targets and accommodates year-round human comfort.

Modeling methods for active envelope strategies are likewise cumbersome. With currently available tools and workflows, it is difficult to express the dynamic, multi-domain effects of new strategies as they relate to established building physics models [13]. Consequently models are often created separately from BEM and then loosely connected through pre- and post-processing of data [23]. This method suffers from poor runtime feedback and excessive manual labor in the reduction of data, factors that limit the application of these methods in the process of building systems design and implementation. Additionally there are two relevant behaviors that are difficult to represent through post-processing: controls, which update systems based on earlier states, and latency-related phenomena such as passive thermal massing or active thermal storage [24].

To expedite the development and integration of active envelope strategies as well as to impact design practices, policy and building codes, models of these strategies must be easy to calibrate, validate, and integrate with current-practice methods. For industrial acceptance, a modeling workflow should promote design iteration through informational feedback to the operator. Such a workflow conforms to the principle of

progressive data input whereby a model offers initial results based on sparse input data and results are refined as the inputs are refined [16]. To enable these qualities, a chosen modeling environment should exhibit adaptivity of modes of operation, encourage hierarchical and modular construction, and be interoperable with other environments (BEMs).

**Active Envelope: Building-Integrated Transparent Concentrating Photovoltaic and Thermal Collector**

A building’s envelope is tasked with controlling the shifting qualities of temperature, sunlight, wind, and moisture while maintaining tempered interior conditions [2,20]. With this gamut of responsibilities, improvements to the envelope are disproportionately consequential to building performance. Further, by integrating energy transformation technologies, the envelope can capture, store, transform, and redistribute energetic resources for use in building systems. A building-integrated, transparent concentrating

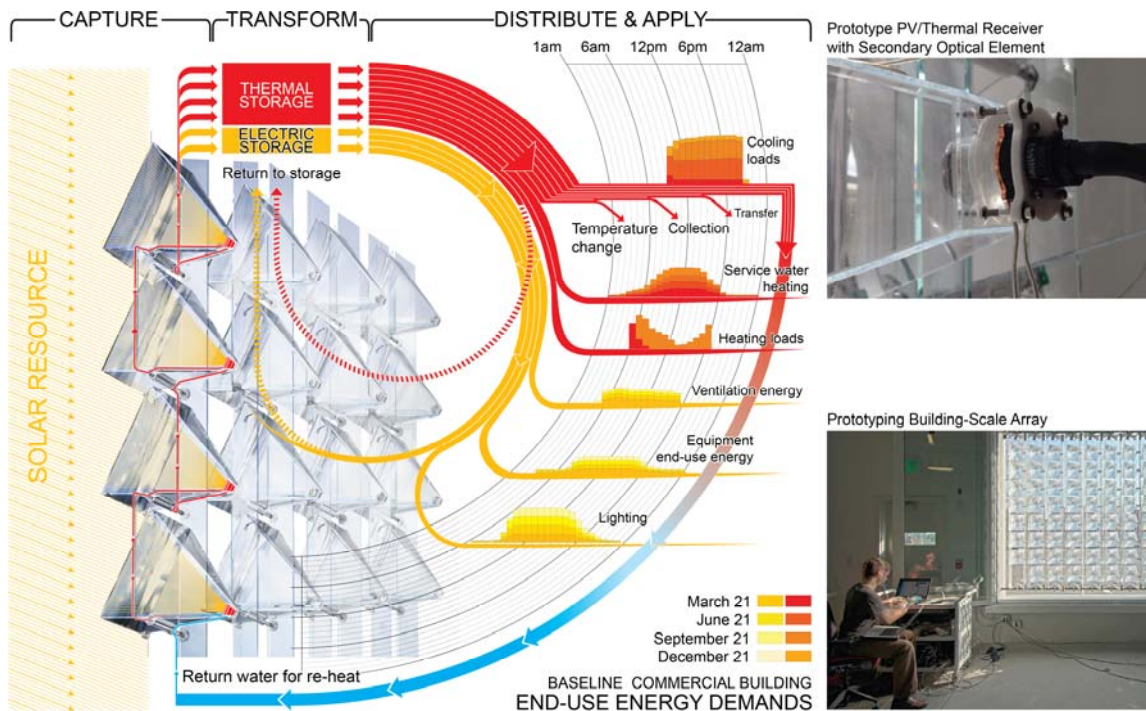


Figure 134. The BITCOPT system. Photographs of CASE Integrated Concentrating Solar Façade (ICSF) installation and data acquisition, with a diagram showing the adaptable energy conversion, storage and redistribution strategy.

photovoltaic and thermal collector (BITCOPT) system (shown in Figure 134) delivers these multiple benefits by intercepting and manipulating the direct-normal component of insolation (IDN), the energetic component largely responsible for elevated cooling loads and uncomfortable, high-contrast lighting conditions in buildings of moderate to deep lease spans [5]. By intercepting IDN but remaining mostly transparent to diffuse insolation (IDiff), the collector provides useful daylighting, maintains views, and reduces heat gain. Simultaneously, BITCOPT produces both electricity and high-quality thermal energy that can drive cooling and dehumidification (via sorption cycles), deliver service hot water and space heating, provide auxiliary electrical generation (via organic-fluid Rankine cycles) [22].

### ***BITCOPT Details***

The framework and results outlined in this paper are applied to a specific BITCOPT technology: the Integrated Concentrating Solar Façade (ICSF) developed at the Center for Architecture Science and Ecology, a research consortium co-hosted by Rensselaer and Skidmore Owings and Merrill LLP (Figure 134) [22]. ICSF is an array of collector modules hung within a curtain wall cassette. The modules are continuously tracked to the sun, each rotating around both horizontal and vertical axes. Each module comprises a flat Fresnel-like primary optical element (POE), a cast secondary optical element (SOE), a high-efficiency concentrator photovoltaic cell (CPV) and a water-block heat exchanger (HX). The last three elements form a sub-assembly, the receiver. The containing cassette is designed with a single-pane, low-iron glazing to the exterior and an insulated glazing unit (IGU) to the interior. As a curtain wall construction the cassette forms the envelope of the building and can be implemented vertically (as a standard façade), horizontally (as an atrium roof or skylight), or tilted.

The CPV within each module produces DC electricity ( $\dot{E}_{gen}$ ), collected from strings of modules wired in series and optimized per-string by a maximum power point routine. Thermal power ( $Q_{gen}$ ) is transferred through the water blocks to a heat transfer fluid (HTF) that circulates through insulated hydronic tubing, transporting thermal energy

from the array. Thermal energy is collected in a storage reservoir of high heat capacity (such as an insulated water tank) from which it can be extracted to drive processes.

Transparency is integral to BITCOPT. Most of the module and the super-structure parts within the window's field of view are constructed from borosilicate glass or clear plastics, so while views directly through the lenses are obscured, at any given time most lines of sight through the array are available and the effect of visual transparency is maintained. Some daylight losses occur due to Fresnel (surface) reflectances as diffuse insolation passes through the clear materials of the modules and super-structure. Therefore BITCOPT separates direct and diffuse insolation, manipulating the two components differently.

### ***Incentive for Model Development and Future Integration***

As a responsive sub-system of a larger building system, BITCOPT cannot be modeled independently without mis-representing behavior such as daylighting control and the enthalpy changes of active thermal storage systems and/or thermal mass within building systems. Co-simulation—whereby a model's sub-models are solved independently, with coupling through discrete domains—is therefore preferred to describe the behavior of a building with active envelope sub-systems. BITCOPT affects multiple values such as daylighting, glazing temperatures, solar heat gain, and zonal loads within the building (in addition to modifying the urban heat island contribution of the building to its local environment, which is beyond the scope of this paper). Because BITCOPT exchanges power with the building's electrical and thermal systems across the entire building, its applications suggests distributing processes likewise throughout the building volume, changing not only the behavior of the building and its systems, but the fundamental design of the building and systems.

This gamut of effects from BITCOPT stands in contrast to the limited effects of alternative technologies for on-site generation (rooftop collectors, semi-transparent thin films, shading louvers, etc) which are not as tightly integrated into a building's fabric and typically must trade-off between daylighting and energy collection [17]. Models of alternative envelope technologies (such as louvered blinds) do not need to address the

multiple physical domains of daylighting, electrical generation, thermal collection, and load reductions simultaneously [15]. The BITCOPT model, however, should be developed in an environment that easily represents differential relationships and controls, meaning that co-simulation with adjoining models become important to system implementation.

### Methods

Previous models of BITCOPT-related systems have been developed towards specific ends [1,6,7] but new development is required to account for the full gamut of the array's effects and to corroborate experimental results. The BITCOPT model in this paper processes inputs of environmental variables and system parameters and outputs of electrical generation, thermal collection, and heat transfer with adjacent systems (Figure 135 and Table 41).

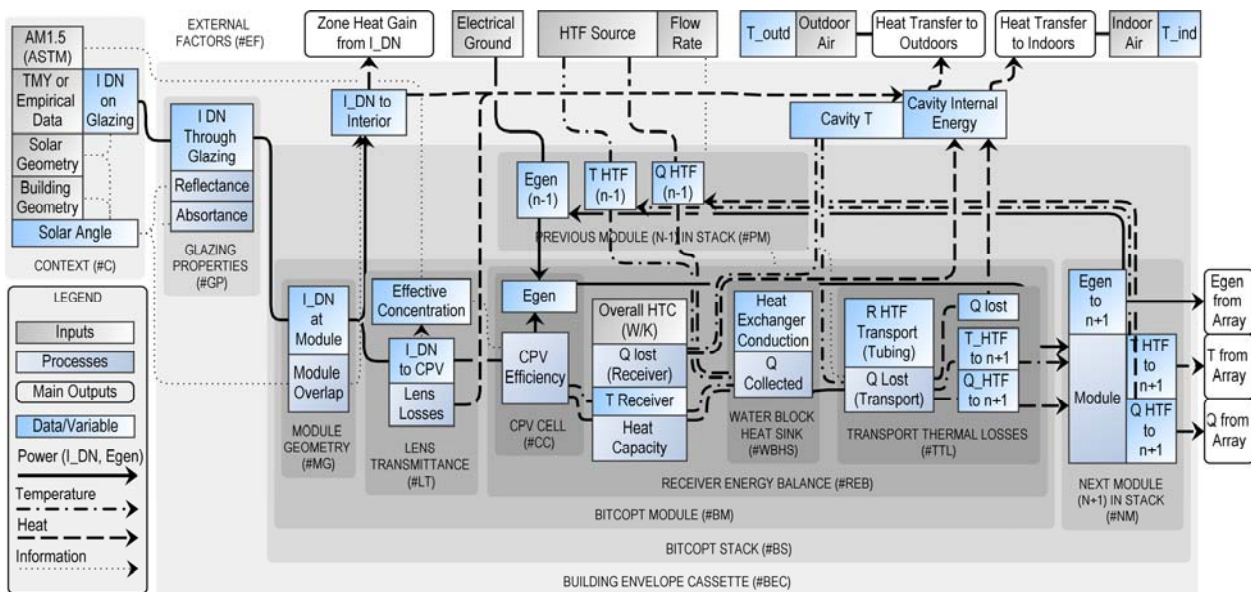


Figure 135. BITCOPT energy balance model and variable flow diagram. Component tags (denoted by #) are referred to in text.

The input and output variables structure is intended to facilitate future integrations of the BITCOPT model with a BEM such as EnergyPlus or DETECT [4], leveraging existing modeling expertise to describe the range of BITCOPT whole building effects. The physics of the BITCOPT model have been developed from roughly-approximated

energy balances and refined as necessary, with the goal of progressing towards more accurate descriptions of the array's behavior in the whole-building context.

### ***Motivation for Investigating Modelica***

Although a dynamic physical system can be modeled in any computational environment, there may be a design advantage to a dynamics-specific environment if it allows a developer to focus more on the system description and less on solution methods. Modelica is one such high-level language for dynamic modeling and has been identified as useful for building modeling, with libraries actively developed and maintained for the purpose [24]. The language purports to speed model development by enforcing the principles of abstraction, modular re-use, and object-oriented structuring. It has been claimed that development of building models in Modelica is more expedient than other common tools [25]. Additionally, both Modelica and select BEM environments support the functional mock-up interface (FMI), a standard for model information interchange and co-simulation [24]. Previous work has focused on using Modelica to model heating, ventilation, and air-conditioning (HVAC), controls, facade-shading systems, and building-integrated solar [11,18]. The language has not yet been applied to an active envelope collector technology. Based on outcomes of the precedent research, it is expected that a streamlined workflow can be created by combining a BITCOPT model (created in Modelica) with BEM through the FMI standard.

## BITCOPT Model Description

The computational model of BITCOPT is a quasi-steady state, lumped-capacitance representation of physical relationships. The relationships form a system of energy balance equations, outlined in Figure 135. The system of equations is solved at discrete time steps to determine the flow of energy between its components and their internal energy states. Although descriptive of the components of a specific technology (ICSF), by describing the transformation of solar resources to electrical and thermal energy flows and modifications to thermal and optical behavior of the building envelope, the model is intended generally to facilitate the modulation of these variables in future (customized) building envelope design processes.

The model's inputs are listed in Table 1.  $I_{DN}$  data is sourced (depending on the mode of analysis, either empirical or extrapolated) from experimental measurements or typical meteorological year (TMY3) data sets. A solar position vector is calculated from time and location data. Using the orientation of the envelope surface into which the BITCOPT is integrated, the angle of incidence ( $\theta_{AOI}$ ) between the solar vector and the surface is calculated [8], as well as the surface-basis orthogonal pitch ( $\theta_{pitch}$ ) and yaw ( $\theta_{yaw}$ ) angles that correspond to the vertical and horizontal excursions of a solar tracking apparatus (Figure 2, #C).

As with two-axis tracking collector systems generally (but unlike static collector systems)  $I_{DN}$  is not reduced by the cosine of  $\theta_{AOI}$  to determine power input to the collector. This factor is used, however, to calculate the insolation flux on an array area to determine momentary collector efficiencies. Additionally, transmittance through the external glazing due to reflectance and absorptance losses ( $T_{Trans,glaz}$ ) is a function of  $\theta_{AOI}$  (Figure 135 #GP). In this study the losses are combined and curve-fit from the bipolar reflectance function (using Snell's Law and assuming an index of refraction of 1.5) and manufacturer's absorptance data [14]. The term  $T_{Trans,glaz,norm}$  is applied to scale  $T_{Trans,glaz}$  to either rated or measured glazing transmittance values.

<b>Model Inputs</b>
Building location
Orientation of BITCOPT envelope facet
BITCOPT array size and configuration
Direct normal insolation ( $I_{DN}$ )
Diffuse insolation ( $I_{Diff}$ )
Heat transfer fluid inlet temperature ( $T_{HTF,in}$ )
Outdoor Dry Bulb Temperature ( $T_{outd}$ )
Zone Mean Air Temperature ( $T_{ind}$ )
<b>Model Outputs</b>
Electrical generation: net ( $\dot{E}_{gen}$ ), efficiency ( $\eta_{Egen}$ )
Thermal collection: net ( $\dot{Q}_{gen}$ ), energy efficiency ( $\eta_{Qgen}$ )
Heat transfer fluid outlet temperature ( $T_{HTF,out}$ )
Heat transfer with outdoors, through glazing ( $\dot{Q}_{outd}$ )
Heat transfer with indoors, through glazing ( $\dot{Q}_{ind}$ )
Direct normal insolation to zone interior ( $I_{DN,ind}$ )
Cavity air temperature ( $T_{cav}$ )

Table 41. Inputs and outputs of active envelope model.

The optical transmission efficiency ( $\eta_{opt}$ ) is a constant in this model, a function of the f-number equivalent of a Fresnel/Kohler-type (non-imaging) lens pair with anti-reflective coating on the SOE [3] (Figure 2, #LT). The theoretical value ( $\eta_{opt} = 88\%$ ) is treated as an upper bound and the efficiency is experimentally determined.

The un-shaded fraction of the POE ( $F_{POE}$ ) must be calculated at each time step as the horizontal and vertical overlap between adjacent modules evolves from hour to hour with tracking geometry.  $F_{POE}$  is interpolated from a two-dimensional lookup table of measurements of the pitch and yaw in the experimental prototype (Figure 2, #MG).

Given these layered attenuations, the solar energy incident on the CPV ( $Q_{DN,CPV}$ ) is determined at a given time step (Equation 59), as is the effective concentration ratio at the CPV ( $X_{eff}$ , Equation 60), which represents flux relative to the ASTM G-173 (AM1.5) standard (Figure 2, #LT).

$$\dot{Q}_{DN,CPV} = I_{DN,cav} A_{POE} F_{POE} \eta_{opt}$$

Equation 59. Solar power incident on CPV (#GP, #MG, #LT).

$$X_{eff,CPV} = \frac{A_{POE}}{A_{SOE}} * \frac{I_{CPV}}{I_{AM1.5}}$$

Equation 60. Effective flux concentration ratio as function of geometric concentration, CPV-incident irradiance, and AM1.5 reference insolation (#LT).

### Module Energy Balance

The central energy flow relationship in the BITCOPT is through the receiver of each module. This energy balance is described in Equation 61 and the control volume boundary is described in Figure 135 (#REB) and Figure 136. Insolation, changes in HTF flow enthalpy, electrical generation, and convective losses (via overall heat transfer coefficients) are considered across the system boundary. For the sake of initial simplification, radiation losses from the receiver to the environment are considered negligible in the current model but this initial assumption will be challenged by the experimental data moving forward and the model will be adjusted accordingly.

$$\begin{aligned}
 m c_{p,receiver} \frac{\partial T_{receiver}}{\partial t} &= \dot{Q}_{DN,CPV} - \dot{E}_{gen} - \dot{m}_{HTF} c_{p,HTF} (T_{HTF,out} - T_{HTF,in}) - U A_{receiver} (T_{receiver} - T_{cav}) \\
 &\quad - (T_{HTF,LMTD} - T_{cav}) / R_{tubing}
 \end{aligned}$$

Equation 61. Energy balance for a module receiver (#REB).

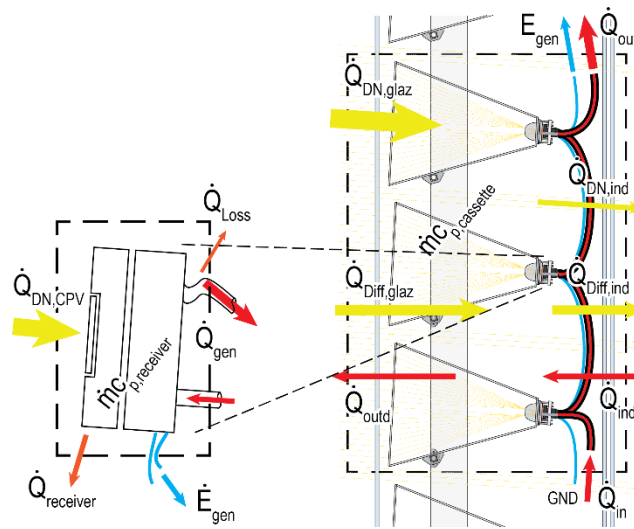


Figure 136. Model control volumes: BITCOPT receiver (left, #BM) and cassette (right, #BEC).

The receiver assembly is treated as a lumped capacitance ( $\dot{m}c_{p,receiver}$ ) comprising the sum of heat capacities of its components save for the SOE, which is isolated from the heat source via a layer of silicone and constructed of glass with low diffusivity. Assuming the surface convection coefficient is below  $20 \text{ W/m}^2$  (reasonable for quiescent air), the receiver's calculated Biot number is less than 0.1, validating the lumped-capacitance assumption (calculation not shown).

### ***Electrical Generation***

The electrical generation from the BITCOPT is a function of  $\dot{Q}_{DN,CPV}$  and the conversion efficiency  $\eta_{Egen,CPV}$ . (Conditioning losses exist as well, but are outside the bounds of the current model).  $\eta_{Egen,CPV}$  is a function of cell temperature  $T_{CPV}$  and  $X_{eff}$  [21].

Heterogeneous shading in serial CPV strings must be considered as a string is current-limited by its least-producing module. Although each CPV is paired to a bypass diodes that protects it from reverse-bias damage, the unshaded CPVs become forward biased and power output from the strings suffers by more than the fraction of shaded array area. Because the installation geometry of the BITCOPT system is assumed to be under the designer's control, we assume all modules in an electrical string (typically one vertical stack of modules) are shaded equally by their neighbors and operate at full power. Shading effects are therefore not modeled presently, although they may be in the future. Experimentally some differential shading does occur in the top-row modules during higher module yaws, which predictably decreases measured electrical output.

To account for power conversion and conditioning, stacks of BITCOPT modules are assumed to be wired in parallel with each other via output-matching DC-DC converters such as those manufactured for panel PV markets. Maximum power point (MPP) tracking is performed for each string and the individual output DC voltages are scaled to match the MPP of the line load (such as a zone-scale low-voltage DC distribution network, or string inverter). Conversion losses are minimized with this technique (to less than 5%, as related through communication with Gene Krzywinski, CTO of eIQ Energy) so the BITCOPT array is currently modeled independently from these effects.

### ***Thermal Collection***

Thermal collection is a function of the energy available at the CPV and the water block heat exchanger characteristics and results in elevation of the HTF temperature (Equation 62). The water block's resistance to heat flow ( $R_{\theta}$ ) is a function of HTF flow rate, but is treated as constant due to the limited range of flow rates in the experimental

setup, and is determined via measurements of CPV, HTF inlet and HTF outlet temperatures.

$$m_{HTF} c_{p,HTF} (T_{HTF,out} - T_{HTF,in}) = (T_{CPV} - T_{HTF,LMTD}) / R_{\theta}$$

Equation 62. Relationship between HTF and CPV driving temperatures and collected heat at module receiver (#WBHS).

### ***Thermal Losses (Receiver and Transport Hydraulics)***

Because the HTF temperature lift across BITCOPT is correlated to collection efficiency, knowledge of the insulation against heat losses is needed to gauge overall system performance. Two resistances in the model account for energy flow across the receiver control volume boundary: heat lost from the receiver surfaces and losses in the hydronic transport. Receiver heat losses are modeled with overall heat transfer coefficients (Equation 63).

$$\dot{Q}_{receiver} = \frac{(T_{receiver} - T_{cav})}{R_{receiver}}; \quad R_{receiver} = \frac{1}{UA_{receiver}}$$

Equation 63. Thermal energy lost at the receiver (#REB).

Transport heat losses are determined by a steady-state model of fluid flow through an insulated pipe with constant surface temperatures, a reasonable assumption due to high insulation value of the assembly and large operational difference between  $T_{HTF}$  and  $T_{cav}$ . (Equation 64). These assumptions dictate constant temperatures in the material of the transport tubing (Equation 65) and a Nusselt number for both HTF and cavity air convections of 3.66 [12].

$$\dot{Q}_{loss} = \frac{(T_{HTF} - T_{cav})}{R_{tubing}}$$

Equation 64. Thermal transport loss as a function of tubing insulation and temperature difference (#TTL).

$$\dot{E}_{internal} = (\dot{Q}_{inlet} - \dot{Q}_{outlet}) - \dot{Q}_{loss} \quad ; \quad \dot{E}_{internal} = 0$$

Equation 65. Energy balance of hydronic tubing (#TTL).

The insulation value ( $R_{tubing}$ ) of the transport tubing assembly is modeled according to material geometry, conductivities, and convection coefficients [12]. The thermal

transport efficiency  $\eta_{Q,tubing}$  is related to tubing wall resistance, HTF mass flow rate, and HTF specific heat (Equation 66).

$$\dot{Q}_{outlet} = \dot{Q}_{inlet} \eta_{Q,tubing} \quad ; \quad \eta_{Q,tubing} = e^{\left(-\frac{1}{R_{tubing} \dot{m}_{HTF} c_{pHTF}}\right)}$$

Equation 66. Thermal transport efficiency of tubing (#TTL).

### **Heat Gain Between Cassette Cavity, Indoors, Outdoors**

Conditions in a curtain wall cavity are difficult to model because insolation, air flow, and pressure, temperature, and moisture gradients converge under fluctuating conditions. The heat transfer described here between the cassette indoors, and outdoors forms the second fundamental energy balance in the BITCOPT system and is currently a simplified representation of an active envelope system, a placeholder for future development. The cassette is considered sealed, with well-mixed air and negligible infiltration. The cassette's heat capacity comprises trapped air, fractions of the interior and exterior glazing, and the tracking components of the BITCOPT. Energy is exchanged with the climate, the occupied zone, and building systems, as detailed in Equation 67 and Figure 136.

$$C_{p,cassette} \frac{dT_{cav}}{dt} = I_{DN,trans,glaz}(A_{glaz} \cos(\theta_{AOI})) - \dot{Q}_{DN,ind} + (A_{glaz})(I_{Diff,cav} - I_{Diff,ind}) \\ + U_{outd} A_{glaz}(T_{outd} - T_{cav}) + U_{ind} A_{glaz}(T_{ind} - T_{cav}) - \dot{E}_{gen} - \dot{Q}_{gen}$$

Equation 67. Energy balance across cassette control volume (#BEC, #EF).

Boundary conditions for the cavity energy simulation include the outdoor dry bulb temperature ( $T_{outd}$ ), gathered from TMY3 data, and a constant-temperature interior ( $T_{ind}$ ). One-dimensional heat transfer between the exterior and the cavity is governed by an overall heat transfer coefficient  $U_{outd}$ .  $U_{outd}$  is calculated from convection on the exterior glazing surface, conduction through the glazing, and interior surface convection (Equation 68). The coefficient to the interior  $U_{ind}$  is similar but refers to the constant  $T_{ind}$ , a lower convection heat transfer, and an insulated glazing unit (Equation 69).

$$U_{outd} = \left( \frac{1}{h_{outd}} + \frac{L_{glass}}{k_{glass}} + \frac{1}{h_{cav}} \right)^{-1}$$

Equation 68. Conductivity across outer cassette glazing (#EF).

$$U_{ind} = \left( \frac{1}{h_{cav}} + \frac{L_{glass}}{k_{glass}} \frac{1}{h_{gap}} + \frac{1}{h_{gap}} + \frac{L_{glass}}{k_{glass}} + \frac{1}{h_{ind}} \right)^{-1}$$

Equation 69. Conductivity across inner cassette glazing (#EF).

### **Reducing Direct Normal Insolation to Building Interior**

Although most direct insolation is gathered by the array, a fraction ( $F_{DN,ind}$ ) passes through the spaces between POEs when the solar vector is near-normal to the array and the angle of incidence ( $\theta_{AOI}$ ) is small. The module lenses are 100% opaque to  $I_{DN}$  (while tracking) but due to array geometry the POEs do not constantly overlap to fill the full aperture of the cassette.  $F_{DN,ind}$  peaks at 15% to 30% for short periods depending on module spacing, and falls to 0% when the array turns far enough ( $15^\circ$ - $25^\circ$  depending on module spacing) around both axes. This area-fraction function is determined through measurements of the prototype and is represented in the model by an interpolated look-up table.

### **Initial Results and Discussion**

To explore the utility of the workflow, this modeling effort has two goals: calibration of the model to experimentally measured results and extrapolation to a BEM-compatible data set. First, the model should reflect the operation of the physical, experimental BITCOPT (currently testing at CASE in New York City). Correlation between collected data and model output serves both to validate the behavior of the model and to highlight aspects of the experiment that are operating as expected (or otherwise). The second goal is to extrapolate the behavior of BITCOPT in a configuration that is compatible with BEM, as a set of data points at hourly intervals with a length of one year, towards the design and estimated values of the system for multiple climate types, during the design process.

For calibration, the model is configured to represent the geometry and material properties during a period of data acquisition. The output of this configuration is compared to empirical electrical generation, thermal collection, and receiver

temperature data from that period by applying measured  $I_{DN}$  and  $T_{HTF,in}$  as boundary conditions.

### **Data Acquisition**

A configuration of the BITCOPT prototype was tested that comprised nine active modules, corresponding to roughly  $1\text{m}^2$  of façade area.  $\dot{E}_{gen}$  data was collected from an electronic load (BK 8500), into which power was sunk from the series-wired modules. The string's MPP was periodically maintained by adjusting the load's voltage input. This data was compared to  $I_{DN}$  measured by two pyrheliometers (Hukseflux DR01) mounted in the tracker.

$\dot{Q}_{gen}$  data was gathered by measuring HTF flow rates, and temperature differences. Flow rates were read with Porter float-type meters with a full-scale reading of 3.3ml/s. Temperatures were measured at inlets and outlets of the water blocks with K-type, sheathed, ungrounded thermocouples (Omega) in contact with HTF. Specific heat of the HTF (distilled water) was calculated continuously relative to measured temperatures. Temperatures at the water block-CPV mating surface were measured with T-type sheathed thermocouples (at two modules). Control was written in LabVIEW, and data logged with NI-9213 and -9205 modules in a cDAQ-9178 chassis.

### **Model Calibration**

In an example data set, modeled  $\dot{E}_{gen}$  and  $\dot{Q}_{gen}$  show good response to the trends in measured  $I_{DN}$  (Figure 137). There are three notable exceptions. Prior to 1:48pm the top row of modules was shaded by the frame of the window in which the prototype is installed. The two deviation spikes at 1:58pm and 2:28pm correspond to deactivation of the tracking, where the prototype lost optical alignment with the sun. Although the insolation focused on the CPV decreased, decreasing electrical generation, energy was still directed to the receiver, increasing thermal collection.

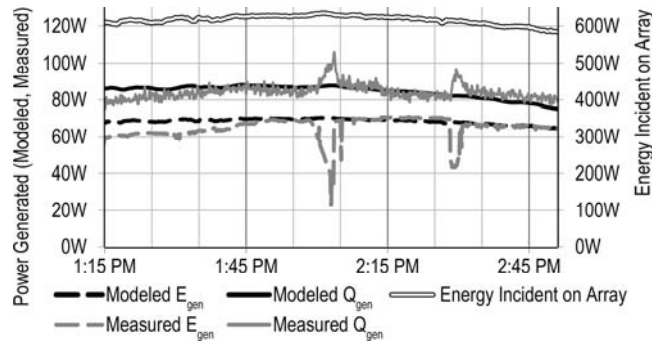


Figure 137. Measured and modeled power generation.

The parameters  $R_{\theta}$ ,  $\eta_{opt}$ , and  $R_{receiver}$  are modeled analytically and their values measured experimentally. They are calibrated to minimize the root mean square (RMS) error between the modeled and measured  $Q_{gen}$ ,  $\dot{E}_{gen}$ , and  $T_{CPV}$  data (relative to sample mean) (Table 42).

Parameters			Measured vs Modeled RMSE		
$R_{\theta}$	$R_{receiver}$	$\eta_{opt}$	$E_{gen}$	$Q_{gen}$	$T_{CPV}$
1.6 K/W	18.7 K/W	57%	10.7%	5.1%	1.2%

Table 42. Parameters for measured-modeled data calibration.

Results of parameter calibration suggest improvements to the BITCOPT prototype. Optical efficiency ( $\eta_{opt}$ ) is low compared to the theoretical value (88%), which suggests lens build quality can be improved. The thermal resistance of the water block ( $R_{\theta}$ ) is higher than the resistance in other considered exchanger designs (1.6 vs 0.2) at similar flow rates) suggesting that a more performance-optimized exchanger would improve collection efficiency.

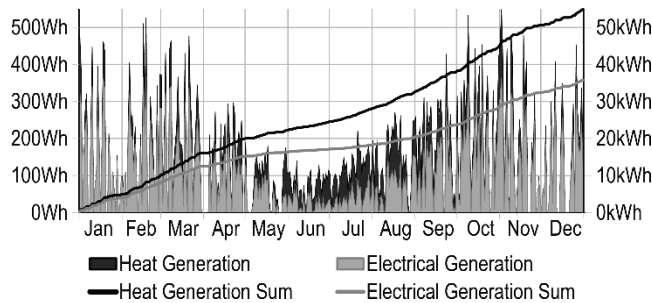


Figure 138. Year-long simulation of energy collection with experimentally-derived model parameters.

The calibrated model is extrapolated to year-long results by using the IDN vector from TMY3 data (New York City climate) as a point of comparison (Figure 138). It's noticeable that the thermal generation is higher, relatively, in the warmer months, possibly due to elevated cavity temperatures (which reduces thermal losses).

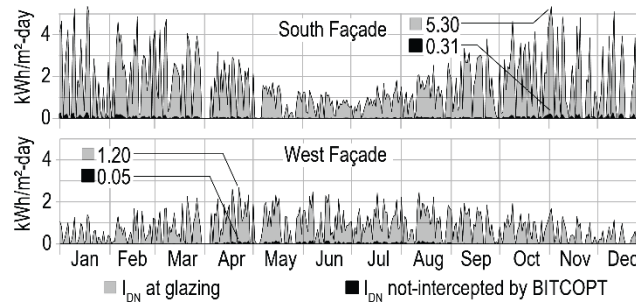


Figure 139. As modeled BITCOPT intercepts 96% (yearly) of  $I_{DN}$  transmitted past exterior glazing of south and west façades.

The reduction of  $I_{DN}$  to the building interior was modeled with New York City TMY3 data (Figure 139). Results indicate that BITCOPT has good potential for daylighting modification, reducing gains from  $I_{DN}$  by 96% relative to a comparable double-skin curtain wall system.

It has been observed that heat lost from BITCOPT will elevate cavity and glazing temperatures, increasing loads during cooling periods, but that the effect is insignificant relative to the reduction of  $I_{DN}$  to the indoors and attendant loads reduction. Future experimentation and modeling will be conducted to challenge these findings in the context of different climate types.

## Conclusion

To explore new workflows for adaptive building technologies, a model was constructed in the Modelica language for a dynamic solar building envelope system. The model was calibrated to experimental results and used to extrapolate full-year data sets (energy generation and the blocking of direct insolation) to facilitate future integration within building energy models. Development in Modelica proved successful, in part by demanding hierarchical structures encouraging users to iteratively increase the complexity of a model's physics. Once calibrated, the model exhibited good

predictive ability and suggested future modifications in the experimental setup and the system development. In the next phase, a functional mockup unit (FMU) of the model will be generated in Modelica to co-simulate with an Energy Plus building model by connecting the models' variables for insolation penetration and glazing temperature to observe the effects of the system on the heating, cooling, and lighting loads of a modeled building. Although the integration of this model with building energy models has not yet been attempted, the framework for that integration is native within the environment, which is expected to facilitate future variations on systems design and customization per variations in local climate conditions, building types, occupation patterns and aesthetic requirements.

## References

1. Amrizal, N., Chemisana, D., and Rosell, J.I. Hybrid photovoltaic–thermal solar collectors dynamic modeling. *Applied Energy*, 0 (2012).
2. Andow, B.C., Krietemeyer, B., Stark, P.R.H., and Dyson, A.H. Performance criteria for dynamic window systems using nanostructured behaviors for energy harvesting and environmental comfort. (2013), 86923V–86923V–11.
3. Benitez, P., Minano, J., Zamora, P., et al. High performance Fresnel-based photovoltaic concentrator. *Optics Express* 18, S1 (2010).
4. Buonomano, A. and Palombo, A. Building energy performance analysis by an in-house developed dynamic simulation code: An investigation for different case studies. *Applied Energy* 113, (2014), 788–807.
5. Chemisana, D., López-Villada, J., Coronas, A., Rosell, J.I., and Lodi, C. Building integration of concentrating systems for solar cooling applications. *Applied Thermal Engineering* 50, 2 (2013), 1472–1479.
6. Chow, T.T. Performance analysis of photovoltaic-thermal collector by explicit dynamic model. *Solar Energy* 75, 2 (2003), 143–152.
7. Craft, J. Simulation, Design and Testing of a Building-Integrated Hybrid Concentrator Photovoltaic System. 2004.
8. Duffie, J.A. and Beckman, W.A. *Solar Engineering of Thermal Processes*. Wiley, 2006.
9. Dyson, A., Ngai, T., and Vollen, J. Characterizing the Problem: Bioenergetic Information Modeling. In *BIM in Academia*. Yale School of Architecture, New Haven, CT, 2011.
10. Esterly, S. and Gelman, R. *2013 Renewable Energy Data Book*. EERE, 2014.
11. Fontanella, G., Basciotti, D., Dubisch, F., et al. Calibration and validation of a solar thermal system model in Modelica. *Building Simulation* 5, 3 (2012), 293–300.
12. Incropera, F. and DeWitt, D. *Fundamentals of Heat and Mass Transfer*. John Wiley, New York, NY, 1996.
13. Kim, D.-W. and Park, C.-S. Difficulties and limitations in performance simulation of a double skin façade with EnergyPlus. *Energy and Buildings* 43, 12 (2011), 3635–3645.
14. LBNL. *Window & Daylighting Software -- WINDOW 6 Research Version*. .

15. LBNL Simulation Research Group and UIUC Building Systems Laboratory. EnergyPlus Engineering Reference. 2013.
16. Marsh, A.J. Performance analysis and conceptual design. 1999. [http://companyshed.com/downloads/documents/Thesis\\_AJMarsh.pdf](http://companyshed.com/downloads/documents/Thesis_AJMarsh.pdf).
17. Miyazaki, T., Akisawa, A., and Kashiwagi, T. Energy savings of office buildings by the use of semi-transparent solar cells for windows. *Renewable Energy* 30, 3 (2005), 281–304.
18. Nouidui, T.S., Wetter, M., and Zuo, W. Functional Mock-Up Unit Import in EnergyPlus For Co-Simulation. *Proceedings of BS2013: 13th Conference of International Building Performance Simulation Association*, (2013).
19. Poirazis, H. *Double Skin Facades for Office Buildings - Literature Review Report*. 2004.
20. Selkowitz, S., Lee, E., and Aschehoug, O. Perspectives on advanced facades with dynamic glazings and integrated lightings controls. *CISBAT* (2003).
21. Spectrolab. C3MJ\_CCA100 data sheet. 2011. <http://www.spectrolab.com/history.htm>.
22. Stark, P.R.H., Jensen, M.K., and Dyson, A.H. *Integrated Concentrating (IC) Solar Façade System*. DOE, 2007.
23. Trcka, M., Wetter, M., and Hensen, J. Comparison of co-simulation approaches for building and HVAC/R system simulation. *submitted for Building simulation conference IBPSA*, (2007).
24. Wetter, M. A view on future building system modeling and simulation. *Building Performance Simulation for Design and Operation*, (2011).
25. Wetter, M. and Haugstetter, C. Modelica versus TRNSYS—A comparison between an equation-based and a procedural modeling language for building energy simulation. *Proc. of the 2nd SimBuild Conference* (2006).